



UNIVERSITÀ
DI PAVIA

PhD IN BIOMEDICAL SCIENCES

DEPARTMENT OF BRAIN AND BEHAVIORAL SCIENCES

UNIT OF NEUROSCIENCE

3D Bioprinting and organoids: a new era in the study of Amyotrophic Lateral Sclerosis

PhD Tutor: Dr. Cristina Cereda

PhD dissertation of
Eveljn Scarian

a.a. 2021-2022

Summary

<i>1. INTRODUCTION</i>	2
1.1 Neurodegenerative diseases	3
1.1.1 Alzheimer’s Disease	5
1.1.2 Parkinson’s Disease	7
1.1.3 Huntington’s Disease.....	9
1.1.4 Amyotrophic Lateral Sclerosis	11
1.1.5 Modeling in the study of NDDs	15
1.2 iPSCs	17
1.2.1 iPSCs modeling	19
1.2.2 iPSCs in the study of NDDs	20
1.3 3D bioprinting	26
1.3.1 History of 3D bioprinting	27
1.3.2 Bioprinting bioplotters.....	28
1.3.3 Bioinks	31
1.3.4 3D bioprinting in the study of NDDs	35
1.4 Organoids.....	37
1.4.1 History of organoids	37
1.4.2 Organoids’ development methods.....	38
1.4.3 Organoids’ applications	41
1.4.4 Organoids in the study of NDDs	44
<i>2. AIM</i>	47
<i>3. MATERIAL AND METHODS</i>	50
3.1 PBMCs reprogramming and iPSCs differentiation	51
3.2 3D bioprinting	55
3.2.1 SA-GEL Hydrogel.....	55
3.2.2 Cellink Bioink Hydrogel	58
3.3 Organoids	62
<i>4. RESULTS</i>	67
4.1 3D bioprinting	68
4.1.1 SA-GEL Hydrogel.....	68
4.1.2 Cellink Bioink Hydrogel	74
4.2 Organoids	83
<i>5. DISCUSSION AND CONCLUSIONS</i>	97
<i>6. REFERENCES</i>	106

1. INTRODUCTION

1.1 Neurodegenerative diseases

Neurodegenerative diseases (NDDs) include a large group of debilitating and still incurable pathologies with a progressive degenerative clinical course, which cause the death of specific neural cell types [1]. They are all aged-related disorders and due to the increasing average age of the population, they are becoming prevalent and, consequently, a serious worldwide diffuse health problem [2]. There are many risk factors associated with NDDs, including genetic and environmental factors, but aging is considered the one with the most impact [3]. These diseases are different in their manifestations because of the different neuronal cells and brain networks affected and the variability of the pathophysiology. Because of the heterogeneity of clinical features and symptoms, the diagnosis of NDDs is difficult, and often can be confirmed only with a neuropathological examination after patient's death [4, 5]. Alzheimer's disease (AD) and other types of dementia, such as Frontotemporal dementia (FTD), manifest memory and cognitive impairment, but other NDDs such as Parkinson's disease (PD), Amyotrophic lateral sclerosis (ALS) and Huntington's disease (HD) affect movement, speaking and breath. Despite their different manifestations they can all manifest in two different forms, the sporadic form and the familiar one, based on familial history, which can be associated or not with specific gene mutations or with a set of susceptible genes, mostly with a dominant inheritance [1]. Some genes are common between NDDs leading to an overlapping between different pathologies, as it was demonstrated in the ALS-FTD spectrum [6] (Figure 1).

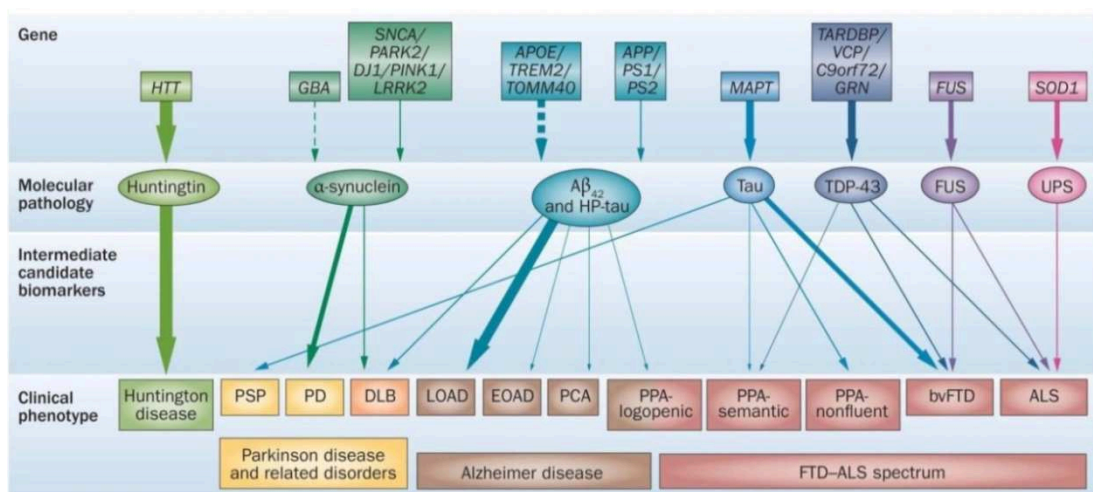


Figure 1. Main genes associated with the different NDDs. PSP= progressive supranuclear palsy, PD= Parkinson disease, DLB= dementia with Lewy bodies, LOAD= late-onset Alzheimer disease, EOAD= early-onset Alzheimer disease, PCA= posterior cortical atrophy, PPA= primary progressive aphasia, bvFTD= behavioral variant frontotemporal dementia, ALS= Amyotrophic lateral sclerosis (modified from Pievani *et al.*, 2014 [7]).

NDDs are characterized by the accumulation of specific proteins. In the context of protein inclusions, the pathologies can be divided in amyloidoses, characterized by Amyloid- β accumulation, tauopathies, with the accumulation of tau protein, α -synucleinopathies, with the accumulation of α -Synuclein, and transactivation response DNA binding protein 43 (TDP-43) proteinopathies. Moreover, in ALS it can be found the accumulation of the Superoxide dismutase protein (SOD) and in HD the accumulation of Huntingtin protein (HTT), general referred as proteinopathies (Table I).

Table I. List of most common misfolded and aggregating proteins and site of aggregation in the main NDDs.

NDD	Misfolded proteins	Aggregates' cellular location
AD	Amyloid- β and tau	Extracellular, cytoplasmatic
PD	α -Synuclein	Cytoplasmatic
ALS	SOD and TDP-43	Cytoplasmatic
HD	HTT	Nuclear

Genes' mutations or sporadic events cause misfolding of proteins and the aggregation into oligomers enriched in β -sheets. These oligomers form fibrillar aggregates and inclusion bodies (Figure 2). Misfolded proteins can spread at different levels, molecular, cellular and regional, by a prion-like principle [8].

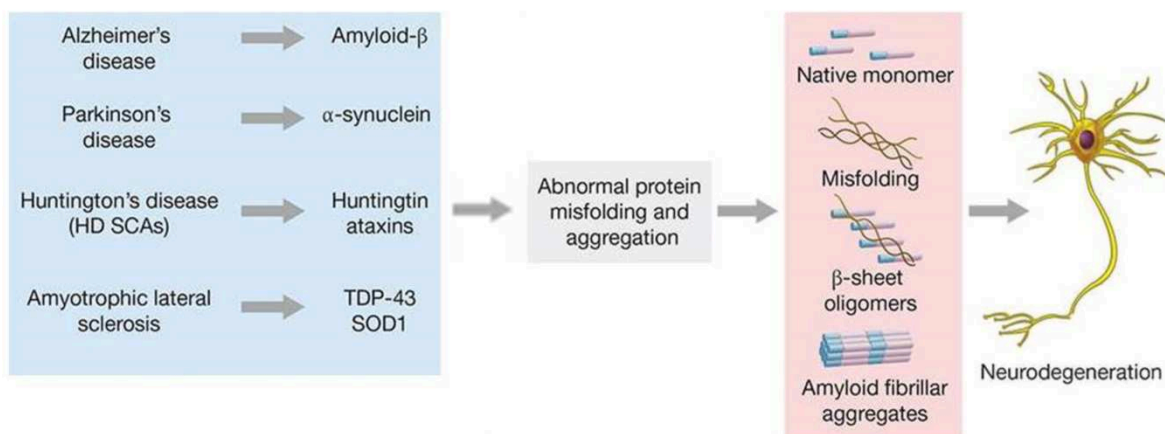


Figure 2. Protein misfolding process in the main NDDs (modified from <https://www.thermofisher.com/it/en/home/references/newsletters-and-journals/bioprobex-journal-of-cell-biology-applications/bioprobex-74/bioprobex-74-antibodies-misfolded-proteins.html>).

Moreover, it was demonstrated that protein aggregates can differ in size and shape [9] [10, 11].

NDDs share many pathological processes such as proteotoxic stress, dysfunction in ubiquitin-proteasomal, autophagosomal and lysosomal systems, oxidative stress and neuroinflammation. All these processes lead to the death of specific neuronal cell types [12].

1.1.1 Alzheimer's Disease

AD is the most common NDD and the most common dementia (50-70% of the cases), affecting at least 27 million people in the world [13] [14]. Over 65 years, the probability of AD doubles every 5 years. Women are more affected with prevalence 1.17 times higher than in men [15]. Moreover, a recent study, demonstrated that the rate of AD deaths increased 146.2% from 2000 to 2018, becoming the fifth cause of death in American old people [16]. The high incidence leads to important costs, including direct costs such as home healthcare, nursing care and long-term care, and indirect ones, such as quality of life and impact on caregivers. It was estimated that the cost for AD was \$305 billion in 2020 [17]. Several risk factors are associated with this pathology, such as head injury, cardiovascular and cerebrovascular disease, depression, smoking, higher parental age, dementia family history, high homocysteine levels and the presence of *APOE* ϵ 4 gene isoform. On the contrary, high education, use of estrogen and anti-inflammatory agents, activities such as playing an instrument or reading, regular aerobic exercise and a healthy diet, decrease AD risk [18].

AD was first described in 1907 by Alois Alzheimer, who noticed brain atrophy and “particular changes in cortical cell clusters” in patients’ autopsies [19, 20]. It manifests with the progressive loss of episodic memory and cognitive functions, followed by language and visuospatial abilities deficiencies. Moreover, symptoms are often accompanied by behavioral disorders [13]. Neuronal death starts in the entorhinal cortex and in the hippocampus, subsequently spreading to other area of the neocortex. It is characterized by extracellular lesions formed by accumulation as senile plaques of $A\beta$ 42 protein, derived from the cleavage of amyloid beta precursor protein (APP) protein, and by intraneuronal inclusions, called neurofibrillary tangles (NFTs), composed of phosphorylated tau protein, which aggregate due to the extracellular β -amyloid deposition [13, 18] (Figure 3).

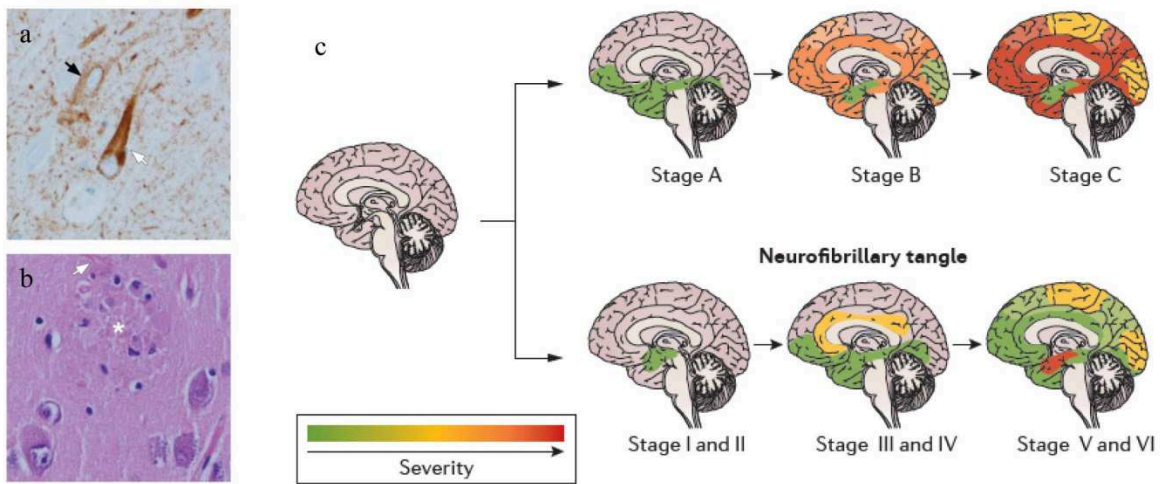


Figure 3. Histological characterization and pathological progression of AD. NFT (white arrow) and a pretangle (black arrow) are visible through immunohistochemistry for phospho-tau (a). Neurite plaques (asterisk) are visible near activated microglia and astrocytes (b). Progression of AD shows that A β deposition commonly precedes neurofibrillar and neurotic changes (c) (modified from Masters *et al.*, 2015 (a and b) [21] and from Dugger *et al.*, 2017 (c) [12]).

Although the accumulation of fibrillar amyloid is the first change in AD, many years can pass prior to the onset of the symptoms. There are three main stages of AD: in the *preclinical* AD there is a pre-symptomatic pathology with first brain changes identifiable by neuroimaging and other biomarkers. Individuals with mild-cognitive impairment and biomarker evidence, who are still able to perform daily life activities, are referred to have *prodromal* AD. Finally, in the stage of *dementia* there is cognitive decline which interferes with life. Positron emission tomography scanning is often used for biomarkers' individuation, such as the ratio A β 1–42 to A β 1–40 in cerebrospinal fluid or in plasma. Moreover, episodic memory tests are commonly used to identify the predementia associated with AD [22, 23]. AD can be inherited as a dominant disorder and it is associated with mutations in three principal genes: *APP* gene on chromosome 21, presenilin 1 (*PSEN 1*) on chromosome 14 and presenilin 2 (*PSEN2*) on chromosome 1. *APP* mutations cause the increase in generation of β -amyloid peptide and its aggregation. *PSEN1* and *PSEN2* mutations interfere with the activity of γ -secretase, enzymes involved in the cleavage of APP protein. Mutations in *APP*, *PSEN1* and *PSEN2* account for 5-10% of AD cases, whereas 90-95% of the cases are not correlated with genes mutations [18].

To date, no pharmacological treatments for AD slow or stop are available. All currently approved drugs are symptomatic agents to improve behavioral and cognitive symptoms. Four cholinesterase inhibitors, Tacrine, no longer available, Donepezil, Rivastigmine and Galantamine, and one N-methyl-D-aspartate receptor antagonist, Memantine, have been approved by the U.S. Food and Drug Administration [24].

1.1.2 Parkinson's Disease

PD is the second most diffuse NDD. In last years, PD had the fastest prevalence and disability growth, becoming one of the main causes of disability in the world [25]. In 2016 there were 6.1 million PD patients with a prevalence increase of 21.7% from 1990 to 2016 [15]. PD affects 1-2 per 1,000 of people, 1% of the population over 65 years and more frequently men than women [26]. Many factors have been linked to this pathology. Exposure to environmental toxins, pesticides, oils, heavy metals, general anesthesia, genetic polymorphisms of cytochrome P450 2D6, and PD family history have been correlated with a major possibility to develop PD, whereas coffee consumption, smoking and physical activity have been found as protective factors [27, 28].

PD was first described by James Parkinson in 1817, who named this pathology “shaking palsy” in his monograph “An essay on the shaking palsy” (reprinted version [29]). It manifests mainly with motor symptoms, such as bradykinesia, postural instability, rigidity and tremor, caused by the degeneration of dopaminergic neurons present in the substantia nigra *pars compacta*, which projects to basal ganglia [30]. Moreover, non-motor symptoms, including olfactive deficits, autonomic dysfunctions, sleep behavior disorders, depression and fatigue have been described in many PD patients and are probably linked to the degeneration of non-dopaminergic neurons, such as noradrenergic, serotonergic, cholinergic and histaminergic ones [31, 32]. PD is characterized by cytoplasmatic inclusions called Lewy bodies, composed mainly of α -synuclein, but also of neurofilament proteins and ubiquitin. A-synuclein is a 140 amino acids protein important for vesicle trafficking and involved in the control of neurotransmitters release. Its oligomers can assume aberrant conformations, called protofibrils, which gradually become insoluble and aggregate in fibrils, which can also spread from cells to other cells [30, 33, 34] (Figure 4). Even if most α -synuclein is located within neurons, oligodendrocytes inclusions were found in midbrain and basal ganglia [35].

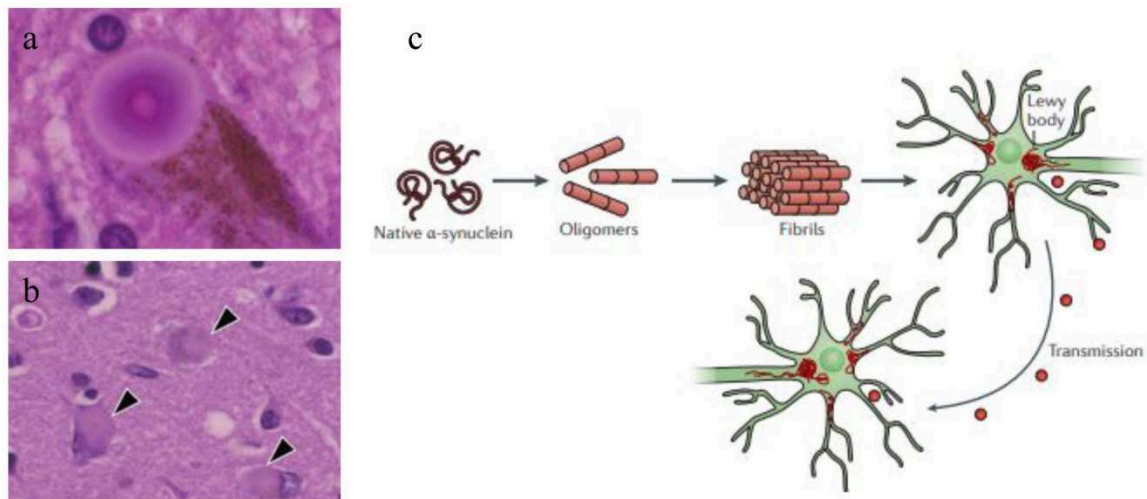


Figure 4. Immunohistochemistry in PD patients and Lewy bodies formation. Lewy bodies are visible through immunohistochemistry in neurons of substantia nigra (a) and of cortex (arrowheads) (b). Lewy bodies are formed of α -synuclein oligomers which aggregate in fibrils and can also spread from cell to cell (c) (modified from Wakabayashi *et al.*, 2013 (a and b) [36] and from Irwin *et al.*, 2013 (c) [37]).

All the theories about PD causes involve α -synuclein aggregation. These include mitochondrial dysfunction, protein clearance systems impairment, oxidative stress and neuroinflammation. Linked to these processes are vesicular transport disruption, microtubular integrity loss, neuronal excitotoxicity, endoplasmic reticulum (ER) impairment and many other events. All these processes lead to cell death through apoptosis or necrosis [38].

As the other NDDs, also PD can manifest in a sporadic form (90%-95% of the cases) or in a familiar one (5%-10% of the cases) with an earlier onset. One of the main genes involved in PD is synuclein alpha (*SNCA*), which encodes for α -synuclein, whereas the most common dominant and recessive mutations occur in leucine rich repeat kinase 2 (*LRRK2*) and Parkin (*PRKN*), respectively. Many other genes have been associated with PD, including PTEN-induced kinase 1 (*PINK1*), glucosylceramidase β (*GBA*), Protein deglycase DJ-1 (*DJ-1*), ATPase cation transporting 13A2 (*ATP13A2*), phospholipase A2 group VI (*PLA2G6*), F-Box Protein 7 (*FBXO7*), GRB10 Interacting GYF Protein 2 (*GIGYF2*) and ubiquitin C-terminal hydrolase L1 (*UCHL1*) [39] (Table II).

Table II. List of PD associated genes (modified from Selvaraj and Piramanayagam, 2019 [39]).

Gene	Protein product	Inheritance
<i>SNCA</i>	α -synuclein	Autosomal dominant
<i>LRRK2</i>	Leucine-rich repeat kinase 2	Autosomal dominant
<i>PRKN</i>	Parkin	Autosomal recessive
<i>PINK1</i>	PTEN-induced putative kinase 1	Autosomal recessive
<i>GBA</i>	β -Glucocerebrosidase	Autosomal dominant
<i>DJ-1</i>	Protein DJ-1	Autosomal recessive
<i>ATP13A2</i>	ATPase 13A2	Autosomal recessive
<i>PLA2G6</i>	Phospholipase A2 Group VI	Autosomal recessive
<i>FBXO7</i>	F-Box protein 7	Autosomal recessive
<i>GIGYF2</i>	GRB10 interacting GYF protein2	Autosomal dominant
<i>UCHL1</i>	Ubiquitin C-Terminal Hydrolase L1	Autosomal dominant

There are only symptomatic therapies for PD, and the most common is treatment with Levodopa, which, since its approval in 1975, has brought to a revolution in PD treatment improving quality of PD patients' lives. Moreover, dopaminergic therapies, such as dopamine agonists, catechol-O-methyltransferase inhibitors and monoamine oxidase B inhibitors, have been approved and have the advantage to address Levodopa shortcomings. Finally, deep brain stimulation has emerged as an alternative for patients who do not respond to medication adjustments [40, 41].

1.1.3 Huntington's Disease

HD is the most common monogenic NDD, with an onset between 30 and 40 years. This disease has a prevalence of 10 per 100,000 people especially between Caucasian, but it was demonstrated that its prevalence varies more than tenfold between different areas, with a lower rate in Eastern population and in South Africa one [42]. Moreover, a recent study analyzed HD diffusion in Italian population, which is characterized by a significant heterogeneity between regions. The Italian prevalence resulted in 3.9/100,000 inhabitants, with a lower rate in a province of Sardinia. Riccò *et al.* (2020) argued that differences found between different regions can be explained by a "founder effect" occurred in the regions with the major prevalence [43].

HD was first described by George Huntington in 1872, who described some American families with choreiform movements associated with psychiatric symptoms [44-46]. This pathology affects central nervous system, especially medium spiny neurons of striatum, causing involuntary movements of face, trunk and limbs, named chorea. However, other symptoms have been reported, such as bradykinesia, dystonia, limb rigidity and cognitive impairment [47].

HD is caused by an autosomal CAG trinucleotide repeat expansion in the *HTT* gene, on chromosome 4. Normal HTT protein is involved in many biological pathways, such as synapses formation, mitochondrial function and axonal transport [47]. *HTT* mutation causes the production of a mutant protein with a longer polyglutamine repeat. People with a protein greater than 39 CAG repeats will develop the pathology, whereas people with a protein between 36 and 39 repeats have a reduced pathology penetrance. Moreover, the age of onset is inversely proportional to the number of repetitions [47, 48]. Being HD a pathology dependent on *HTT* CAG repeats, the major risk factor is CAG repeat length, but also CAG instability, which can lead to gene expansion. Moreover, genetic factors have been identified to play the major role in the progression of HD [49]. It was widely demonstrated that anticipation can occur when gene is passed through paternal line, being male gametes more prone to mutations than female ones [50-52]. Mutant HTT affects transcription factors regulation, protein homeostasis, mitochondrial pathways, alters lysosomal and autophagy functions, affects axonal transport and synaptic plasticity, and causes proteins aggregation. Moreover, it was demonstrated that it causes astrocytes dysfunction and microglia activation [47]. Mutant HTT protein is cleaved into toxic fragments containing the polyQ expansion contributing to neurons death. A recent study demonstrated that inclusions' distribution and density is not correlated with pathology stage, however, infers *HTT* expansion degree [53]. Riguet *et al.* (2021) discovered that in inclusions formation also cytoplasmic and cytoskeletal proteins are involved. Moreover, they found that nuclear and cytoplasmic inclusions show distinct ultrastructural properties and distinct biochemical compositions [54] (Figure 5).

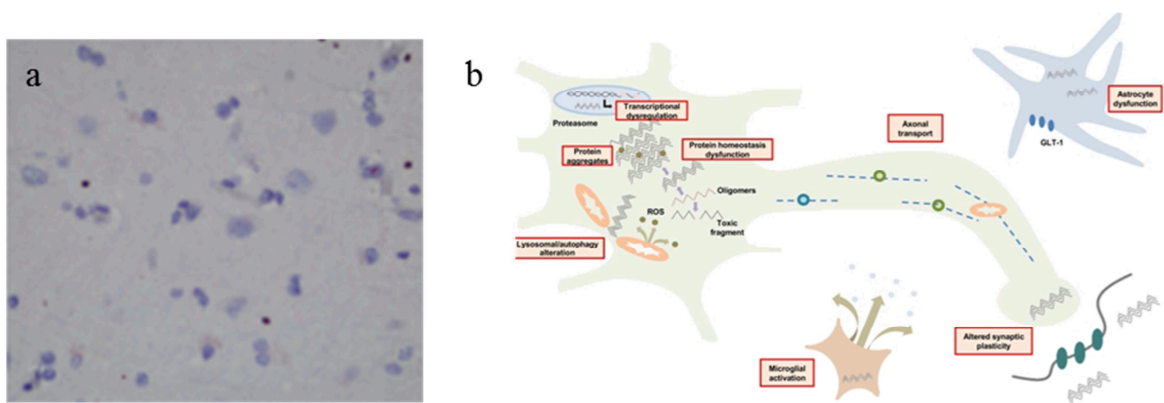


Figure 5. HTT inclusions and pathways affected by mutant HTT. Immunostaining of the prefrontal cortex allows the identification of mutant HTT inclusions (a). Mutations in *HTT* gene affect many biological pathways (b) (modified from Hickman *et al.*, 2022 (a) [53] and from Gatto *et al.*, 2020 (b) [47]).

To date, no effective cures or treatments for pathology modification exist. Tetrabenazine, which prevents dopamine and serotonin absorption, and Deutetrabenazine, a vesicular monoamine transporter 2 inhibitor, have been approved for the treatment of HD associated chorea [55].

1.1.4 Amyotrophic Lateral Sclerosis

ALS, also known as Lou Gehrig's disease, is a rare NDD which affects upper and lower motor neurons (MNs) of cortex, brainstem and spinal cord, leading to muscle atrophy, weakness and spasticity. Death occurs due to paralysis within three to five years after the onset of symptoms [1].

A recent metanalysis study reported that ALS prevalence fluctuates from 1.57 per 100,000 persons to 9.62 per 100,000 persons and the incidence from 0.42 per 100,000 persons-year to 2.76 per 100,000 persons-year. Moreover, higher rates are found in developed regions, probably due to the higher possibility to have an adequate diagnosis and to a more severe population aging, while a decline in ALS incidence was observed in older age group, probably due to under-diagnosis in older patients, who often manifest comorbidities [56]. ALS is characterized by sexual dimorphism with a higher risk for men to develop the disease. Therefore, it was suggested a possible protective role of female hormones, especially estrogen and progesterone [57]. Their protective effects were attributed to a direct influence on muscular and neuronal cells and to a reduction in neuroinflammation [58, 59]. A decreased ALS risk was also associated with the treatment with oral contraceptives [60] while testosterone was associated with a higher risk [61]. Other factors have been associated with ALS, such as older age, ALS family history, body mass index, smoking, virus infections, comorbid conditions, exposition to heavy metals and pesticides and traumatic brain injuries [62, 63]. Moreover, Dickerson *et al.* (2018) found an

association between ALS and specific occupations, such as forestry, agriculture, fishing, hunting and construction works [64]. A relationship between ALS development and air-pollution was also suggested [65]. Recently, a study on 188 ALS patients from northern New England and Ohio identified head trauma, electrical burns and lead exposure as factors with a higher correlation with ALS development [66].

ALS was first described as “sclérose latérale amyotrophique” by Jean-Martin Charcot in 1869, bringing together neurological characteristics which were considered as diverse disorders. “Sclérose latérale” indicates glial cells which replace degenerated MNs leading to the hardening of lateral cortico-spinal tract, while the word “amyotrophique” refers to the atrophy and degeneration of muscles [67]. ALS can be classified based on the site of onset in bulbar or spinal ALS. Bulbar ALS is a more severe form and is characterized by difficult, slow and distorted speech [68]. Moreover, in primary lateral sclerosis, upper MNs are primarily affected, whereas progressive muscle atrophy affects primarily lower MNs [6]. There are several possible cellular mechanisms which might cause ALS, but an exact pathway is still not known. Moreover, genetic and phenotypic variations have been observed between patients and make the understanding of disease mechanism more difficult. Possible mechanisms include RNA metabolism alterations, impairing in protein homeostasis and in DNA repair, excitotoxicity caused by glutamate, oxidative stress, neuroinflammation, mitochondrial dysfunction, defects in nucleocytoplasmic transport, vesicular and axonal transport and oligodendrocytes dysfunction [69]. Moreover, different studies have demonstrated an active role of glial cells in ALS pathology, inasmuch astrocytes and microglia are the major player in neuroinflammatory response, causing an important gliosis effect [70-72].

Insoluble intracellular inclusions, containing SOD1 (about 2% of the cases), TDP-43 (about 97% of the cases) or Fused in Sarcoma (FUS) (about 1% of the cases) proteins, were found in MNs but also in oligodendrocytes and astrocytes [73, 74]. Protein aggregation and the spatiotemporal symptoms spread, have suggested a prion-like propagation, as observed in other NDDs [74]. TDP-43 inclusions are divided in skein-like inclusions and round inclusions, with differences in the formation process. Lewy-body like inclusions, a form of round inclusions, have been also found in a little percentage of sporadic ALS (sALS) cases [75]. Moreover, Bunina bodies, are round eosinophilic inclusions, immunonegative for TDP-43 but immunopositive for transferrin, cystatin C, peripherin and sortilin-related receptor CNS expressed 2. They are considered to originate from Golgi apparatus or rough ER, and often localized in the proximity of skein-like inclusions [75, 76]. Finally, a recent study demonstrated that autophagy is a common

degradation pathway for both Bunina bodies and TDP-43 skein-like inclusions [76] (Figure 6).

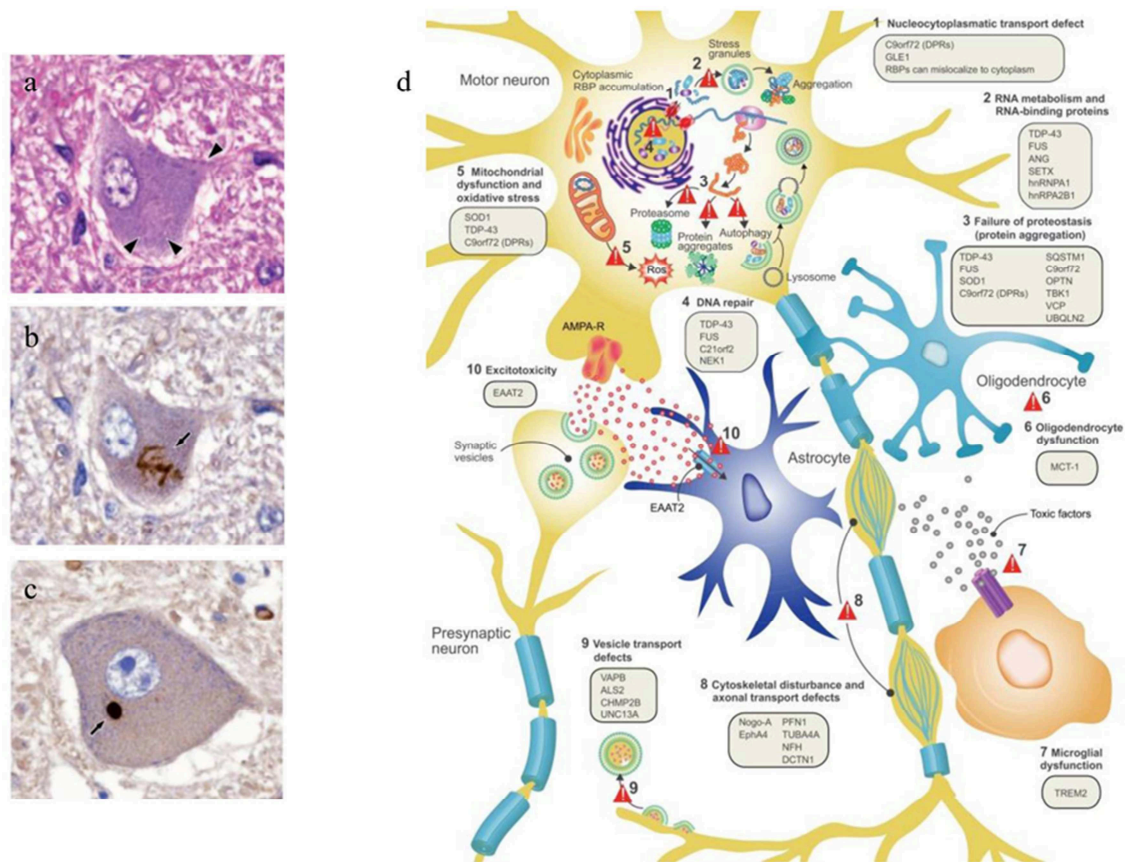


Figure 6. ALS inclusions and pathways affected in ALS pathogenesis. ALS inclusions are Bunina Bodies (arrowheads) (a), skein-like inclusions (b) and round inclusions (arrow) (c). Mutations in ALS associated genes affect different biological pathways (d) (modified from Mori *et al.*, 2019 (a, b and c) [76] and from Van Damme *et al.*, 2017 (d) [77]).

sALS represents 90% of the cases, whereas familial ALS 10% of the patients, with an autosomal dominant inheritance in most of the cases [1]. Both sporadic and familial ALS can be caused by mutations in different genes (Table III).

Table III. List of most common ALS associated genes (modified from Corcia *et al.*, 2017 [78]).

Gene	Protein product	Inheritance
<i>SOD1</i>	Superoxide dismutase 1	Autosomal dominant Autosomal recessive
<i>TARDBP</i>	TAR DNA-binding protein 43	Autosomal dominant
<i>FUS/TSL</i>	Fusion malignant liposarcoma	Autosomal dominant Autosomal recessive
<i>VCP</i>	Valosin-containing protein	Autosomal dominant
<i>C9orf72</i>	Chromosome 9 open reading frame 72	Autosomal dominant
<i>VAPB</i>	Vesicle-associated membrane protein B	Autosomal dominant
<i>OPT</i>	Optineurin	Autosomal dominant Autosomal recessive
<i>UBQLN2</i>	Ubiquilin 2	X-linked
<i>ATXN2</i>	Ataxin-2	Autosomal dominant
<i>ANG</i>	Angiogenin	Autosomal dominant
<i>FIG4</i>	Phosphoinositide 5- phosphatase	Autosomal dominant

The first gene discovered as associated with ALS pathogenesis is *SOD1*, localized on chromosome 21. *SOD1* is a metalloenzyme of 153 aminoacids which converts superoxide free radicals (O_2^-) into hydrogen peroxide (H_2O_2) and O_2 . Mutations in this gene cause oxidative stress, mitochondrial toxicity, inflammation and protein aggregation [1, 79-81].

TARDBP encodes for the protein TDP-43, a RNA-binding protein that regulates different pathways such as transcription, translation and splicing. As already mentioned, TDP-43 is the main component of ALS associated inclusions, inasmuch mutations in *TARDBP* gene cause TDP-43 mislocalization in cytoplasm, its ubiquitination and hyperphosphorylation, its truncation forming toxic fragments and aggregation [1, 82, 83]. Moreover, it was demonstrated that mutations in *VCP* gene, involved in different pathways such as regulation of cell cycles, autophagosome maturation, mitophagic process and the ubiquitin-proteasome system, are often associated with the presence of ubiquitin and TDP-43

inclusions. *VCP* gene shows phenotypic pleiotropy, inasmuch mutations in this gene have been found also in other pathologies such as FTD [6].

As previous described also mutations in *FUS/TSN* gene, which encodes for a 526 amino acid protein involved in DNA repair [6], can cause protein aggregates often positive also to TDP-43, p62 and ubiquitin [84].

Finally, the last gene correlated with ALS pathogenesis, among the most common ones, is *C9orf72*, a gene often associated with autophagy [85, 86]. Expansions of the hexanucleotide GGGGCC over an arbitrary cut-off of 30 repeats can lead to loss or toxic gain of function of the gene [87]. Histopathologically, mutations in *C9orf72* cause TDP-43 inclusions, RNA foci comprising *C9orf72* repeat RNA and dipeptide repeat proteins [1, 88].

Till now, Riluzole, a glutamate antagonist, is the only drug approved for the treatment of ALS in Europe [89].

1.1.5 Modeling in the study of NDDs

In last years, many studies have focused on the pathogenesis of NDDs, but the exact causes of these chronic pathologies are still unknown. Specific diagnostic biomarkers are not available, except in some cases in which the genetic mutation is causative of the disease [12]. Therefore, it is even more important to find a good model to study the aetiopathogenesis of these diseases. Animal models have been the most studied for many years, starting from more simple ones such as nematode worms, baker's yeast and fruit flies to more complex ones such as mice and rats [90-94]. The improvement in molecular techniques has revolutionized the study with animal models. The recombinant DNA cloning consists in the joining of DNA fragments with plasmids and vectors for the amplification in bacterial hosts. This technique allowed, for the first time, beyond the increase of the knowledge about genes, the manipulation and modification of genes and the mass production of proteins [95, 96]. More recently, the possibility to site-direct gene editing have opened the possibility to new transgenic approaches, such as the "knocking-out" of specific genes involved in NDDs, and the "knocking-in" of corrected ones. These techniques have allowed the production of many different animal models [97]. Moreover, the advances in DNA sequencing and in bioinformatic technologies have lead access to the genome profiling of all living organisms [98].

However, animal models could not recapitulate the entire sequence of NDDs events that occur in humans, lacking in neuronal circuit, glial, vascular and immunologic complexity [99].

In vitro models have emerged as fundamental tools for the study of single cells and of their environment [100]. The first step in the use of cell cultures for the study of brain tissue was achieved in 1962 by Bousquet and Meunier. They obtained cells from embryonic rat spinal cord and ganglia and cultured them on a collagen-coated glass, obtaining the first organotypic culture [101]. From this first study organotypic cultures have been obtained from different brain areas, despite the many difficulties in their preparing and maintaining and their huge variability [100].

For this reason, the use of immortalized cell lines has emerged as an alternative to remove the need of tissues as sources [100]. Immortalized cells lines have many advantages such as commercial availability, continuous proliferation, low cost and their easy handling. Moreover, many of them have a human origin [102]. The most used immortalized cell line in the study of NDDs is the human neuroblastoma cell line SH-SY5Y. SH-SY5Y cells show a neurite structure and express immature neuronal markers [103, 104]. These cells can furthermore be differentiated into specific neuronal phenotypes with the use of various reagents. Differentiated SH-SY5Y cells express mature neuronal markers and exhibit elongated neurites and a low proliferation rate. However, they do not have the electrophysiological characteristics of mature neurons. The addition of neurotoxic agents to the cell medium can lead to toxicity in these cells and to their death, mimicking what happens in NDDs [102, 103, 105]. However, immortalized cell lines often present genetic and metabolic modifications when compared to human cells [106]. In this field, it was largely demonstrated that environmental modification methods can represent promising tools to obtain immortalized cell lines for research and clinical use [107]. Human *post-mortem* tissues can also provide important information. However, some limitations include their limited availability, the fact that they can lack of some precious information, and the fact that they do not provide data about disease progression [108].

More recently, the use of stem cell technology has emerged for the substitution of lost neurons, but also for their use as immunomodulators and neuroprotectors. Stem cells are a cellular type presents in living organisms [109] and they are characterized by two main properties, the capacity to self-renew and to differentiate [110, 111]. There are different types of stem cells [112]:

- Totipotent stem cells: represented by early zygote and early blastomeres. They can differentiate into cells of the whole organism, allowing the differentiation of embryo and extra-embryonic structures.

-Pluripotent stem cells: represented by embryonic stem cells (ESCs), which are isolated by the blastocyst and can differentiate into all the embryo tissues except the placenta, and by induced pluripotent stem cells (iPSCs), derived from adult somatic cells.

-Multipotent stem cells: tissue-somatic stem cells which can differentiate only into the cell types of the original tissue.

-Oligopotent stem cells: can differentiate into limited number of cell types.

-Unipotent stem cells: can differentiate into only one cell type.

Beyond the use of stem cells, three-dimensional (3D) cultures have recently raised also for the study of the nervous system [113-115]. It was largely demonstrated that culturing in 3D mimics better the environment and the factors present in the tissue than the traditional two-dimensional (2D) cultures [116-118]. Usually, 3D cultures are classified into non-scaffold, scaffold-based 3D culture systems and hybrid 3D culture systems. In the first system, cells are grown in 3D self-assembled spherical clusters (aggregates or spheroids) without the adding of biomaterials, whereas in scaffold-based 3D cultures cells are seeding or dispersing into a 3D solid or liquid matrix. Moreover, in hybrid 3D culture models, spheroids are incorporated into 3D polymeric scaffolds [108, 118]. Among the 3D technologies, two of the main known are the 3D bioprinting and the organoids 3D technology.

1.2 iPSCs

iPSCs are stem cells obtained from somatic cells with the use of defined pluripotency associated factors. Together with ESCs, they belong to the group of pluripotent stem cells, which means that they can proliferate and differentiate in all the three primary germ layers and to the germ cells that give origin to gametes [119].

The history of pluripotent stem cells began in 1998. In that year, Thomson *et al.* obtained ESCs from the inner cell mass of cultured blastocysts. Obtained ESCs had normal karyotype and expressed the typical markers of primate ESCs. Moreover, they did not express the markers of other early lineages, and, after *in vitro* proliferation, they maintained the potential to form trophoblast and to derivivate the three embryonic germ layers [120].

However, the use of pre-implantation embryos carries with it ethical limitations, since the embryo is destroyed to obtain ESCs. Moreover, the use of cells derived from ESCs differentiation could be a potential problem for immunological rejection after cells transplantation. Donor cells differentiated from ESCs have their own human leukocytes antigen proteins which could induce an immunological response in the recipient's immune

system after transplantation, leading to immune rejection. Furthermore, the use of immunosuppressive drugs, to avoid this effect, could bring to serious side effects [119, 121, 122].

The described issues persuaded in 2006 Takahashi and Yamanaka to search a way to obtain pluripotent stem cells from adults' cells. They supposed that the factors that permit to maintain the ESCs identity could be used to induce pluripotency in somatic cells. They discovered that the expression of four transcription factors (Oct4, Sox2, Klf4 and c-Myc), emerged from a list of 24 candidate-reprogramming factors, and since then called "Yamanaka factors", were sufficient to induce pluripotency in somatic cells. They successfully reprogrammed mouse fibroblasts into iPSCs and a year later they replicated the same experiment with human fibroblast [123, 124]. Moreover, in the same year, the group of Thomson identified a different combination of factors (Oct 3/4, Sox2, Nanog, and Lin 28) which allowed the generation of iPSCs [125]. The low rate of efficacy using the Yamanaka and the Thomson's factors, induced researchers to find molecules which improve the efficacy, also called "enhancers", and molecules which oppose to reprogramming, also called "barriers" [126]. Among them, the long non-coding RNAs LincRoR and Let7 act as "enhancer" and as "barrier", respectively [127, 128].

The reproducibility of the iPSCs reprogramming protocol and its simplicity encouraged many laboratories to improve the reprogramming technique. Over the years, many different delivery methods, to introduce reprogramming factors in the cells, have been developed. Such methods include integrative systems, in which exogenous genetic material is integrated into a host genome, and non-integrative systems, which do not involve an integration of genetic material into the host system [126]. Integrative systems include viral vectors (lentivirus, inducible lentivirus and retrovirus) [123, 125, 129] and non-viral vectors (plasmids and transposons) [130-132]. Non-integrative systems include viral vectors (adenovirus and Sendai virus) [133, 134] and non-viral vectors (episomal DNA vectors, mRNA and proteins) [135-138].

Today, iPSCs are widely used in different fields such as disease modeling, regenerative medicine, in which damaged or degenerated tissues are repaired with the help of iPSCs cultured, differentiated in laboratory and then transplanted, drug discovery and cytotoxicity studies, inasmuch iPSCs cells resemble better the human physiology than animal models [139-141].

Despite the numerous advantages provided by the use of iPSCs, it is important to highlight the genomic instability of this type of cells. iPSCs can, in fact, transform into tumor cells in consequence of oncogenic properties of the reprogramming cocktail or due to the use of

integrating vectors. Moreover, they can undergo variations in gene expression, DNA methylation, somatic mutations etc. [122, 142, 143].

1.2.1 iPSCs modeling

As already mentioned, animal models are commonly used for the study of different pathologies. However, interspecies differences between animals and humans do not allow a complete parallelism between animal disease and human pathology [141]. For example, it was noted that there are not reasonable correlates of human neuropsychiatric disorders in animals [144]. Many problems emerged also in drug trials: Tirizalad, a drug investigated in acute ischemic stroke, was successful in animal studies, but was correlated with increased death risk and dependency in humans [145]. Moreover, the use of patient-derived cells is complicated by the unavailability of extensive sources of some types of cells, such as brain and heart cells [146].

For these reasons, iPSCs, which can be obtained from patients' accessible cells, such as peripheral blood mononuclear cells (PBMCs) and fibroblasts, are seen as optimal alternatives. Furthermore, their self-renewal property is essential to obtain a large quantity of cell types. Finally, iPSCs' use promotes approaches of personalized disease modeling, because of their patients' derivation [141].

One of the first uses of iPSCs in disease modeling is the study of genetic-associated pathologies. iPSCs are derived from mutated patients and compared to the ones of healthy subjects or to isogenic controls. Moreover, they can be differentiated into disease relevant cells for the identification of the disease-related pathways [141]. iPSCs allow the generation of different cell types, which is important in pathologies as ALS or AD, in which there is the involvement of both neuron and glial cells [147]. Gene editing allows the introduction of specific disease-associated mutations. Gene editing on iPSCs have improved with the emergence of original technologies, such as zinc finger nucleases [148], CRISPR Cas9 system [149-151] and transcription activator like effector nucleases [152, 153].

Beyond the use in the study of mutations-associated pathologies, iPSCs are also useful in the modeling of sporadic forms of the diseases, even if it is more difficult due the fact that sporadic diseases are often correlated to environmental factors and due to the line-to-line variations intrinsic of iPSCs [147].

Since iPSCs share the indefinite proliferation capacity, different metabolic signatures and the expression of oncogenic markers like c-Myc with cancer cells, they can be used to develop models of carcinogenesis *in vitro* [154, 155]. Till now, different studies have used

iPSCs in the study of many cancer types, including glioblastoma [156-158], gastrointestinal cancers [159, 160], oral mucosa cancers [161], blood cells cancers [49, 162, 163], liver cancers [164], pancreatic cancers [165], osteosarcoma [166] etc. Moreover, many cancer-prone diseases, such as Li–Fraumeni syndrome [167, 168] and Noonan syndrome [169, 170] have been studied with the use of iPSCs.

iPSCs have been used for the study of cardiomyopathies [171-175] and of bones diseases [176, 177]. More recently, organ-on-chip technology, microfluidic cell culture system on which iPSCs- derived cells are cultured to have controlled and dynamic conditions, have been used for the study of cardiological pathologies [178-180], kidney injuries [181, 182] and progeria syndrome [183, 184]. Finally, iPSCs can be targets for viral infections for viral diseases studies [185].

Advances in xenotransplantation technology have also allowed the development of complex iPSCs-derived human tissues [186].

A challenging in the use of iPSCs, especially in the study of developmental pathologies and NDDs, is the fact that the functional tissue derived from iPSCs differentiation often resembles embryonic and not adult cell types. One possible solution has been the use of aging-associated stressors, which are able to induce cell aging. It has been noted that the same effect could be achieved by the use of ectopically express gene products, such as progerin. Finally, a direct reprogramming from patients' cells into lineage-specific cells does not erase cellular aging [147, 187].

1.2.2 iPSCs in the study of NDDs

The use of iPSCs has emerged as an essential tool for the study of NDDs' mechanisms and treatments, due to their capacity to differentiate into both neural and glial cells [188].

iPSCs in the study of AD

More than 50 studies focused on the use of iPSCs-derived neurons in AD. Many studies have demonstrated that iPSCs-derived neurons reflect the typical AD biomarkers found also *in vivo* [189, 190], including A β accumulation and tau hyperphosphorylation [146, 191-194]. AD patients iPSCs-derived cholinergic neurons showed a major vulnerability to cell death with an increase in cell apoptosis when stimulated with glutamate [195]. Glutamatergic neurons derived from iPSCs of patients carrying *APP*^{V717I} mutation were used to study the alteration in APP subcellular distribution and in β - and γ -secretases cleavage [196]. Moreover, neurons carrying *APP*^{V717I} or *APP*^{K670N/M671L} mutations showed

reduced mitophagy and defects in endocytosis [197]. Oxidative stress was furthermore demonstrated in iPSCs-derived neurons carrying *APP*^{E693A} mutation [198].

Also mutations in *PSEN* have been studied through the use of iPSCs. In 2011, Yagi *et al.* generated for the first time iPSCs carrying *PSEN1*^{A246E} and *PSEN*^{N141I} mutations from fibroblasts. They demonstrated that in these cells A β 42 production is enhanced and that γ -secretase inhibitors reduces both A β 40 and A β 42 [199]. In 2013, Woodruff *et al.* demonstrated that *PSEN1* mutation acts via a gain of function of γ -secretases [200]. Moreover, *PSEN1*^{A246E}, *PSEN1*^{V89L}, and *PSEN1*^{L150P} mutations were correlated with a more sensibility to A β toxicity and to oxidative stress [191, 201]. Thanks to iPSCs modeling, *PSEN* mutations were associated with alterations in autophagic, apoptotic, ubiquitin proteasome, mitophagic and endo-lysosomal pathways [193, 202-204] and with transcriptomic genes deregulation [205].

As regard to sporadic AD, iPSCs-derived neurons from sporadic patients exhibited mitochondrial dysfunctions, oxidative stress, activation of the ER, DNA damage and increase in A β toxicity [191, 195, 206, 207]. Moreover, in 2017 Armijo *et al.* demonstrated that familiar AD iPSCs-derived neurons are more susceptible to A β 1-42 oligomers than the ones from sporadic AD patients and from healthy subjects [201].

Curiously, no study has reported the presence of neurofibrillary tangles, probably due to the fact that iPSC-derived neurons do not achieve the complete maturation [188, 208].

iPSCs were also used to study sporadic AD risk genes, and among them *APOE*. It was demonstrated that iPSCs-derived neurons carrying *APOE4* produce more A β and have higher levels of phosphorylated tau [209, 210]. Furthermore, they exhibited endosome abnormalities and defects in autophagy and mitophagy pathways [197, 207].

Astrocytes are involved in both neurotransmitter recycling and perform metabolic functions [211-213]. AD iPSCs-derived astrocytes exhibited a minor complexity and aberrant marker localization when compared to normal ones [214]. Thanks to single-cell analysis, Liao *et al.* (2016) demonstrated that astrocytes contribute deeply to A β accumulation [215].

Microglia acts as brain immune cells, synapses pruning and in removing protein aggregates such as A β plaques [22, 216, 217]. Genome-Wide Association Studies have allowed the identification of numerous microglia genes associated with a major risk of AD development, such as *CD33*, *HLA-DRB1*, *TREM2*, *INPP5D*, *MS4A64*, *CASS4* and *SPI1* [218]. It was widely demonstrated that, while microglia derived from healthy patients' iPSCs are capable in phagocytosis, in synaptic pruning and in A β uptake [219, 220], microglia derived from iPSCs of sporadic AD patients show alteration in phagocytic

pathway and in cytokines release [221]. Moreover, *APOE4* microglia showed alteration in gene expression indicating a pro-inflammatory phenotype [209]. iPSCs-derived microglia carrying *TREM2*^{W50C} and *TREM2*^{T66M} mutations manifested reduced viability and impaired phagocytosis [221, 222].

Finally, oligodendrocytes are glial cells involved in the generation of myelin sheath and in the regulation of metabolic waste of the brain [223]. AD patients and animal models manifest white matter loss and oligodendrocytes dysfunction [224, 225]. Oligodendrocytes have been successfully obtained from iPSCs, but, till now, their role as AD models have not been studied [190].

iPSCs in the study of PD

In PD, dopaminergic neurons of the *pars compact* of the substantia nigra are lost and for this reason iPSCs are usually differentiated in this type of cells [30]. iPSCs-derived dopaminergic neurons have been used to study both sporadic and familiar PD. To date, more than 300 mutated iPSC-derived neuronal lines have been generated [226]. In 2011, Seibler *et al.* demonstrated that *PINK1* mutated iPSCs-derived neurons have defects in autophagic clearance of mitochondria due to a block in *PRKN* translocation [227]. Moreover, it was demonstrated that neurons derived from PD patients carrying *PINK* or *PRKN* mutations show α -synuclein increase and mitochondrial susceptibility [228-230], whereas neurons with *GBA* mutations showed a decrease in activity and in dopamine levels [231], ER stress, autophagic/lysosomal dysfunction [232] and α -synuclein aggregation [233]. Furthermore, in 2018 Schöndorf *et al.* demonstrated that *GBA* mutations cause alterations in mitochondrial morphology and functions associated with an increase in reactive oxygen species levels [233]. In 2017, Son *et al.* investigated *LRRK2* mutations, differentiating mutated iPSCs in neuronal and intestinal phenotypes, inasmuch *LRRK2* mutations are involved in both PD and gastrointestinal diseases. They demonstrated that mutations in this gene cause changes in gene expression of intestinal cells, providing a good model for the study of PD pathophysiology [234]. Moreover, *LRRK2* mutations in iPSCs-derived dopaminergic neurons have been associated with mitochondrial deficits [235, 236], α -synuclein aggregation [237, 238] and impaired endocytosis [239, 240]. As regard to *SNCA* gene the most commonly alterations studied through iPSCs are A53T and multiplication of *SNCA* [241]. In *SNCA* mutated iPSCs-derived neurons one of the most common alterations is mitochondrial impairment [242-244]. Moreover, different studies have demonstrated that *SNCA* iPSCs-derived neurons have increased sensitivity to mitochondrial oxidative stress induced by toxins [245-247]. *SNCA* iPSCs-derived neurons

have higher levels of α -synuclein phosphorylation and aggregates formation [248-250]. Misfolded protein aggregates result in ER stress and in the activation of the unfolded protein response in *SNCA*-mutated iPSCs-derived neurons [251, 252]. *SNCA* mutations were also associated with an increase in cell death, with deregulation in dopaminergic differentiation genes and with impairment in neurite growth and length [250, 251, 253]. Finally, *DJ-1* mutations were associated with oxidative stress and lysosomal dysfunctions [254-256].

Despite the different mutations, iPSCs derived from PD patients exhibit α -synuclein accumulation, oxidative stress damage, mitochondrial damage and anomalies in proteolytic systems [244, 257-259]. Recently, it has been demonstrated that iPSCs are a good tool also to characterize early-onset PD, in which genetic mutations are not well characterized, showing an increase in soluble form of α -synuclein protein, decrease in lysosomal proteins and accumulation of phosphoprotein kinase C_{α} [260].

As regard to cell transplantation, many studies have demonstrated that iPSCs-derived dopaminergic neurons can be used to rescue motor deficits in animal models [261-263].

Although most of the studies investigated neuronal functions, there are many evidence on the role of glial cells in PD. However, studies using iPSCs-derived glial cells remain rare. It was demonstrated that in co-cultures of iPSCs-derived neurons and astrocytes, astrocytes have a protective effect rescuing differentiation deficits and mitochondrial dysfunctions associated with treatment with rotenone and potassium cyanide [264]. Moreover, di Domenico *et al.* (2018) demonstrated that the co-culturing of iPSCs-derived dopaminergic neurons with astrocytes mutated in *LRRK2* exert a neurodegenerative phenotype, while the co-culture with healthy oligodendrocytes does not have this effect [238]. More recently, Azevedo *et al.* (2022) obtained oligodendrocytes from patients iPSCs revealing an impairment in their maturation [265] and Badanjak's group (2021) demonstrated that PD iPSCs-derived microglia have an upregulation of interleukin 10 and interleukin 1 B genes and a higher phagocytic capacity [266].

iPSCs in the study of HD

Many animal models have been developed for the study of HD. However, most therapies effective in animals have failed in human trials. The majority of mouse models have a greater number of CAG repeats than humans. For this reason, iPSCs are now even more important for the study of this pathology [267-269].

HD iPSCs were first obtained in 2008 by Park *et al.* They generated iPSCs with 72 CAG repeats and differentiated them in neural precursors [270]. Moreover, in 2010 Zhang *et al.*

obtained iPSCs with the same repeat number from fibroblasts and differentiated them in striatal mature neurons, which exhibited mitochondrial dysfunctions and a decrease in glutamate transporters and BDNF transcription [271]. An *et al.* (2012) reported the target correction of CAG repeat in HD iPSCs, providing for the first time an unbiased isogenic control for mutated iPSCs [272]. Different studies demonstrated that HD-iPSCs show dysregulation in various cellular processes, β -catenin phosphorylation, SOD1 accumulation, dysregulation in p53 expression, enhancing in lysosomal activity and many transcriptional changes related to genes involved in cell cycles, axonal and neuronal development, and cell signaling [273-275]. Liu *et al.* (2017) investigated proteasomal activity and the expression of FOXO proteins in HD, inasmuch FOXO proteins have a role in metabolism, longevity, cellular proliferation and stress tolerance. They found that HD-iPSCs express higher levels of FOXO1 and FOXO4, and consequently a higher proteasomal activity [276]. Moreover, it was demonstrated an increase in HD-iPSCs calcium store-operated channels [277].

In the field of transplantations, in 2013 Delli Carri *et al.* induced iPSCs to become GABAergic neurons, which were transplanted into rats. Transplanted neurons matured and led to restoration of motorial behavior [278]. It was also proved that iPSCs transplantation could improve memory and functional recovery [279]. In 2017, Al-Gharaibeh *et al.* demonstrated that corrected HD iPSCs-derived neural stem cells transplanted into a HD murine model maintain the ability to survive and differentiate in neurons, improving locomotor functions [280]. Moreover, it was proved that iPSCs-derived neuron progenitor cells transplanted into adult mouse brain differentiate in mature neurons [281].

Finally, glial cells' role in HD has been widely studied. Merienne *et al.* (2019) reported that in HD mouse models upregulated genes were most of all represented in glial cells. HD iPSCs-derived astrocytes have been studied since 2012 [282]. In that year, Joupperi *et al.* observed vacuolation in these cells, pathological hallmark already seen in patients' lymphocytes [281]. Moreover, astrocytes' abnormalities were found in *post mortem* brain tissues and animal models of HD [283]. More recently, astrocytes were obtained from HD monkey iPSCs. Astrocytes showed HTT aggregates, impairment in glutamate clearance and in mitochondrial functions, resistance to oxidative stress and abnormal electrophysiological properties [284]. In the same year, Garcia *et al.* confirmed the electrophysiological abnormalities in HD iPSCs-derived astrocytes and demonstrated that HD astrocytes in co-culture reduce the support on neurons' maturation and to their protection [285].

iPSCs in the study of ALS

Finally, multiple groups have derived MNs from ALS affected patients iPSCs, finding different phenotypes [286]. In 2014, Kiskinis *et al.* reprogrammed fibroblasts from patients carrying *SOD1*^{A4V} mutation. MNs derived from obtained iPSCs had the trend to undergo apoptosis, manifested mitochondrial dysfunctions, reduced soma size and shorter processes. Moreover, authors found, through transcriptomic analyses, alteration in genes involved in the organization of cytoskeleton [287]. In the same year, Chen *et al.* reported neurofilaments inclusions and neurite degeneration in iPSCs-derived MNs carrying *SOD1*^{D90A} mutation and defects in mitochondrial function and structures in MNs with A4V mutation [288]. More recently, Park *et al.* (2016) demonstrated that *SOD1*^{G93A} MNs derived from mouse iPSCs manifest pathological hallmarks, such as SOD1 aggregates and reduced cell variability [289].

Other studies have reported the involvement of unfolded protein response system and of ER stress in *SOD1*, *C9orf72* and *FUS* mutations [290]. Pathological aggregations have been also found in iPSCs-derived MNs *SOD1*^{L144FVX} and *SOD1*^{N139K} [291, 292].

As regard to *C9orf72* mutations, different studies have shown the presence of RNA foci in mutant iPSCs-derive neurons, inasmuch RNA-binding proteins, including FUS and TDP-43, can interact with GGGGCC RNA repeat [293-296]. More recently, it was demonstrated that poly (GR) binds to mitochondrial proteins, leading to impairment in mitochondria activity and to oxidative stress [297]. Moreover, mutated iPSCs-derived neurons showed stress cytotoxicity and misregulation in genes involved in neural differentiation, cell adhesion and synaptic transmission [293, 294]. Many studies have also described reduction in cell viability and increased susceptibility to excitotoxicity, probably due to the elevated presence of Ca²⁺ permeable glutamatergic ionotropic receptors [295, 296, 298].

TDP-43 is the main constituent of protein aggregates found in ALS patients. TDP-43 aggregation is a constant characteristic found in iPSCs-derived MNs carrying different *TARDBP* mutations [299-301]. Many studies have also reported that iPSCs-derived neurons carrying *TDP-43*^{A90V} and *TDP-43*^{M337V} manifest vulnerability to stress-induced cytotoxicity and misregulation in RNA metabolism and cytoskeleton functions [302, 303]. Moreover, both Egawa *et al.* (2012) and Fujimori *et al.* (2018) reported a reduced neurite length [301, 302].

As regard to *FUS* mutations, FUS aggregations were found in iPSCs-derived MNs by different studies [304-306]. De Santis *et al.* (2017) revealed, thanks to the use of mutated and isogenic iPSCs, that *FUS* mutations deregulate several microRNAs involved in MNs survival and apoptotic factors [307]. Oxidative stress increased cellular death, impaired

DNA-damage response and reduced neurite length. Axonal swelling and an alteration in mitochondrial potential were found [305, 308-310].

In general, iPSCs-derived MNs have allowed the modeling of axonal abnormalities and the axonal growth impairment typical of ALS pathogenesis [301, 311, 312].

As for other NDDs, the role of glial cells has been studied with the use of iPSCs also in ALS. It was demonstrated that astrocytes derived from iPSCs of ALS patients mutated in *TARDBP* exhibit cell defects such as TDP-43 proteinopathy and cell death [313]. sALS iPSCs-derived astrocytes transplanted into the spinal cord of mice induced the reduction of neurons number and of the inhibitory inputs to MNs, ubiquitin aggregation and neurofilaments disorganization [314]. Furthermore, co-cultures of MNs and astrocytes led to the accumulation of cytoplasmic TDP-43, oxidative stress, ER stress, mitochondrial impairment and synaptic degeneration [315].

Other studies have pointed out that transplantation of iPSC-derived glia-rich progenitors, which subsequently gave rise to astrocytes, in spinal cord of ALS mice and rats, improved motor functions and life, acting on the activation of protein kinase B signals [316, 317].

Microglia has also been identified as a player in ALS progression, inasmuch it is activated in the area of MNs degeneration and contributing to their death [318].

Different studies have suggested that transplantation of iPSCs-derived glial precursor cells may ameliorate the environment around MNs. However, till now, there is still much to do for efficient employment of iPSCs-derived microglia and astrocytes for treatment of ALS [319].

1.3 3D bioprinting

Additive manufacturing (AM), which consists in joining materials to make objects from computer-aided design (CAD) model data, has emerged in last years in many industry sectors. One of the most known implementations of AM is 3D printing, which is now used in many industrial sectors, such as automobile, aviation, electronics etc. Moreover, it is now used in biomedical sciences to develop surgical equipment, medical devices, implants and prosthetics. 3D bioprinting is an extended application of AM emerged from 3D printing, allowing the integration of living cells with printing biomaterials called bioinks to mimic the natural cellular architecture [320, 321].

1.3.1 History of 3D bioprinting

Modern bioprinting is founded on the so-called “biofabrication”, first defined by US Defence Advanced Research Projects Agency as “the use of biological materials and mechanisms for construction”, to indicate methods to create 3D structures which mimic biological growth mechanisms [322]. This term is now used in the fields of Tissue Engineering (TE) and of Regenerative Medicine (RM) indicating the application of strategies of 3D manufacturing for the positioning and manipulation of cells. Bioprinting is for this reason defined as a process of biofabrication used in TE and RM (Figure 7) [322].

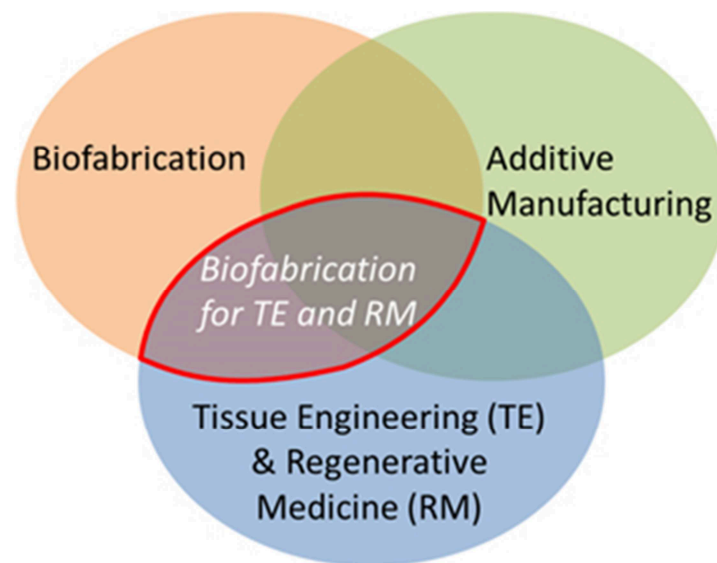


Figure 7. Venn diagram of the relations between Biofabrication, AM and the fields of TE and RM (modified from Groll *et al.*, 2016 [322]).

The term “bioprinting” was firstly used in 2004 in the title “Workshop on Bioprinting, Biopatterning and Bioassembly”. In a subsequently report, Mironov, Reis and Derby declared: “For the purpose of the meeting, bioprinting was defined as: the use of material transfer process for patterning and assembling biologically relevant materials-molecules, cells, tissues, and biodegradable biomaterials- with a prescribed organization to accomplish one or more biological functions” [323]. However, only in 2010 the term bioprinting was first defined by Guillemot *et al.* as “the use of computer-aided transfer processes for patterning and assembling living and non-living materials with a prescribed 2D or 3D organization in order to produce bioengineered structures serving in regenerative medicine, pharmacokinetic and basic cell biology studies” [324, 325].

As regard to practical use of bioprinting, the first step was the creation of the first polymeric scaffold for the cultivation of cells in 1974 by Robert Langer [326]. In 1988, Klebe *et al.* used a standard inkjet printer to deposit cells by a micropositioning method

called cytoscribing [327]. In 1999, the first laser bioprinter was used to deposit living cells [328], whereas in 2002, Landers *et al.* developed the first extrusion-based bioprinting technology, later commercialized as “3D Bioplotter” [329]. Moreover, the year later Wilson and Boland developed the first inkjet bioprinter. The system allowed the creation of a bioink consisting of a mixture of cells, medium and serum [330]. From that year, further improvements in bioink and printing systems have been done. The first 3D bioprinting company was founded in 2007 from Organovo Company, with the aim to develop and commercialize models of tissues for disease modeling and drug screening. Many other companies emerged in the field of bioprinter systems, such as the RegenHu and the Envision-Tec, which developed bioprinters for research uses. Moreover, the increase demand of cost effective bioprinters, opened to a new industry of low-cost and affordable bioprinters. Simultaneously, new companies for the development of printable bioinks emerged. Among them, the most predominant are CELLINK, Allevi and Advanced Biomatrix [331].

1.3.2 Bioprinting bioplotters

The principal components of bioprinting are:

- Bioplotter: allows the deposition of the bioink in a software-controlled mode.
- Bioink: compound on which cells are seeded for their printing. It can be formed of different biomaterials.

All bioplotters require some characteristics: high throughput, high resolution, nontoxicity, the capacity to dispense many biomaterials with different viscosity simultaneously and the capacity to maintain cell viability [332].

Bioplotters share common elements:

- Robotic motion system that moves in x-y-z axis
- Nozzles
- Sterile chamber with a laminar flow
- Software which allows the control of speed and pressure [332].

There are four different bioprinting techniques and consequently four bioplotters types (Figure 8):

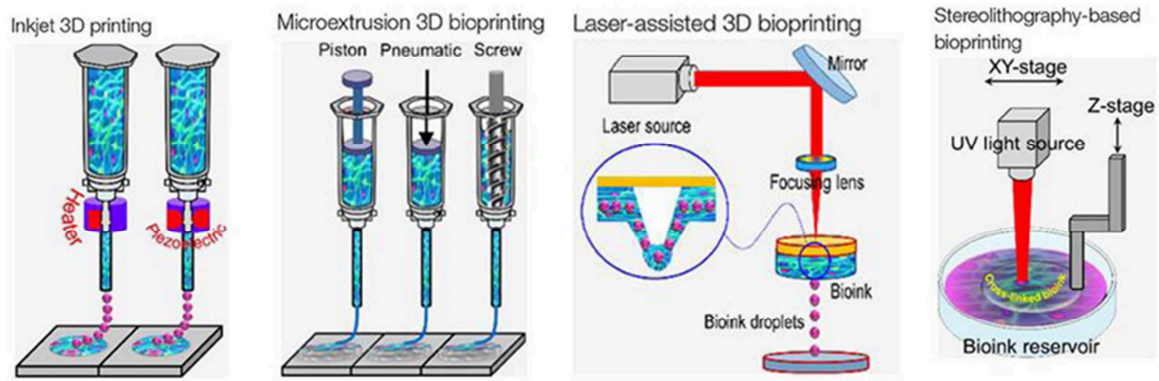


Figure 8. Different bioprinting techniques (modified from Ramadan *et al.*, 2020 [321]).

1. InkJet-based bioprinting

It originates from the classical 2D paper-based office inkjet printers. It is a non-contact technique in which bioink droplets are deposited on a substrate using nozzles and replicating the CAD model. This technique is divided into two different subtypes: thermal and piezoelectric [321]. Thermal inkjet bioprinter is composed by an ink chamber with nozzles and heating elements. A current pulse is applied to the heat element generating a bubble that forces the bioink out. The high temperature can denaturize hydrogel materials, but the heating time is so short that does not allow the detriment of biocomponents [333, 334]. Piezoelectric technique uses an electric charge which is applied to piezocrystals. The induced vibration of piezocrystals forces the bioink out [334].

The advantages of this technique include the low cost, high speed and the possibility to obtain heterogeneous tissue structures with high cell viability. However, inkjet bioprinting requires bioinks with a low viscosity [321, 335].

2. Microextrusion bioprinting

It is a technique in which bioinks are dispensed through a nozzle applying a pressure and using a pneumatic or mechanical (piston or screw-driven) system, under the control of a robotic arm. It allows the extrusion of filaments instead of a single droplet.

With the pneumatic system the testing of various bioinks with different viscosity is possible by the control of pressure and gating time. In the piston-driven deposition there is a direct control over the flow whereas in the screw-driven deposition a higher pressure is allowed with the possibility to have a major spatial control [321, 334, 335].

This technique is the best method for the creation of large-scale constructs using bioinks of different viscosity [336]. However, this technique allows low resolution and can lead to a loss of cell variability and of tissue structure, due the high extrusion pressure [337]. An example of extrusion bioplotter is the Cellink BioX (Cellink AB) (Figure 9).



Figure 9. Cellink BioX bioplotter (<https://www.cellink.com/product/bio-x/>)

3. Laser-based bioprinting

It is a non-contact and nozzle-free technique to precisely deposit bioink onto a substrate. Cells are excited by the energy of a laser to create a precise pattern. The laser pulse is passed through a ribbon coated with an absorbing layer. It allows the transfer of hydrogel droplets from a donor slide to a receiving substrate. There are two types of laser-based direct writing, the laser-induced forward transfer and the matrix-assisted pulsed laser evaporation direct writing, which uses a lower pulse [321, 334, 335].

Laser-based bioprinting offers many advantages: cells can be seeded on high density with single-cell resolution and high speed [321, 324, 338]. Moreover, a real-time monitoring is allowed [339]. However, it was demonstrated that excessive temperature generated by the laser may affect cells viability [340].

4. Stereolithography-based bioprinting

In this technique a UV light or a laser are directed onto a photopolymerizable liquid polymer, allowing the cross-linking of the polymer itself. Many polymerizations' cycles are repeated and, in every cycle, a thin layer is created till the build of the 3D structure in a layer-by-layer mode.

This technology allows a high resolution and the absence of shear stress. However, UV exposure can cause cell damage [321, 335, 341].

1.3.3 Bioinks

As previously explained, a bioink can be composed of different biomaterials which are printed with cells. A first definition for biomaterials was “non-vital materials used in medical devices, intended to interact with biological systems”, as they were used only for medical devices [342, 343]. Today, biomaterials are considered as “any material, except to drugs, that interacts with living tissues and performs a particular function without causing adverse effects” [342-344].

A good biomaterial must have some characteristics: biocompatibility, high quality physical and chemical properties and biodegradability. It must be biofunctional, bioinert and sterilizable [342] [345] [346]. As regard to toxicity, there are many *in vitro* and *in vivo* tests used to analyze the potential effects on cells [342]. Furthermore, a biomaterial is chosen on the base of chemical, physical and biological properties [343, 345].

We can distinguish two printing methods: scaffold-based bioprinting and scaffold-free bioprinting. In the first method there is the use of an exogenous scaffold as a mechanical support during the development of the tissue. It is a more economic method, and it requires a lower density of cells. However, the scaffold can reduce cell-to-cell interactions and it can be subjected to degradation [335, 347]. In scaffold-free bioprinting cells are leaved to generate adjacent tissue architecture on their own. Multicellular building blocks, such as tissue strands, pellets and spheroids, are printed, fuse together and release autonomously the extracellular matrix (ECM) components. This method reduces the toxicity on the cells, lacking an exogenous material, increases cell-to-cell interactions and reduces the post-bioprinting maturation. However, advantages include the need of a higher cell number, the low scalability and the lack of mechanical integrity [335, 347]. A synergic approach associates microscaffolds and spheroid or other hybrid constructs. For example, in the “lockeyballs” technique”, microscaffolds help spheroids to fuse together and provide mechanical integrity [335, 348]. Depending on the choice of the scaffold the selected biomaterials could vary.

Till now, many are the biomaterials developed, but the ones with the best characteristics are hydrogels, carbon-based nanomaterials, nanofibers, nanoparticles and self-assembling peptides.

Hydrogels

Hydrogels are the most used biomaterials thanks to their capacity to provide a hydrated and supportive environment for cells [343, 349]. They are composed of natural or synthetic polymers. Natural polymers include alginate, collagen, cellulose, fibrin and chitosan and

and β -D-mannuronate (M). The G-blocks are the only ones that are involved in the gelation with divalent cation [360] (Figure 11).

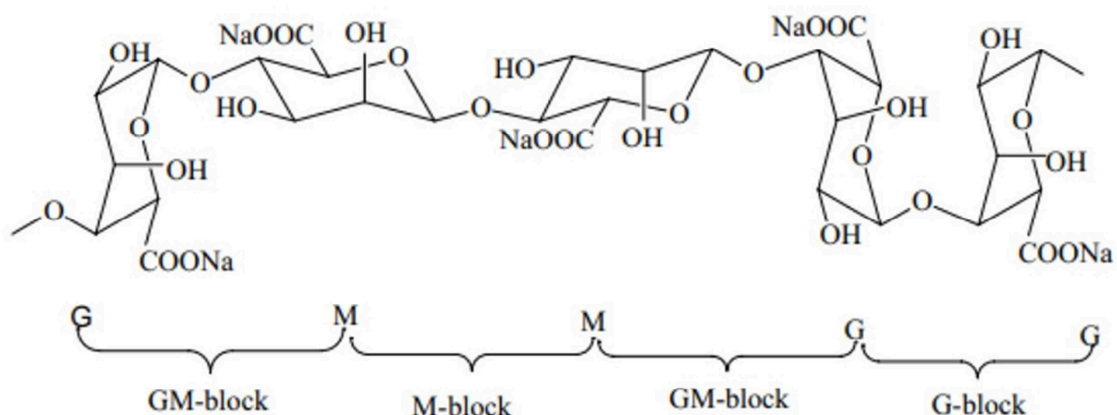


Figure 11. Chemical structure of alginate (modified from Sahoo and Biswal, 2021 [360]).

Sodium alginate (SA) is one of the most used hydrogels. It allows a good biocompatibility and can be crosslinked using divalent cations such as Ca^{2+} [358, 360].

Cellulose is the most abundant natural polymer prevalently obtained from wood. It is an organic polysaccharide with a molecular structure similar to starch with several β (1 \rightarrow 4) linked D-glucose units [357] (Figure 12) .

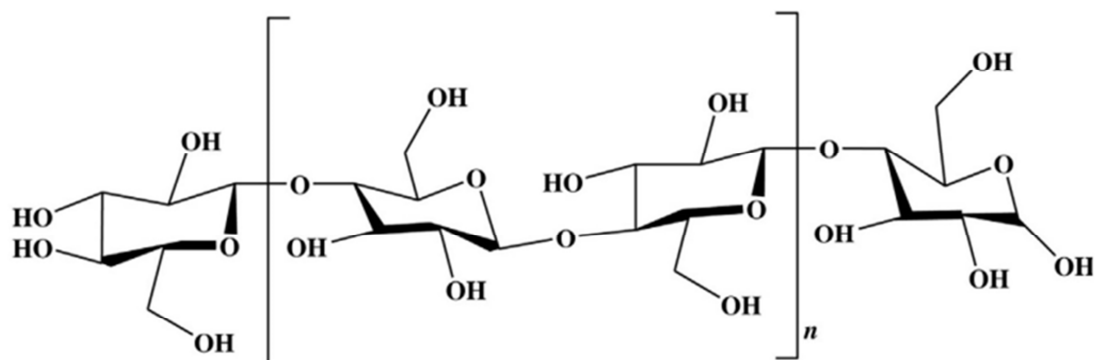


Figure 12. Chemical structure of cellulose (modified from Deskmukh *et al.*, 2017 [357]).

Cellulose has optimal properties for 3D bioprinting, such as biocompatibility, biodegradability, and high mechanical strength [357, 361]. For its qualities, cellulose-based hydrogels have found applications in different fields, including biomedical applications, drug delivery, wound healing and TE [362].

Carbon-based biomaterials

Neural cells have the property to generate and transmit electrical stimuli, and, for this reason, it is even more important to perform electroactive biomaterials to model brain tissue. Carbon-based biomaterials, such as graphene and carbon nanotubes, are emerging as important tools in the study of brain for their chemical, physical and mechanical properties [343, 363]. Carbon nanotubes have demonstrated promising results in nerve regeneration studies, despite safety issues, such as the production of free radicals and the consequently oxidative stress, and the induction of DNA damage and inflammation [364]. Graphene is composed of a layer of carbon atoms arranged in a hexagonal honeycomb lattice. It should be coated with pre-coating layer for the improving of cell-substrate adhesion. Graphene-composed nanomaterials have emerged for multiple applications such as biosensors, nanocarriers and neural degeneration [363].

Nanofibers

Nanofibers were developed for the reproduction of structures such as axons, collagen fibers and capillaries [343, 365]. Electrospinning is the most applied technique to produce nanofibers of different polymeric materials. The advantages of this system are the simplicity, the reproducibility, and its capacity to produce fibers with different diameters and topographical features [366-369]. Moreover, electrospun nanofibers have a large surface-area/volume ratio which promotes cell attachment, functionalization and molecule loading [368].

Many different materials, both synthetic and natural, but also composite polymers, have been used to produce nanofibrous scaffolds [369]. Cellulose nanofibrils have been widely studied in the field of 3D bioprinting, because the high surface area and the uniform particle size distribution allow a stable self-assembled structure. They can be divided in three categories based on the source and processing: microfibrillated cellulose, nanocrystalline cellulose, and bacterial nanocellulose [370, 371].

Nowadays, nanofiber scaffolds are largely used in musculoskeletal TE, vascular TE, skin TE, neural TE, and for the controlled delivery of drugs, DNA and proteins [372].

Nanoparticles

Nanoparticles were developed for drug delivery through the brain blood barrier, because this structure interferes with the passage of drugs to the brain. For this reason, it is even more important to develop a system which allows drugs to achieve therapeutics levels. Nanoparticles possess many important characteristics: small size and vast surface and

surface-volume ratios. Additionally, they contrast the low solubility, the short circulation half-life and the unstable bioactivity of molecules [373, 374].

They can be composed of various materials, including metals, ceramics, oxides, polymers and salts. In particular, silica nanoparticles are preferred because of their porous structure and their good biocompatibility [343, 373].

Self-assembling peptides

Self-assembling peptides are monomers or amino acid sequences that form autonomously nanostructures, including tubes, rods and sheets. They can differ for their biochemical and physicochemical activities on the base of morphology, size and accessibility [343, 375]. Moreover, the self-assembling can be controlled acting on pH, ionic strength, enzymatic triggers and temperature. Self-assembling peptides hydrogels are applied in many different fields, from TE to drug deliver. They share many characteristics, including a good biocompatibility and excellent bioactive properties [376]. The advantages of self-assembling peptides structures are the ease of synthesis and their biocompatibility [377, 378]. Different types of self-assembling peptides can be enumerated, including dipeptides, the simplest blocks, which can assemble in nanoscale structures. Moreover, the surfactant-like peptides are characterized by an amphiphilic structure which minimizes the contact with water, to form more complex structures such as nanotubes and nanovesicles [375, 379].

1.3.4 3D bioprinting in the study of NDDs

From the development of the first polymeric scaffold in 1974, advances have been done in the use of 3D bioprinting in many different fields [320, 380]. It is now widely used in the creation of skin [381-383], cardiac [384, 385], cartilage [386, 387], bone tissues etc. [388-391].

Human nervous system is more complex than other tissues and for this reason the use of 3D bioprinting in this field is emerged later [392]. Studies have focused on the encapsulation of neural cells into hydrogels. In 2013, Owens *et al.* used mouse bone marrow stem cells and Schwann cells for the printing of a synthetic nerve graft [393]. The year later, Lorber printed rat retinal ganglion cells and glia cells, demonstrating that the printing does not affect viability and growth [394]. In 2016, Gu *et al.* encapsulated neural stem cells (NSCs) into a hydrogel composed of agarose, alginate and carboxymethyl-chitosan [395]. More recently, Abelseth *et al.* (2019) encapsulated neural aggregates

derived from human iPSCs and demonstrated that cells maintain a good viability after printing and neurite extension during the culture for 41 days [396].

In the study of AD, yet in 2011 Altunbas *et al.* studied self-assembling peptides hydrogels as vehicles for the release of curcumin compounds [397]. More recently, it was demonstrated that the use of hydrogels composed of gellan gum and xanthan gum for the delivery of Resveratrol improves its effect compared to orally administered resveratrol suspension [398].

Also nanoparticles have been studied for drug delivery. It was demonstrated that the delivery of both acetylcholinesterase inhibitors and curcumin, using this type of biomaterials, has positive effects in amnesic mice increasing [399, 400]. Moreover, nanoparticles were used for the delivery of epigallocatechin-3-gallate, antioxidants and vaccines against A β peptides and pathological phosphorylated tau protein [401, 402]. Finally, self-assembling peptides have been used for the delivery of the neuroprotective peptide humanin in an AD mice and vaccines [403, 404]. Furthermore, it was demonstrated that amyloid nanofibrils are a good tool for the development of stem cells and have a positive influence on neurogenesis [405, 406].

Gelatin-based hydrogels were also used for dopamine delivery in the treatment of PD. It was demonstrated that both dextran/GEL and chitosan/GEL hydrogels allow a good drug delivery leading to a motor improvement in PD mice [407, 408]. Hydrogels were also used for neurotrophic factors delivery [409, 410], whereas nanoparticles were used for the subadministration of Levodopa, with the abolishing of adverse effects such as dyskinesia, and of dopamine agonists, such as bromocriptine, and NADPH oxidase inhibitors [411-413]. Additionally, Abdelrahman *et al.* (2022) encapsulated dopaminergic neurons in self-assembling tetrapeptide scaffolds and demonstrated that cells maintain the electrophysiological activity and that the co-culture with endothelial cells promotes neurite outgrowth and a network formation [414].

Compared to AD and PD, few authors have worked on the use of 3D bioprinting for the study of ALS and HD. As regard to HD, studies have focused principally on the use of microcarries, such as microspheres, for the delivery of neurotrophic factors [415-417]. More recently, it was demonstrated that the administration of selenium nanoparticles in a HD models of *Caenorhabditis elegans* reduces neuronal death, improves behavioral symptoms and protects animals in stress conditions [418].

Moreover, in 2018, Adil *et al.* generated striatal progenitors within a PNIPAAm-PEG hydrogel. They demonstrated that the transplantation of obtained striatal progenitors slows disease progression, increases the survival and improves the coordination in HD mice.

Moreover, the progenitors developed medium spiny neurons phenotype and formed synapses [419].

As regard to ALS, in 2018, Osaky *et al.* obtained a motor unit model using a collagen/matrigel microfluidic device, co-culturing MN spheroids and 3D muscle fiber bundles [420]. Different studies have demonstrated that hydrogels can be used as delivery vehicles and imaging probes. In a recent study, glial progenitor cells embedded in hyaluronic acid-based hydrogel were transplanted in spinal cords of ALS pigs and dogs. The follow-up magnetic resonance imaging and histopathology demonstrated successful placement of cells and the safety of the procedure [421]. Furthermore, adipose stem cells encapsulated in methacrylated gellan gum/hyaluronic acid hydrogel stay *in vitro* for 14 days and are visible as hyperintense signal in magnetic resonance imaging for 24 h after transplantation [422, 423]. Moreover, nanoparticles were used for the delivery of Riluzole and of the antioxidant cerium oxide [424-426].

1.4 Organoids

The term “organoid” have been used several times in the history of biomedicine [427]. In the 20th century, it was used as a synonym of “organelle” [428], whereas in oncology it was widely used for indicate a tumor with a complex tissue-like structure [429, 430]. The modern definition of organoids refers to cells that self-organize in a 3D environment and differentiate into functional cell types, recapitulating the *in vivo* organ [427, 431]. They can be derived from tissues’ fragments, ESCs, iPSCs and neonatal or adult stem cells [432, 433]. Organoids are a useful and versatile tool for the study of brain development and functions, but also for disease modeling [434].

1.4.1 History of organoids

A first step in the field of organoids was achieved in 1910. In this year, Wilson *et al.* demonstrated that if a sponge is dissociated into cells and its cells are then reaggreated, they recognize to form a new sponge [435]. This first experiment demonstrated that adult cells have the potential to specify a multicellular structure [427]. Subsequently, other authors used the same methods of disaggregation and reaggregation on more complex animals, confirming that some types of cells carry information to reorganize themselves [427, 436, 437]. It was demonstrated that type specificity is stronger than species specificity, allowing the formation of aggregates formed of cells of different species but with a similar histological phenotype [438]. Moreover, different studies have demonstrated

the importance of inductive signals in the formation of self-organizing structures [439, 440] and have focused on the forces involved in cells' adhesion [441-443].

At the beginning of their use, organoids were obtained only from animals' tissues and most of all for the study of embryogenesis [427]. Furthermore, human organoids production depended on tissues' fragments from fetuses, children or adults. Epidermal organoids were obtained from human keratinocytes [444], simple neuronal organoids from brain cells [445-447] and thymocytes aggregates were used for the study of T-cells [448].

A great improvement in the use of organoids was made by the development of human ESCs and iPSCs, leading to the possibility to use patients' cells as starting materials for organoids [427]. First studies used ESCs and iPSCs derived from mice for the production of gut organoids [449] cardiac organoids [450] and liver organoids [451]. Moreover, in 2009, Sato *et al.* obtained intestinal organoids starting from adult intestinal stem cells. Stem cells self-organized in Matrigel and differentiated into crypt-villus structures [452]. A first example of brain organoids was made in 2008 by Eiraku *et al.* They generated cerebral cortex tissue allowing the self-aggregation of mouse ESCs. The obtained cortical neurons were functional, transplantable and formed connections. Moreover, the cortical tissue was composed of four distinct zones (ventricular, early and late cortical-plate and Cajal-Retzius cell zones) [453]. With the advances in ESCs and iPSCs technologies and with the increase of their availability, human organoids have become even more studied and are now used for the study of many different tissues and pathologies [427].

1.4.2 Organoids' development methods

It is widely accepted that there are different ways to develop organoids. First of all, as already mentioned, organoids can be derived from differentiated cells or from stem cells. Moreover, they can be developed using printed or shaped scaffold or only cells [427]. The simplest organoids are those obtained from single cells, such the ones obtained by Sato *et al.* in 2009, starting from single intestinal stem cells [427, 452]. Obviously, this type of organoids does not resemble the complexity of the full organ. To obtain more realistic organoids often more than one type of stem cells are required although scaffolds may or may not be needed [427].

There are four methods used for organoids' generation (Figure 13):

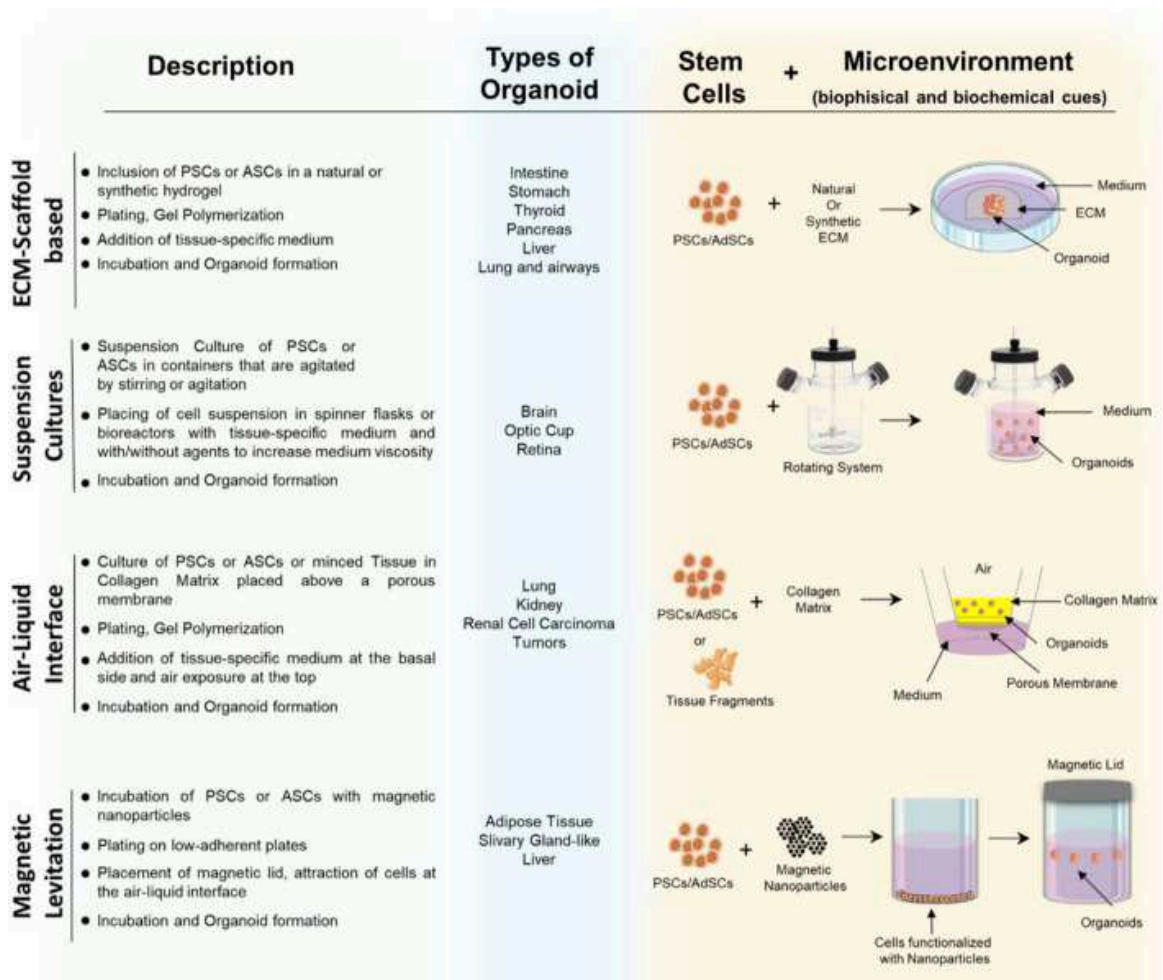


Figure 13. Different methods for organoids development (modified from Tortorella *et al.*, 2022 [454])

1. ECM-scaffold based

This technique consists in the generation of organoids by including stem cells in an environment that mimics ECM and it is the most common method used. In the years many different authors have developed organoids using this method for the study of different tissues [455-458].

Scaffolds consist in natural or synthetic hydrogels, as the ones already mentioned for 3D bioprinting, and bioactive chemical and biological molecules [454, 459]. In a recent study it was demonstrated that the presence of soft hydrogels accelerates the differentiation of organoids from iPSCs [460]. However, the stiffness of hydrogels can influence cell migration and spreading [461]. Hydrogels are supplemented with ECM components and the most used is the basement membrane extract, derived from murine sarcoma. The basement membrane extract is often named as Matrigel, Cultrex, or Geltrex [461, 462]. Matrigel has demonstrated many advantages in terms of biomimicry to native ECM, of cytocompatibility and of enhancing of cell biological events such as cell adhesion and differentiation [462, 463]. However, it was demonstrated that it has limited utility for

organoids for the development of drugs and for regenerative medicine, because of its tumor-derived origin, its high cost, its safety issues and the batch-to-batch variation. For these reasons, different groups have searched substitutes for Matrigel [464, 465]. Recently, Kim *et al.* (2022) have developed gastrointestinal tissue-derived ECM hydrogels, which have been proven suitability for the modeling of gastrointestinal diseases, for drug development and for tissue regeneration [465].

2. Suspension cultures

As already mentioned, ECM supports introduce biological variability and lead to high costs and xenogenic problems [465]. Suspension cultures technique consists in the culture of cells in floating conditions with the use of spinner flasks or rotating bioreactors (Figure 14).

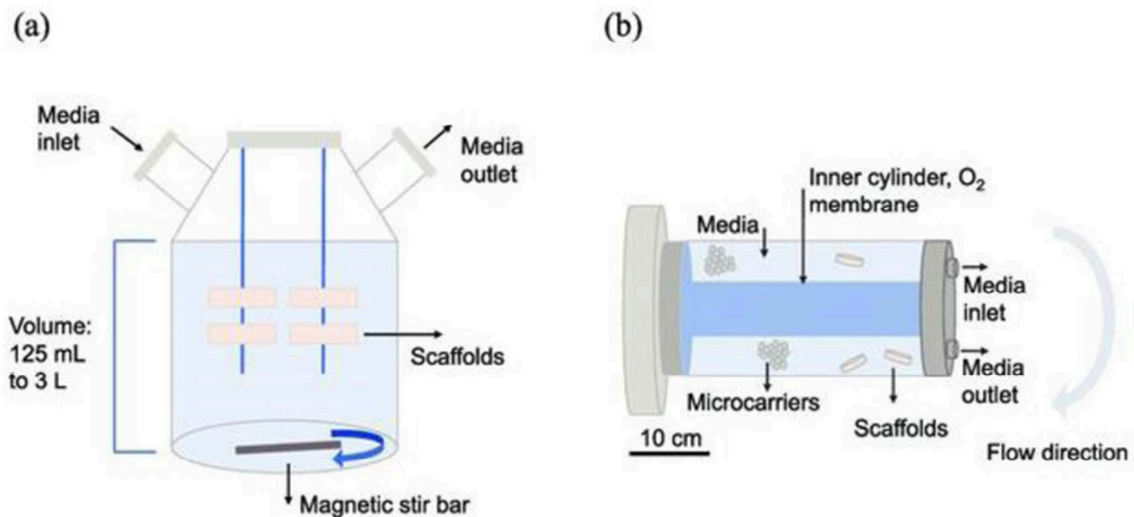


Figure 14. Spinner flask (a) and rotating bioreactor (b) (modified from Burova *et al.*, 2019 [466]).

With this method rotating cell culture systems are generated [459, 467, 468]. The advantages of this type of cultures include a major reproducibility and standardization, and a larger scale-up. Both bioreactors and spinner flasks are used to have controlled microenvironments in order to regulate cell growth, their differentiation and organoids development [469]. Spinner flasks are widely used for their availability and their easy setup [470, 471]. There are three main classes of bioreactors: cell expansion bioreactors, used principally for cell expansion, TE bioreactors, which allow the development of large 3D grafts overcoming the limitation in oxygen and nutrients diffusion, and organ-on-chip systems, which use a small amount of cells grown in micrometer-scaled wells [469]. Although the many advantages of both bioreactors and spinner flasks they shear different

issues, including the high volumes and the difficult to manufactures [472]. Alternatively, cells can be cultured in low-adherent or hydrophilic treated cell culture plates in floating conditions using an orbital shaker, with a more simple, less expensive and with a high throughput method [459].

3. Air–liquid interface (ALI)

In this method, stem cells are exposed to the culture medium, on one side, and to the air on the other side. In ALI cultures, cells are first grown on a permeable filter, and, once they reach confluence, media is removed from one side of the filter leaving the cells exposed to air [473]. ALI method allows the oxygenation of cells and the supply of the nutrients [473-475]. On the other side, one of the major limitations is that ALI cultures are a static culture system and do not allow to study dynamic processes [473].

4. Magnetic levitation

Cells are tagged with magnetic nanoparticles and then exposed to a magnetic field. That allows their levitation to the liquid–air interface and their aggregation, the generation of components of the ECM and subsequently multilayered tissue [459, 476, 477]. This system does not require scaffolds and substrates, leaving cells to produce their own bio-matrices, avoiding xenotopic problems. Moreover, it allows the replication of necrotic and hypoxic regions [459, 477].

Finally, organoids can also be generated by unguided or guided methods. In unguided methods stem cells aggregates and differentiate without the need of external factors and *stimuli*, whereas in guided methods there is the supplementation of external factors, such as morphogens [478].

1.4.3 Organoids’ applications

Organoids represent, as 3D bioprinting, an improvement in the generation of model systems. Cell types resemble better and are grown in similar conditions to those of the human body [479, 480]. For these reasons, the organoids systems have emerged in different fields [480]. Their uses include (Figure 15):

- Basic research: such as studies on the developmental processes, on cell-to-cell interactions, on external *stimuli* and on cell homeostasis.
- Biobanking: patient cells are used to generate organoids and stored as future sources
- Disease modeling: organoids are used to understand the mechanisms of human diseases

- Precision medicine: patient-derived organoids are used to test drugs and as sources for regenerative medicine.

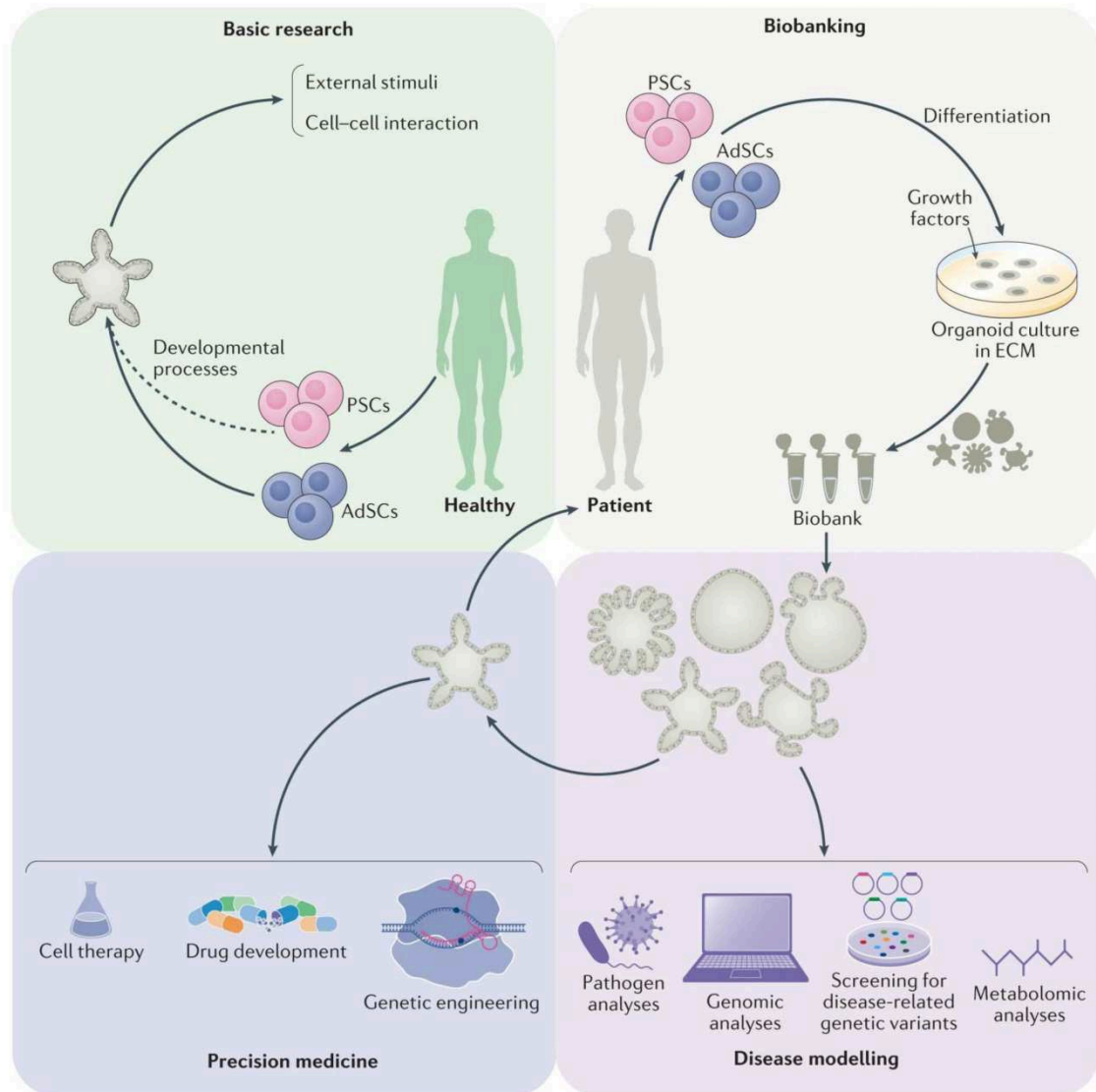


Figure 15. Different applications of human organoids (modified from Kim *et al.*, 2020 [480]).

As regard to disease modeling, human organoids have many advantages compared to animal models. First of all, as already described for iPSCs and their use in 3D bioprinting, organoids allow a more accurate representation of human tissue. Deriving from human cells they do not manifest the differences, both physiological and pathological, of animal models. Moreover, they provide a larger quantity of material, are more accessible and allow faster and more powerful outcomes [480-482].

Organoids are now widely used for the modeling of different systems, especially for those systems which imply different cells' types. In heart modeling cardiomyocytes are the main cells of interest. These cells are not easily available and for this reason the main method for their derivation is stem cells differentiation. Moreover, organoids allow the study of other

cardiac cells, including cardiac fibroblasts and endothelial cells [483]. Cardiac organoids have been developed both as spheroids and by combining cells with ECM [484-487]. Furthermore, in 2017 Devarasetty *et al.* demonstrated that cardiomyocytes organoids maintain the capacity to beat as organ's cells [488].

Similar to cardiac systems, liver has one main cells type, the hepatocytes, and other secondary cells, such as hepatic stellate cells, Kupffer cells and hepatic endothelial cells. In 2013, Takebe *et al.* obtained organoids from iPSCs-derived hepatic cells within Matrigel. They demonstrated that obtained organoids have a gene expression similar to liver buds, form vasculature after transplantation and show functions similar to liver [489]. Moreover, in 2019 Wu *et al.* produced hepatobiliary organoids for the study of hepatogenesis [490, 491]. Liver organoids have been also studied for response to *stimuli*. In a spheroidal model it was demonstrated that cells response to toxins such as lead and mercury. This characteristic enables the use of organoids for environmental studies and for drug discovery [492].

Brain includes different types of cells: neurons, microglia, oligodendrocytes, astrocytes, pericytes and endothelial cells. One of the first experiments with brain organoids allowed the formation of multiple brain structures starting from iPSCs included in Matrigel, without the need of growth factors [493]. The most complete organoids model is a model developed in 2018 by Nzou *et al.*, which includes all the main cell types and a blood brain barrier formed of endothelial cells and pericytes [494].

Human lungs are exposed to many airborne dangers, including pollutants and smoke, and for this reasons respiratory diseases are considered one of the major cause of human morbidity [495]. Lung can be separated into airway models, including Clara, goblet, and ciliated cells and alveolus models, which cells are primary type I pneumocytes [496]. Rock *et al.* (2009) were one of the first groups to develop a tracheospheroid model [497]. Since then, many progresses have been done and now lung organoids possess different compartments and alveolar structures [498, 499]. Moreover, thanks to the ALI method, organoids models for airway studies, with structures which resemble bronchioles, and for the modeling of lung injuries, have been developed [500-502].

Finally, organoids have been used to study the gastrointestinal tract, which includes enteroendocrine cells, enterocytes and Paneth cells. One of the most complete organoids models was obtained in 2011 by Sato and *et al.* They differentiated stem cells in Matrigel and were able to obtain all the major cells of the gut [503]. Moreover, gut organoids were obtained for the modeling of bacterial infections to study the epithelial barrier properties, of nutrient transportation and absorption [504-507].

With the improvement of organoids protocols, this 3D technique is now used for the modeling of other body compartments. Organoids are now used for the study of kidney, reproductive organs, retina, thyroid etc. [508-513].

Despite the organ studied, organoids systems intrinsically have a big degree of complexity and variability, which is often difficult to understand, and for these reasons there is the need of standardized protocols [480].

Recent studies have focused on the development of vascular organoids systems. Progresses have been done with blood vessel organoids and cases of vascularization have been reported after transplantation [489, 514, 515]. However, vascularization of organoids remains a great obstacle [480, 516].

Finally, one of the most promising approaches is the incorporation of organoids into microfluidic devices, in the so-called organ-on-chip. It allows the simulation of fluid flows for the exchange of nutrients and molecules [496, 517]. This approach leads to different advantages in the study of tumors, allowing the mimicking of the metastasis and angiogenesis potential [518-520]. Moreover, it is fundamental for the study of organs which are constantly exposed to air and nutrients flows, such as lung and gastrointestinal tract [517, 521, 522].

1.4.4 Organoids in the study of NDDs

As described for 3D bioprinting, also organoids have been widely used for the study and the modeling of NDDs [434, 523].

Organoids in the study of AD

AD is characterized by A β deposits. For many years, iPSCs derived neurons have been used for the study of the deposition process. However, in these studies, A β were secreted in the media and removed during cell feeding, not allowing the formation of deposits. On the contrary, organoids provide a 3D environment for the formation of aggregates [196, 523-525]. One of the first 3D models of AD was obtained by Choi *et al.* in 2014. They embedded neuronal precursor cell lines overexpressing *APP* in Matrigel and obtained a 3D model which showed A β deposition [526]. Further studies using *APP* and *PSEN* mutated organoids confirmed these findings [525, 527-529]. Moreover, Gonzalez *et al.* (2018) demonstrated that AD organoids develop structures similar to amyloid plaques and NFTs [528].

In 2018, Lin *et al.* studied the role of microglia in protein aggregates clearance. They co-cultured familiar AD derived forebrain organoids with *APOE* mutated microglia cells

generated from iPSCs. They showed that microglia carrying *APOE4* variant have longer processes and a minor capacity to uptake A β aggregates. Moreover, neurons of organoids near mutated microglia exhibited a higher level of tau and A β phosphorylation [209].

Organoids have been also used for assessing the effect of pharmacological substances in the treatment of AD. The first attempt was done in 2014 using β - or γ -secretase inhibitors. Authors demonstrated that these inhibitors attenuated the pathology [526]. More recently, Raja *et al.* (2016) demonstrated that the use of γ -secretase inhibitor compound E or BACE-1 β -secretase inhibitor reverses amyloid and tau pathology [527].

Organoids in the study of PD

A first characterization of midbrain organoids was done in 2016 by Jo *et al.*, and it was found that they have a great potential for the study of PD onset and characteristics [530]. It was demonstrated that these organoids are composed of dopaminergic neurons and that organoids carrying *LRRK2*^{G2019S} mutation have a decreased numbers of this type of cells [531]. Recently, Jarazo *et al.* (2022) obtained midbrain organoids from iPSCs of *PINK1* mutated patients. They found that proteins involved in cell cycle, differentiation, autophagy, mitophagy and apoptosis are differentially expressed in mutated organoids when compared to control ones and that they manifest also firing abnormalities. They demonstrated that the treatment with the compound 2-hydroxypropyl- β -cyclodextrin resolves the impairment in mitophagy and in dopaminergic differentiation [532]. Finally, it was found that midbrain organoids are composed of dopaminergic neurons interspersed with astrocytes as in the physiologic brain environment, with potential therapeutic outcomes for transplantation [533].

Organoids in the study of HD

To date, only few studies have focused on organoids for the study of HD and ALS.

In 2018, Conforti *et al.* developed cerebral organoids, containing predominantly cortical neurons, using iPSCs from HD patients, finding that the mutation of *HTT* leads to aberrant neuronal maturation and to cell disorganization. Moreover, they proved that the downregulation of mutated *HTT* is efficient in rescuing the defects in neuroectodermal development [534]. Similarly, Zhang *et al.* (2020) demonstrated that HD organoids have a smaller size than isogenic control ones. Mutated organoids had a lower number of neuroepithelial structures, an aberrant development and cells' disorganization. Moreover, they treated organoids with KU60019, an antagonist of the Ataxia-telangiectasia mutated kinase, involved in HD pathology, finding an improvement in the development of neuroepithelial progenitors [535]. More recently, Metzger *et al.* (2022) developed HD

organoids for drug screening and tested the bromodomain inhibitors. They found that these drugs revert the phenotypes induced by the *HTT* mutation [536]. In the same year, it was found an accumulation of the heat shock transcription factor 1 in the mitochondria of HD organoids, and that the peptide inhibitor DH1 successfully abolishes mitochondrial abnormalities [537].

It should be noted that these studies have a limit in the fact that they describe only cortical neurons, and not medium spiny neurons, which are the cells more involved in HD [534]. In the future, the generation of forebrain organoids will improve the study of HD allowing to study the hypothesis of a BDNF deficit in HD [538, 539]. Moreover, microfluidic devices could improve the study the cortico-striatal network. In this sense, in 2018 Virlogeux *et al.* reconstructed a HD corticostriatal network with on-a-chip approach, demonstrating presynaptic defects in HD cells [540].

Organoids in the study of ALS

The study of ALS is intrinsically correlated with the study of neuromuscular junctions. In 2018, Osaki *et al.*, using the organ-on-chip system, studied the characteristics of ALS iPSCs-MNs, such as the speed and the length of neurite elongation, and tested the effects of rapamycin and bosutinib [420]. In 2020, Martins *et al.* used iPSCs derived axial stem cells to generate spinal cord neurons and skeletal muscle cells which generated spontaneously neuromuscular organoids [541]. More recently, Pereira *et al.* (2021) generated sensorimotor organoids containing functional neuromuscular junctions, finding that ALS organoids show impairment of the neuromuscular junctions [542].

Organoids were also used for the study of ALS specific mutations. In 2021, Szebényi *et al.* demonstrated that ALI-generated organoids derived from ALS/FTD patients' iPSCs and carrying *C9orf72* expansion, show aberrations at astroglia and neuron levels, such as DNA damage and alterations of the autophagy signaling [543]. More recently, organoids were used to study TDP-43 ALS. Proteins extracts of TDP-43 ALS postmortem spinal cord were injected into iPSCs-derived cerebral organoids, demonstrating that the injection induces the formation of TDP-43 pathology with a spreading process into the cerebral organoids. Moreover, the injection causes astrogliosis, cellular apoptosis and DNA damage [544].

2. AIM

NDDs are a wide group of neurological debilitating disorders which are becoming prevalent because of the increasing average age of the population [1]. Many studies have focused on modeling and drug discovery of these pathologies; however, until now, only symptomatic treatments are available. Furthermore, animal models are not able to summarize all the characteristics of these diseases, whereas 2D cell cultures are not adequate for the study of cell-to-cell and cell-to-environment interactions [99]. In last years, 3D cells cultures are emerging as new promising models for the study of the aetiopathogenesis of different disease, but there is still much to do in the field of NDDs. Two of the most diffuse 3D techniques are 3D Bioprinting and organoids [118].

Aim of this study was to investigate the use of these two new techniques as promising tools for the study of ALS.

We obtained iPSCs from PBMCs of a healthy subject and a sALS patient and differentiated them into NSCs. Control (CTRL) and sALS NSCs were then used for hydrogel inclusion and 3D printing and for the generation of organoids.

In the first part of this work, we focused on 3D bioprinting technique and we characterized two types of hydrogels. The first hydrogel was a homemade bioink composed of SA and GEL, compounds which were previously demonstrated to allow growth and cells development [358, 359]. We tested different SA and GEL concentrations and printing temperatures to assess best printability conditions. Moreover, we evaluated different sterilization methods. We then developed a 3D printing protocol for extrusion-based bioprinting. NSCs were included and printed in the 6% SA-4% GEL hydrogel and differentiated firstly into MNs progenitors (MNPs) and finally into MNs using a protocol set up by our group. Every step of differentiation was characterized for cells viability and proliferation, while confocal microscopy was performed to analyze the typical markers of each differentiation step. Moreover, we evaluated hydrogel for the capacity to allow the maintenance of the electrophysiological characteristics of included cells. NSC34 cells were included and printed in the hydrogel and tested for their ability to produce action potentials. In parallel we assessed a commercialized hydrogel, Cellink Bioink, composed of cellulose nanofibrils and alginate. As for homemade hydrogel, we performed mechanical assays, testing moisture, swelling and porosity. We then included and printed NSCs in the hydrogel, which were differentiated into MNPs and MNs. As for 6% SA-4% GEL hydrogel, we tested each differentiation step for cell viability and we performed immunofluorescence (IF) analysis for differentiation markers. Moreover, the high quality of RNA obtained from the constructs, allowed us to perform a RT-qPCR to have a

quantitative analysis of markers expression. Finally, we analyzed the electrophysiological characteristics of included NSC34.

In the second part of this work, we assessed a protocol for MNs organoids (MNOs) formation. NSCs from healthy and sALS iPSCs were cultured in floating conditions and differentiated into MNOs. We firstly performed some morphological analysis, evaluating organoids area during the differentiation protocol and the roundness of both CTRL and sALS mature MNOs. We then characterized MNOs for the expression of Nestin, marker of undifferentiated cells, GFAP and TUBB3 as markers of glial and neurons cells respectively, ISL1 and HB9 as markers of MNs. Finally, we performed bulk RNA-seq on 2D cultured MNs and on MNOs, obtained from both CTRL and sALS NSCs. We evaluated the number of deregulated genes (DE) and obtained volcano plots, PCA graphic and heatmaps of DE genes. We then analyzed common DE genes between sALS 2D cultured MNs and MNOs and identified the cell types in the two groups. Finally, we analyzed the cellular categories of the DE genes in the two groups and validated some of the most significant DE ECM-related genes found in MNOs transcriptomic analysis.

3. MATERIAL AND METHODS

3.1 PBMCs reprogramming and iPSCs differentiation

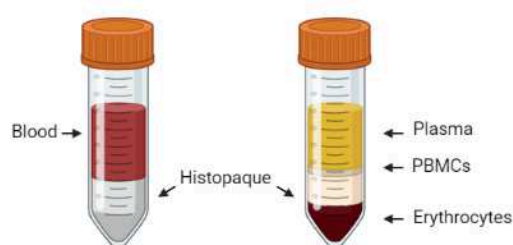
Patients Enrolment

PBMCs were isolated from a healthy CTRL and a sALS patient. The sALS patient was diagnosed at the IRCCS Mondino Foundation (Pavia, Italy) and tested for genetic mutations with Next Generation Sequencing (NGS) as described in Filosto *et al.*, 2018 [545]. The CTRL subject was recruited at IRCCS Policlinico S.Matteo Foundation (Pavia, Italy) and was interviewed on personal health history to avoid pathologies.

The study design was examined by the IRBs of the enrolling Institutions and all the participants signed the informed consensus.

PBMCs isolation

Total blood was obtained from the CTRL subject and the sALS patient and conserved into Ethylenediaminetetraacetic acid tubes to avoid coagulation. PBMCs isolation was performed in sterile environment within 24 h after the blood collection using Ficoll-Histopaque®-1077 (Sigma-Aldrich, USA) and following manufacturer's instructions. An equal volume of blood was added to an equal volume of Histopaque and then centrifuged in order to separate PBMCs from plasma and erythrocytes (Figure 16). Isolated PBMCs' layer was then mixed with 1X PBS (Sigma-Aldrich, USA) and further centrifuged for a complete separation from plasma. Cells viability was determined by Trypan Blue Exclusion Test (Sigma-Aldrich, USA) using the TC20™ Automated Cell Counter (Bio-Rad, USA). PBMCs were preserved in Fetal Bovine Serum (Euroclone, Italy) and 10% dimethyl sulfoxide (Sigma-Aldrich, USA) and placed at -80°C in a container which provides a slow rate of cooling. After 24 h cells were stored in liquid nitrogen.



Created in BioRender.com 

Figure 16. Separation of PBMCs. PBMCs are separated from plasma and erythrocytes by centrifugation (created with Biorender.com).

PBMCs reprogramming

PBMCs reprogramming was performed following a protocol already set up by our group [546].

5×10^5 cells were suspended in a PBMCs medium composed of StemPro™-34 + SCF 100 ng/mL, FLT-3 100 ng/mL, IL-3 20 ng/mL and IL-6 20 ng/mL in a 24 well-plate. After 4 days cells were transduced with virus obtained from CytoTune®-iPS 2.0 Sendai Reprogramming Kit (ThermoFisher Scientific, USA) using the following formula:

$$\text{Volume } (\mu\text{L}) = \frac{\text{MOI (CIU/cell)} \cdot \text{n. of cells}}{\text{titer of virus (CIU/mL)} \cdot 10^{-3}(\text{mL}/\mu\text{L})}$$

MOI: virus-dependent number. KOS=5, hc-Myc=5, hKlf4=3

Titer of virus: lot-dependent number

The medium was replaced after 24 h with fresh complete PBMCs medium to remove the reprogramming vectors. Cells were plated on a vitronectin-coated culture dish and cultured 7 days in complete StemPro™-34 medium (ThermoFisher Scientific, USA).

The medium was then changed to Essential 8™ Medium (ThermoFisher Scientific, USA) until iPSCs colonies formation. iPSCs colonies were manually picked and plated on vitronectin-coated well and splitted using 0.5 mM Ethylenediaminetetraacetic acid (Euroclone, Italy) for 3 passages. Cells were finally collected and cryopreserved in Essential 8™ Medium and 10% dimethyl sulfoxide (Figure 17).

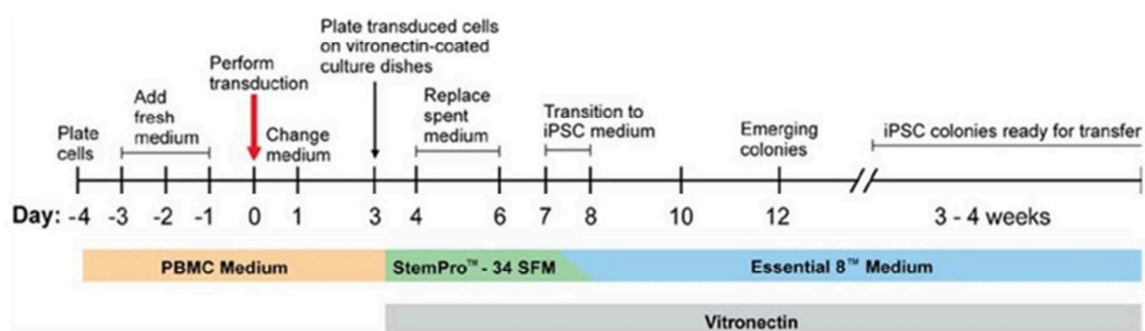


Figure 17. PBMCs reprogramming protocol.

https://tools.thermofisher.com/content/sfs/manuals/cytotune_ips_2_0_sendai_reprog_kit_man.pdf

iPSCs differentiation into NSCs

iPSCs obtained from the CTRL subject and the sALS patient were differentiated into NSCs in 2D. iPSCs were grown on vitronectin and when they reached 60-70% of confluence the medium was changed with the NSCs Differentiation Medium composed of Neurobasal 2X (ThermoFisher Scientific, USA) and Neural Induction Supplement 2X (ThermoFisher Scientific Inc., USA). Cells were cultured in this medium for 7 days for the complete differentiation into NSCs and at day 8 the medium was changed with the Expansion Medium composed of Neurobasal 2X, Advanced DMEM/F12 2X (ThermoFisher Scientific, USA) and Neural Induction Supplement 50X.

NSCs differentiation in 2D

NSCs were differentiated first into MNPs and then into MNs, as depicted in figure 18.

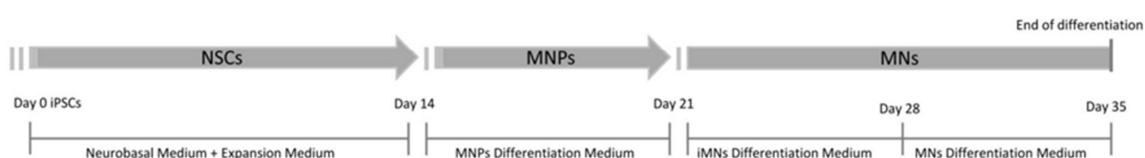


Figure 18. NSCs differentiation protocol (modified from Scarian *et al.*, 2022 [547]).

NSCs were cultured for 7 days with MNPs Differentiation Medium composed of Neurobasal 2X, Advanced DMEM/F12 2X, Neural induction supplement 50X, 0.1 μ M Retinoic Acid (RA) (Sigma-Aldrich, USA) and 0.5 μ M Purmorphamine (ThermoFisher Scientific, USA) for the formation of MNPs. MNPs were then differentiated into immature MNs (iMNs) within 7 days, in suspension condition, in a medium composed of Neurobasal 2X, Advanced DMEM/F12 2X, 0.5 μ M RA, 0.1 μ M Purmorphamine, 10ng/mL GDNF (ThermoFisher Scientific, USA), 10ng/mL IGF (ThermoFisher Scientific, USA) and 10ng/mL BDNF (ThermoFisher Scientific, USA). iMNs were finally plated on vitronectin and induced to mature into MNs with the addition of 0.1 μ M Compound E (Santa Cruz Biotechnology, USA) for 7 days, as previously described [548].

Immunofluorescence analysis

IF analysis was performed at each stage of differentiation process. 2D cultured cells were fixed in 4% paraformaldehyde (ThermoFisher Scientific, USA) and blocked in 5 % Normal Goat Serum (ThermoFisher Scientific, USA) and 0.1 % tween (Sigma-Aldrich, USA). Cells were then incubated in primary antibody at 4°C overnight (Table IV). Nestin is an intermediated filament protein of cytoskeleton, expressed during cells development [549, 550]; SOX2 is a transcription factor involved in self-renewal maintenance [551,

552]; SOX1 is a transcription factor expressed during neurogenesis [553, 554]; PAX6 is a transcription factor expressed during embryonic development [555]. MNPs were marked for Olig2 which is involved in the differentiation of MNs and oligodendrocytes [556] and PAX6 [555], which is also present in NSCs. Finally, MNs were marked for TUBB3, a marker involved in axon guidance and maintenance [557, 558] and ChAT involved in the biosynthesis of acetylcholine [559].

After washes in cold 1X PBS, cells were incubated in secondary antibody at room temperature (RT) (Table IV) and then washed in 1X PBS and one time in distilled water (dH₂O). 2D cultured cells were mounted with Prolong® Gold anti-fade reagent DAPI (ThermoFisher Scientific, USA), dried, nail-polished and analyzed by confocal microscopy (Olympus Fluoview, FV10i, Japan).

Table IV. List of antibodies used for the IF analysis of 2D cultured cells (modified from Scarian *et al.*, 2022 [547]).

Primary Antibody	Secondary Antibody
Nestin 1:250 (Abcam, UK)	CFTM 594 goat anti-mouse 1:500 (Sigma-Aldrich, USA)
SOX2 1:400 (Proteintech, USA)	CFTM 488A goat anti-rabbit 1:500 (Sigma-Aldrich, USA)
SOX1 1:400 (Abcam, UK)	CFTM 488A goat anti-rabbit 1:500 (Sigma-Aldrich, USA)
PAX6 1:250 (ThermoFisher Scientific, USA)	CFTM 594 goat anti-mouse 1:500 (Sigma-Aldrich, USA)
Olig2 1:500 (Novus Biologicals, USA)	CFTM 488A goat anti-rabbit 1:500 (Sigma-Aldrich, USA)
TUBB3 1:400 (Abcam, UK)	CFTM 488A goat anti-rabbit 1:500 (Sigma-Aldrich, USA)
ChAT 1:400 (Novus Biologicals, USA)	CFTM 594 goat anti-mouse 1:500 (Sigma-Aldrich, USA)

3.2 3D bioprinting

We tested two different hydrogels. The first hydrogel was composed by SA and GEL and was developed in our laboratory. The second hydrogel was Cellink Bioink (IK-102000; Cellink, Sweden), a commercial bioink composed of cellulose nanofibrils and alginate already used for the study of human NSCs [560].

3.2.1 SA-GEL Hydrogel

Hydrogel preparation

Different concentrations of SA and GEL were tested as reported in table V (Table V). The correct concentration of SA (Sigma-Aldrich, USA) and GEL (Sigma-Aldrich, USA) were first weighted and dissolved separately in sterile 1X PBS. GEL solution was heated at 72°C for complete dissolution and SA solution was finally added. SA-GEL solution was homogenized and sterilized prior to the bioprinting process. Moreover, two different temperatures, 25°C and 37°C, were tested setting in each case the optimal pressure of printing.

Table V. Parameters tested for hydrogel preparation (modified from Fantini *et al.*, 2019 [546])

Hydrogel type	SA	GEL	Printing Temperature (°C)	Printing Pressure (kPa)
1	6%	4%	25°C	45-70
2	6%	4%	37°C	30-50
3	4%	4%	25°C	35-60
4	4%	4%	37°C	30-40

Hydrogel sterilization

Four different sterilization methods were tested: filtration, autoclaving, UV exposure and pasteurization as described in Fantini *et al.* (2019) [546]. In the first method, SA and GEL, dissolved in 1X PBS, were passed into a 0.20 µm filter (Corning, USA). UV exposure consists in the exposure of SA and GEL powders to UV rays. In pasteurization process, SA and GEL solutions were heated at 72°C. Finally, the last method consisted in the autoclaving of SA and GEL solutions at 121°C.

Bioprinting parameters

SA-GEL bioink was printed using the Bioplotter Cellink BioX (Cellink AB, Sweden), which was provided with HEPA filters for sterile environment maintenance. Cartridges were provided with a 0.41 mm nozzle and the pressure was manually controlled. The STL grid model (FreeCAD©, ver. 0.16) was designed using the open-source CAD software. Slic3r (version 1.2.9) was used to assess splicing process. The print-head speed was 600 mm/min and layer heights were 0.4 mm.

NSCs bioprinting

NSCs, differentiated from iPSCs of both CTRL and sALS subjects, were encapsulated in sterilized SA-GEL hydrogel and printed using the Cellink BioX and the parameters already described in Fantini *et al.* [546]. 6×10^5 cells/mL NSCs were mixed in the hydrogel using two syringes and a luer connector. Constructs were then crosslinked using 2% CaCl₂ diluted in dH₂O to harden the structures. NSCs were then cultured in the Expansion Medium as previously described (see chapter 3.1 “PBMCs reprogramming and iPSCs differentiation”, paragraph “iPSCs differentiation into NSCs”).

NSCs differentiation in SA-GEL hydrogel

Printed NSCs were cultured in Expansion Medium to allow proliferation. NSCs were then differentiated into MNPs and MNs as previously described for 2D differentiation (see chapter 3.1 “PBMCs reprogramming and iPSCs differentiation”, paragraph “NSCs differentiation in 2D”), with the difference that cells are not cultured in suspension but remain in the hydrogel constructs.

Proliferation-viability assay

The crosslinking causes the hardening of the constructs, and, for this reason, it was impossible to perform the Trypan Blue exclusion assay. Therefore, viability was evaluated using the LIVE/DEAD Viability Assay (ThermoFisher Scientific, USA). Viability was evaluated at days 0, 3, 7, 10, 14 and 20 after the printing during the differentiation process into MNs. Constructs were incubated in 0.75 μM calcein AM (ThermoFisher Scientific, USA), which indicates intracellular esterase activity staining living cells, and in 1 μM ethidium homodimer-1 (ThermoFisher Scientific, USA), which stains dead cells indicating the loss of plasma membrane activity. After 45 min, constructs were washed with 1X PBS and examined at an EVOS™ XL Core Imaging System microscope (Thermofisher Scientific, USA).

Immunofluorescence analysis

IF analysis was performed at each stage of differentiation process.

Cells printed in 6% SA-4% GEL hydrogel were fixed in 4% paraformaldehyde and blocked in 5 % Normal Goat Serum and 0.1 % tween. Constructs were then incubated in primary antibody at 4°C overnight (Table VI). After washes in cold 1X PBS, constructs were incubated in secondary antibody at 4°C, washed in 1X PBS and then in dH₂O. Finally, constructs were mounted with Polyvinyl alcohol mounting medium with DABCO® anti-fadig (Sigma-Aldrich, USA), dried, nail-polished and analyzed by confocal microscopy (Olympus Fluoview, FV10i, Japan). 3D constructs images were acquired every 15 µm and 3D reconstructions were performed using the microscope software. Image analysis was performed using Fiji-Imagej free software (<https://imagej.net/Fiji/Downloads>).

Table VI. List of antibodies used for the IF analysis of 3D constructs (modified from Scarian *et al.*, 2022 [547]).

Primary Antibody	Secondary Antibody
Nestin 1:100 (Abcam, UK)	CFTM 594 goat anti-mouse 1:500 (Sigma-Aldrich, USA)
SOX2 1:250 (Proteintech, USA)	CFTM 488A goat anti-rabbit 1:500 (Sigma-Aldrich, USA)
SOX1 1:200 (Abcam, UK)	CFTM 488A goat anti-rabbit 1:400 (Sigma-Aldrich, USA)
PAX6 1:100 (ThermoFisher Scientific, USA)	CFTM 594 goat anti-mouse 1:400 (Sigma-Aldrich, USA)
Olig2 1:400 (Novus Biologicals, USA)	CFTM 488A goat anti-rabbit 1:500 (Sigma-Aldrich, USA)
TUBB3 1:400 (Abcam, UK)	CFTM 488A goat anti-rabbit 1:500 (Sigma-Aldrich, USA)
ChAT 1:200 (Novus Biologicals, USA)	CFTM 594 goat anti-mouse 1:400 (Sigma-Aldrich, USA)

Analysis of electrophysiological characteristics of included cells

NSC34 cells were used for the evaluation of the electrophysiological characteristics of included cells, as they resemble many of the characteristics of human MNs. Cells were first differentiated in 2D using a Differentiation Medium composed of DMEM High Glucose (Carlo Erba, Italy), 1% penicillin/streptomycin (Carlo Erba, Italy), 1% L-glutamine (Carlo

Erba, Italy) and 10 μ M all-trans RA. The differentiation was morphological evaluated at the optical microscope EVOS™ XL Core Imaging System (Thermofisher Scientific, USA) at day 0, 1, 4, 7, 11 and 14.

1×10^6 NSC34 were encapsulated in SA-GEL hydrogel and printed with the parameters described above (see chapter 3.2.1 “SA-GEL Hydrogel”, paragraph “Bioprinting parameters”).

Since NSC34 do not fire autonomously, cells were treated with 15 mM KCl at 37°C in order to induce them to produce action potentials. Simultaneously, cells left in 1X PBS at 37°C were used as control sample. After the treatment, an IF analysis with the antibody c-Fos (Santa Cruz Biotechnology, USA; dilution 1:300), a marker of neuronal activity often expressed when neurons fire action potentials [561], was performed. Finally, cells were analyzed by confocal microscopy (Olympus Fluoview, FV10i, Japan).

3.2.2 Cellink Bioink Hydrogel

Hydrogel characterization

Moisture

Moisture assay was performed as described by Shawan *et al.* (2019) [562] and modified from Piola *et al.* (2022) [563]. Moisture was evaluated for constructs composed only of the hydrogel Cellink Bioink and for constructs composed of cells medium DMEM Low Glucose (Carlo Erba, Italy) and hydrogel in a 1:10 proportion. After hydration in dH₂O constructs were weighted and then dried at 37°C. Moisture percentage was evaluated using the following formula:

$$\mathbf{Moisture(\%)} = \left[\frac{W^H - W^D}{W^H} \right] \times 100$$

W^H : weight of hydrated prints

W^D : weight of constructs after drying

Swelling

Swelling ratio (S) was evaluated as described by Asohan *et al.* (2022) [564] and by Piola *et al.* (2022) [563]. Both constructs composed only of the hydrogel and of cells medium and hydrogel were dried at 37°C and weighted. They were then rehydrated in dH₂O and weighted after water removing at different time point (0, 1, 3, 6 and 24 h). The formula for the calculation of the swelling ratio is:

$$S = \left[\frac{W^H - W^D}{W^D} \right] \times 100$$

W^H : weight of hydrated constructs

W^D : weight of dehydrated constructs

Moreover, the mass swelling ratio (Q) was calculated using the following formula:

$$Q = \frac{W^H}{W^D}$$

W^H : weight of hydrated constructs

W^D : weight of dehydrated constructs

Porosity

Porosity, of both printed constructs composed of only hydrogel and of constructs composed of cells medium and hydrogel, was evaluated using the liquid displacement method as described by Piola et al. (2022) [563]. A known volume of absolute ethanol (Carlo Erba, Italy) was weighted and then the constructs were immersed. After 5 min the weight of ethanol plus the constructs was calculated and at the end the ethanol without the constructs was weighted again.

The porosity percentage was calculated using the following formula:

$$Porosity (\%) = \left[\frac{W^1 - W^3}{W^2 - W^3} \right] \times 100$$

W^1 : weight of pure ethanol

W^2 : weight of ethanol and the submerged construct

W^3 : weight of ethanol after construct removal

NSCs bioprinting

NSCs differentiated from iPSCs of both CTRL and sALS subjects, were encapsulated in sterilized Cellink Bioink and printed using the Bioplotter Cellink BioX (Cellink, Sweden). 6×10^5 cells/mL NSCs were mixed, using two syringes and a luer connector, with the bioink in a 1:10 proportion. The printing was performed following manufacture's recommendation (BPR-IK-102000, Cellink) and the parameters previously described. The printing was performed using a 0,41 mm nozzle (23G) at 25°C, at a pressure between 45 and 70 kPa and a printing speed of 600 mm/min. The ionic agent provided with the bioink (Cellink, Sweden) was then used to crosslink the constructs. NSCs were then cultured in the Expansion Medium as previously described.

NSCs Differentiation in Cellink Bioink Hydrogel

NSCs from sALS and CTRL subjects were differentiated as previously described (see chapter 3.2.1 "SA-GEL Hydrogel", paragraph "NSCs differentiation in SA-GEL hydrogel").

Proliferation-viability assay

Viability was evaluated at days 0, 3, 7, 10, 14 and 20 after the printing during the differentiation process into MNs, as previously described (see chapter "3.2.1 SA-GEL Hydrogel", paragraph "Proliferation-viability assay").

Immunofluorescence

IF was performed at each stage of differentiation process as described (see chapter 3.2.1 "SA-GEL Hydrogel", paragraph "Immunofluorescence analysis").

IF quantification was performed for every confocal slice of the 3D constructs. Corrected total cell fluorescence analysis (CTCF) on the cell colony was obtained using the following formula [565] (<http://theolb.readthedocs.io/en/latest/imaging/measuring-cellfluorescence-using-imagej.html#measuring-cell-fluorescence-using-imagej>. Accessed on 13 January 2021).

$$\text{CTCF} = \text{Integrated Density} - (\text{Area of selected cell} \times \text{Mean fluorescence of background readings})$$

CTCF of the first layer was set to 1.0 and the relative fluorescence intensity of the other layers was calculated as the ratio of the layer CTFC to that of the first layer [566].

RT-qPCR

RNA was extracted from NSCs, MNPs and MNs, cultured both in 2D and 3D conditions, using TRIzol® (ThermoFisher Scientific, USA) and following manufacturer's instructions. After the evaluation of its quality and quantity using Nanodrop One C spectrophotometer (Thermofisher Scientific, USA), 1000 ng were reversed-transcribed using iScriptcDNA Synthesis Kit (BioRad, Italy) and following the manufacturer's protocol. A quantitative chain reaction was carried out on 1 µL of cDNA using the CFX Connect™ Real-Time PCR Detection System (BioRad, Italy) and the SYBR Green Master Mix (BioRad, Italy). The expression of the genes in Table VII was performed at 60°C. Cycle threshold (Ct) values were normalized with *GAPDH*. $2\Delta Ct$ method was used to detect differences between genes expression.

Table VII. List of primers used for RT-qPCR of 3D constructs (modified from Scarian *et al.*, 2022 [547]).

Gene	Primer sequences (5'-3')	Annealing Temperature
<i>Nestin</i>	F GGA AGA GAA CCT GGG AAA GG R GAT TCA GCT CTG CCT CAT CC	60° C
<i>SOX2</i>	F AGTCTCCAAGCGACGAAAAA R TTTCACGTTTGCAACTGTCC	60° C
<i>SOX1</i>	F AAATACTGGAGACGAACGCC R AACCCAAGTCTGGTGTGTCAGC	60° C
<i>PAX6</i>	F TGTGTGCTCTGAAGGTCAGG R CTGGAGCTCTGTTTGGAAGG	60° C
<i>Olig2</i>	F CCCTAAAGGTGCGGATGCTT R CTGGATGCGATTTGAGGAGC	60° C
<i>TUBB3</i>	F CAGATGTTGATGCCAAGAA R GGGATCCACTCCACGAAGTA	60° C
<i>MAP2</i>	F AGGGCTGGTAGGTTGGATCT R TGTGTCTCTGCCTTTGTATC	60° C
<i>GAPDH</i>	F CAG CAA GAG CAC AAG AGG AAG R CAA CTG TGA GGA GGG GAG ATT	60° C

Electrophysiological analysis of included NSC34 cells

1X10⁶ NSC34 were encapsulated in Cellink Bioink and printed with the parameters described above. The electrophysiological analysis of included cells was performed as

previously described (see chapter 3.2.1 “SA-GEL Hydrogel”, paragraph “Analysis of electrophysiological characteristics of included cells”).

3.3 Organoids

Organoids generation protocol

CTRL and sALS NSCs were splitted using StemPro Acutase (Life Technologies,USA) in order to obtain single-cells and break aggregates and then filtrated using a 40 μm cell strainer (Corning Inc., USA). Dissociated cells were counted using the TC20™ Automated Cell Counter (Bio-Rad, USA) and 4×10^6 NSCs were seeded on a non-coated 6-well plate. Cells were then cultured in floating condition at 95 rpm using an Orbi-Shaker CO₂ (Benchmark Scientific) for the formation of organoids. They were then differentiated, using the culture media described above, for the formation of MNP organoids (MNPOs) and then of MNOs (Figure 19). Organoids were cultured for 28 days and no longer because they started to disaggregate and lose the roundness.

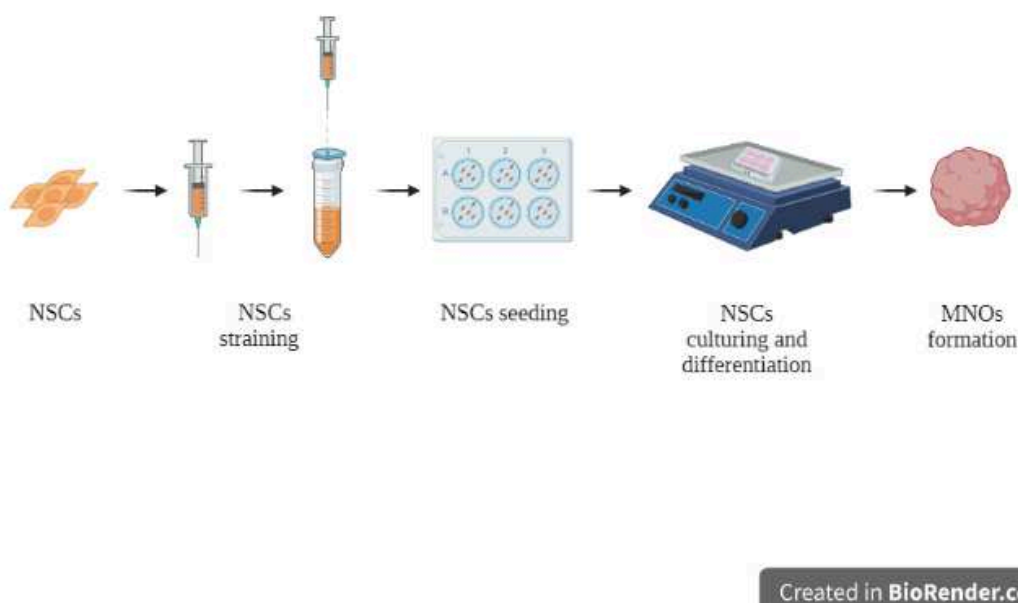


Figure 19. Organoids generation protocol. NSCs are strained and differentiated in floating condition for the formation of organoids (created with Biorender.com).

Organoids morphological characterization

The different steps of organoids formation were evaluated by bright field using EVOS™ XL Core Imaging System. Area at days 1, 7, 14, 21, and 28 was calculated using ImageJ Software. Moreover, from bright-field images, organoids roundness was evaluated at day 28.

Immunofluorescence analysis

The IF protocol described above was modified for MNOs with minor modifications (see chapter 3.2.1 “SA-GEL Hydrogel”, paragraph “Immunofluorescence analysis”). Table VIII shows the antibodies used for the IF analysis.

Confocal microscopy was used to acquire images and IF quantification was acquired using ImageJ Software. Neurites length and the thickness of GFAP positive layer was evaluated from IF images. Quantification was performed on total area subtracted from the background.

Table VIII. List of antibodies used for MNOs IF analysis.

Primary Antibody	Secondary Antibody
Nestin 1:100 (Abcam, UK)	CFTM 594 goat anti-mouse 1:500 (Sigma-Aldrich, USA)
GFAP 1:100 (Santa Cruz Biotechnology, USA)	CFTM 594 goat anti-mouse 1:500 (Sigma-Aldrich, USA)
TUBB3 1:500 (Abcam, UK)	CFTM 488A goat anti-rabbit 1:500 (Sigma-Aldrich, USA)
ISL 1:100 (ThermoFisher Scientific, USA)	CFTM 488A goat anti-rabbit 1:500 (Sigma-Aldrich, USA)
HB9 1:100 (Santa Cruz Biotechnology, USA)	CFTM 594 goat anti-mouse 1:500 (Sigma-Aldrich, USA)

Bulk RNA sequencing (RNA-seq)

500 ng of total RNA from 2D MNs and from MNOs, from both CTRL and sALS subjects, were used for libraries preparation. RNA was depleted from ribosomal RNA using RiboCop V1.3 (Lexogen, Austria) and CORALL Total RNA-Seq Library Prep Kit (Lexogen, Austria) was used for libraries preparation. Quality of libraries was detected using 4200 Tape Station (Agilent Technologies, USA) with a “DNA High sensitivity” assay (Agilent Technologies, USA), whereas quantification was performed using High Sensitivity dsDNA assay (ThermoFisher Scientific, USA) with a Qubit device (ThermoFisher Scientific, USA). Sequencing was performed using Illumina NextSeq 500 (Illumina, USA) and FastQ files were generated via Illumina bcl2fastq2, version 2.17.1.14 (<http://support.illumina.com/downloads/bcl-2fastq-conversion-software-v217.html>).

Bioinformatics' analysis

Bioinformatics' data analysis pipeline was used to process the FastQ files generated by the sequencing through Unique Molecular Identifiers (UMI) extraction, trimming, alignment and quality control steps. In the first step UMIs were removed, inasmuch CORALL libraries contain N12 UMI at the start of Read 1. Later, poly(A) sequences at the 3' end of Read 1 and poly(T) sequences at the 5' end of Read 2 were trimmed. Trimmed reads were then aligned through STAR using Gencode Release h38 (GRCh38) as human genome reference. FeatureCounts software was used for gene and transcript abundance computing using the "stranded forward" option. The R package DESeq2 was used for differential expression analysis. Genes with $\log_2(\text{condition sample/control donor}) \geq 1$ and false discovery rate ≤ 0.1 were considered differentially expressed (DE) [567]. R software was used for the generation of heatmaps (heatmap.2 function from the R ggplots package), PCA plot (prcomp function from the R ggplots package) and gene ontology (GO) Chord plot (GOChord function from the R GOplot package) [568]. enrichR web tool was used for functional enrichment analysis [569], whereas deconvolution analysis was performed using the CIBERSORTx web tool (<https://cibersortx.stanford.edu/>)

RT-qPCR

Several genes emerged from RNA-seq were validated through RT-qPCR. 250 ng of total RNA were reverse transcribed using iScriptcDNA Synthesis Kit and qPCR was performed using the CFX Connect™ Real-Time PCR Detection System and the SYBR Green Master Mix, as previously described. The expression of the genes in Table IX was performed at 60°C (Table IX).

Table IX. List of primers used for RT-qPCR validation.

Gene	Primer Sequences (5'-3')	Annealing Temperature
<i>OPN</i>	F TGAAACGAGTCAGCTGGATG R TGAAATTCATGGCTGTGGAA	60 °C
<i>NCAN</i>	F TTTGGTGGTTCTGCATGTGT R CAGGGGCACTACCAATGTCT	60 °C
<i>TIMP1</i>	F AAGGCTCTGAAAAGGGCTTC R GAAAGATGGGAGTGGGAACA	60 °C
<i>FLOT1</i>	F CCAGCCTGAACCATGTTTTT R CCATGGCGAGTGTAACCTT	60 °C
<i>CTSL</i>	F GTGGACATCCCTAAGCAGGA R TTTCAAATCCGTAGCCAACC	60 °C
<i>LOXL1</i>	F CACCAGCATTACCACAGCAT R CCTGGGTATGAGAGGTGCAT	60 °C
<i>FNI</i>	F CAGTGGGAGACCTCGAGAAG R GTCCCTCGGAACATCAGAAA	60 °C
<i>TIMP2</i>	F GAAAAAGCTGGGTCTTGCTG R AGTGTCTCGGAGGCTGAGAA	60 °C
<i>APP</i>	F CACAGAGAGAACCACCAGCA R ACATCCGCCGTAAAAGAATG	60 °C
<i>COL9A2</i>	F CCTTCTGTCTGGGACTCAGG R GGTAACAGCCGAATGATGCT	60 °C
<i>OTX2</i>	F CAACAGCAGAATGGAGGTCA R AGCTGGGCTCCAGATAGACA	60 °C
<i>COL4A4</i>	F TGGTAAAACCATGACGCAA R TGCTAATGTCGCATCTCTGG	60 °C
<i>GAPDH</i>	F CAGCAAGAGCACAAGAGGAAG R CAACTGTGAGGAGGGGAGATT	60 °C

Statistical analysis

Tests were performed at least three times to observe measurements' reproducibility. Statistical analyses were performed using GraphPad Prism (GraphPad Prism 8) and data were presented as mean \pm SEM. T-test, followed by Mann-Whitney test, was performed in the analysis between two groups, and ANOVA, followed by Bonferroni test, when comparison between more than two groups occurred. A p-value < 0.05 was considered statistically significant.

4. RESULTS

4.1 3D bioprinting

4.1.1 SA-GEL Hydrogel

4% SA-6% GEL hydrogel shows the best characteristics for printability

We tested for printability quality two different concentrations of SA and GEL. SA confers rigidity to the constructs, whereas GEL, derived from collagen, mimics the ECM [359]. The first type of hydrogel was composed of 4% SA and 4% GEL, whereas the second one of 6% SA and 4% GEL. As reported in table V (page 55) we tested two different temperatures (25°C and 37°C) and different printing pressures. We observed that both types of hydrogels printed at 37°C required lower printing pressures (30-50 kPa for the 6% SA-4% GEL hydrogel and 30-40 kPa for the 4% SA-4% GEL hydrogel) than hydrogels printed at 25°C (45-70 kPa for the 6% SA-4% GEL hydrogel and 35-60 kPa for the 4% SA-4% GEL hydrogel). In fact, GEL is a temperature-dependent biomaterial and liquefies with the increase of temperature. Moreover, the 6% SA-4% GEL hydrogel required a higher printing pressure when printed at 25°C compared to the hydrogel composed of 4% SA and 4% GEL, printed at the same temperature. That indicates a major viscosity because of the higher SA concentration.

We assessed printing repeatability of the different types of hydrogels, testing daily fresh hydrogels for 3 days consecutively and printing grids with 10x10x1.2 mm dimensions. By a camera, we obtained planar images which were analyzed by ImageJ software, measuring grid side and grid gap (Figure 20). We found statistically significant differences between hydrogel type 1 (6% SA-4% GEL printed at 25°C) and hydrogel type 4 (4% SA-4% GEL printed at 37°C) for both sides (Figure 20 b) and gaps (Figure 20 c) (*p<0.05) due to different temperature parameters and SA concentration. Moreover, we found a statistically significant difference in side parameter (Figure 20 b) between hydrogel type 3 (4% SA-4% GEL printed at 25°C) and hydrogel type 4 (4% SA-4% GEL printed at 37°C) due to different printing temperatures. Moreover, hydrogel types 2 (6% SA-4% GEL printed at 37°C) and 4 (4% SA-4% GEL printed at 37°C) showed a higher variability in printability, as demonstrated by the higher SEM.

These results allowed us to conclude that the hydrogel type 1 (6% SA-4% GEL printed at 25° C at a pressure between 45 and 70 kPa) has the best characteristics for the printing.

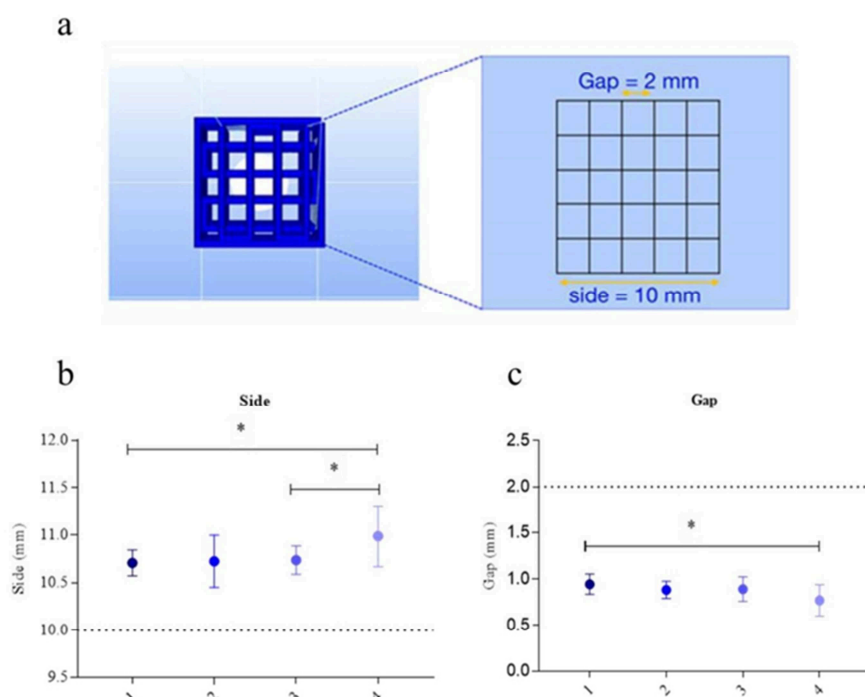


Figure 20. Mechanical characterization of SA-GEL hydrogels. Different SA and GEL concentrations and printing temperatures were tested for printing (see Table V). FREE-CAD images of grids with gap and side dimensions were obtained (a). Side values were measured for all hydrogel types showing statistically significant differences between type 1 and 4 (* $p < 0.05$) and between type 3 and 4 (* $p < 0.05$) (b). Gap values for all hydrogel types were calculated, showing a statistically significant difference between type 1 and type 4 (* $p < 0.05$) (c). Dotted lines indicate the reference value used to evaluate the printing accuracy. Data were analyzed using ANOVA, followed by the Bonferroni test. (GraphPad Prism 8). Error bars indicate SEM (modified from Fantini *et al.*, 2019 [546]).

Pasteurization is the best sterilization method for the 6% SA-4% GEL hydrogel

Sterilization is essential for cells culturing, and, unlike commercial hydrogels which are already sterilized, homemade hydrogels need a sterilization process prior to the printing. We tested three different methods for the sterilization (UV exposure, autoclaving and filtration) and pasteurization. As shown in table X only pasteurization was compatible with both SA and GEL (Table X). Both compounds, and especially SA, were sensitive to UV exposure; autoclaving caused the viscosity loss of both SA and GEL, and finally filtration was not possible due to the polymeric nature of both SA and GEL.

For these reasons, we decided to pasteurize the hydrogel prior to use in a 72°C bath for 1 h.

Table X. Methods tested for SA-GEL hydrogel sterilization

Methods	SA	GEL
UV	X	✓
Autoclaving	X	X
Filtration	X	X
Pasteurization	✓	✓

NSCs maintain a good viability when printed and differentiated in 6% SA-4% GEL hydrogel

We printed NSCs in 6% SA-4% GEL hydrogel and differentiated them into MNPs, iMNs, and finally into MNs. To assess the viability of printed cells during the differentiation, we performed a LIVE/DEAD assay at each stage of the differentiation process. As shown in figure 21, although cell viability reported some degree of variability, during the differentiation process an increase is evident. We found statistically significant differences between NSCs and iMNs (day 0 vs. 14, ** $p < 0.01$), between NSCs and MNs (day 0 vs day 20, *** $p < 0.001$) and between MNPs and MNs (day 7 vs day 20, ** $p < 0.01$).

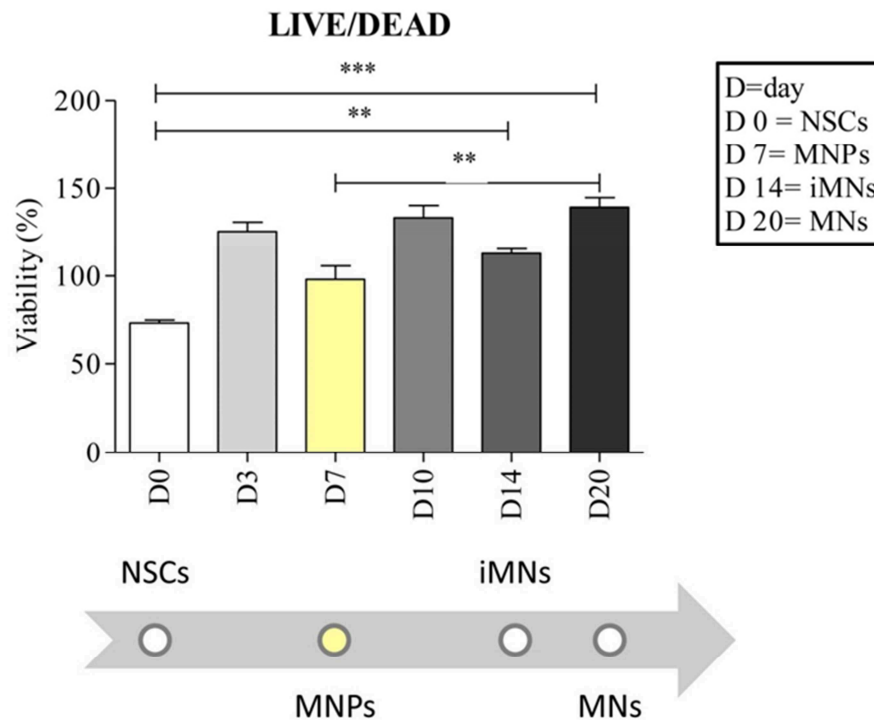


Figure 21. Viability assay performed on cells during the differentiation process in 6% SA-4% GEL hydrogel. On the Y-axis the viability percentage is indicated. Cell viability was evaluated at days (D) 0, 3, 7, 10, 14 and 20 after NSCs printing and the beginning of differentiation into MNs. After 7 days, cells reach the stage of MNPs (yellow bar), the first stage of cell specialization into MNs, and viability is increased by 34% compared to day 0, whereas at day 14 they reach the stage of iMNs with an increase in viability of 53% compared to day 0. At day 20, NSCs are differentiated into MNs with an increase of viability of 90% when compared to day 0. Statistically significant differences were found between NSCs and iMNs (day 0 vs 14, ** $p < 0.01$), between NSCs and MNs (day 0 vs day 20, *** $p < 0.001$) and between MNPs and MNs (day 7 vs day 20, ** $p < 0.01$). Data were analyzed using ANOVA, followed by the Bonferroni test (GraphPad Prism 8). Error bars indicate SEM.

Including and printing in 6% SA-4% GEL hydrogel does not interfere with the differentiation process

We printed NSCs in 6% SA-4% GEL hydrogel and differentiated them into MNs. At each differentiation stage, we performed an IF analysis for the typical markers of the stage and we analyzed them at confocal microscope. For the characterization of NSCs we used Nestin, SOX2, SOX1 and PAX6. For the MNPs stage, we stained cells with Olig2 and PAX6 and MNs were marked for TUBB3 and ChAT. We noticed that the hydrogel allowed both CTRL and sALS cell colonies formation, and that they expressed the markers of each differentiation step (Figure 22). We observed high background fluorescence, represented by the diffuse green color, which did not permit to do quantification analyses, as the calculation of CTCF.

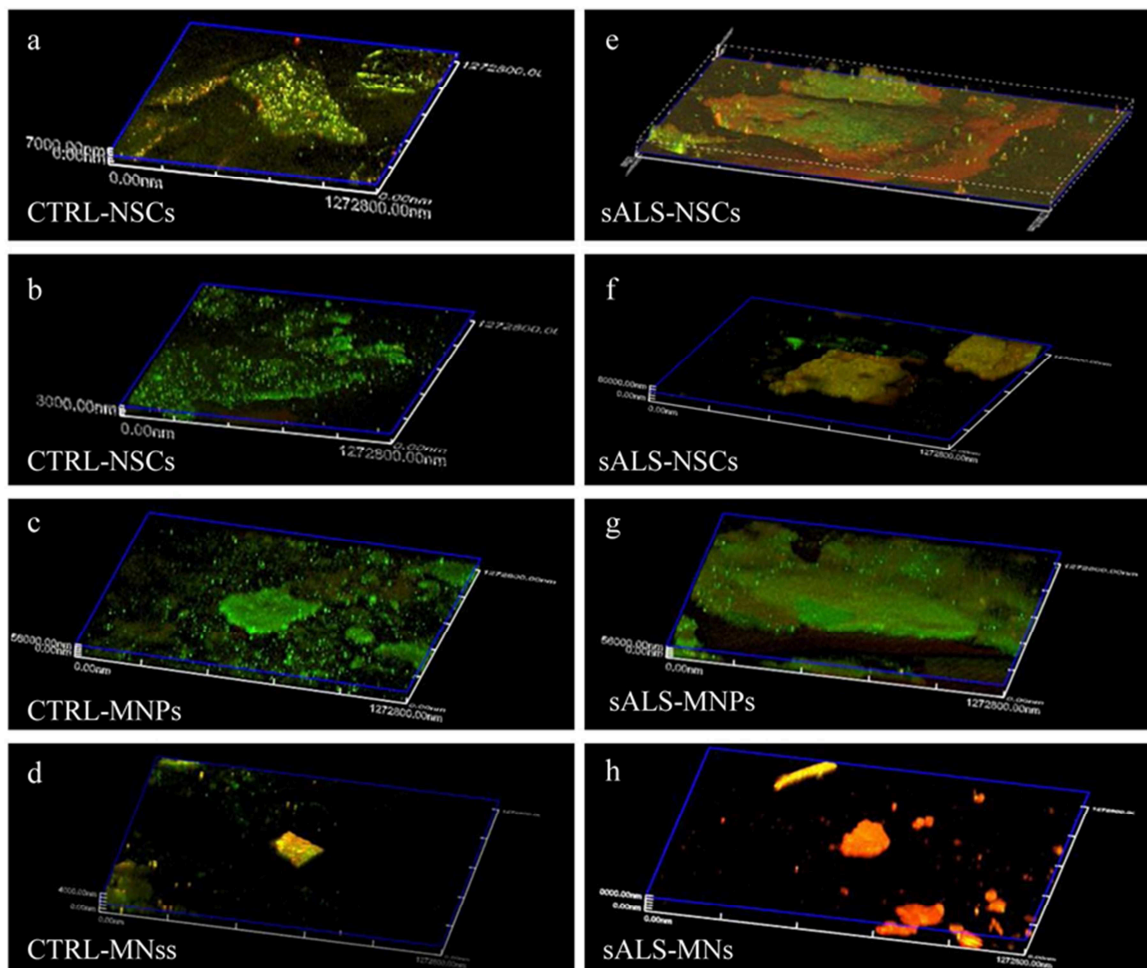


Figure 22. IF analysis performed on CTRL and sALS cells included in 6% SA-4%GEL hydrogel, at each differentiation step. NSCs from CTRL and sALS subject were printed in 6% SA-4% GEL hydrogel and differentiated into MNPs and MNs. Cells expressed the typical markers of each stage of differentiation: NSCs expressed Nestin=green and SOX2=red (a and e); NSCs expressed SOX1=green and PAX6=red (b and f); MNPs expressed Olig2=green and PAX6= red (c and g); MNs expressed TUBB3= green and ChAT=red (d and h). Images come from videos acquired through confocal microscopy.

The videos acquired through confocal microscopy show the thickness of the colonies, which is not possible to appreciate from 2D images (Figure 23).

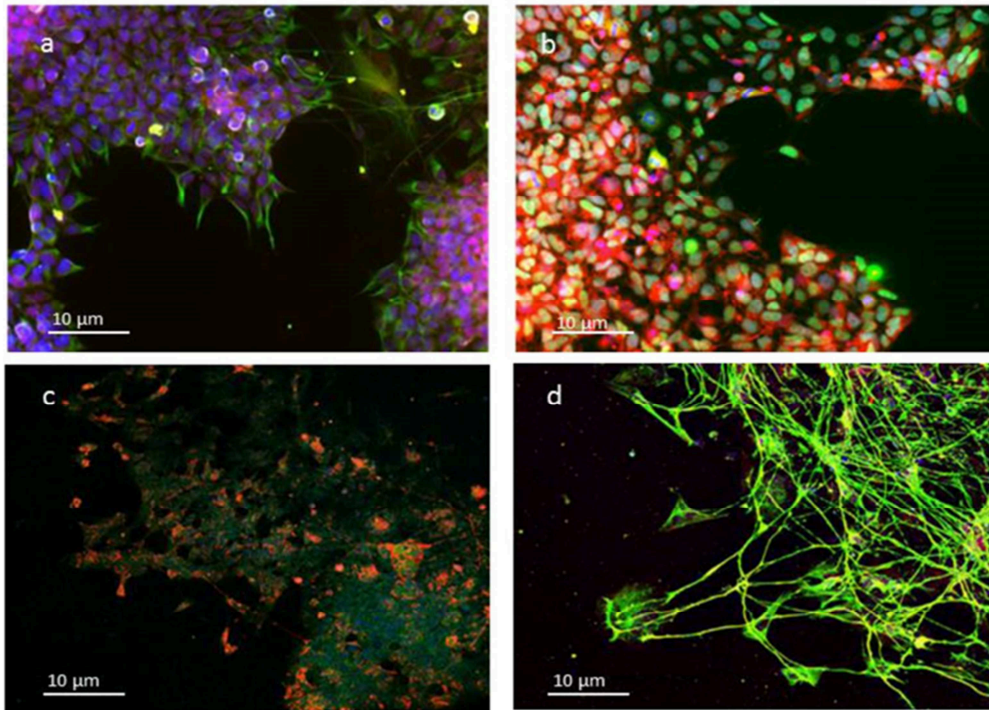


Figure 23. IF of 2D cells. NSCs expressed the typical markers Nestin=green and SOX2=red (a) and SOX1=green and PAX6=red NSCs (b). MNPs expressed Olig2=green and PAX6=red (c), whereas MNs expressed TUBB3=green and ChAT=red (d). Nuclei were stained with DAPI (blue). Scale bar= 10μm (modified from Scarian *et al.*, 2022 [547]).

NSC34 maintain their electrophysiological characteristics when printed in 6% SA- 4% GEL hydrogel

We used NSC34 cells, a mouse spinal cord x neuroblastoma hybrid cell line, to test the cells electrophysiological behavior after printing. NSC34 share many characteristics with human MNs. We first developed a differentiation protocol to bring cells to the more mature stage.

We noticed that, already at day 1 after differentiation starting, cells began to show propagations. At the end of the differentiation protocol, cells have changed their morphology and aggregated in colonies. Moreover, they showed a huge number of propagations and connections (Figure 24).

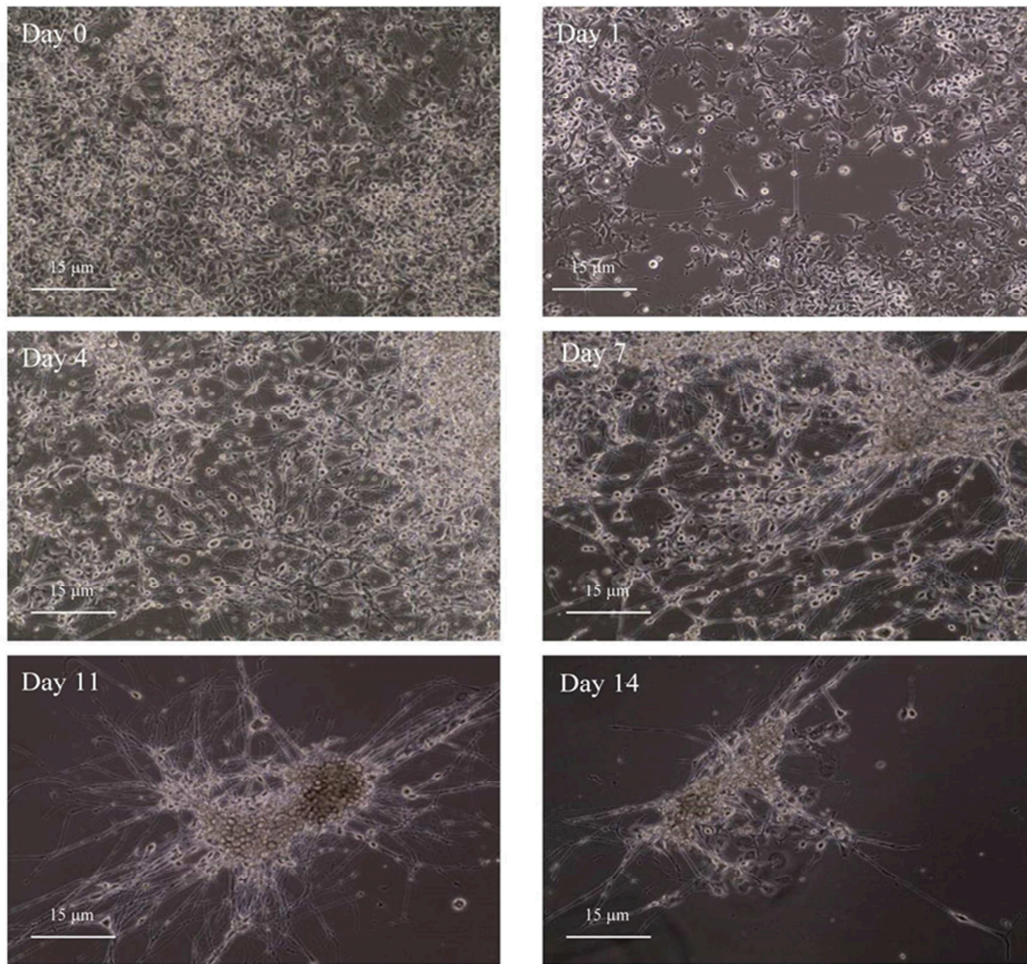


Figure 24. Optical microscope images of NSC34 during differentiation process. NSC34 were differentiated in DMEM High Glucose, 1% penicillin/streptomycin, 1% L-glutamine and 10 µM RA for 14 days. The differentiation process was evaluated at days 0, 1, 4, 7, 11 and 14 using the optical microscope EVOS™ XL Core Imaging System. Cells showed propagations already at day 1 and then, at day 7, grouped in colonies and interconnected between themselves. Scale bar= 15 µm (modified from Scarian *et al.*, 2022 [547]).

At the end of the differentiation process, we performed an IF analysis for the neuronal activity marker c-Fos, after the inducing of cell firing with 15 mM KCl.

As shown in figure 25 we found that the treatment with 15mM KCl induced cells firing (** $p < 0.01$), in both 2D and 3D conditions, allowing us to conclude that the inclusion in the hydrogel did not interfere with the firing capacity of included NSC34.

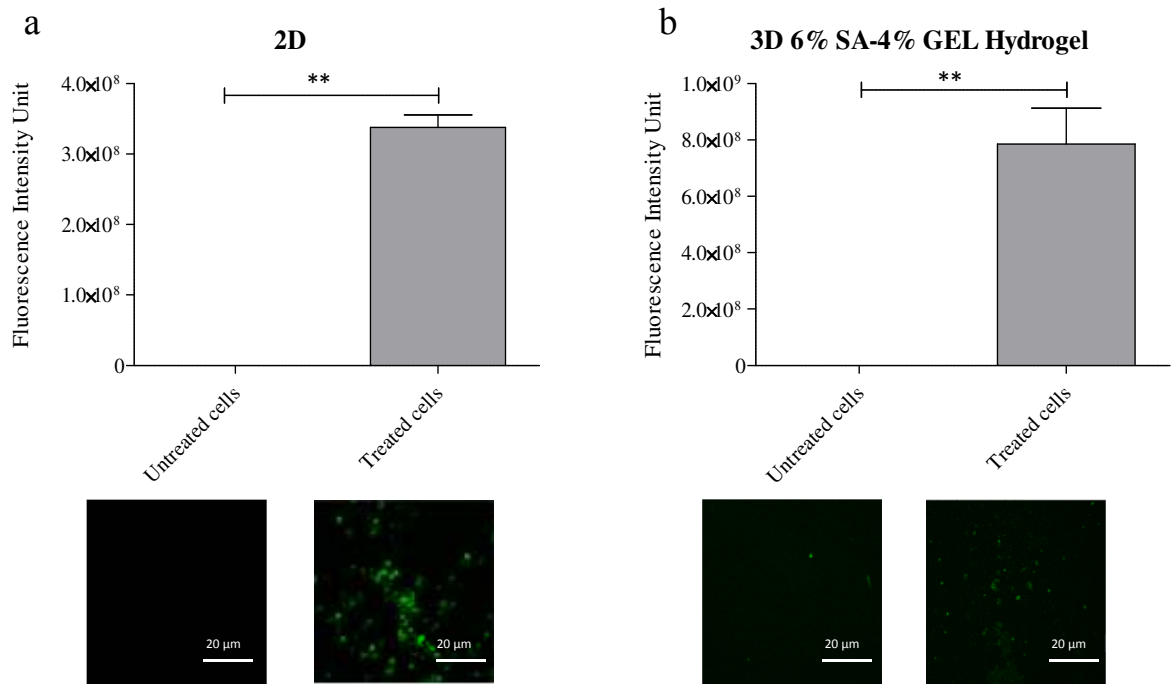


Figure 25. IF analysis for the electrophysiological characterization of NSC34 included in 6% SA-4% GEL hydrogel. On the Y-axis the fluorescence intensity unit value is indicated. NSC34 cells, both in 2D (a) and 3D (b) were induced firing through 15 mM KCl. In both 2D and 3D, cells fire after the treatment. Data were analyzed using a t-test followed by the Mann–Whitney test. ** $p < 0.01$ (GraphPad Prism 8). Error bars indicate SEM. Scale bar = 20 μm .

4.1.2 Cellink Bioink Hydrogel

Cellink Bioink hydrogel shows good characteristics for cells culture

Moisture, swelling ratio and porosity were evaluated for both printed constructs composed of only Cellink Bioink and for constructs composed of culture medium and culture medium + hydrogel in 1:10 ratio.

Moisture test was performed to measure the water content. This parameter is very important to test the integrity of the hydrogel, correlating with the capacity to maintain dimension stability. In both types of constructs, we found a moisture percentage above 95% (95.46% for the first type of constructs and 95.55% for the second one) without significant differences (Figure 26), indicating a great amount of water content and a good capacity to maintain dimension stability.

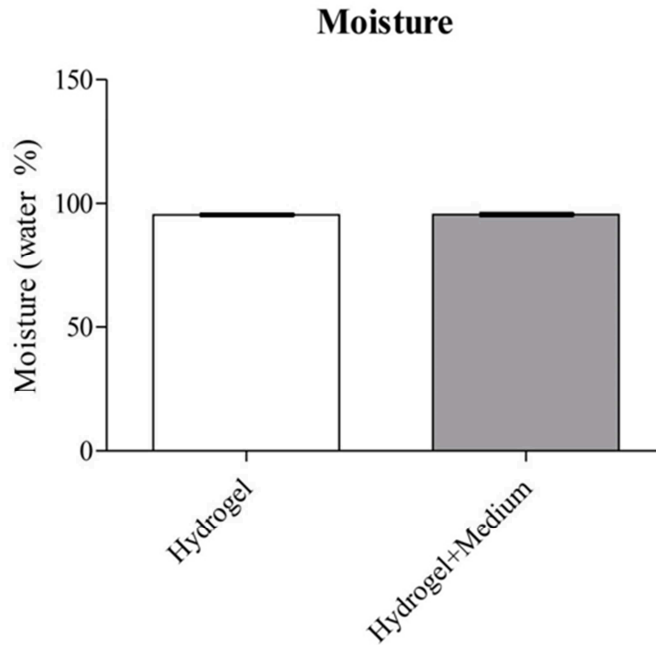


Figure 26. Moisture percentage analysis. Moisture percentage was evaluated in both constructs composed of only Cellink Bioink (Hydrogel) and in constructs composed of the hydrogel and culture medium (Hydrogel + Medium). On the Y-axis the moisture percentage is indicated. In both types of construct the moisture was above 95% without significant differences. Data were analyzed using a t-test followed by the Mann–Whitney test. Error bars indicate SEM (GraphPad Prism 8) (modified from Scarian *et al.*, 2022 [547]).

We evaluated the swelling of the hydrogel. Swelling is the ability to absorb water and, for this reason, is directly linked to moisture. In figure 27 we can notice that in both types of constructs, the one composed of only hydrogel and the one composed of hydrogel + culture medium, the swelling ratio increased after water submersion, reaching a plateau after three hours (T-3h). This plateau lays at approximately 40% for constructs composed only of the hydrogel, and at approximately 55% for the constructs composed of hydrogel + culture medium, indicating that constructs could no longer change shape.

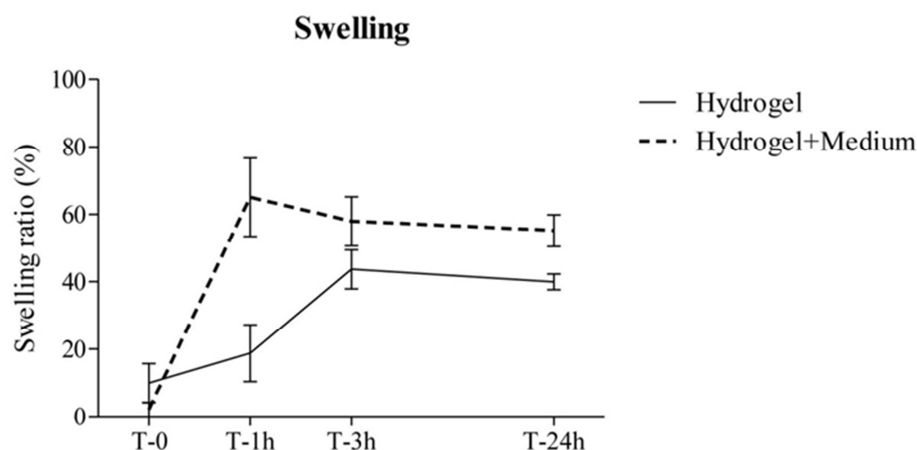


Figure 27. Swelling ratio analysis. Swelling ratio was evaluated in both constructs composed of only Cellink Bioink (Hydrogel) and in constructs composed of hydrogel + culture medium (Hydrogel + Medium). On the Y-axis the swelling ratio is indicated. After three hours (T-3h) in dH₂O the swelling ratio in both types of constructs reaches a plateau. Data were analyzed using a t-test followed by the Mann–Whitney test. Error bars indicate SEM (GraphPad Prism 8) (modified from Scarian *et al.*, 2022 [547]).

Moreover, the mass swelling ratio of both types of constructs, at each time point, did not exceed the value of 2 (Table XI). A low mass swelling ratio is preferred since its value affects the geometry of the structures. A small mass swelling ratio allows only minimal change in the geometry [564, 570].

Table XI. Mass swelling ratio of printed structures (modified from Scarian *et al.*, 2022 [547]).

Type of constructs	Mass swelling ratio
Hydrogel T-0h	1,10
Hydrogel + Medium T-0h	1,02
Hydrogel T-1h	1,19
Hydrogel + Medium T-1h	1,65
Hydrogel T-3h	1,44
Hydrogel + Medium T-3h	1,58
Hydrogel T-24h	1,40
Hydrogel + Medium T-24h	1,55

Finally, porosity indicates the amount of pore space in the hydrogel and is linked with nutrient and oxygen diffusion. Results of porosity test showed that the constructs composed of both hydrogel + cell medium had a higher porosity percentage (near 36%) when compared to the ones composed of only Cellink Bioink, which reaches a value near 27% (Figure 28).

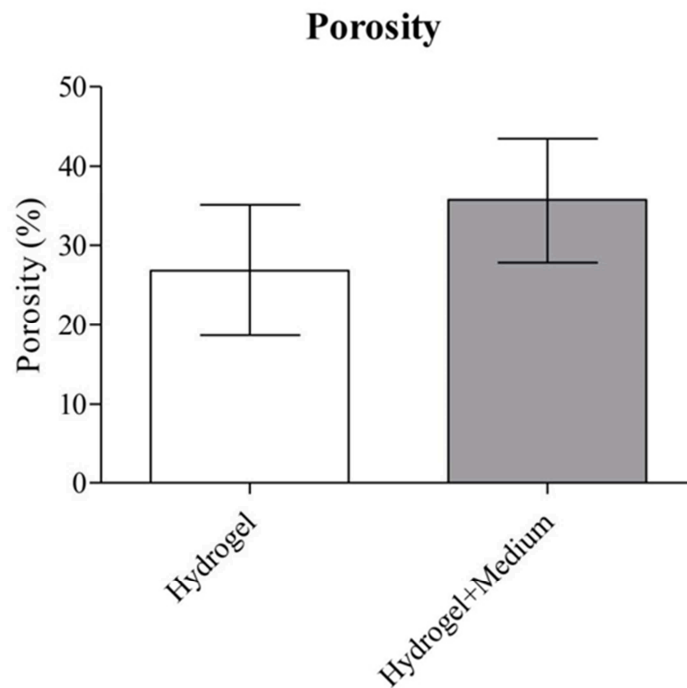


Figure 28. Porosity percentage analysis. Porosity percentage was evaluated in both constructs composed of only Cellink Bioink (Hydrogel) and in constructs composed of the hydrogel + culture medium (Hydrogel + Medium). On the Y-axis the porosity percentage is indicated. In the first type of construct the porosity percentage reaches a value near 27%, whereas in the second type of construct the value increases to 36%. Data were analyzed using a t-test followed by the Mann–Whitney test. Error bars indicate SEM (GraphPad Prism 8) (modified from Scarian *et al.*, 2022 [547]).

Printing in Cellink Bioink allows a good viability of cells during 3D differentiation

We performed LIVE/DEAD viability assay to evaluate the capability of cells to proliferate during the differentiation process in Cellink Bioink. We first included NSCs in the hydrogel and printed them at 25 °C at a pressure between 45 and 70 kPA. LIVE/DEAD assay was performed at each differentiation step.

We observed an increase in cell viability when cells are printed and differentiated in 3D. Moreover, we found statistically significant differences between NSCs and iMNs (day 0 vs. 14, ** $p < 0.01$), between NSCs and MNs (day 0 vs. 20, *** $p < 0.001$) and between MNPs and MNs (day 7 vs. 20, ** $p < 0.01$) (Figure 29), indicating that the hydrogel and the printing process did not interfere with cells viability.

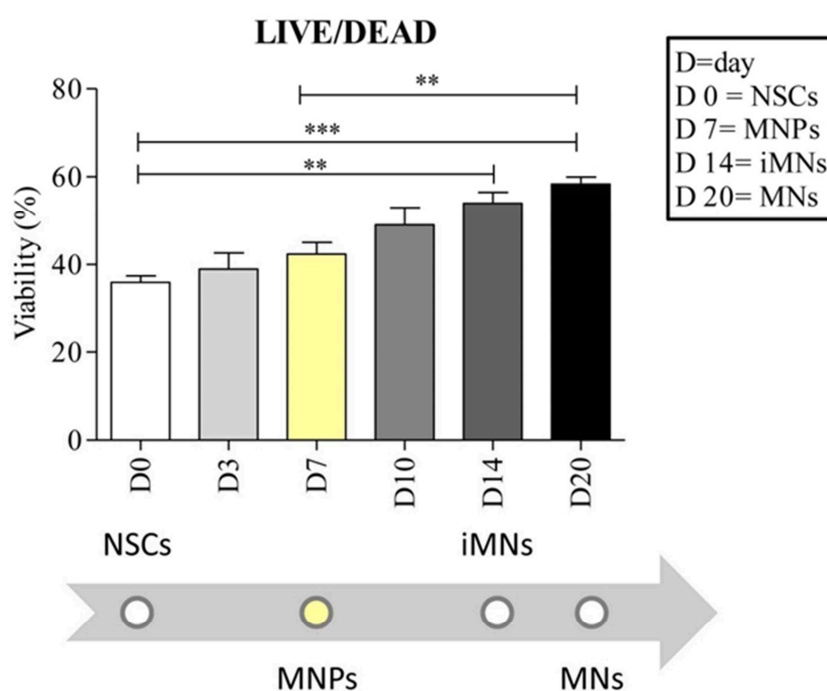


Figure 29. Viability assay performed on cells during differentiation process in Cellink Bioink hydrogel. On the Y-axis the viability percentage is indicated. The cell viability was evaluated at day 0, 3, 7, 10, 14 and 20 after NSCs printing and the beginning of differentiation into MNs. After 7 days cells reach the stage of MNPs (yellow bar), the first stage of cell specialization into MNs, and viability is increased by 18% compared to day 0, whereas at day 14 they reach the stage of iMNs with an increase in viability of 50% compared to day 0. At day 20 NSCs are differentiated into MNs with an increase of viability of 62% compared to day 0. Statistically significant differences were found between NSCs and iMNs (day 0 vs. 14, ** $p < 0.01$), between and MNs (day 0 vs. 20, *** $p < 0.001$) and between MNPs and MNs (day 7 vs. 20, ** $p < 0.01$). Data were analyzed using ANOVA, followed by the Bonferroni test. Error bars indicate SEM (GraphPad Prism 8) (modified from Scarian *et al.*, 2022 [547]).

NSCs maintain differentiation capability when printed in Cellink Bioink hydrogel

As for 6% SA-4% GEL hydrogel, we tested if Cellink Bioink hydrogel allowed the correct differentiation of NSCs into MNs. We printed NSCs and differentiated them in Cellink Bioink hydrogel as previously described, and then we performed an IF analysis for the markers of the differentiation stages. Finally, we analyzed cells at confocal microscope.

From the 3D reconstruction we noticed that both CTRL and sALS cells, at each step, formed colonies and expressed the typical markers of the differentiation stage. These results allowed us to conclude that the inclusion and printing in the hydrogel did not interfere with the correct differentiation process (Figure 30). Moreover, as for 6% SA-4% GEL hydrogel, it is evident the thickness of the colonies which we cannot be appreciated in 2D confocal images (Figure 23).

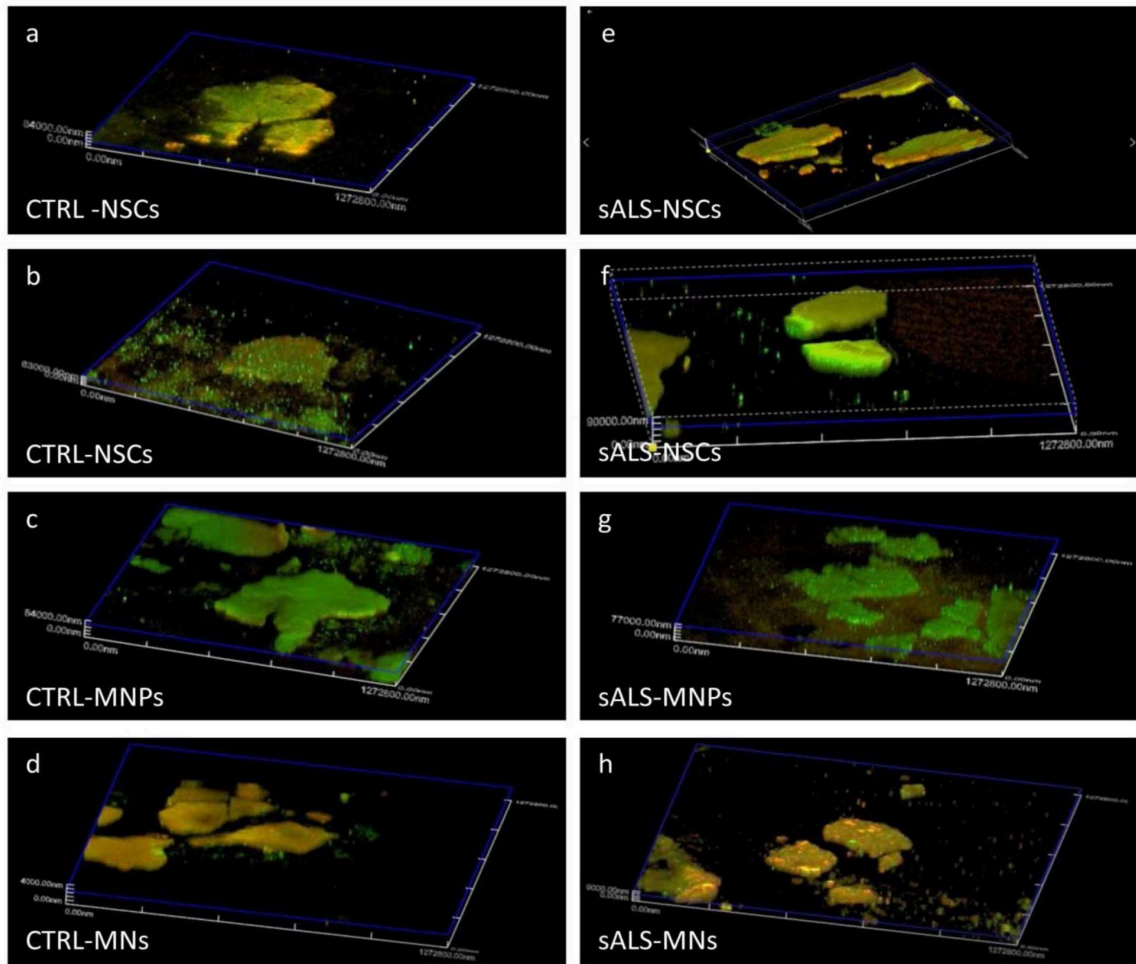


Figure 30. IF analysis performed on CTRL and sALS cells included in Cellink Bioink hydrogel, at each differentiation step. NSCs from CTRL and sALS subject were printed in Cellink Bioink hydrogel and differentiated into MNPs and MNs. Cells express the typical markers of differentiation at each stage: NSCs express Nestin=green and SOX2=red (a and e); NSCs express SOX1=green and PAX6=red (b and f); MNPs express Olig2=green and PAX6= red (c and g); MNs express TUBB3= green and ChAT=red (d and h). Images come from videos acquired through confocal microscopy (available at <https://www.mdpi.com/article/10.3390/ijms23105344/s1>) (modified from Scarian *et al.*, 2022 [547]).

Finally, we performed CTCF analysis for the different layers of the confocal reconstruction, normalizing the first layer to 1. We found that, for almost every differentiation step, the layer at approximately 75 μm from the beginning of the construct is the one with the maximum IF intensity (Figure 31).

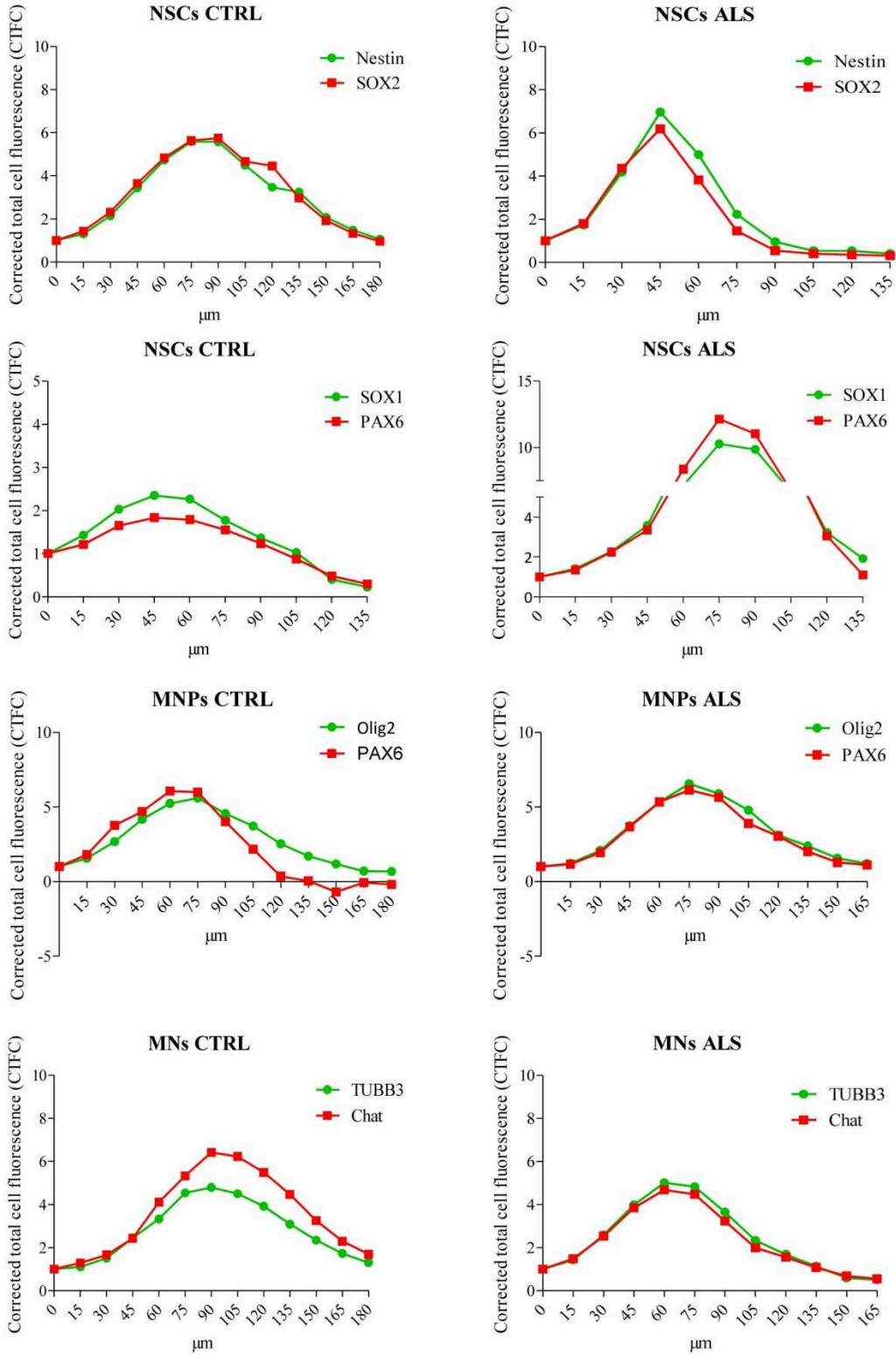


Figure 31. CTCF in 3D constructs layers. We calculated CTCF value for each layer of NSCs, MNPs and MNs of both CTRL and sALS constructs. On the Y-axis the CTCF value is indicated. CTCF of the first layer was normalized to 1. At each differentiation stage the layer around 75μm is the one with the maximum IF intensity (modified from Scarian *et al.*, 2022 [547])

4.1.4 RT-qPCR confirms the good differentiation in 3D

To have a more quantitative measure of marker's expression and confirm the correct differentiation of NSCs, from both CTRL and sALS subjects, in Cellink Bioink, we performed a RT-qPCR for the expression of *Nestin*, *SOX2*, *SOX1*, *PAX6* in NSCs, *PAX6* and *Olig2* in MNPs, *TUBB3* and *MAP2* in MNs. As we can notice in Figure 32, cells, at each differentiation step, expressed the expected markers, confirming that Cellink Bioink did not interfere with differentiation.

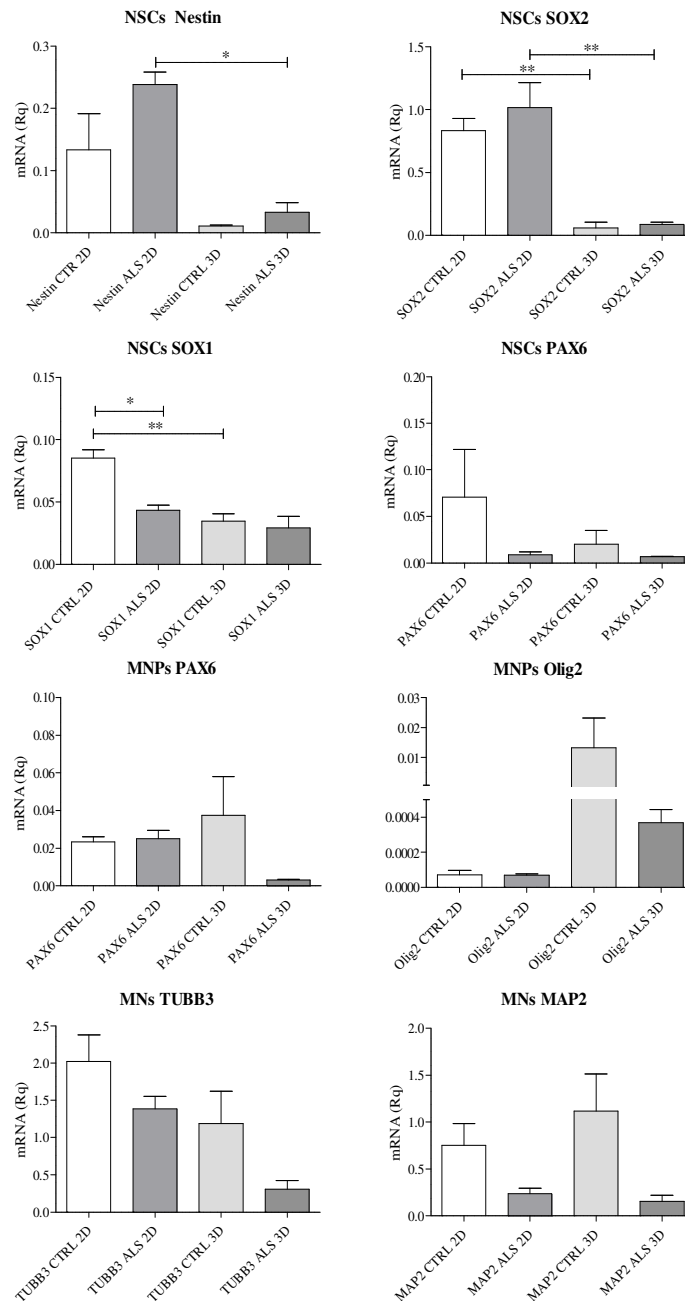


Figure 32. RT-qPCR with the markers of each differentiation step. The differentiation was confirmed using different markers for each stage: *Nestin*, *SOX2*, *SOX1* and *PAX6* for NSCs, *PAX6* and *MAP2* for MNPs, *TUBB3* and *MAPP2* for MNs. On the Y-axis the Rq value is indicated. Data were analyzed using ANOVA, followed by the Bonferroni test. * p < 0.05; ** p < 0.01 (GraphPad Prism 8). Error bars indicate SEM (modified from Scarian *et al.*, 2022 [547]).

We can notice that 3D cultured NSCs showed a reduction in *Nestin*, *SOX2* and *SOX1* expressions when compared to 2D condition (*p < 0.05 and ** p < 0.01). Furthermore, sALS NSCs showed, both in 2D and 3D, a higher expression of *Nestin* and *SOX2* when compared to CTRL cells, whereas they showed a reduction of *SOX1* and *PAX6*.

We also found that sALS MNPs, especially in 3D, showed a lower expression of *PAX6* and *Olig2*. Moreover, in both sALS and CTRL, 3D printed MNPs showed a higher *Olig2* expression.

sALS cells expressing MNs markers, showed a reduction when compared to CTRL, both in 2D and in 3D. Finally, 3D CTRL MNs showed an increase in *MAP2* expression and a reduction in *TUBB3* expression when compared to 2D cultured cells.

Printing process in Cellink Bioink hydrogel does not interfere with the electrophysiological characteristics of NSC34

As with 6% SA-4% GEL hydrogel, we performed a c-Fos assay to evaluate the electrophysiological characteristics of differentiated NSC34.

We found that, both 2D and 3D-cultured cells, showed a statistically significant increasing of firing after the KCl treatment (** p < 0.01). The analysis of the IF intensity allowed us to conclude that the hydrogel and the printing process did not interfere with the electrophysiological characteristics of NSC34. Moreover, we noticed that untreated 3D NCS34 showed a low firing intensity, which was not observed in 2D cultures, probably due to a background fluorescence caused by the hydrogel itself (Figure 33).

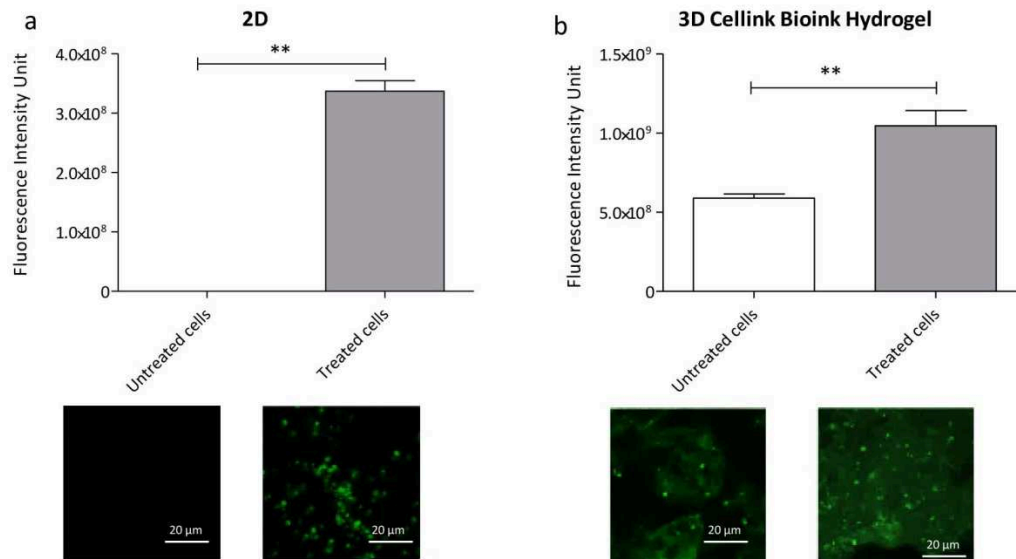


Figure 33. IF analysis for the electrophysiological characterization of NSC34 included in Cellink Bioink hydrogel. On the Y-axis the fluorescence intensity unit value is indicated. NSC34 cells, both in 2D (a) and 3D (b) were induced to produce action potentials through 15 mM KCl. In both 2D and 3D cells fire after the treatment. Data were analyzed using a t-test followed by the Mann–Whitney test. ** $p < 0.01$ (GraphPad Prism 8). Error bars indicate SEM. Scale bar = 20 μm (modified from Scarian *et al.*, 2022 [547]).

4.2 Organoids

Morphological characterization shows an alteration in sALS MNOs

We evaluated by bright field the morphological characteristics of organoids at days 1, 7, 14, 21 and 28. At day 1 organoids began to form and at day 7 they are NSCs organoids. We then began the differentiation to MNOs. At day 14 they reached the stage of MNPOs, at day 21 the stage of immature MNOs and at day 28 the stage of MNOs. By bright field we noticed that during the differentiation process there was an increase of both CTRL and sALS organoids area (Figure 34).

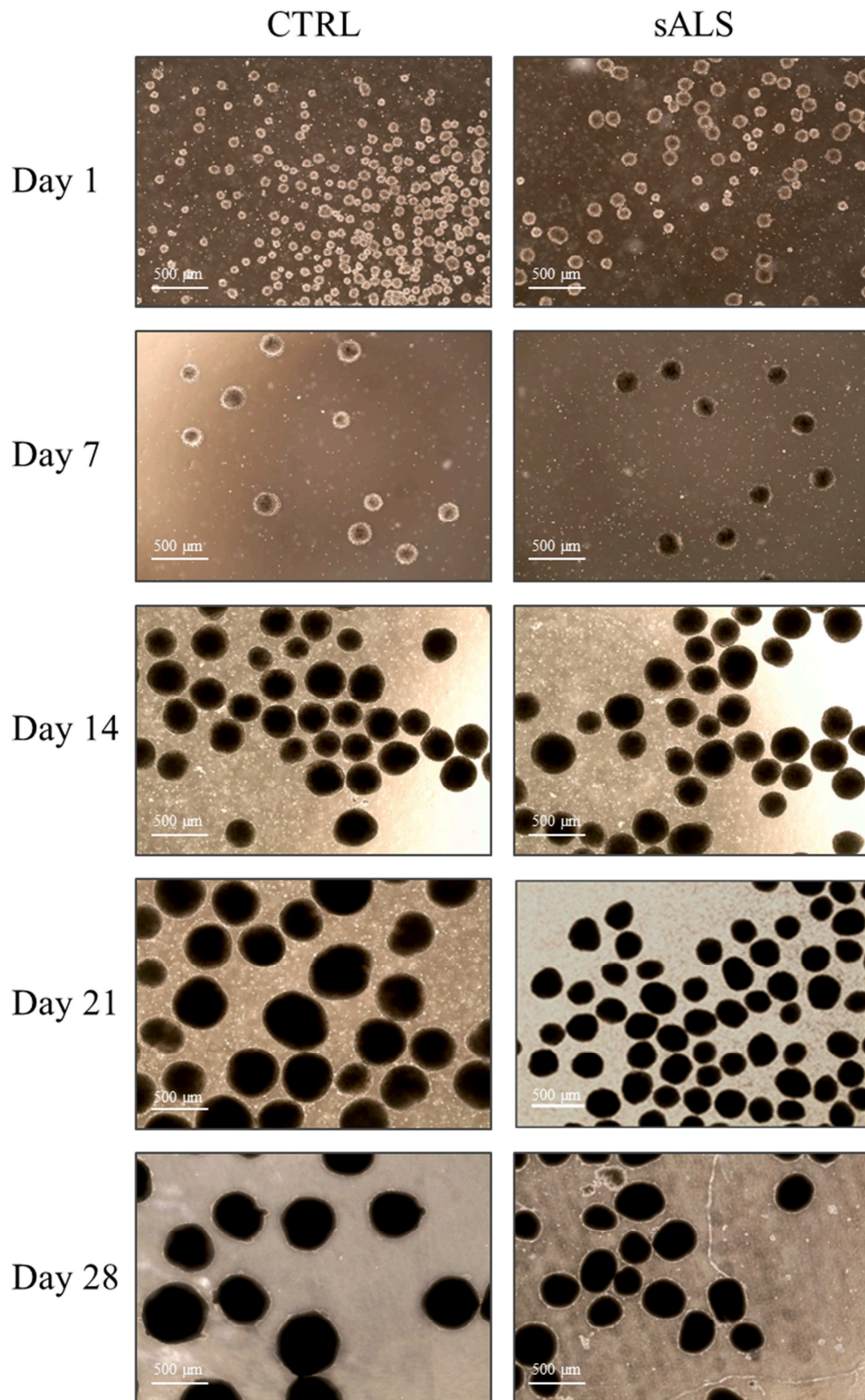


Figure 34. Bright-field images at days 1, 7, 14, 21 and 28 of CTRL and sALS organoids during differentiation. NSCs were differentiated for 28 days to obtain MNOs. Organoids area showed an increase during the differentiation process. Scale bar= 500 μm .

Moreover, we measured the area at the different days using ImageJ software (Figure 35 a). Till day 7, sALS organoids showed a bigger area when compared to CTRL ones, although without statistically significant differences (Figure 35 b). This trend started to revert from day 10. Until the end of differentiation, CTRL organoids were bigger than sALS ones, with significant differences at days 17 (***) $p < 0.001$), 21 (*) $p < 0.05$), 24 (*) $p < 0.05$) and 28 (*) $p < 0.05$).

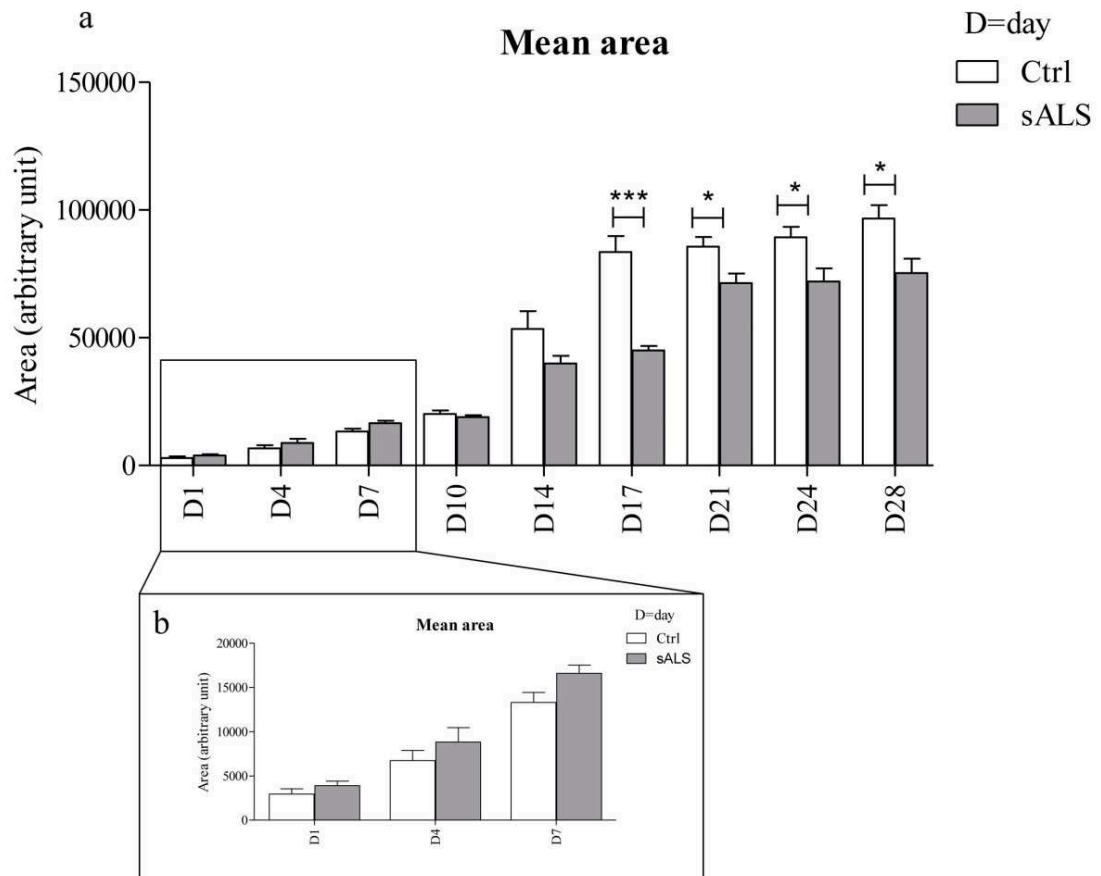


Figure 35. Analysis of CTRL and sALS organoids area during differentiation. Area at days 1, 4, 7, 10, 14, 17, 21, 24 and 28 was calculated using ImageJ software (a). sALS organoids seemed to have a bigger area than CTRL organoids without significant differences at days 1, 4 and 7 (b). From day 10 the trend is inverted, and CTRL organoids showed a bigger area with significant differences at days 17 (***) $p < 0.001$), 21 (*) $p < 0.05$), 24 (*) $p < 0.05$) and 28 (*) $p < 0.05$). Data were analyzed using a t-test followed by the Mann–Whitney test (GraphPad Prism 8). Error bars indicate SEM.

Finally, we evaluated the roundness of organoids at day 28, stage at which they are completely differentiated into MNOs, finding that CTRL MNOs showed a more regular shape when compared to sALS MNOs (* $p < 0.05$) (Figure 36).

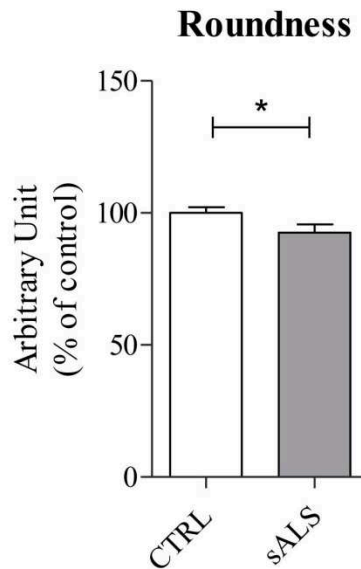


Figure 36. Analysis of CTRL and sALS MNOs roundness at day 28. Roundness was evaluated at day 28 using ImageJ software. CTRL MNOs showed a more regular shape when compared to sALS one (* $p < 0.05$). Data were analyzed using a t-test followed by the Mann–Whitney test (GraphPad Prism 8). Error bars indicate SEM.

Immunofluorescence analysis demonstrates that sALS MNOs have an increase in Nestin expression and a decrease in neurite length

We first performed an IF analysis using Nestin as a marker of undifferentiated cells [549]. Images confirmed the morphological characterization yet observed by bright field. As shown in Figure 37, sALS MNOs exhibited a more irregular shape when compared to CTRL (Figure 37 a and b). Moreover, with the ImageJ analysis we found a significant increase in Nestin expression in sALS MNOs when compared to CTRL (* $p < 0.05$) (Figure 37 c), suggesting the major presence of undifferentiated cells. Finally, we measured the length of neurites in Nestin positive cells. ImageJ analysis showed a decreased in the length of sALS neurites (**** $p < 0.0001$) (Figure 37 d).

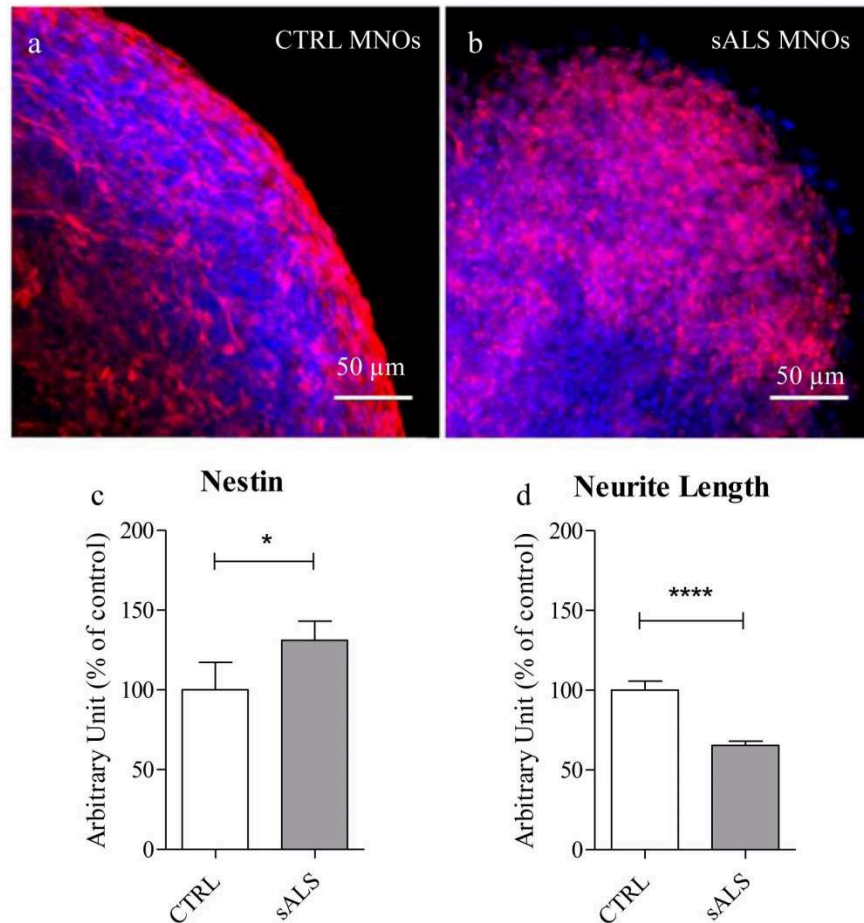


Figure 37. IF analysis for Nestin of CTRL and sALS MNOs. NSCs from both CTRL and sALS iPSCs were differentiated into MNOs. MNOs were then stained with Nestin= red and nuclei were stained with DAPI= blue (a and b). sALS MNOs showed an increase in Nestin positive cells (c) and a decrease neurite length (d). Scale bar= 50μm. Data were analyzed using a t-test followed by the Mann–Whitney test. **** p < 0.0001, * p < 0.05 (GraphPad Prism 8). Error bars indicate SEM.

sALS MNOs show an increasing trend in GFAP expression and a decreasing trend in TUBB3 expression. GFAP+ layer thickness results higher in sALS MNOs

We stained MNOs with markers of both glial (GFAP) [571] [572] neural cells (TUBB3) [557] (Figure 38 a and b). The ImageJ analysis revealed that, even if it was not found any significant difference between CTRL and sALS MNOs as regard to GFAP and TUBB3 expression, there was an increasing trend for GFAP and a decreasing trend for TUBB3 in sALS MNOs when compared to CTRL ones (Figures 38 c and d). Moreover, we found a significant increase in the thickness of GFAP+ layer in sALS MNOs when compared to CTRL (**p<0.001), indicating a major presence of gliosis (Figure 38 e). Moreover, the IF analysis confirmed the more irregular shape of sALS MNOs when compared to CTRL.

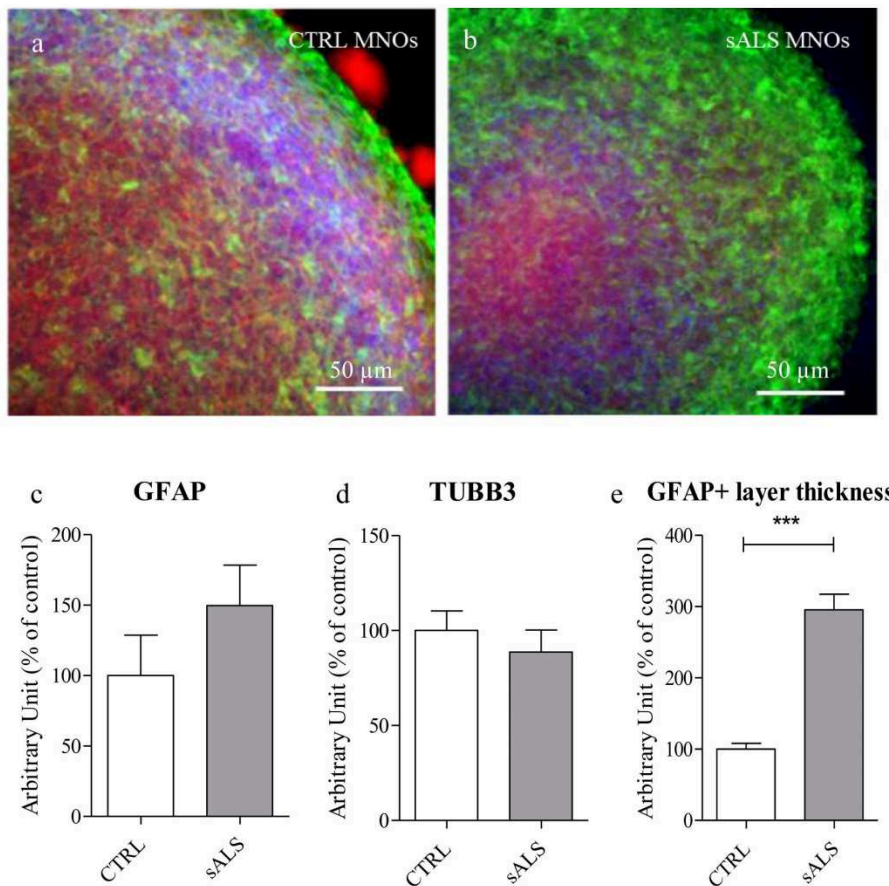


Figure 38. IF analysis for GFAP and TUBB3 of CTRL and sALS MNOs. NSCs from both CTRL and sALS iPSCs were differentiated into MNOs. MNOs were stained with GFAP=green and TUBB3=red and nuclei were stained with DAPI=blue (a and b). sALS MNOs showed an increasing trend in GFAP expression (c) and a decreasing trend in TUBB3 expression (d) when compared to CTRL MNOs, although without statistically significant differences. Moreover, sALS MNOs showed an increase in GFAP+ layer thickness (e). Data were analyzed using a t-test followed by the Mann-Whitney test. *** $p < 0.001$ (GraphPad Prism 8). Error bars indicate SEM.

sALS MNOs shows a decrease in MNs markers expression

We stained MNOs for two MNs markers, the insulin enhancer protein (ISL1) [573, 574] and the MNs homeobox gene (HB9) [575, 576]. We noticed also from these IF analyses that the border of sALS MNOs resulted more irregular when compared to CTRL ones (Figure 39 a and b). Moreover, the ImageJ analysis revealed a decreasing trend in ISL1 expression and a statistically significant decrease in HB9 expression in sALS MNOs (**** $p < 0.0001$), indicating a decrease in MNs number in sALS MNOs (Figure 39 c and d).

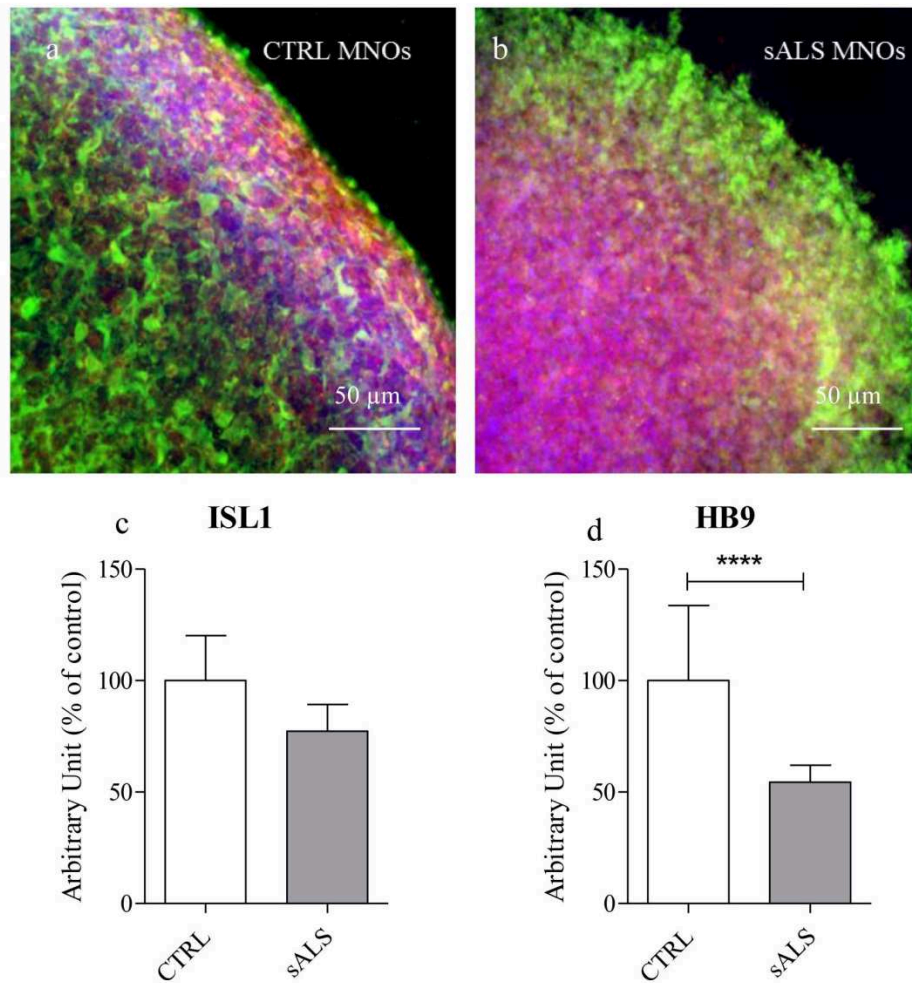


Figure 39. IF analysis for ISL1 and HB9 of CTRL and sALS MNOs. NSCs from both CTRL and sALS iPSCs were differentiated into MNOs. MNOs were stained with ISL1=green and HB9=red and nuclei were stained with DAPI=blue (a and b). sALS MNOs showed a decrease trend in ISL1 expression (c) and a statistically significant decrease in HB9 expression (d) when compared to CTRL MNOs. Data were analyzed using a t-test followed by the Mann–Whitney test. **** $p < 0.0001$ (GraphPad Prism 8). Error bars indicate SEM.

Bulk RNA-seq on CTRL and sALS 2D MNs and MNOs

A bulk RNA-seq analysis was performed to analyze the differences in transcriptome profiles not only between 2D MNs and MNOs but also between CTRL and sALS. As shown in table XII, when we compared sALS 2D MNs with CTRL 2D MNs, we found 382 DE genes, 71 downregulated and 311 upregulated. The number of DE genes was increased when we compared sALS MNOs with CTRL MNOs. In this case we found 2929 DE genes, 1322 downregulated and 1607 upregulated.

Table XII. Number of DE genes in the two groups

Groups	Number of DE genes	Dowregulated genes	Upregulated genes
sALS 2D MNs vs CTRL 2D MNs	382	71	311
sALS MNOs vs CTRL MNOs	2929	1322	1607

Considering the resulting transcripts, we constructed volcano plots to highlight all statistically significant DE genes between the four groups: sALS 2D MNs vs CTRL 2D MNs (Figure 40 a), sALS MNOs vs CTRL MNOs (Figure 40 b), CTRL MNOs vs CTRL 2D MNs (Figure 40 c) and sALS MNOs vs sALS 2D MNs (Figure 40 d).

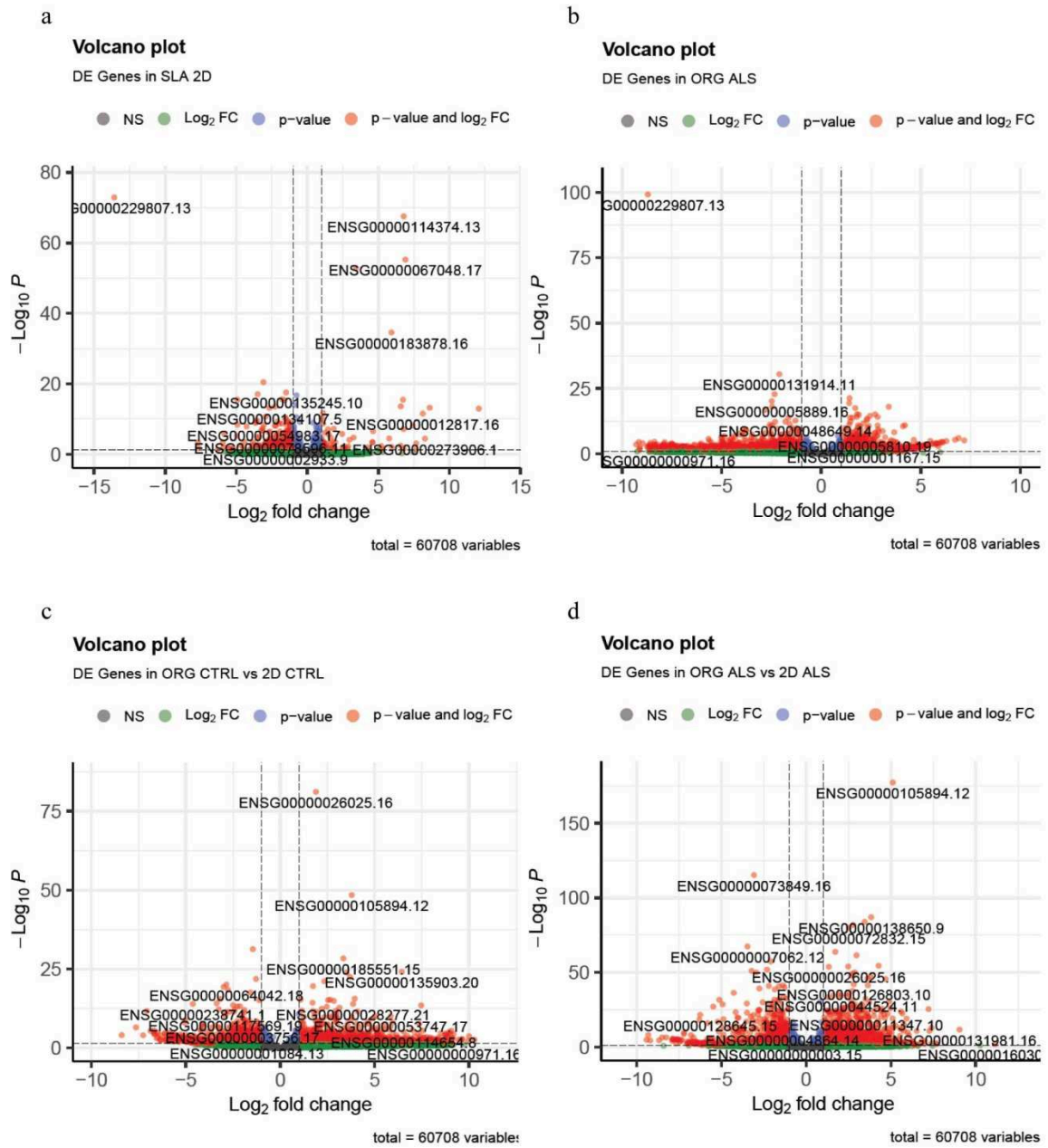


Figure 40. Volcano plots from bulk RNA-seq analysis. Volcano plots were obtained for DE genes for sALS 2D MNs vs CTRL 2D MNs (a), for sALS MNOs vs CTRL MNOs (b), for CTRL MNOs vs CTRL 2D MNs (c) and for sALS MNOs vs sALS 2D MNs (d). Genes with $|\log_2(\text{disease sample/healthy donor})| \geq 1$ and false discovery rate ≤ 0.1 were considered DE. Red dots are significantly up- and downregulated genes, whereas blue, green and grey ones are DE genes that are not significant. NS=non-significant; log₂FC = satisfying fold change criteria; P: satisfying p-value criteria; P and log₂FC: satisfying both fold change and p-value cut-off.

A principal component analysis (PCA) of 200 top DE genes in all groups was performed. As shown in figure 41 a division between the four groups is evident. Furthermore, the division between CTRL MNOs and sALS MNOs is more evident than the one between CTRL and sALS 2D MNs.

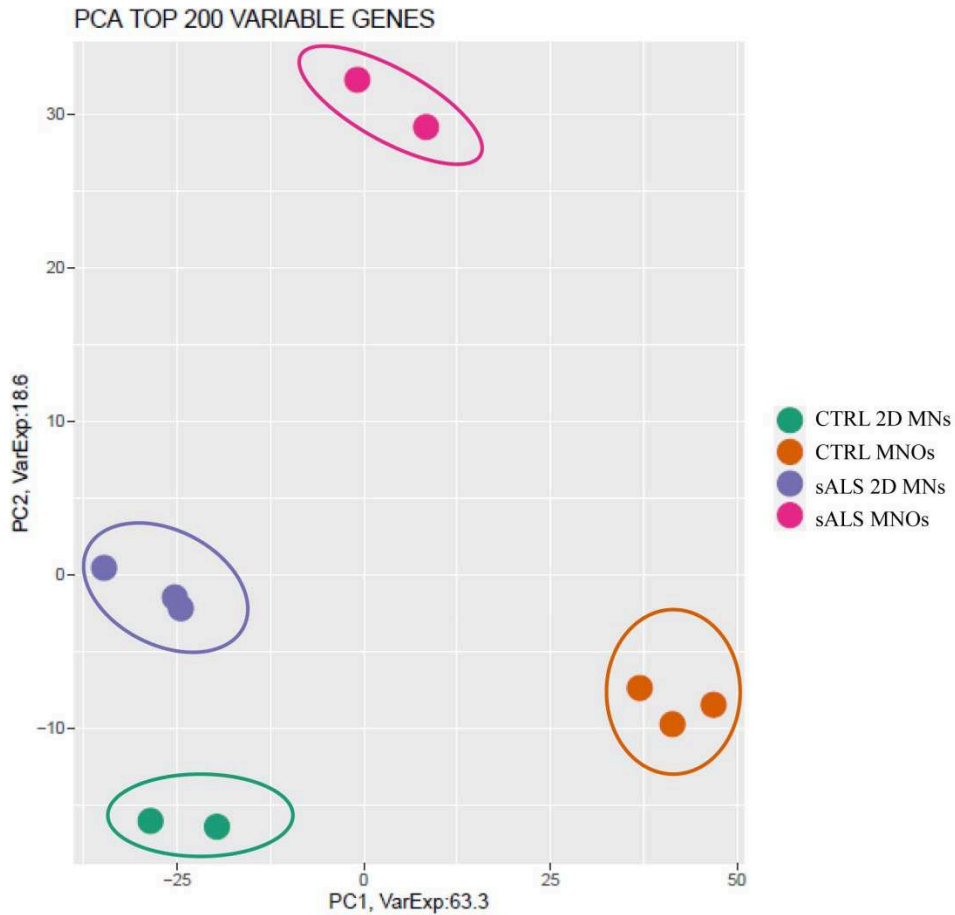


Figure 41. PCA of 200 top DE genes. PCA was performed between CTRL 2D MNS (green dots), CTRL MNOs (orange dots), sALS 2D MNS (violet dots) and sALS MNOs (pink dots). On the X-axis the value of the principal component 1 (PC1) is indicated. On the Y-axis the value of the principal component 2 (PC2) is indicated. The division between the four groups, and especially between CTRL MNOs and sALS MNOs, is evident.

Moreover, the heatmaps of 60 top DE genes of the four groups showed their different expression profiles (Figure 42).

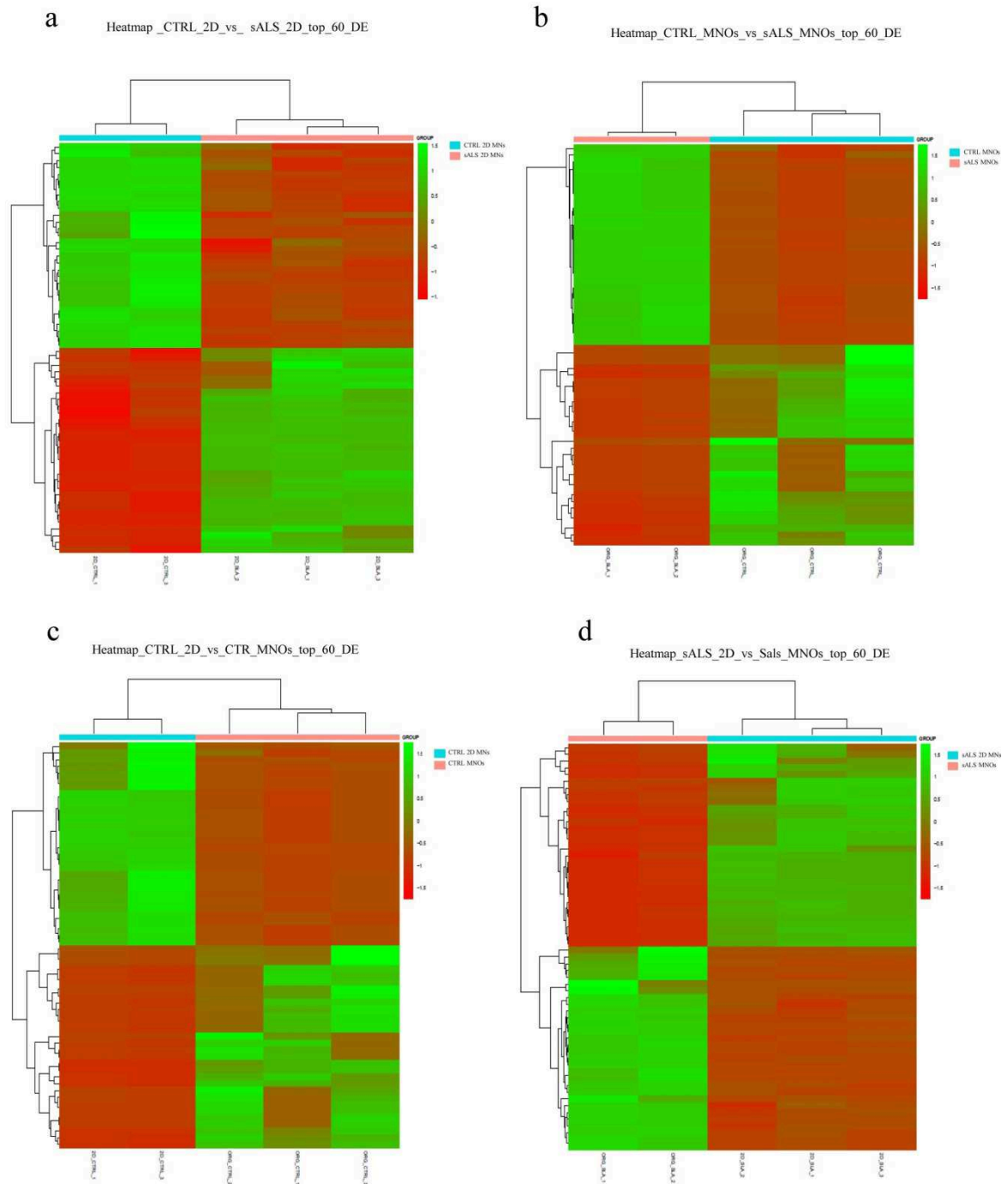


Figure 42. Heatmaps of the 60 top DE genes. Heatmaps were obtained for all the groups: CTRL 2D MNs (blue bar) vs sALS 2D MNs (pink bar) (a), CTRL MNOs (blue bar) vs sALS MNOs (pink bar) (b), CTRL 2D MNs (blue bar) vs CTRL MNOs (pink bar) (c) and sALS 2D MNs (blue bar) vs sALS MNOs (pink bar) (d). There is an evident division between the four groups' expression profiles.

We compared the DE genes of sALS 2D MNs and sALS MNOs and we found 116 common DE genes (Figure 43 a). Among these genes, only two are classified as glial proteins. The analysis of cell populations in these two groups by RNA-seq deconvolution confirmed the presence of oligodendrocytes and astrocytes in MNOs (Figure 43 c), which were not found in 2D MNs (Figure 43 b).

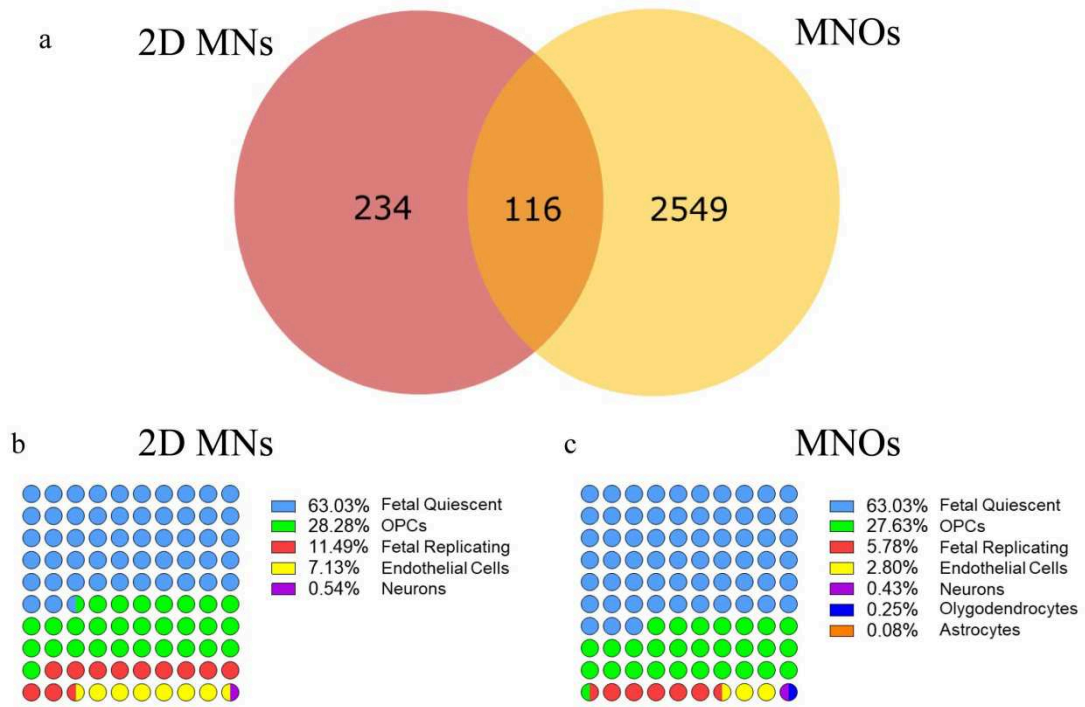


Figure 43. Number of DE genes of sALS 2D MNs and sALS MNOs and deconvolution analysis. The analysis of DE genes showed that 2D MNs and 2D MNOs share 116 DE genes (a). The analysis of cell populations individuated oligodendrocytes and astrocytes in MNOs (c), which are not present in 2D MNs (b).

Finally, we performed a GO term enrichment analysis for DE genes in sALS 2D MNs vs CTRL 2D MNs and sALS MNOs vs CTRL MNOs for both upregulated and downregulated DE genes together. Analyzing the GO chords, we found that, whereas in sALS 2D MNs the DE genes were involved in nervous system development, neuron projection morphogenesis, regulation of inclusion body assembly and chemical synaptic transmission (Figure 44 a), the DE genes in sALS MNOs were related to ECM organization, axogenesis, axon guidance, extracellular structure organization and external encapsulating structure organization (Figure 44 b).

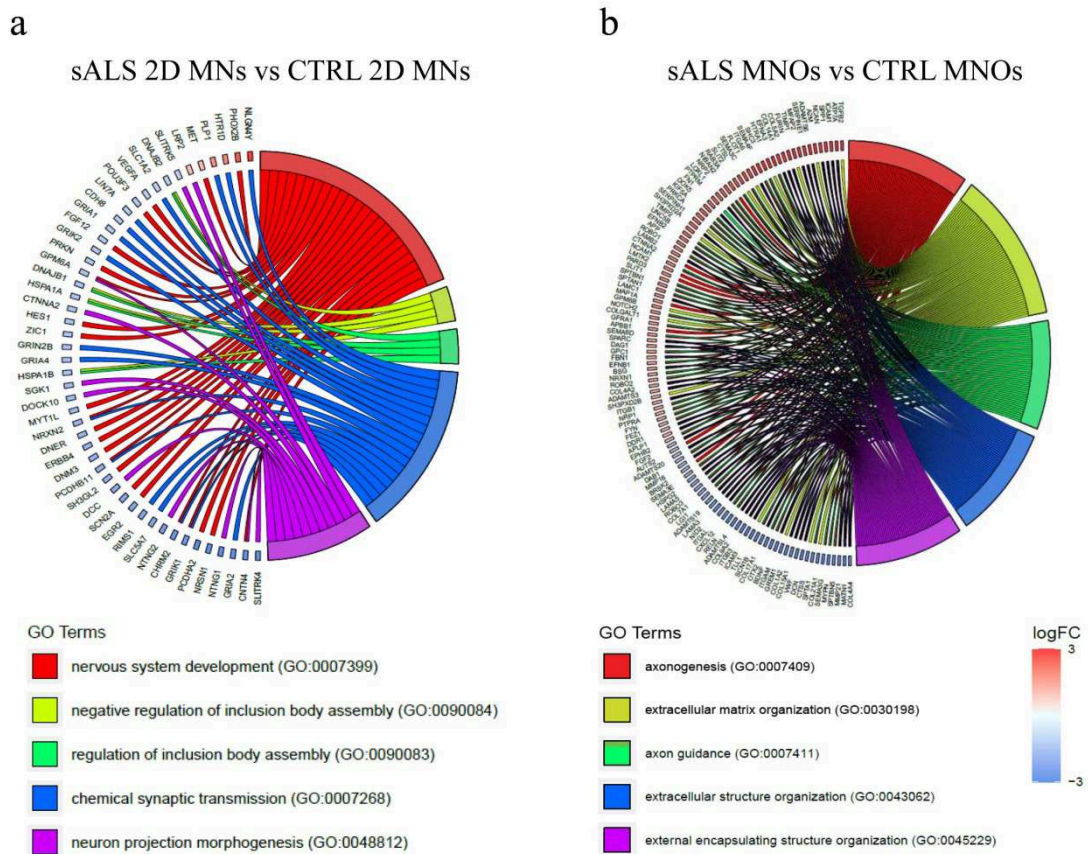


Figure 44. Gene ontology analysis of cellular components category. A GO analysis comparing sALS 2D MNs vs CTRL 2D MNs (a) and sALS MNOs vs CTRL MNOs (b) for all DE genes was performed. In sALS 2D MNs the DE genes were involved in nervous system development, neuron projection morphogenesis, regulation of inclusion body assembly and chemical synaptic transmission (a), in sALS MNOs the DE genes were related to ECM organization, axonogenesis, axon guidance, extracellular structure organization and external encapsulating structure organization (b). Color refers to different pathways connected to respective DE.

We validated by RT-qPCR some ECM-related genes found in MNOs, and we confirmed the upregulation in sALS MNOs of osteopontin (*OPN*) gene expression (* $p < 0.05$), the increasing trend of Neurocan (*NCAN*), TIMP Metallopeptidase Inhibitor 1 and 2 (*TIMP1* and *TIMP2*), Flotillin 1 (*FLOT1*), Cathepsin L1 (*CTSL*), Lysyl Oxidase Like 1 (*LOXLI*), Fibronectin 1 (*FNI*) and Amyloid β Precursor Protein (*APP*) genes expression and the decreasing trend of Collagen type IX alpha 2 chain (*COL9A2*), Orthodenticle Homeobox 2 (*OTX2*), and Collagen type IV alpha 4 chain (*COL4A4*) genes expression (Figure 45).

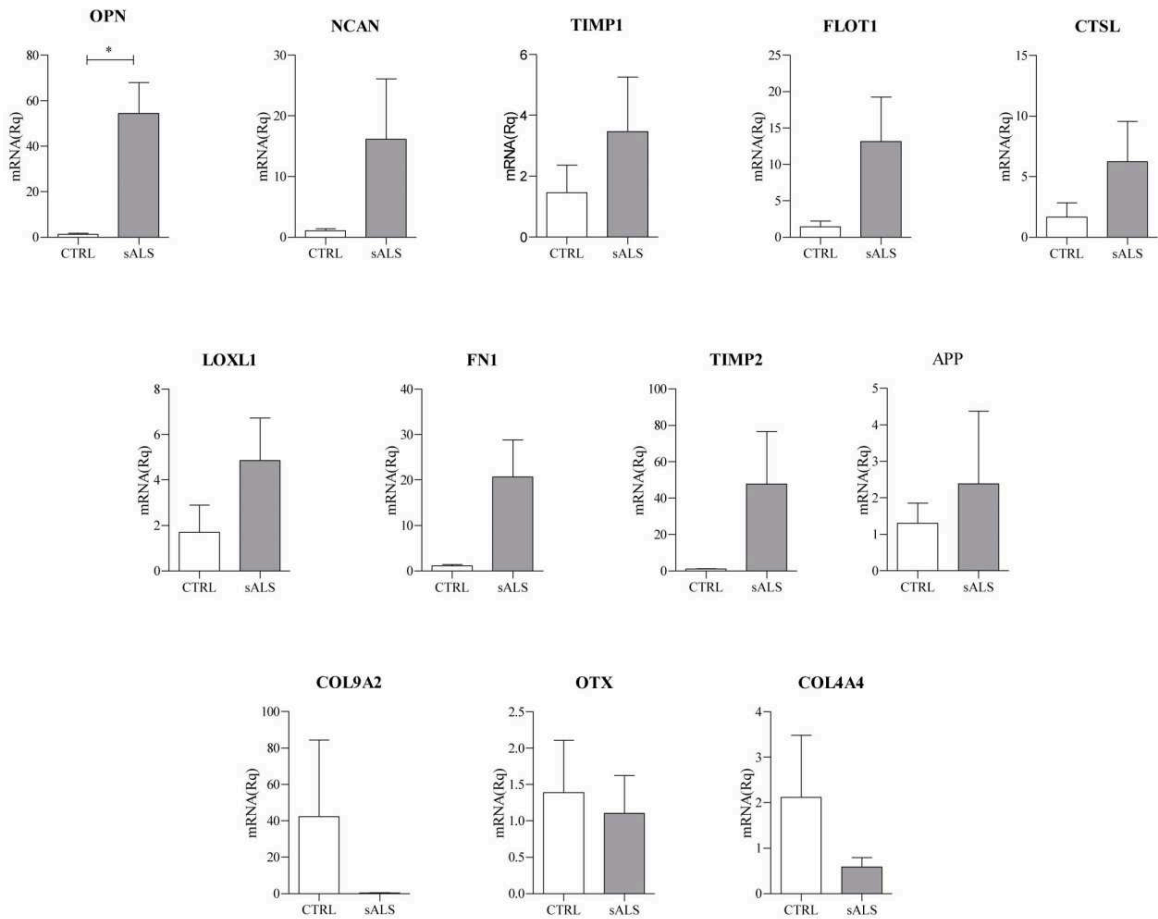


Figure 45. Validation by RT-qPCR of ECM-related genes. Deregulation in sALS MNOs of ECM-related genes (*OPN*, *NCAN*, *TIMP1*, *FLOT1*, *CTSL*, *LOXLI*, *FN1*, *TIMP2*, *APP*, *COLP9A2*, *OTX*, *COLA4A*) was validated by RT-qPCR. The upregulation of the first 9 genes and the downregulations of the last 3 genes were confirmed. On the Y-axis the Rq value is indicated. Data were analyzed using a t-test followed by the Mann–Whitney test. * $p < 0.05$ (GraphPad Prism 8). Error bars indicate SEM.

5. DISCUSSION AND CONCLUSIONS

NDDs are becoming a great problem due to their increasing rate in the world. They are the causes of difficulties in patients' lives and economy costs for the society [2, 17].

It is even more important to find a good model for the study of their aetiopathogenesis, and in last years many *in vitro* and *in vivo* models have emerged [94, 100].

3D cellular models are emerging as innovative cell culture systems inasmuch they can mimic better the physiological environment in which cells live and show the interaction between cells [118]. Two of the main 3D techniques are 3D bioprinting and organoids. In this study we developed new 3D models for the study of ALS pathology differentiating both CTRL and sALS NSCs into MNs.

As regard to 3D bioprinting, we studied two different types of hydrogels, a homemade and a commercial one. We wanted to test if a homemade hydrogel could be a good alternative to a more expensive commercial one. For both the hydrogels we first performed mechanical tests, and then they were tested for cell viability, for their capacity to allow NSCs differentiation into MNs and for their electrophysiological characteristics. These experiments allowed us to compare the two different hydrogels.

We first developed a homemade hydrogel composed of SA and GEL, testing different concentrations for printability and different sterilization methods. We concluded that the best concentrations of SA and GEL are 6% and 4% respectively, and the best parameters for printing are a temperature of 25°C and a printing pressure between 35 and 70 kPa. This hydrogel allowed a good printing resolution and the maintenance of constructs' shape. Moreover, we tested different methods of hydrogel sterilization, concluding that pasteurization was the only method compatible with both SA and GEL.

In parallel, we tested the mechanical characteristics (moisture, swelling and porosity) of Cellink Bioink, a commercial bioink composed of cellulose nanofibrils and alginate. We tested both constructs composed only of the hydrogel and constructs composed of hydrogel and cell medium. We found that the moisture in both the construct types exceeds 95%. Moisture indicates the water content of the structures, and it facilitates solubility and compounds diffusion [562, 577]. Precedent studies have already reported a moisture percentage above 90%, indicating a high amount of water in gelatin-based hydrogels [562, 563]. Moreover, prior research showed that the presence of hydrophilic groups in the hydrogel, which in Cellink Bioink are represented by the hydroxyl groups on the surface of the cellulose fibers and by the inherent hydrophilicity of alginate [578, 579], can affect the water content [562].

Moisture properties are directly linked to swelling ratio, which indicates the hydrogel ability to absorb water. The higher is the swelling ratio, the higher is the capacity of the

hydrogel to change its shape and break in a hydrated environment. Furthermore, crosslinking can reduce the space available for water in the hydrogel and, consequently, reduce the swelling ratio [564]. In our experiments, we found that constructs composed of both hydrogel and culture medium showed a higher swelling ratio when compared to the ones composed of only hydrogel. However, the swelling ratio of both the types of constructs reached a plateau around 3h after submersion, remarking the impossibility to change shape anymore. Finally, we tested porosity, an index of empty spaces in the hydrogel, linked with nutrient and oxygen diffusion [562]. We found that constructs composed of both hydrogel and cell medium showed a higher porosity percentage when compared to constructs composed of only hydrogel. This data allowed us to conclude that the addition of culture medium enables constructs to have a major nutrient diffusion.

Both 6% SA-4% GEL and Cellink Bioink hydrogels were tested to ascertain that they allow cells to maintain a good viability and proliferation during the differentiation process. We found that, in both the hydrogel types, viability is increased during differentiation. However, we noticed that, whereas Cellink Bioink allows a constant increase in cell proliferation and viability, in 6% SA-4% GEL hydrogel cells viability undergoes a non-significant decrease at days 7 and 14. Even so, our data suggested that both 6% SA-4% GEL homemade hydrogel and commercial Cellink Bioink allow a good viability during the differentiation process.

The second step was to verify if cells, during the differentiation into MNs, expressed the typical markers of each step, to confirm the optimal differentiation process in 3D. At this purpose, we characterized NSCs with the typical markers Nestin [549] [550], SOX2 [551, 552], SOX1 [553, 554], PAX6 [555], MNPs with the markers PAX6 and Olig2 [556] and MNs with the markers TUBB3 [557, 558] and ChAT [559]. In both the types of hydrogels, we found, through confocal microscopy images, that during the differentiation both CTRL and sALS cells form colonies, which expressed the typical markers of the steps. When compared to 2D cultured cells, 3D constructs images showed the thickness of the colonies and allowed the study of cells organization and interconnections, as was already demonstrated in precedent studies [395, 580]. Surprisingly, 6% SA-4% GEL hydrogel showed a more evident background which did not allow to calculate the CTCF and have a quantification analysis of the markers expression. Cellink Bioink, on the contrary, showed less background fluorescence and the CTCF calculation revealed that the layer around 75 μm from the beginning of the construct is the one with the maximum IF intensity for almost every differentiation step in both CTRL and sALS conditions. Moreover, to confirm the results, we performed an RT-qPCR for the markers of the differentiation steps. This

analysis was possible only for Cellink Bioink hydrogel, because of the poor quality of RNA extracted from cells included in 6% SA-4% GEL hydrogel. It was already demonstrated that the low yield of RNA obtained from encapsulated cells is a result of complexing between negatively charged RNA and positively charged matrix [581, 582]. By RT-qPCR we confirmed that Cellink Bioink did not interfere with the expression of the typical differentiation markers, besides for the expression of NSCs. An expression reduction after printing was already reported by Jeon *et al.* (2017) for the *ASGR1* gene [583]. We noticed that differences between CTRL and sALS are maintained after printing and that *Nestin* and *SOX2* have a higher expression, both in 2D and in 3D, in sALS NSCs than in CTRL ones, whereas *SOX1* and *PAX6* are more expressed in CTRL. Different studies considered *Nestin* and *SOX2* as markers of more “immature” NSCs, inasmuch they are a marker of undifferentiated nervous cells before the exit of cell cycle and commitment and a marker involved in self-renewal, respectively [549, 551, 580]. *PAX6* and *SOX1* are considered markers of more “mature” NSCs: *PAX6* is a marker also of MNPs and *SOX1* was found to typify activated neural stem progenitors and to be a neuroectodermal lineage marker at first stages of development [554, 584, 585]. For these reasons, we concluded that sALS NSCs seemed to be less differentiated than CTRL ones. In MNPs we observed a higher expression of *PAX6* in CTRL cells when compared to sALS MNPs, suggesting that sALS MNPs differentiate earlier than CTRL ones since *PAX6* is expressed also in more undifferentiated cells as NSCs. The high expression of *PAX6* indicates the presence of immature MNPs in CTRL cultures and thus a mixed population of mature and immature MNPs. Moreover, we observed that *PAX6* expression was low in both NSCs and MNPs. A precedent study found that stem cells undergo low to high *PAX6* levels during differentiation to neural stem cells, vanishing with the reaching of a more differentiated stadium [586]. Finally, we noticed that both CTRL and sALS printed MNPs, showed an increase in *Olig2* expression when compared to 2D cultured cells, indicating that the inclusion and printing in the hydrogel promotes MNPs maturation. At the step of MNs, we noticed a reduction of sALS cells expressing MNs markers. That aspect allows us to suppose a MNs death, which is a hallmark of ALS pathology. Moreover, in CTRL 3D cultured cells, we found an increase in *MAP2* expression and a decrease in *TUBB3* expression, when compared to 2D cultured cells. Precedent studies demonstrated that *TUBB3* is a marker of iMNs [587, 588], whereas *MAP2* a marker of MNs in a more mature stadium [588, 589]. These results allowed us to conclude that the 3D environment increases the differentiation of CTRL MNPs into MNs.

Finally, we tested both 6% SA-4% GEL and Cellink Bioink hydrogels, in order to understand if included and printed NSC34 maintain their electrophysiological activity. We choose this type of cells inasmuch it was already demonstrated that they are a good model for the study of MNs. They share many characteristics with MNs (i.e. expression of ChAT, generation of action potentials, expression of neurofilament triplet proteins) and they recapitulate MNs development in an immortalized system. Furthermore, when stimulated with KCl, they are able to produce action potentials [590]. We tried different methods, such as patch clamp or Multi-Electrode Array, but, unfortunately, we did not obtain good data. The hydrogels formed a film around the cell membranes which prevented the adhesion of the patch pipette or to the Multi-Electrode Array electrodes.

Since different studies analyzed the electrophysiological characteristics of cells by IF or immunohistochemistry [591-593], we decided to perform an IF staining for the action potential marker c-Fos. We found that both types of hydrogels did not interfere with the capacity of cells to produce action potentials. However, we noticed that, meanwhile in 6% SA-4% GEL hydrogel untreated cells did not show any fluorescence intensity, Cellink Bioink included untreated cells showed a low fluorescence intensity, probably due to intrinsic autofluorescence of the bioink, as already seen in other hydrogels [566, 594]. Nevertheless, in both types of hydrogels, printed cells behave as 2D cultured cells, increasing their electrophysiological activity after 15mM KCl treatment, allowing us to conclude that both hydrogels did not interfere with the firing of included NSC34.

In the second part of this work, we focused on the optimization of a protocol for MNOs differentiation and their characterization. We differentiated CTRL and sALS NSCs in floating conditions and we obtained, after 28 days, MNOs. We compared the area of CTRL and sALS MNOs during all the formation and differentiation process. We found that till day 7 the area of sALS MNOs seemed to be higher than the one of CTRL MNOs, and that this trend is inverted from day 10, probably due to death of MNs caused by the pathology itself [300, 595, 596]. Smaller organoids were also observed in other neuronal pathological conditions, such as microencephaly and autoimmune diseases [597] [598]. The different size of sALS organoids compared to CTRL ones could also be due to a delay in the development of sALS MNOs. The delay could be not linked to the pathology, even if there are not evidences in this regard. Moreover, measuring the roundness at day 28, we found that CTRL MNOs exhibited a more regular shape than sALS ones.

We then performed IF analyses to characterize cells in both CTRL and sALS MNOs. We first marked MNOs with Nestin, as a marker of undifferentiated and immature cells [549].

We found an increase in Nestin expressing cells in sALS MNOs when compared to CTRL ones, allowing us to conclude that sALS MNOs presented a major number of undifferentiated cells. Similar results were found by RT-qPCR in NSCs included in 3D bioprinted constructs [547]. Furthermore, precedent works demonstrated a high presence and proliferation of Nestin positive NSCs in ALS animals, linked to the attempt to repair degenerated MNs [599-601]. Moreover, we measured neurites lengths of Nestin positive organoids cells, demonstrating a decrease in sALS neurites length when compared to CTRL ones, as already demonstrated by previous studies on ALS MNs [311, 602, 603].

We further stained MNOs with GFAP and TUBB3, markers of glial and neuron cells respectively [557, 558, 571, 572]. We found an increasing trend for GFAP and a decreasing trend for TUBB3 expression in sALS MNOs when compared to CTRL, and a significant increase in GFAP+ layer in sALS MNOs. These data confirmed an active gliosis in ALS. Different studies have demonstrated that astrocytes and microglia have an active role in ALS pathology, leading to an inflammatory response and to an important gliosis effect [71, 604-606]. Moreover, in 2007 Guan *et al.* found that the increase in *Nestin* expression in ALS affected mice was linked to the presence of reactive glia [600]. Furthermore, the data about *TUBB3* confirmed what found in RT-qPCR analysis in Cellink Bioink study, both for 2D and 3D cultured cells [547].

Finally, we marked MNOs for ISL1 and HB9. We found a reduction of both ISL1 and HB9 expression in sALS MNOs when compared to CTRL ones, suggesting a decrease in MNs number in sALS, inasmuch different studies found that ISL1 is essential for MNs development and maturation [573, 574] and that HB9 is involved in MNs differentiation [575, 576].

We then performed a bulk RNA-seq analysis on both CTRL and sALS 2D MNs and MNOs, to investigate the differences in transcriptome profiles between CTRL and sALS cells and between 2D cultured MNs and MNs developed in a 3D culture. Comparing sALS and CTRL 2D cultured MNs we found 382 DE genes (71 downregulated and 311 upregulated) meaning a different expression profile caused by the pathology itself, as previously demonstrated in PBMCs [607, 608] and in plasma derived from ALS patients [609]. Moreover, we found that the number of DE genes was increased when we compared sALS and CTRL MNOs with 2929 DE genes (1322 downregulated and 1607 upregulated). This data allows us to suppose that, with the use of MNOs, there is the possibility to study the deregulation of different pathways.

On these data, we constructed volcano plots to analyze the significant DE genes in all the four analyzed groups, confirming the different alteration degree in MNOs vs 2D MNs and

in ALS vs CTRL. We found a tenfold increase in the number of DE genes between CTRL and sALS MNOs. This data suggests an exacerbation of pathological signature of ALS. The PCA of 200 top DE genes allowed us to identify the evident division between the four groups' expression profiles with a larger difference between CTRL MNOs sALS MNOs, confirming the data about the number of DE genes. The division between CTRL and sALS 2D cultured MNs confirmed the differences found in plasma and PBMCs of ALS patients when compared to CTRL ones [608, 609]. The division of the four groups was further confirmed analyzing the heatmaps of 60 top DE genes.

Comparing the DE genes of sALS 2D MNs and sALS MNOs we found 116 common DE genes. Interestingly, only two of the 116 DE genes were related to glial proteins, suggesting the presence of glial population cells in MNOs but not in 2D cultured MNs. Through the analysis of cell populations in these two groups by RNA-seq deconvolution, we confirmed this hypothesis, finding oligodendrocytes and astrocytes in MNOs but not in 2D cultured cells. In last years, many studies have underlined the possibility to investigate glia formation and development using organoids. Moreover, only 3D models allow the possibility to study the cell heterogeneity and cell to cell interactions [610, 611].

Finally, we performed a GO term enrichment analysis on DE genes between sALS and CTRL 2D MNs and between sALS and CTRL MNOs. As regard to cellular processes category, we found that in both 2D cultures and in MNOs the DE genes were related to the nervous system, e.g. to synapses and to axogenesis. However, only in MNOs we found a deregulation in genes involved in ECM structure and organization. Numerous studies have demonstrated that ALS pathology could be related to a disruption of the ECM, precluding the normal communication between neurons [612-614]. For this reason, we decided to validate some of the most significant DE ECM-related genes. We confirmed the upregulation of *OPN*, *NCAN*, *TIMP1*, *FLOT1*, *CTSL*, *LOXL1*, *FNI*, *TIMP2* and *APP* and the downregulation of *COL9A2*, *OTX2* and *COL4A4* expressions.

OPN [615], *NCAN* [616-618], *TIMPs* genes (both *TIMP1* and *TIMP2*) [619], *FLOT1* [620, 621], *CTSL* [622-624] and *LOXL1* [625-627] are involved in ECM remodeling and turnover. *CTSL* [620, 621], *APP* [628], *OTX2* [629, 630], *COL9A2* [631] and *COL4A4* [632] interact with different ECM protein and structures. *FNI* [633] and *APP* are involved in cell migration, signaling and adhesion. Moreover, *CTSL* [622] and *OTX2* [629, 630] are involved in axon growth and guidance. These data allowed us to suppose that the deregulation of these genes can cause a disruption in physiological functions of ECM, leading to a stop in the communication between cells. Interesting, all the above cited genes were found implicated in ALS pathology. *OPN* is one of the most expressed proteins by

activated microglia and was linked to ALS associated neuroinflammation, but also with secretory and autophagy pathway defects [634, 635], whereas *OTX2* has protective roles in ALS models [636]. *NCAN* was already found upregulated in ALS transgenic rats [637] and it was demonstrated that an increase in its expression causes an inhibition in excitatory conduction and in axonal growth [638], whereas the elevated levels of *TIMPI* in ALS patients were correlated with MNs and muscles degeneration, because of its implication in tissue remodeling [639, 640]. *TIMP2*, *FLOT1* and *LOXLI* expressions were found increased in NDDs [627, 639, 641-643], whereas *CTSL* and *APP* were found increased both in muscles and serum of ALS patients and ALS animals models [644-646]. *FNI* was found dysregulated in ALS and AD and correlated with the duration of illness [647, 648]. Finally, both *COL9A2* and *COL4A4* deregulation was found in ALS patients in precedent studies [649, 650].

These data confirmed that MNOs organoids recapitulate many of the hallmarks associated with ALS pathology, pointing out the importance of ECM.

In conclusion, we demonstrated the efficacy of the use of 3D bioprinting and organoids, two of the main important 3D techniques, as promising tools for the study of ALS pathology. Both allowed NSCs culture and differentiation into MNs in an environment which better mimics the physiological characteristics of the tissue, allowing the study of interactions between cells.

Moreover, whereas 3D bioprinting demonstrated the possibility to study also the electrophysiological characteristics of cells, in our MNOs model we found ALS pathological hallmarks, such as gliosis, decreased level of mature MNs and a smaller length of neuritis. Finally, Bulk RNA-seq analysis and the deconvolution analysis showed the deregulation of ECM-related genes and the presence of oligodendrocytes and astrocytes in MNOs, allowing the study of their functions and relative pathways.

Limits of the study and future perspectives

A limitation of our study consists in the lack of biological repeats: in both 3D bioprinting and organoids experiments we compared cells obtained from one sALS patient and one CTRL subject. A future perspective will be the improvement of our study with the extension of the cohort. Moreover, as regards to 3D bioprinting, our future aim is to study the presence of other cell types, including glial cells such as astrocytes and oligodendrocytes. We will perform RNA-seq experiments also on 3D constructs as well as electrophysiological analyses on MNOS, for a more exhaustive comparison between 3D

bioprinting and organoids. Another limit of this study is the fact that the different steps of MNOs are not well characterized. A more detailed study on the different steps of MNOs formation is needed.

Despite the limitations of our study, we demonstrated that both 3D bioprinting and MNOs models open the possibility to the generation of a realistic neuron tissue, with implication in the finding of new therapeutic targets for the study of ALS and in performing drug screening tests, as already happened for other pathologies [651-653].

6. REFERENCES

- [1] O. Pansarasa *et al.*, "Biomarkers in Human Peripheral Blood Mononuclear Cells: The State of the Art in Amyotrophic Lateral Sclerosis," (in eng), *Int J Mol Sci*, vol. 23, no. 5, Feb 25 2022, doi: 10.3390/ijms23052580.
- [2] K. Mayne, J. A. White, C. E. McMurrin, F. J. Rivera, and A. G. de la Fuente, "Aging and Neurodegenerative Disease: Is the Adaptive Immune System a Friend or Foe?," (in eng), *Front Aging Neurosci*, vol. 12, p. 572090, 2020, doi: 10.3389/fnagi.2020.572090.
- [3] Y. Hou *et al.*, "Ageing as a risk factor for neurodegenerative disease," (in eng), *Nat Rev Neurol*, vol. 15, no. 10, pp. 565-581, 10 2019, doi: 10.1038/s41582-019-0244-7.
- [4] B. Grandal Leiros *et al.*, "Prevalence and concordance between the clinical and the post-mortem diagnosis of dementia in a psychogeriatric clinic," (in eng), *Neurologia (Engl Ed)*, vol. 33, no. 1, pp. 13-17, 2018 Jan - Feb 2018, doi: 10.1016/j.nrl.2016.04.011.
- [5] M. Bruzova, R. Rusina, Z. Stejskalova, and R. Matej, "Autopsy-diagnosed neurodegenerative dementia cases support the use of cerebrospinal fluid protein biomarkers in the diagnostic work-up," (in eng), *Sci Rep*, vol. 11, no. 1, p. 10837, 05 25 2021, doi: 10.1038/s41598-021-90366-5.
- [6] E. Scarian, G. Fiamingo, L. Diamanti, I. Palmieri, S. Gagliardi, and O. Pansarasa, "The Role of VCP Mutations in the Spectrum of Amyotrophic Lateral Sclerosis- Frontotemporal Dementia," (in eng), *Front Neurol*, vol. 13, p. 841394, 2022, doi: 10.3389/fneur.2022.841394.
- [7] M. Pievani, N. Filippini, M. P. van den Heuvel, S. F. Cappa, and G. B. Frisoni, "Brain connectivity in neurodegenerative diseases--from phenotype to proteinopathy," (in eng), *Nat Rev Neurol*, vol. 10, no. 11, pp. 620-33, Nov 2014, doi: 10.1038/nrneurol.2014.178.
- [8] C. Soto and S. Pritzkow, "Protein misfolding, aggregation, and conformational strains in neurodegenerative diseases," (in eng), *Nat Neurosci*, vol. 21, no. 10, pp. 1332-1340, 10 2018, doi: 10.1038/s41593-018-0235-9.
- [9] W. Qiang, W. M. Yau, J. X. Lu, J. Collinge, and R. Tycko, "Structural variation in amyloid- β fibrils from Alzheimer's disease clinical subtypes," (in eng), *Nature*, vol. 541, no. 7636, pp. 217-221, 01 12 2017, doi: 10.1038/nature20814.
- [10] S. Narasimhan *et al.*, "Pathological Tau Strains from Human Brains Recapitulate the Diversity of Tauopathies in Nontransgenic Mouse Brain," (in eng), *J Neurosci*, vol. 37, no. 47, pp. 11406-11423, 11 22 2017, doi: 10.1523/JNEUROSCI.1230-17.2017.
- [11] J. L. Guo *et al.*, "Distinct α -synuclein strains differentially promote tau inclusions in neurons," (in eng), *Cell*, vol. 154, no. 1, pp. 103-17, Jul 03 2013, doi: 10.1016/j.cell.2013.05.057.
- [12] B. N. Dugger and D. W. Dickson, "Pathology of Neurodegenerative Diseases," (in eng), *Cold Spring Harb Perspect Biol*, vol. 9, no. 7, Jul 2017, doi: 10.1101/cshperspect.a028035.
- [13] M. V. F. Silva, C. M. G. Loures, L. C. V. Alves, L. C. de Souza, K. B. G. Borges, and M. D. G. Carvalho, "Alzheimer's disease: risk factors and potentially protective measures," (in eng), *J Biomed Sci*, vol. 26, no. 1, p. 33, May 09 2019, doi: 10.1186/s12929-019-0524-y.
- [14] X. X. Zhang, Y. Tian, Z. T. Wang, Y. H. Ma, L. Tan, and J. T. Yu, "The Epidemiology of Alzheimer's Disease Modifiable Risk Factors and Prevention," (in eng), *J Prev Alzheimers Dis*, vol. 8, no. 3, pp. 313-321, 2021 2021, doi: 10.14283/jpad.2021.15.
- [15] G. D. Collaborators, "Global, regional, and national burden of Alzheimer's disease and other dementias, 1990-2016: a systematic analysis for the Global Burden of

- Disease Study 2016," (in eng), *Lancet Neurol*, vol. 18, no. 1, pp. 88-106, 01 2019, doi: 10.1016/S1474-4422(18)30403-4.
- [16] "2020 Alzheimer's disease facts and figures," (in eng), *Alzheimers Dement*, Mar 10 2020, doi: 10.1002/alz.12068.
- [17] W. Wong, "Economic burden of Alzheimer disease and managed care considerations," (in eng), *Am J Manag Care*, vol. 26, no. 8 Suppl, pp. S177-S183, 08 2020, doi: 10.37765/ajmc.2020.88482.
- [18] A. Kumar , J. Sidhu , A. Goyal , and J. Tsao "Alzheimer Disease," in *StatPearls [Internet]*. StatPearls Publishing, 2022, p. 29763097.
- [19] H. J. Möller and M. B. Graeber, "The case described by Alois Alzheimer in 1911. Historical and conceptual perspectives based on the clinical record and neurohistological sections," (in eng), *Eur Arch Psychiatry Clin Neurosci*, vol. 248, no. 3, pp. 111-22, 1998, doi: 10.1007/s004060050027.
- [20] J. A. Soria Lopez, H. M. González, and G. C. Léger, "Alzheimer's disease," (in eng), *Handb Clin Neurol*, vol. 167, pp. 231-255, 2019, doi: 10.1016/B978-0-12-804766-8.00013-3.
- [21] C. L. Masters, R. Bateman, K. Blennow, C. C. Rowe, R. A. Sperling, and J. L. Cummings, "Alzheimer's disease," (in eng), *Nat Rev Dis Primers*, vol. 1, p. 15056, 10 2015, doi: 10.1038/nrdp.2015.56.
- [22] R. A. Hickman, A. Faustin, and T. Wisniewski, "Alzheimer Disease and Its Growing Epidemic: Risk Factors, Biomarkers, and the Urgent Need for Therapeutics," (in eng), *Neurol Clin*, vol. 34, no. 4, pp. 941-953, 11 2016, doi: 10.1016/j.ncl.2016.06.009.
- [23] P. S. Aisen, G. A. Jimenez-Maggiara, M. S. Rafii, S. Walter, and R. Raman, "Early-stage Alzheimer disease: getting trial-ready," (in eng), *Nat Rev Neurol*, vol. 18, no. 7, pp. 389-399, 07 2022, doi: 10.1038/s41582-022-00645-6.
- [24] J. Cummings, "New approaches to symptomatic treatments for Alzheimer's disease," (in eng), *Mol Neurodegener*, vol. 16, no. 1, p. 2, 01 13 2021, doi: 10.1186/s13024-021-00424-9.
- [25] Z. Ou *et al.*, "Global Trends in the Incidence, Prevalence, and Years Lived With Disability of Parkinson's Disease in 204 Countries/Territories From 1990 to 2019," (in eng), *Front Public Health*, vol. 9, p. 776847, 2021, doi: 10.3389/fpubh.2021.776847.
- [26] O. B. Tysnes and A. Storstein, "Epidemiology of Parkinson's disease," (in eng), *J Neural Transm (Vienna)*, vol. 124, no. 8, pp. 901-905, 08 2017, doi: 10.1007/s00702-017-1686-y.
- [27] F. N. Emamzadeh and A. Surguchov, "Parkinson's Disease: Biomarkers, Treatment, and Risk Factors," (in eng), *Front Neurosci*, vol. 12, p. 612, 2018, doi: 10.3389/fnins.2018.00612.
- [28] D. Belvisi *et al.*, "Risk factors of Parkinson disease: Simultaneous assessment, interactions, and etiologic subtypes," (in eng), *Neurology*, vol. 95, no. 18, pp. e2500-e2508, 11 03 2020, doi: 10.1212/WNL.00000000000010813.
- [29] J. Parkinson, "An essay on the shaking palsy. 1817," (in eng), *J Neuropsychiatry Clin Neurosci*, vol. 14, no. 2, pp. 223-36; discussion 222, 2002, doi: 10.1176/jnp.14.2.223.
- [30] D. W. Dickson, "Neuropathology of Parkinson disease," (in eng), *Parkinsonism Relat Disord*, vol. 46 Suppl 1, pp. S30-S33, Jan 2018, doi: 10.1016/j.parkreldis.2017.07.033.
- [31] H. M. Lee and S. B. Koh, "Many Faces of Parkinson's Disease: Non-Motor Symptoms of Parkinson's Disease," (in eng), *J Mov Disord*, vol. 8, no. 2, pp. 92-7, May 2015, doi: 10.14802/jmd.15003.

- [32] H. Tibar *et al.*, "Non-Motor Symptoms of Parkinson's Disease and Their Impact on Quality of Life in a Cohort of Moroccan Patients," (in eng), *Front Neurol*, vol. 9, p. 170, 2018, doi: 10.3389/fneur.2018.00170.
- [33] L. Stefanis, " α -Synuclein in Parkinson's disease," (in eng), *Cold Spring Harb Perspect Med*, vol. 2, no. 2, p. a009399, Feb 2012, doi: 10.1101/cshperspect.a009399.
- [34] A. L. Mahul-Mellier *et al.*, "The process of Lewy body formation, rather than simply α -synuclein fibrillization, is one of the major drivers of neurodegeneration," (in eng), *Proc Natl Acad Sci U S A*, vol. 117, no. 9, pp. 4971-4982, 03 03 2020, doi: 10.1073/pnas.1913904117.
- [35] K. Wakabayashi, S. Hayashi, M. Yoshimoto, H. Kudo, and H. Takahashi, "NACP/ α -synuclein-positive filamentous inclusions in astrocytes and oligodendrocytes of Parkinson's disease brains," (in eng), *Acta Neuropathol*, vol. 99, no. 1, pp. 14-20, Jan 2000, doi: 10.1007/pl00007400.
- [36] K. Wakabayashi, K. Tanji, S. Odagiri, Y. Miki, F. Mori, and H. Takahashi, "The Lewy body in Parkinson's disease and related neurodegenerative disorders," (in eng), *Mol Neurobiol*, vol. 47, no. 2, pp. 495-508, Apr 2013, doi: 10.1007/s12035-012-8280-y.
- [37] D. J. Irwin, V. M. Lee, and J. Q. Trojanowski, "Parkinson's disease dementia: convergence of α -synuclein, tau and amyloid- β pathologies," (in eng), *Nat Rev Neurosci*, vol. 14, no. 9, pp. 626-36, Sep 2013, doi: 10.1038/nrn3549.
- [38] J. Jankovic and E. K. Tan, "Parkinson's disease: etiopathogenesis and treatment," (in eng), *J Neurol Neurosurg Psychiatry*, vol. 91, no. 8, pp. 795-808, 08 2020, doi: 10.1136/jnnp-2019-322338.
- [39] S. Selvaraj and S. Piramanayagam, "Impact of gene mutation in the development of Parkinson's disease," (in eng), *Genes Dis*, vol. 6, no. 2, pp. 120-128, Jun 2019, doi: 10.1016/j.gendis.2019.01.004.
- [40] M. J. Armstrong and M. S. Okun, "Diagnosis and Treatment of Parkinson Disease: A Review," (in eng), *JAMA*, vol. 323, no. 6, pp. 548-560, 02 11 2020, doi: 10.1001/jama.2019.22360.
- [41] T. Ntetsika, P. E. Papatoma, and I. Markaki, "Novel targeted therapies for Parkinson's disease," (in eng), *Mol Med*, vol. 27, no. 1, p. 17, 02 25 2021, doi: 10.1186/s10020-021-00279-2.
- [42] M. D. Rawlins *et al.*, "The Prevalence of Huntington's Disease," (in eng), *Neuroepidemiology*, vol. 46, no. 2, pp. 144-53, 2016, doi: 10.1159/000443738.
- [43] M. Riccò, L. Vezzosi, F. Balzarini, G. Gualerzi, and S. Ranzieri, "Prevalence of Huntington Disease in Italy: a systematic review and meta-analysis," (in eng), *Acta Biomed*, vol. 91, no. 3-S, pp. 119-127, 04 10 2020, doi: 10.23750/abm.v91i3-S.9441.
- [44] G. Huntington, "On chorea. George Huntington, M.D.," (in eng), *J Neuropsychiatry Clin Neurosci*, vol. 15, no. 1, pp. 109-12, 2003, doi: 10.1176/jnp.15.1.109.
- [45] K. B. Bhattacharyya, "The story of George Huntington and his disease," (in eng), *Ann Indian Acad Neurol*, vol. 19, no. 1, pp. 25-8, 2016 Jan-Mar 2016, doi: 10.4103/0972-2327.175425.
- [46] G. Huntington, "On Chorea," *Medical and Surgical Reporter*, vol. 26, 1872.
- [47] E. M. Gatto, N. G. Rojas, G. Persi, J. L. Etcheverry, M. E. Cesarini, and C. Perandones, "Huntington disease: Advances in the understanding of its mechanisms," (in eng), *Clin Park Relat Disord*, vol. 3, p. 100056, 2020, doi: 10.1016/j.prdoa.2020.100056.
- [48] P. McColgan and S. J. Tabrizi, "Huntington's disease: a clinical review," (in eng), *Eur J Neurol*, vol. 25, no. 1, pp. 24-34, 01 2018, doi: 10.1111/ene.13413.

- [49] M. P. Chao *et al.*, "Human AML-iPSCs Reacquire Leukemic Properties after Differentiation and Model Clonal Variation of Disease," (in eng), *Cell Stem Cell*, vol. 20, no. 3, pp. 329-344.e7, 03 02 2017, doi: 10.1016/j.stem.2016.11.018.
- [50] N. G. Ranen *et al.*, "Anticipation and instability of IT-15 (CAG)_n repeats in parent-offspring pairs with Huntington disease," (in eng), *Am J Hum Genet*, vol. 57, no. 3, pp. 593-602, Sep 1995.
- [51] R. A. Roos, "Huntington's disease: a clinical review," (in eng), *Orphanet J Rare Dis*, vol. 5, p. 40, Dec 20 2010, doi: 10.1186/1750-1172-5-40.
- [52] S. Migliore, J. Jankovic, and F. Squitieri, "Genetic Counseling in Huntington's Disease: Potential New Challenges on Horizon?," (in eng), *Front Neurol*, vol. 10, p. 453, 2019, doi: 10.3389/fneur.2019.00453.
- [53] R. A. Hickman, P. L. Faust, K. Marder, A. Yamamoto, and J. P. Vonsattel, "The distribution and density of Huntingtin inclusions across the Huntington disease neocortex: regional correlations with Huntingtin repeat expansion independent of pathologic grade," (in eng), *Acta Neuropathol Commun*, vol. 10, no. 1, p. 55, 04 19 2022, doi: 10.1186/s40478-022-01364-1.
- [54] N. Riguet *et al.*, "Nuclear and cytoplasmic huntingtin inclusions exhibit distinct biochemical composition, interactome and ultrastructural properties," (in eng), *Nat Commun*, vol. 12, no. 1, p. 6579, 11 12 2021, doi: 10.1038/s41467-021-26684-z.
- [55] K. T. Potkin and S. G. Potkin, "New directions in therapeutics for Huntington disease," (in eng), *Future Neurol*, vol. 13, no. 2, pp. 101-121, May 2018, doi: 10.2217/fnl-2017-0035.
- [56] L. Xu *et al.*, "Global variation in prevalence and incidence of amyotrophic lateral sclerosis: a systematic review and meta-analysis," (in eng), *J Neurol*, vol. 267, no. 4, pp. 944-953, Apr 2020, doi: 10.1007/s00415-019-09652-y.
- [57] F. Trojsi, G. D'Alvano, S. Bonavita, and G. Tedeschi, "Genetics and Sex in the Pathogenesis of Amyotrophic Lateral Sclerosis (ALS): Is There a Link?," (in eng), *Int J Mol Sci*, vol. 21, no. 10, May 21 2020, doi: 10.3390/ijms21103647.
- [58] J. Kim, T. Y. Kim, K. S. Cho, H. N. Kim, and J. Y. Koh, "Autophagy activation and neuroprotection by progesterone in the G93A-SOD1 transgenic mouse model of amyotrophic lateral sclerosis," (in eng), *Neurobiol Dis*, vol. 59, pp. 80-5, Nov 2013, doi: 10.1016/j.nbd.2013.07.011.
- [59] M. Heitzer *et al.*, "Administration of 17 β -Estradiol Improves Motoneuron Survival and Down-regulates Inflammation Activation in Male SOD1(G93A) ALS Mice," (in eng), *Mol Neurobiol*, vol. 54, no. 10, pp. 8429-8443, Dec 2017, doi: 10.1007/s12035-016-0322-4.
- [60] J. P. K. Rooney *et al.*, "A case-control study of hormonal exposures as etiologic factors for ALS in women: Euro-MOTOR," (in eng), *Neurology*, vol. 89, no. 12, pp. 1283-1290, Sep 19 2017, doi: 10.1212/WNL.0000000000004390.
- [61] R. M. Pfeiffer *et al.*, "Identifying potential targets for prevention and treatment of amyotrophic lateral sclerosis based on a screen of medicare prescription drugs," (in eng), *Amyotroph Lateral Scler Frontotemporal Degener*, vol. 21, no. 3-4, pp. 235-245, 05 2020, doi: 10.1080/21678421.2019.1682613.
- [62] L. Belbasis, V. Bellou, and E. Evangelou, "Environmental Risk Factors and Amyotrophic Lateral Sclerosis: An Umbrella Review and Critical Assessment of Current Evidence from Systematic Reviews and Meta-Analyses of Observational Studies," (in eng), *Neuroepidemiology*, vol. 46, no. 2, pp. 96-105, 2016, doi: 10.1159/000443146.
- [63] E. Longinetti and F. Fang, "Epidemiology of amyotrophic lateral sclerosis: an update of recent literature," (in eng), *Curr Opin Neurol*, vol. 32, no. 5, pp. 771-776, 10 2019, doi: 10.1097/WCO.0000000000000730.

- [64] A. S. Dickerson, J. Hansen, M. A. Kioumourtzoglou, A. J. Specht, O. Gredal, and M. G. Weisskopf, "Study of occupation and amyotrophic lateral sclerosis in a Danish cohort," (in eng), *Occup Environ Med*, vol. 75, no. 9, pp. 630-638, 09 2018, doi: 10.1136/oemed-2018-105110.
- [65] M. Seelen *et al.*, "Long-Term Air Pollution Exposure and Amyotrophic Lateral Sclerosis in Netherlands: A Population-based Case-control Study," (in eng), *Environ Health Perspect*, vol. 125, no. 9, p. 097023, 09 27 2017, doi: 10.1289/EHP1115.
- [66] A. S. Andrew *et al.*, "Risk factors for amyotrophic lateral sclerosis: A regional United States case-control study," (in eng), *Muscle Nerve*, vol. 63, no. 1, pp. 52-59, 01 2021, doi: 10.1002/mus.27085.
- [67] Charcot J-M and J. A., "Deux cas d'atrophie musculaire progressive avec lesions de la substance grise et des faisceaux antero-lateraux de la moelle epiniere," *Arch Physiol Neurol Pathol*, pp. p. 744-54., 1869.
- [68] P. Masrori and P. Van Damme, "Amyotrophic lateral sclerosis: a clinical review," (in eng), *Eur J Neurol*, vol. 27, no. 10, pp. 1918-1929, 10 2020, doi: 10.1111/ene.14393.
- [69] R. Mejzini, L. L. Flynn, I. L. Pitout, S. Fletcher, S. D. Wilton, and P. A. Akkari, "ALS Genetics, Mechanisms, and Therapeutics: Where Are We Now?," (in eng), *Front Neurosci*, vol. 13, p. 1310, 2019, doi: 10.3389/fnins.2019.01310.
- [70] E. Trias, S. Ibarburu, R. Barreto-Núñez, and L. Barbeito, "Significance of aberrant glial cell phenotypes in pathophysiology of amyotrophic lateral sclerosis," (in eng), *Neurosci Lett*, vol. 636, pp. 27-31, 01 01 2017, doi: 10.1016/j.neulet.2016.07.052.
- [71] K. Yamanaka and O. Komine, "The multi-dimensional roles of astrocytes in ALS," (in eng), *Neurosci Res*, vol. 126, pp. 31-38, Jan 2018, doi: 10.1016/j.neures.2017.09.011.
- [72] P. Cassina, E. Miquel, L. Martínez-Palma, and A. Cassina, "Glial Metabolic Reprogramming in Amyotrophic Lateral Sclerosis," (in eng), *Neuroimmunomodulation*, vol. 28, no. 4, pp. 204-212, 2021, doi: 10.1159/000516926.
- [73] C. G. Chisholm, J. J. Y. Yerbury, and L. McAlary, "Protein Aggregation in Amyotrophic Lateral Sclerosis," in *Spectrums of Amyotrophic Lateral Sclerosis: Heterogeneity, Pathogenesis and Therapeutic Directions*, J. W. S. Ltd. Ed., 2021, ch. 6.
- [74] L. McAlary, Y. L. Chew, J. S. Lum, N. J. Geraghty, J. J. Yerbury, and N. R. Cashman, "Amyotrophic Lateral Sclerosis: Proteins, Proteostasis, Prions, and Promises," (in eng), *Front Cell Neurosci*, vol. 14, p. 581907, 2020, doi: 10.3389/fncel.2020.581907.
- [75] Y. Miki *et al.*, "Colocalization of Bunina bodies and TDP-43 inclusions in a case of sporadic amyotrophic lateral sclerosis with Lewy body-like hyaline inclusions," (in eng), *Neuropathology*, vol. 38, no. 5, pp. 521-528, Oct 2018, doi: 10.1111/neup.12484.
- [76] F. Mori, Y. Miki, T. Kon, K. Tanji, and K. Wakabayashi, "Autophagy Is a Common Degradation Pathway for Bunina Bodies and TDP-43 Inclusions in Amyotrophic Lateral Sclerosis," (in eng), *J Neuropathol Exp Neurol*, vol. 78, no. 10, pp. 910-921, 10 01 2019, doi: 10.1093/jnen/nlz072.
- [77] P. Van Damme, W. Robberecht, and L. Van Den Bosch, "Modelling amyotrophic lateral sclerosis: progress and possibilities," (in eng), *Dis Model Mech*, vol. 10, no. 5, pp. 537-549, 05 2017, doi: 10.1242/dmm.029058.
- [78] P. Corcia *et al.*, "Genetics of amyotrophic lateral sclerosis," (in eng), *Rev Neurol (Paris)*, vol. 173, no. 5, pp. 254-262, May 2017, doi: 10.1016/j.neurol.2017.03.030.

- [79] O. Pansarasa, M. Bordoni, L. Diamanti, D. Sproviero, S. Gagliardi, and C. Cereda, "SOD1 in Amyotrophic Lateral Sclerosis: "Ambivalent" Behavior Connected to the Disease," (in eng), *Int J Mol Sci*, vol. 19, no. 5, May 03 2018, doi: 10.3390/ijms19051345.
- [80] M. Bordoni *et al.*, "Nuclear Phospho-SOD1 Protects DNA from Oxidative Stress Damage in Amyotrophic Lateral Sclerosis," (in eng), *J Clin Med*, vol. 8, no. 5, May 22 2019, doi: 10.3390/jcm8050729.
- [81] E. Obrador, R. Salvador-Palmer, R. López-Blanch, A. Jihad-Jebbar, S. L. Vallés, and J. M. Estrela, "The Link between Oxidative Stress, Redox Status, Bioenergetics and Mitochondria in the Pathophysiology of ALS," (in eng), *Int J Mol Sci*, vol. 22, no. 12, Jun 14 2021, doi: 10.3390/ijms22126352.
- [82] M. Giannini, A. Bayona-Feliu, D. Sproviero, S. I. Barroso, C. Cereda, and A. Aguilera, "TDP-43 mutations link Amyotrophic Lateral Sclerosis with R-loop homeostasis and R loop-mediated DNA damage," (in eng), *PLoS Genet*, vol. 16, no. 12, p. e1009260, 12 2020, doi: 10.1371/journal.pgen.1009260.
- [83] T. R. Suk and M. W. C. Rousseaux, "The role of TDP-43 mislocalization in amyotrophic lateral sclerosis," (in eng), *Mol Neurodegener*, vol. 15, no. 1, p. 45, 08 15 2020, doi: 10.1186/s13024-020-00397-1.
- [84] H. X. Deng *et al.*, "FUS-immunoreactive inclusions are a common feature in sporadic and non-SOD1 familial amyotrophic lateral sclerosis," (in eng), *Ann Neurol*, vol. 67, no. 6, pp. 739-48, Jun 2010, doi: 10.1002/ana.22051.
- [85] A. E. Renton *et al.*, "A hexanucleotide repeat expansion in C9ORF72 is the cause of chromosome 9p21-linked ALS-FTD," (in eng), *Neuron*, vol. 72, no. 2, pp. 257-68, Oct 20 2011, doi: 10.1016/j.neuron.2011.09.010.
- [86] M. DeJesus-Hernandez *et al.*, "Expanded GGGGCC hexanucleotide repeat in noncoding region of C9ORF72 causes chromosome 9p-linked FTD and ALS," (in eng), *Neuron*, vol. 72, no. 2, pp. 245-56, Oct 20 2011, doi: 10.1016/j.neuron.2011.09.011.
- [87] J. Beckers, A. K. Tharkeshwar, and P. Van Damme, "C9orf72 ALS-FTD: recent evidence for dysregulation of the autophagy-lysosome pathway at multiple levels," (in eng), *Autophagy*, vol. 17, no. 11, pp. 3306-3322, 11 2021, doi: 10.1080/15548627.2021.1872189.
- [88] R. Balendra and A. M. Isaacs, "C9orf72-mediated ALS and FTD: multiple pathways to disease," (in eng), *Nat Rev Neurol*, vol. 14, no. 9, pp. 544-558, Sep 2018, doi: 10.1038/s41582-018-0047-2.
- [89] M. Hinchcliffe and A. Smith, "Riluzole: real-world evidence supports significant extension of median survival times in patients with amyotrophic lateral sclerosis," (in eng), *Degener Neurol Neuromuscul Dis*, vol. 7, pp. 61-70, 2017, doi: 10.2147/DNND.S135748.
- [90] V. Khurana and S. Lindquist, "Modelling neurodegeneration in *Saccharomyces cerevisiae*: why cook with baker's yeast?," (in eng), *Nat Rev Neurosci*, vol. 11, no. 6, pp. 436-49, 06 2010, doi: 10.1038/nrn2809.
- [91] A. Ruetenik and A. Barrientos, "Exploiting Post-mitotic Yeast Cultures to Model Neurodegeneration," (in eng), *Front Mol Neurosci*, vol. 11, p. 400, 2018, doi: 10.3389/fnmol.2018.00400.
- [92] F. M. Ribeiro, E. R. Camargos, L. C. de Souza, and A. L. Teixeira, "Animal models of neurodegenerative diseases," (in eng), *Braz J Psychiatry*, vol. 35 Suppl 2, pp. S82-91, 2013, doi: 10.1590/1516-4446-2013-1157.
- [93] G. D. Colpo, F. M. Ribeiro, N. P. Rocha, and A. L. Teixeira, "Animal Models for the Study of Human Neurodegenerative Diseases," in *Animal Models for the Study of Human Diseases*, 2017, pp. 1109-1129.

- [94] W. Yang, X. Chen, S. Li, and X. J. Li, "Genetically modified large animal models for investigating neurodegenerative diseases," (in eng), *Cell Biosci*, vol. 11, no. 1, p. 218, Dec 21 2021, doi: 10.1186/s13578-021-00729-8.
- [95] J. A. Lepasant, "The promises of neurodegenerative disease modeling," (in eng), *C R Biol*, vol. 338, no. 8-9, pp. 584-92, 2015 Aug-Sep 2015, doi: 10.1016/j.crv.2015.06.018.
- [96] S. Khan *et al.*, "Role of Recombinant DNA Technology to Improve Life," (in eng), *Int J Genomics*, vol. 2016, p. 2405954, 2016, doi: 10.1155/2016/2405954.
- [97] X. Zhu, Y. Zhang, X. Yang, C. Hao, and H. Duan, "Gene Therapy for Neurodegenerative Disease: Clinical Potential and Directions," (in eng), *Front Mol Neurosci*, vol. 14, p. 618171, 2021, doi: 10.3389/fnmol.2021.618171.
- [98] J. M. Heather and B. Chain, "The sequence of sequencers: The history of sequencing DNA," (in eng), *Genomics*, vol. 107, no. 1, pp. 1-8, Jan 2016, doi: 10.1016/j.ygeno.2015.11.003.
- [99] T. M. Dawson, T. E. Golde, and C. Lagier-Tourenne, "Animal models of neurodegenerative diseases," (in eng), *Nat Neurosci*, vol. 21, no. 10, pp. 1370-1379, 10 2018, doi: 10.1038/s41593-018-0236-8.
- [100] A. Slanzi, G. Iannoto, B. Rossi, E. Zenaro, and G. Constantin, "Models of Neurodegenerative Diseases," (in eng), *Front Cell Dev Biol*, vol. 8, p. 328, 2020, doi: 10.3389/fcell.2020.00328.
- [101] J. BOUSQUET and J. M. MEUNIER, "[Organotypic culture, on natural and artificial media, of fragments of the adult rat hypophysis]," (in fre), *C R Seances Soc Biol Fil*, vol. 156, pp. 65-7, 1962.
- [102] S. Cetin, D. Knez, S. Gobec, J. Kos, and A. Pišlar, "Cell models for Alzheimer's and Parkinson's disease: At the interface of biology and drug discovery," (in eng), *Biomed Pharmacother*, vol. 149, p. 112924, May 2022, doi: 10.1016/j.biopha.2022.112924.
- [103] J. Kovalevich and D. Langford, "Considerations for the use of SH-SY5Y neuroblastoma cells in neurobiology," (in eng), *Methods Mol Biol*, vol. 1078, pp. 9-21, 2013, doi: 10.1007/978-1-62703-640-5_2.
- [104] L. M. de Medeiros *et al.*, "Cholinergic Differentiation of Human Neuroblastoma SH-SY5Y Cell Line and Its Potential Use as an In vitro Model for Alzheimer's Disease Studies," (in eng), *Mol Neurobiol*, vol. 56, no. 11, pp. 7355-7367, Nov 2019, doi: 10.1007/s12035-019-1605-3.
- [105] D. G. Brown and H. J. Wobst, "Opportunities and Challenges in Phenotypic Screening for Neurodegenerative Disease Research," (in eng), *J Med Chem*, vol. 63, no. 5, pp. 1823-1840, 03 12 2020, doi: 10.1021/acs.jmedchem.9b00797.
- [106] K. Gordon *et al.*, "Immortality, but not oncogenic transformation, of primary human cells leads to epigenetic reprogramming of DNA methylation and gene expression," (in eng), *Nucleic Acids Res*, vol. 42, no. 6, pp. 3529-41, Apr 2014, doi: 10.1093/nar/gkt1351.
- [107] Y. Wang, S. Chen, Z. Yan, and M. Pei, "A prospect of cell immortalization combined with matrix microenvironmental optimization strategy for tissue engineering and regeneration," (in eng), *Cell Biosci*, vol. 9, p. 7, 2019, doi: 10.1186/s13578-018-0264-9.
- [108] E. G. Z. Centeno, H. Cimarosti, and A. Bithell, "2D versus 3D human induced pluripotent stem cell-derived cultures for neurodegenerative disease modelling," (in eng), *Mol Neurodegener*, vol. 13, no. 1, p. 27, 05 22 2018, doi: 10.1186/s13024-018-0258-4.
- [109] F. Sivandzade and L. Cucullo, "Regenerative Stem Cell Therapy for Neurodegenerative Diseases: An Overview," (in eng), *Int J Mol Sci*, vol. 22, no. 4, Feb 22 2021, doi: 10.3390/ijms22042153.

- [110] R. Sakthiswary and A. A. Raymond, "Stem cell therapy in neurodegenerative diseases: From principles to practice," (in eng), *Neural Regen Res*, vol. 7, no. 23, pp. 1822-31, Aug 15 2012, doi: 10.3969/j.issn.1673-5374.2012.23.009.
- [111] K. Sugaya and M. Vaidya, "Stem Cell Therapies for Neurodegenerative Diseases," (in eng), *Adv Exp Med Biol*, vol. 1056, pp. 61-84, 2018, doi: 10.1007/978-3-319-74470-4_5.
- [112] W. Zakrzewski, M. Dobrzyński, M. Szymonowicz, and Z. Rybak, "Stem cells: past, present, and future," (in eng), *Stem Cell Res Ther*, vol. 10, no. 1, p. 68, 02 26 2019, doi: 10.1186/s13287-019-1165-5.
- [113] A. M. Hopkins, E. DeSimone, K. Chwalek, and D. L. Kaplan, "3D in vitro modeling of the central nervous system," (in eng), *Prog Neurobiol*, vol. 125, pp. 1-25, Feb 2015, doi: 10.1016/j.pneurobio.2014.11.003.
- [114] Y. T. Dingle *et al.*, "Three-Dimensional Neural Spheroid Culture: An In Vitro Model for Cortical Studies," (in eng), *Tissue Eng Part C Methods*, vol. 21, no. 12, pp. 1274-83, Dec 2015, doi: 10.1089/ten.TEC.2015.0135.
- [115] M. Ahn, F. Kalume, R. Pitstick, A. Oehler, G. Carlson, and S. J. DeArmond, "Brain Aggregates: An Effective In Vitro Cell Culture System Modeling Neurodegenerative Diseases," (in eng), *J Neuropathol Exp Neurol*, vol. 75, no. 3, pp. 256-62, Mar 2016, doi: 10.1093/jnen/nlv025.
- [116] F. Pampaloni, E. G. Reynaud, and E. H. Stelzer, "The third dimension bridges the gap between cell culture and live tissue," (in eng), *Nat Rev Mol Cell Biol*, vol. 8, no. 10, pp. 839-45, Oct 2007, doi: 10.1038/nrm2236.
- [117] M. Ravi, V. Paramesh, S. R. Kaviya, E. Anuradha, and F. D. Solomon, "3D cell culture systems: advantages and applications," (in eng), *J Cell Physiol*, vol. 230, no. 1, pp. 16-26, Jan 2015, doi: 10.1002/jcp.24683.
- [118] S. A. Langhans, "Three-Dimensional," (in eng), *Front Pharmacol*, vol. 9, p. 6, 2018, doi: 10.3389/fphar.2018.00006.
- [119] S. Moradi *et al.*, "Research and therapy with induced pluripotent stem cells (iPSCs): social, legal, and ethical considerations," (in eng), *Stem Cell Res Ther*, vol. 10, no. 1, p. 341, 11 21 2019, doi: 10.1186/s13287-019-1455-y.
- [120] J. A. Thomson *et al.*, "Embryonic stem cell lines derived from human blastocysts," (in eng), *Science*, vol. 282, no. 5391, pp. 1145-7, Nov 1998.
- [121] C. J. Taylor, E. M. Bolton, and J. A. Bradley, "Immunological considerations for embryonic and induced pluripotent stem cell banking," (in eng), *Philos Trans R Soc Lond B Biol Sci*, vol. 366, no. 1575, pp. 2312-22, Aug 12 2011, doi: 10.1098/rstb.2011.0030.
- [122] V. Volarevic *et al.*, "Ethical and Safety Issues of Stem Cell-Based Therapy," (in eng), *Int J Med Sci*, vol. 15, no. 1, pp. 36-45, 2018, doi: 10.7150/ijms.21666.
- [123] K. Takahashi and S. Yamanaka, "Induction of pluripotent stem cells from mouse embryonic and adult fibroblast cultures by defined factors," (in eng), *Cell*, vol. 126, no. 4, pp. 663-76, Aug 2006, doi: 10.1016/j.cell.2006.07.024.
- [124] K. Takahashi *et al.*, "Induction of pluripotent stem cells from adult human fibroblasts by defined factors," (in eng), *Cell*, vol. 131, no. 5, pp. 861-72, Nov 2007, doi: 10.1016/j.cell.2007.11.019.
- [125] J. Yu *et al.*, "Induced pluripotent stem cell lines derived from human somatic cells," (in eng), *Science*, vol. 318, no. 5858, pp. 1917-20, Dec 21 2007, doi: 10.1126/science.1151526.
- [126] A. E. Omole and A. O. J. Fakoya, "Ten years of progress and promise of induced pluripotent stem cells: historical origins, characteristics, mechanisms, limitations, and potential applications," (in eng), *PeerJ*, vol. 6, p. e4370, 2018, doi: 10.7717/peerj.4370.

- [127] Y. Wang *et al.*, "Endogenous miRNA sponge lincRNA-RoR regulates Oct4, Nanog, and Sox2 in human embryonic stem cell self-renewal," (in eng), *Dev Cell*, vol. 25, no. 1, pp. 69-80, Apr 15 2013, doi: 10.1016/j.devcel.2013.03.002.
- [128] K. A. Worringer *et al.*, "The let-7/LIN-41 pathway regulates reprogramming to human induced pluripotent stem cells by controlling expression of prodifferentiation genes," (in eng), *Cell Stem Cell*, vol. 14, no. 1, pp. 40-52, Jan 02 2014, doi: 10.1016/j.stem.2013.11.001.
- [129] K. Kaji, K. Norrby, A. Paca, M. Mileikovsky, P. Mohseni, and K. Woltjen, "Virus-free induction of pluripotency and subsequent excision of reprogramming factors," (in eng), *Nature*, vol. 458, no. 7239, pp. 771-5, Apr 09 2009, doi: 10.1038/nature07864.
- [130] K. Okita *et al.*, "A more efficient method to generate integration-free human iPS cells," (in eng), *Nat Methods*, vol. 8, no. 5, pp. 409-12, May 2011, doi: 10.1038/nmeth.1591.
- [131] K. Woltjen *et al.*, "piggyBac transposition reprograms fibroblasts to induced pluripotent stem cells," (in eng), *Nature*, vol. 458, no. 7239, pp. 766-70, Apr 09 2009, doi: 10.1038/nature07863.
- [132] R. P. Davis *et al.*, "Generation of induced pluripotent stem cells from human foetal fibroblasts using the Sleeping Beauty transposon gene delivery system," (in eng), *Differentiation*, vol. 86, no. 1-2, pp. 30-7, 2013 Jul-Sep 2013, doi: 10.1016/j.diff.2013.06.002.
- [133] M. Stadtfeld, M. Nagaya, J. Utikal, G. Weir, and K. Hochedlinger, "Induced pluripotent stem cells generated without viral integration," (in eng), *Science*, vol. 322, no. 5903, pp. 945-9, Nov 2008, doi: 10.1126/science.1162494.
- [134] N. Fusaki, H. Ban, A. Nishiyama, K. Saeki, and M. Hasegawa, "Efficient induction of transgene-free human pluripotent stem cells using a vector based on Sendai virus, an RNA virus that does not integrate into the host genome," (in eng), *Proc Jpn Acad Ser B Phys Biol Sci*, vol. 85, no. 8, pp. 348-62, 2009.
- [135] K. Okita, M. Nakagawa, H. Hyenjong, T. Ichisaka, and S. Yamanaka, "Generation of mouse induced pluripotent stem cells without viral vectors," (in eng), *Science*, vol. 322, no. 5903, pp. 949-53, Nov 07 2008, doi: 10.1126/science.1164270.
- [136] F. Jia *et al.*, "A nonviral minicircle vector for deriving human iPS cells," (in eng), *Nat Methods*, vol. 7, no. 3, pp. 197-9, Mar 2010, doi: 10.1038/nmeth.1426.
- [137] L. Warren *et al.*, "Highly efficient reprogramming to pluripotency and directed differentiation of human cells with synthetic modified mRNA," (in eng), *Cell Stem Cell*, vol. 7, no. 5, pp. 618-30, Nov 2010, doi: 10.1016/j.stem.2010.08.012.
- [138] D. Kim *et al.*, "Generation of human induced pluripotent stem cells by direct delivery of reprogramming proteins," (in eng), *Cell Stem Cell*, vol. 4, no. 6, pp. 472-6, Jun 05 2009, doi: 10.1016/j.stem.2009.05.005.
- [139] V. K. Singh, M. Kalsan, N. Kumar, A. Saini, and R. Chandra, "Induced pluripotent stem cells: applications in regenerative medicine, disease modeling, and drug discovery," (in eng), *Front Cell Dev Biol*, vol. 3, p. 2, 2015, doi: 10.3389/fcell.2015.00002.
- [140] M. Ohnuki and K. Takahashi, "Present and future challenges of induced pluripotent stem cells," (in eng), *Philos Trans R Soc Lond B Biol Sci*, vol. 370, no. 1680, p. 20140367, Oct 19 2015, doi: 10.1098/rstb.2014.0367.
- [141] C. Wiegand and I. Banerjee, "Recent advances in the applications of iPSC technology," (in eng), *Curr Opin Biotechnol*, vol. 60, pp. 250-258, 12 2019, doi: 10.1016/j.copbio.2019.05.011.
- [142] M. A. Blasco, M. Serrano, and O. Fernandez-Capetillo, "Genomic instability in iPS: time for a break," (in eng), *EMBO J*, vol. 30, no. 6, pp. 991-3, Mar 16 2011, doi: 10.1038/emboj.2011.50.

- [143] S. Yamanaka, "Induced pluripotent stem cells: past, present, and future," (in eng), *Cell Stem Cell*, vol. 10, no. 6, pp. 678-684, Jun 14 2012, doi: 10.1016/j.stem.2012.05.005.
- [144] E. J. Nestler and S. E. Hyman, "Animal models of neuropsychiatric disorders," (in eng), *Nat Neurosci*, vol. 13, no. 10, pp. 1161-9, Oct 2010, doi: 10.1038/nn.2647.
- [145] N. B. Robinson *et al.*, "The current state of animal models in research: A review," (in eng), *Int J Surg*, vol. 72, pp. 9-13, Dec 2019, doi: 10.1016/j.ijisu.2019.10.015.
- [146] Y. Shi, H. Inoue, J. C. Wu, and S. Yamanaka, "Induced pluripotent stem cell technology: a decade of progress," (in eng), *Nat Rev Drug Discov*, vol. 16, no. 2, pp. 115-130, 02 2017, doi: 10.1038/nrd.2016.245.
- [147] D. Hockemeyer and R. Jaenisch, "Induced Pluripotent Stem Cells Meet Genome Editing," (in eng), *Cell Stem Cell*, vol. 18, no. 5, pp. 573-86, 05 2016, doi: 10.1016/j.stem.2016.04.013.
- [148] D. Hockemeyer *et al.*, "Efficient targeting of expressed and silent genes in human ESCs and iPSCs using zinc-finger nucleases," (in eng), *Nat Biotechnol*, vol. 27, no. 9, pp. 851-7, Sep 2009, doi: 10.1038/nbt.1562.
- [149] L. Cong *et al.*, "Multiplex genome engineering using CRISPR/Cas systems," (in eng), *Science*, vol. 339, no. 6121, pp. 819-23, Feb 15 2013, doi: 10.1126/science.1231143.
- [150] O. Shalem *et al.*, "Genome-scale CRISPR-Cas9 knockout screening in human cells," (in eng), *Science*, vol. 343, no. 6166, pp. 84-87, Jan 03 2014, doi: 10.1126/science.1247005.
- [151] C. De Masi, P. Spitalieri, M. Murdocca, G. Novelli, and F. Sangiuolo, "Application of CRISPR/Cas9 to human-induced pluripotent stem cells: from gene editing to drug discovery," (in eng), *Hum Genomics*, vol. 14, no. 1, p. 25, 06 26 2020, doi: 10.1186/s40246-020-00276-2.
- [152] M. Christian *et al.*, "Targeting DNA double-strand breaks with TAL effector nucleases," (in eng), *Genetics*, vol. 186, no. 2, pp. 757-61, Oct 2010, doi: 10.1534/genetics.110.120717.
- [153] D. Hockemeyer *et al.*, "Genetic engineering of human pluripotent cells using TALE nucleases," (in eng), *Nat Biotechnol*, vol. 29, no. 8, pp. 731-4, Jul 07 2011, doi: 10.1038/nbt.1927.
- [154] H. M. Chao and E. Chern, "Patient-derived induced pluripotent stem cells for models of cancer and cancer stem cell research," (in eng), *J Formos Med Assoc*, vol. 117, no. 12, pp. 1046-1057, Dec 2018, doi: 10.1016/j.jfma.2018.06.013.
- [155] M. X. Doss and A. Sachinidis, "Current Challenges of iPSC-Based Disease Modeling and Therapeutic Implications," (in eng), *Cells*, vol. 8, no. 5, 04 30 2019, doi: 10.3390/cells8050403.
- [156] S. H. Stricker *et al.*, "Widespread resetting of DNA methylation in glioblastoma-initiating cells suppresses malignant cellular behavior in a lineage-dependent manner," (in eng), *Genes Dev*, vol. 27, no. 6, pp. 654-69, Mar 15 2013, doi: 10.1101/gad.212662.112.
- [157] I. Sancho-Martinez *et al.*, "Establishment of human iPSC-based models for the study and targeting of glioma initiating cells," (in eng), *Nat Commun*, vol. 7, p. 10743, Feb 22 2016, doi: 10.1038/ncomms10743.
- [158] M. Paolillo, S. Comincini, and S. Schinelli, "In Vitro Glioblastoma Models: A Journey into the Third Dimension," (in eng), *Cancers (Basel)*, vol. 13, no. 10, May 18 2021, doi: 10.3390/cancers13102449.
- [159] S. Miyazaki *et al.*, "A Cancer Reprogramming Method Using MicroRNAs as a Novel Therapeutic Approach against Colon Cancer: Research for Reprogramming of Cancer Cells by MicroRNAs," (in eng), *Ann Surg Oncol*, vol. 22 Suppl 3, pp. S1394-401, Dec 2015, doi: 10.1245/s10434-014-4217-1.

- [160] C. C. Ku *et al.*, "Generation of Human Stomach Cancer iPSC-Derived Organoids Induced by," (in eng), *Cells*, vol. 11, no. 2, 01 06 2022, doi: 10.3390/cells11020184.
- [161] K. Miyoshi *et al.*, "Generation of human induced pluripotent stem cells from oral mucosa," (in eng), *J Biosci Bioeng*, vol. 110, no. 3, pp. 345-50, Sep 2010, doi: 10.1016/j.jbiosc.2010.03.004.
- [162] A. G. Kotini *et al.*, "Stage-Specific Human Induced Pluripotent Stem Cells Map the Progression of Myeloid Transformation to Transplantable Leukemia," (in eng), *Cell Stem Cell*, vol. 20, no. 3, pp. 315-328.e7, 03 02 2017, doi: 10.1016/j.stem.2017.01.009.
- [163] H. Kim and C. Schaniel, "Modeling Hematological Diseases and Cancer With Patient-Specific Induced Pluripotent Stem Cells," (in eng), *Front Immunol*, vol. 9, p. 2243, 2018, doi: 10.3389/fimmu.2018.02243.
- [164] H. J. Kim *et al.*, "Establishment of Hepatocellular Cancer Induced Pluripotent Stem Cells Using a Reprogramming Technique," (in eng), *Gut Liver*, vol. 11, no. 2, pp. 261-269, Mar 15 2017, doi: 10.5009/gnl15389.
- [165] K. Noguchi *et al.*, "Susceptibility of pancreatic cancer stem cells to reprogramming," (in eng), *Cancer Sci*, vol. 106, no. 9, pp. 1182-7, Sep 2015, doi: 10.1111/cas.12734.
- [166] D. F. Lee *et al.*, "Modeling familial cancer with induced pluripotent stem cells," (in eng), *Cell*, vol. 161, no. 2, pp. 240-54, Apr 09 2015, doi: 10.1016/j.cell.2015.02.045.
- [167] R. Zhou, A. Xu, J. Gingold, L. C. Strong, R. Zhao, and D. F. Lee, "Li-Fraumeni Syndrome Disease Model: A Platform to Develop Precision Cancer Therapy Targeting Oncogenic p53," (in eng), *Trends Pharmacol Sci*, vol. 38, no. 10, pp. 908-927, 10 2017, doi: 10.1016/j.tips.2017.07.004.
- [168] H. Kim *et al.*, "Oncogenic role of SFRP2 in p53-mutant osteosarcoma development via autocrine and paracrine mechanism," (in eng), *Proc Natl Acad Sci U S A*, vol. 115, no. 47, pp. E11128-E11137, 11 20 2018, doi: 10.1073/pnas.1814044115.
- [169] S. Mulero-Navarro *et al.*, "Myeloid Dysregulation in a Human Induced Pluripotent Stem Cell Model of PTPN11-Associated Juvenile Myelomonocytic Leukemia," (in eng), *Cell Rep*, vol. 13, no. 3, pp. 504-515, Oct 20 2015, doi: 10.1016/j.celrep.2015.09.019.
- [170] R. Li *et al.*, "Generation of an induced pluripotent stem cell line (TRNDi003-A) from a Noonan syndrome with multiple lentigines (NSML) patient carrying a p.Q510P mutation in the PTPN11 gene," (in eng), *Stem Cell Res*, vol. 34, p. 101374, 01 2019, doi: 10.1016/j.scr.2018.101374.
- [171] L. Han *et al.*, "Study familial hypertrophic cardiomyopathy using patient-specific induced pluripotent stem cells," (in eng), *Cardiovasc Res*, vol. 104, no. 2, pp. 258-69, Nov 01 2014, doi: 10.1093/cvr/cvu205.
- [172] A. Tanaka *et al.*, "Endothelin-1 induces myofibrillar disarray and contractile vector variability in hypertrophic cardiomyopathy-induced pluripotent stem cell-derived cardiomyocytes," (in eng), *J Am Heart Assoc*, vol. 3, no. 6, p. e001263, Nov 11 2014, doi: 10.1161/JAHA.114.001263.
- [173] P. W. Burridge, S. Diecke, E. Matsa, A. Sharma, H. Wu, and J. C. Wu, "Modeling Cardiovascular Diseases with Patient-Specific Human Pluripotent Stem Cell-Derived Cardiomyocytes," (in eng), *Methods Mol Biol*, vol. 1353, pp. 119-30, 2016, doi: 10.1007/7651_2015_196.
- [174] S. P. Wyles *et al.*, "Modeling structural and functional deficiencies of RBM20 familial dilated cardiomyopathy using human induced pluripotent stem cells," (in eng), *Hum Mol Genet*, vol. 25, no. 2, pp. 254-65, Jan 15 2016, doi: 10.1093/hmg/ddv468.

- [175] K. Musunuru *et al.*, "Induced Pluripotent Stem Cells for Cardiovascular Disease Modeling and Precision Medicine: A Scientific Statement From the American Heart Association," (in eng), *Circ Genom Precis Med*, vol. 11, no. 1, p. e000043, 01 2018, doi: 10.1161/HCG.0000000000000043.
- [176] J. J. Hwang, J. Choi, Y. A. Rim, Y. Nam, and J. H. Ju, "Application of Induced Pluripotent Stem Cells for Disease Modeling and 3D Model Construction: Focus on Osteoarthritis," (in eng), *Cells*, vol. 10, no. 11, 11 05 2021, doi: 10.3390/cells10113032.
- [177] M. Csobonyeiova, S. Polak, A. Nicodemou, R. Zamborsky, and L. Danisovic, "iPSCs in Modeling and Therapy of Osteoarthritis," (in eng), *Biomedicines*, vol. 9, no. 2, Feb 12 2021, doi: 10.3390/biomedicines9020186.
- [178] M. Abulaiti *et al.*, "Establishment of a heart-on-a-chip microdevice based on human iPSC cells for the evaluation of human heart tissue function," (in eng), *Sci Rep*, vol. 10, no. 1, p. 19201, 11 05 2020, doi: 10.1038/s41598-020-76062-w.
- [179] V. Paloschi *et al.*, "Organ-on-a-chip technology: a novel approach to investigate cardiovascular diseases," (in eng), *Cardiovasc Res*, vol. 117, no. 14, pp. 2742-2754, 12 17 2021, doi: 10.1093/cvr/cvab088.
- [180] E. L. Doherty, W. Y. Aw, A. J. Hickey, and W. J. Polacheck, "Microfluidic and Organ-on-a-Chip Approaches to Investigate Cellular and Microenvironmental Contributions to Cardiovascular Function and Pathology," (in eng), *Front Bioeng Biotechnol*, vol. 9, p. 624435, 2021, doi: 10.3389/fbioe.2021.624435.
- [181] S. Kim and S. Takayama, "Organ-on-a-chip and the kidney," (in eng), *Kidney Res Clin Pract*, vol. 34, no. 3, pp. 165-9, Sep 2015, doi: 10.1016/j.krcp.2015.08.001.
- [182] R. Paoli and J. Samitier, "Mimicking the Kidney: A Key Role in Organ-on-Chip Development," (in eng), *Micromachines (Basel)*, vol. 7, no. 7, Jul 20 2016, doi: 10.3390/mi7070126.
- [183] J. Ribas *et al.*, "Biomechanical Strain Exacerbates Inflammation on a Progeria-on-a-Chip Model," (in eng), *Small*, vol. 13, no. 15, 04 2017, doi: 10.1002/smll.201603737.
- [184] L. Atchison, H. Zhang, K. Cao, and G. A. Truskey, "A Tissue Engineered Blood Vessel Model of Hutchinson-Gilford Progeria Syndrome Using Human iPSC-derived Smooth Muscle Cells," (in eng), *Sci Rep*, vol. 7, no. 1, p. 8168, 08 15 2017, doi: 10.1038/s41598-017-08632-4.
- [185] F. G. Lafaille *et al.*, "Impaired intrinsic immunity to HSV-1 in human iPSC-derived TLR3-deficient CNS cells," (in eng), *Nature*, vol. 491, no. 7426, pp. 769-73, Nov 29 2012, doi: 10.1038/nature11583.
- [186] R. G. Rowe and G. Q. Daley, "Induced pluripotent stem cells in disease modelling and drug discovery," (in eng), *Nat Rev Genet*, vol. 20, no. 7, pp. 377-388, 07 2019, doi: 10.1038/s41576-019-0100-z.
- [187] Z. Chen *et al.*, "Reprogramming progeria fibroblasts re-establishes a normal epigenetic landscape," (in eng), *Aging Cell*, vol. 16, no. 4, pp. 870-887, 08 2017, doi: 10.1111/acel.12621.
- [188] H. Okano and S. Morimoto, "iPSC-based disease modeling and drug discovery in cardinal neurodegenerative disorders," (in eng), *Cell Stem Cell*, vol. 29, no. 2, pp. 189-208, 02 03 2022, doi: 10.1016/j.stem.2022.01.007.
- [189] L. Li, J. Chao, and Y. Shi, "Modeling neurological diseases using iPSC-derived neural cells : iPSC modeling of neurological diseases," (in eng), *Cell Tissue Res*, vol. 371, no. 1, pp. 143-151, 01 2018, doi: 10.1007/s00441-017-2713-x.
- [190] M. Barak *et al.*, "Human iPSC-Derived Neural Models for Studying Alzheimer's Disease: from Neural Stem Cells to Cerebral Organoids," (in eng), *Stem Cell Rev Rep*, vol. 18, no. 2, pp. 792-820, 02 2022, doi: 10.1007/s12015-021-10254-3.

- [191] A. Ochalek *et al.*, "Neurons derived from sporadic Alzheimer's disease iPSCs reveal elevated TAU hyperphosphorylation, increased amyloid levels, and GSK3B activation," (in eng), *Alzheimers Res Ther*, vol. 9, no. 1, p. 90, Dec 01 2017, doi: 10.1186/s13195-017-0317-z.
- [192] M. Ortiz-Virumbrales *et al.*, "CRISPR/Cas9-Correctable mutation-related molecular and physiological phenotypes in iPSC-derived Alzheimer's PSEN2," (in eng), *Acta Neuropathol Commun*, vol. 5, no. 1, p. 77, 10 27 2017, doi: 10.1186/s40478-017-0475-z.
- [193] M. Wezyk *et al.*, "Overactive BRCA1 Affects Presenilin 1 in Induced Pluripotent Stem Cell-Derived Neurons in Alzheimer's Disease," (in eng), *J Alzheimers Dis*, vol. 62, no. 1, pp. 175-202, 2018, doi: 10.3233/JAD-170830.
- [194] K. H. Chang *et al.*, "Modeling Alzheimer's Disease by Induced Pluripotent Stem Cells Carrying APP D678H Mutation," (in eng), *Mol Neurobiol*, vol. 56, no. 6, pp. 3972-3983, Jun 2019, doi: 10.1007/s12035-018-1336-x.
- [195] L. Duan, B. J. Bhattacharyya, A. Belmadani, L. Pan, R. J. Miller, and J. A. Kessler, "Stem cell derived basal forebrain cholinergic neurons from Alzheimer's disease patients are more susceptible to cell death," (in eng), *Mol Neurodegener*, vol. 9, p. 3, Jan 2014, doi: 10.1186/1750-1326-9-3.
- [196] C. R. Muratore *et al.*, "The familial Alzheimer's disease APPV717I mutation alters APP processing and Tau expression in iPSC-derived neurons," (in eng), *Hum Mol Genet*, vol. 23, no. 13, pp. 3523-36, Jul 2014, doi: 10.1093/hmg/ddu064.
- [197] E. F. Fang *et al.*, "Mitophagy inhibits amyloid- β and tau pathology and reverses cognitive deficits in models of Alzheimer's disease," (in eng), *Nat Neurosci*, vol. 22, no. 3, pp. 401-412, 03 2019, doi: 10.1038/s41593-018-0332-9.
- [198] T. Kondo *et al.*, "Modeling Alzheimer's disease with iPSCs reveals stress phenotypes associated with intracellular A β and differential drug responsiveness," (in eng), *Cell Stem Cell*, vol. 12, no. 4, pp. 487-96, Apr 2013, doi: 10.1016/j.stem.2013.01.009.
- [199] T. Yagi *et al.*, "Modeling familial Alzheimer's disease with induced pluripotent stem cells," (in eng), *Hum Mol Genet*, vol. 20, no. 23, pp. 4530-9, Dec 2011, doi: 10.1093/hmg/ddr394.
- [200] G. Woodruff *et al.*, "The presenilin-1 Δ E9 mutation results in reduced γ -secretase activity, but not total loss of PS1 function, in isogenic human stem cells," (in eng), *Cell Rep*, vol. 5, no. 4, pp. 974-85, Nov 27 2013, doi: 10.1016/j.celrep.2013.10.018.
- [201] E. Armijo, C. Gonzalez, M. Shahnawaz, A. Flores, B. Davis, and C. Soto, "Increased susceptibility to A β toxicity in neuronal cultures derived from familial Alzheimer's disease (PSEN1-A246E) induced pluripotent stem cells," (in eng), *Neurosci Lett*, vol. 639, pp. 74-81, 02 2017, doi: 10.1016/j.neulet.2016.12.060.
- [202] J. K. Lee *et al.*, "Acid sphingomyelinase modulates the autophagic process by controlling lysosomal biogenesis in Alzheimer's disease," (in eng), *J Exp Med*, vol. 211, no. 8, pp. 1551-70, Jul 28 2014, doi: 10.1084/jem.20132451.
- [203] J. Yang *et al.*, "Early pathogenic event of Alzheimer's disease documented in iPSCs from patients with PSEN1 mutations," (in eng), *Oncotarget*, vol. 8, no. 5, pp. 7900-7913, Jan 31 2017, doi: 10.18632/oncotarget.13776.
- [204] P. Martín-Maestro *et al.*, "Mitophagy Failure in Fibroblasts and iPSC-Derived Neurons of Alzheimer's Disease-Associated Presenilin 1 Mutation," (in eng), *Front Mol Neurosci*, vol. 10, p. 291, 2017, doi: 10.3389/fnmol.2017.00291.
- [205] A. A. Sproul *et al.*, "Characterization and molecular profiling of PSEN1 familial Alzheimer's disease iPSC-derived neural progenitors," (in eng), *PLoS One*, vol. 9, no. 1, p. e84547, 2014, doi: 10.1371/journal.pone.0084547.

- [206] M. A. Israel *et al.*, "Probing sporadic and familial Alzheimer's disease using induced pluripotent stem cells," (in eng), *Nature*, vol. 482, no. 7384, pp. 216-20, Jan 2012, doi: 10.1038/nature10821.
- [207] J. H. Birnbaum *et al.*, "Oxidative stress and altered mitochondrial protein expression in the absence of amyloid- β and tau pathology in iPSC-derived neurons from sporadic Alzheimer's disease patients," (in eng), *Stem Cell Res*, vol. 27, pp. 121-130, 03 2018, doi: 10.1016/j.scr.2018.01.019.
- [208] K. Imaizumi *et al.*, "Controlling the Regional Identity of hPSC-Derived Neurons to Uncover Neuronal Subtype Specificity of Neurological Disease Phenotypes," (in eng), *Stem Cell Reports*, vol. 5, no. 6, pp. 1010-1022, Dec 08 2015, doi: 10.1016/j.stemcr.2015.10.005.
- [209] Y. T. Lin *et al.*, "APOE4 Causes Widespread Molecular and Cellular Alterations Associated with Alzheimer's Disease Phenotypes in Human iPSC-Derived Brain Cell Types," (in eng), *Neuron*, vol. 98, no. 6, pp. 1141-1154.e7, 06 27 2018, doi: 10.1016/j.neuron.2018.05.008.
- [210] A. R. Wadhvani, A. Affaneh, S. Van Gulden, and J. A. Kessler, "Neuronal apolipoprotein E4 increases cell death and phosphorylated tau release in alzheimer disease," (in eng), *Ann Neurol*, vol. 85, no. 5, pp. 726-739, 05 2019, doi: 10.1002/ana.25455.
- [211] C. Eroglu and B. A. Barres, "Regulation of synaptic connectivity by glia," (in eng), *Nature*, vol. 468, no. 7321, pp. 223-31, Nov 11 2010, doi: 10.1038/nature09612.
- [212] M. Bélanger, I. Allaman, and P. J. Magistretti, "Brain energy metabolism: focus on astrocyte-neuron metabolic cooperation," (in eng), *Cell Metab*, vol. 14, no. 6, pp. 724-38, Dec 07 2011, doi: 10.1016/j.cmet.2011.08.016.
- [213] N. J. Allen and C. Eroglu, "Cell Biology of Astrocyte-Synapse Interactions," (in eng), *Neuron*, vol. 96, no. 3, pp. 697-708, Nov 01 2017, doi: 10.1016/j.neuron.2017.09.056.
- [214] V. C. Jones, R. Atkinson-Dell, A. Verkhratsky, and L. Mohamet, "Aberrant iPSC-derived human astrocytes in Alzheimer's disease," (in eng), *Cell Death Dis*, vol. 8, no. 3, p. e2696, 03 2017, doi: 10.1038/cddis.2017.89.
- [215] M. C. Liao *et al.*, "Single-Cell Detection of Secreted A β and sAPP α from Human IPSC-Derived Neurons and Astrocytes," (in eng), *J Neurosci*, vol. 36, no. 5, pp. 1730-46, Feb 03 2016, doi: 10.1523/JNEUROSCI.2735-15.2016.
- [216] M. Prinz and J. Priller, "Microglia and brain macrophages in the molecular age: from origin to neuropsychiatric disease," (in eng), *Nat Rev Neurosci*, vol. 15, no. 5, pp. 300-12, May 2014, doi: 10.1038/nrn3722.
- [217] S. Hong, L. Dissing-Olesen, and B. Stevens, "New insights on the role of microglia in synaptic pruning in health and disease," (in eng), *Curr Opin Neurobiol*, vol. 36, pp. 128-34, Feb 2016, doi: 10.1016/j.conb.2015.12.004.
- [218] J. Penney, W. T. Ralvenius, and L. H. Tsai, "Modeling Alzheimer's disease with iPSC-derived brain cells," (in eng), *Mol Psychiatry*, vol. 25, no. 1, pp. 148-167, 01 2020, doi: 10.1038/s41380-019-0468-3.
- [219] J. Muffat *et al.*, "Efficient derivation of microglia-like cells from human pluripotent stem cells," (in eng), *Nat Med*, vol. 22, no. 11, pp. 1358-1367, 11 2016, doi: 10.1038/nm.4189.
- [220] E. M. Abud *et al.*, "iPSC-Derived Human Microglia-like Cells to Study Neurological Diseases," (in eng), *Neuron*, vol. 94, no. 2, pp. 278-293.e9, Apr 19 2017, doi: 10.1016/j.neuron.2017.03.042.
- [221] P. W. Brownjohn *et al.*, "Functional Studies of Missense TREM2 Mutations in Human Stem Cell-Derived Microglia," (in eng), *Stem Cell Reports*, vol. 10, no. 4, pp. 1294-1307, 04 10 2018, doi: 10.1016/j.stemcr.2018.03.003.

- [222] P. Garcia-Reitboeck *et al.*, "Human Induced Pluripotent Stem Cell-Derived Microglia-Like Cells Harboring TREM2 Missense Mutations Show Specific Deficits in Phagocytosis," (in eng), *Cell Rep*, vol. 24, no. 9, pp. 2300-2311, 08 28 2018, doi: 10.1016/j.celrep.2018.07.094.
- [223] L. Dimou and M. Simons, "Diversity of oligodendrocytes and their progenitors," (in eng), *Curr Opin Neurobiol*, vol. 47, pp. 73-79, 12 2017, doi: 10.1016/j.conb.2017.09.015.
- [224] S. E. Nasrabady, B. Rizvi, J. E. Goldman, and A. M. Brickman, "White matter changes in Alzheimer's disease: a focus on myelin and oligodendrocytes," (in eng), *Acta Neuropathol Commun*, vol. 6, no. 1, p. 22, 03 02 2018, doi: 10.1186/s40478-018-0515-3.
- [225] E. Papuč and K. Rejdak, "The role of myelin damage in Alzheimer's disease pathology," (in eng), *Arch Med Sci*, vol. 16, no. 2, pp. 345-351, 2020, doi: 10.5114/aoms.2018.76863.
- [226] J. Tran, H. Anastacio, and C. Bardy, "Genetic predispositions of Parkinson's disease revealed in patient-derived brain cells," (in eng), *NPJ Parkinsons Dis*, vol. 6, p. 8, 2020, doi: 10.1038/s41531-020-0110-8.
- [227] P. Seibler, J. Graziotto, H. Jeong, F. Simunovic, C. Klein, and D. Krainc, "Mitochondrial Parkin recruitment is impaired in neurons derived from mutant PINK1 induced pluripotent stem cells," (in eng), *J Neurosci*, vol. 31, no. 16, pp. 5970-6, Apr 2011, doi: 10.1523/JNEUROSCI.4441-10.2011.
- [228] Y. Imaizumi *et al.*, "Mitochondrial dysfunction associated with increased oxidative stress and α -synuclein accumulation in PARK2 iPSC-derived neurons and postmortem brain tissue," (in eng), *Mol Brain*, vol. 5, p. 35, Oct 06 2012, doi: 10.1186/1756-6606-5-35.
- [229] S. Y. Chung *et al.*, "Parkin and PINK1 Patient iPSC-Derived Midbrain Dopamine Neurons Exhibit Mitochondrial Dysfunction and α -Synuclein Accumulation," (in eng), *Stem Cell Reports*, vol. 7, no. 4, pp. 664-677, 10 2016, doi: 10.1016/j.stemcr.2016.08.012.
- [230] H. Bogetofte *et al.*, "Mutation Causes Metabolic Disturbances and Impaired Survival of Human iPSC-Derived Neurons," (in eng), *Front Cell Neurosci*, vol. 13, p. 297, 2019, doi: 10.3389/fncel.2019.00297.
- [231] C. M. Woodard *et al.*, "iPSC-derived dopamine neurons reveal differences between monozygotic twins discordant for Parkinson's disease," (in eng), *Cell Rep*, vol. 9, no. 4, pp. 1173-82, Nov 20 2014, doi: 10.1016/j.celrep.2014.10.023.
- [232] H. J. Fernandes *et al.*, "ER Stress and Autophagic Perturbations Lead to Elevated Extracellular α -Synuclein in GBA-N370S Parkinson's iPSC-Derived Dopamine Neurons," (in eng), *Stem Cell Reports*, vol. 6, no. 3, pp. 342-56, Mar 08 2016, doi: 10.1016/j.stemcr.2016.01.013.
- [233] D. C. Schöndorf *et al.*, "The NAD⁺ Precursor Nicotinamide Riboside Rescues Mitochondrial Defects and Neuronal Loss in iPSC and Fly Models of Parkinson's Disease," (in eng), *Cell Rep*, vol. 23, no. 10, pp. 2976-2988, 06 05 2018, doi: 10.1016/j.celrep.2018.05.009.
- [234] M. Y. Son *et al.*, "Distinctive genomic signature of neural and intestinal organoids from familial Parkinson's disease patient-derived induced pluripotent stem cells," (in eng), *Neuropathol Appl Neurobiol*, vol. 43, no. 7, pp. 584-603, Dec 2017, doi: 10.1111/nan.12396.
- [235] L. H. Sanders *et al.*, "LRRK2 mutations cause mitochondrial DNA damage in iPSC-derived neural cells from Parkinson's disease patients: reversal by gene correction," (in eng), *Neurobiol Dis*, vol. 62, pp. 381-6, Feb 2014, doi: 10.1016/j.nbd.2013.10.013.

- [236] J. Walter *et al.*, "Neural Stem Cells of Parkinson's Disease Patients Exhibit Aberrant Mitochondrial Morphology and Functionality," (in eng), *Stem Cell Reports*, vol. 12, no. 5, pp. 878-889, 05 14 2019, doi: 10.1016/j.stemcr.2019.03.004.
- [237] M. Nguyen and D. Krainc, "LRRK2 phosphorylation of auxilin mediates synaptic defects in dopaminergic neurons from patients with Parkinson's disease," (in eng), *Proc Natl Acad Sci U S A*, vol. 115, no. 21, pp. 5576-5581, 05 22 2018, doi: 10.1073/pnas.1717590115.
- [238] A. di Domenico *et al.*, "Patient-Specific iPSC-Derived Astrocytes Contribute to Non-Cell-Autonomous Neurodegeneration in Parkinson's Disease," (in eng), *Stem Cell Reports*, vol. 12, no. 2, pp. 213-229, 02 12 2019, doi: 10.1016/j.stemcr.2018.12.011.
- [239] P. Y. Pan *et al.*, "Parkinson's Disease-Associated LRRK2 Hyperactive Kinase Mutant Disrupts Synaptic Vesicle Trafficking in Ventral Midbrain Neurons," (in eng), *J Neurosci*, vol. 37, no. 47, pp. 11366-11376, 11 22 2017, doi: 10.1523/JNEUROSCI.0964-17.2017.
- [240] N. Connor-Robson *et al.*, "An integrated transcriptomics and proteomics analysis reveals functional endocytic dysregulation caused by mutations in LRRK2," (in eng), *Neurobiol Dis*, vol. 127, pp. 512-526, 07 2019, doi: 10.1016/j.nbd.2019.04.005.
- [241] S. Avazzadeh, J. M. Baena, C. Keighron, Y. Feller-Sanchez, and L. R. Quinlan, "Modelling Parkinson's Disease: iPSCs towards Better Understanding of Human Pathology," (in eng), *Brain Sci*, vol. 11, no. 3, Mar 14 2021, doi: 10.3390/brainsci11030373.
- [242] A. Flierl *et al.*, "Higher vulnerability and stress sensitivity of neuronal precursor cells carrying an alpha-synuclein gene triplication," (in eng), *PLoS One*, vol. 9, no. 11, p. e112413, 2014, doi: 10.1371/journal.pone.0112413.
- [243] J. Arias-Fuenzalida *et al.*, "FACS-Assisted CRISPR-Cas9 Genome Editing Facilitates Parkinson's Disease Modeling," (in eng), *Stem Cell Reports*, vol. 9, no. 5, pp. 1423-1431, 11 14 2017, doi: 10.1016/j.stemcr.2017.08.026.
- [244] R. M. Brazdis *et al.*, "Demonstration of brain region-specific neuronal vulnerability in human iPSC-based model of familial Parkinson's disease," (in eng), *Hum Mol Genet*, vol. 29, no. 7, pp. 1180-1191, 05 08 2020, doi: 10.1093/hmg/ddaa039.
- [245] S. D. Ryan *et al.*, "Isogenic human iPSC Parkinson's model shows nitrosative stress-induced dysfunction in MEF2-PGC1 α transcription," (in eng), *Cell*, vol. 155, no. 6, pp. 1351-64, Dec 05 2013, doi: 10.1016/j.cell.2013.11.009.
- [246] I. Prots *et al.*, " α -Synuclein oligomers induce early axonal dysfunction in human iPSC-based models of synucleinopathies," (in eng), *Proc Natl Acad Sci U S A*, vol. 115, no. 30, pp. 7813-7818, 07 24 2018, doi: 10.1073/pnas.1713129115.
- [247] M. H. R. Ludtmann *et al.*, " α -synuclein oligomers interact with ATP synthase and open the permeability transition pore in Parkinson's disease," (in eng), *Nat Commun*, vol. 9, no. 1, p. 2293, 06 12 2018, doi: 10.1038/s41467-018-04422-2.
- [248] U. Dettmer *et al.*, "Parkinson-causing α -synuclein missense mutations shift native tetramers to monomers as a mechanism for disease initiation," (in eng), *Nat Commun*, vol. 6, p. 7314, Jun 16 2015, doi: 10.1038/ncomms8314.
- [249] G. Kouroupi *et al.*, "Defective synaptic connectivity and axonal neuropathology in a human iPSC-based model of familial Parkinson's disease," (in eng), *Proc Natl Acad Sci U S A*, vol. 114, no. 18, pp. E3679-E3688, 05 02 2017, doi: 10.1073/pnas.1617259114.
- [250] O. Zygogianni, N. Antoniou, M. Kalomoiri, G. Kouroupi, E. Taoufik, and R. Matsas, "In Vivo Phenotyping of Familial Parkinson's Disease with Human

- Induced Pluripotent Stem Cells: A Proof-of-Concept Study," (in eng), *Neurochem Res*, vol. 44, no. 6, pp. 1475-1493, Jun 2019, doi: 10.1007/s11064-019-02781-w.
- [251] S. M. Heman-Ackah *et al.*, "Alpha-synuclein induces the unfolded protein response in Parkinson's disease SNCA triplication iPSC-derived neurons," (in eng), *Hum Mol Genet*, vol. 26, no. 22, pp. 4441-4450, 11 15 2017, doi: 10.1093/hmg/ddx331.
- [252] F. Zambon *et al.*, "Cellular α -synuclein pathology is associated with bioenergetic dysfunction in Parkinson's iPSC-derived dopamine neurons," (in eng), *Hum Mol Genet*, vol. 28, no. 12, pp. 2001-2013, 06 15 2019, doi: 10.1093/hmg/ddz038.
- [253] L. Lin, J. Göke, E. Cukuroglu, M. R. Dranias, A. M. VanDongen, and L. W. Stanton, "Molecular Features Underlying Neurodegeneration Identified through In Vitro Modeling of Genetically Diverse Parkinson's Disease Patients," (in eng), *Cell Rep*, vol. 15, no. 11, pp. 2411-26, 06 14 2016, doi: 10.1016/j.celrep.2016.05.022.
- [254] L. F. Burbulla *et al.*, "Dopamine oxidation mediates mitochondrial and lysosomal dysfunction in Parkinson's disease," (in eng), *Science*, vol. 357, no. 6357, pp. 1255-1261, 09 22 2017, doi: 10.1126/science.aam9080.
- [255] C. Y. Xu *et al.*, "DJ-1 Inhibits α -Synuclein Aggregation by Regulating Chaperone-Mediated Autophagy," (in eng), *Front Aging Neurosci*, vol. 9, p. 308, 2017, doi: 10.3389/fnagi.2017.00308.
- [256] T. Ahfeldt *et al.*, "Pathogenic Pathways in Early-Onset Autosomal Recessive Parkinson's Disease Discovered Using Isogenic Human Dopaminergic Neurons," (in eng), *Stem Cell Reports*, vol. 14, no. 1, pp. 75-90, 01 14 2020, doi: 10.1016/j.stemcr.2019.12.005.
- [257] K. Shiba-Fukushima *et al.*, "Evidence that phosphorylated ubiquitin signaling is involved in the etiology of Parkinson's disease," (in eng), *Hum Mol Genet*, vol. 26, no. 16, pp. 3172-3185, 08 15 2017, doi: 10.1093/hmg/ddx201.
- [258] H. Fukusumi *et al.*, "Alpha-synuclein dynamics in induced pluripotent stem cell-derived dopaminergic neurons from a Parkinson's disease patient (PARK4) with SNCA triplication," (in eng), *FEBS Open Bio*, vol. 11, no. 2, pp. 354-366, 02 2021, doi: 10.1002/2211-5463.13060.
- [259] J. Okarmus *et al.*, "Identification of bioactive metabolites in human iPSC-derived dopaminergic neurons with PARK2 mutation: Altered mitochondrial and energy metabolism," (in eng), *Stem Cell Reports*, vol. 16, no. 6, pp. 1510-1526, 06 08 2021, doi: 10.1016/j.stemcr.2021.04.022.
- [260] A. H. Laperle *et al.*, "iPSC modeling of young-onset Parkinson's disease reveals a molecular signature of disease and novel therapeutic candidates," (in eng), *Nat Med*, vol. 26, no. 2, pp. 289-299, 02 2020, doi: 10.1038/s41591-019-0739-1.
- [261] M. Wernig *et al.*, "Neurons derived from reprogrammed fibroblasts functionally integrate into the fetal brain and improve symptoms of rats with Parkinson's disease," (in eng), *Proc Natl Acad Sci U S A*, vol. 105, no. 15, pp. 5856-61, Apr 2008, doi: 10.1073/pnas.0801677105.
- [262] S. Wang *et al.*, "Autologous iPSC-derived dopamine neuron transplantation in a nonhuman primate Parkinson's disease model," (in eng), *Cell Discov*, vol. 1, p. 15012, 2015, doi: 10.1038/celldisc.2015.12.
- [263] B. Song *et al.*, "Human autologous iPSC-derived dopaminergic progenitors restore motor function in Parkinson's disease models," (in eng), *J Clin Invest*, vol. 130, no. 2, pp. 904-920, 02 03 2020, doi: 10.1172/JCI130767.
- [264] F. Du, Q. Yu, A. Chen, D. Chen, and S. S. Yan, "Astrocytes Attenuate Mitochondrial Dysfunctions in Human Dopaminergic Neurons Derived from iPSC," (in eng), *Stem Cell Reports*, vol. 10, no. 2, pp. 366-374, 02 13 2018, doi: 10.1016/j.stemcr.2017.12.021.

- [265] C. Azevedo *et al.*, "Parkinson's disease and multiple system atrophy patient iPSC-derived oligodendrocytes exhibit alpha-synuclein-induced changes in maturation and immune reactive properties," (in eng), *Proc Natl Acad Sci U S A*, vol. 119, no. 12, p. e2111405119, 03 22 2022, doi: 10.1073/pnas.2111405119.
- [266] K. Badanjak *et al.*, "iPSC-Derived Microglia as a Model to Study Inflammation in Idiopathic Parkinson's Disease," (in eng), *Front Cell Dev Biol*, vol. 9, p. 740758, 2021, doi: 10.3389/fcell.2021.740758.
- [267] R. Chang, X. Liu, S. Li, and X. J. Li, "Transgenic animal models for study of the pathogenesis of Huntington's disease and therapy," (in eng), *Drug Des Devel Ther*, vol. 9, pp. 2179-88, 2015, doi: 10.2147/DDDT.S58470.
- [268] L. Liu *et al.*, "Induced Pluripotent Stem Cells in Huntington's Disease: Disease Modeling and the Potential for Cell-Based Therapy," (in eng), *Mol Neurobiol*, vol. 53, no. 10, pp. 6698-6708, 12 2016, doi: 10.1007/s12035-015-9601-8.
- [269] M. Csobonyeiova, S. Polak, and L. Danisovic, "Recent Overview of the Use of iPSCs Huntington's Disease Modeling and Therapy," (in eng), *Int J Mol Sci*, vol. 21, no. 6, Mar 24 2020, doi: 10.3390/ijms21062239.
- [270] I. H. Park *et al.*, "Disease-specific induced pluripotent stem cells," (in eng), *Cell*, vol. 134, no. 5, pp. 877-86, Sep 2008, doi: 10.1016/j.cell.2008.07.041.
- [271] N. Zhang, M. C. An, D. Montoro, and L. M. Ellerby, "Characterization of Human Huntington's Disease Cell Model from Induced Pluripotent Stem Cells," (in eng), *PLoS Curr*, vol. 2, p. RRN1193, Oct 2010, doi: 10.1371/currents.RRN1193.
- [272] M. C. An *et al.*, "Genetic correction of Huntington's disease phenotypes in induced pluripotent stem cells," (in eng), *Cell Stem Cell*, vol. 11, no. 2, pp. 253-63, Aug 03 2012, doi: 10.1016/j.stem.2012.04.026.
- [273] H. i. Consortium, "Induced pluripotent stem cells from patients with Huntington's disease show CAG-repeat-expansion-associated phenotypes," (in eng), *Cell Stem Cell*, vol. 11, no. 2, pp. 264-78, Aug 2012, doi: 10.1016/j.stem.2012.04.027.
- [274] W. J. Szlachcic, P. M. Switonski, W. J. Krzyzosiak, M. Figlerowicz, and M. Figiel, "Huntington disease iPSCs show early molecular changes in intracellular signaling, the expression of oxidative stress proteins and the p53 pathway," (in eng), *Dis Model Mech*, vol. 8, no. 9, pp. 1047-57, Sep 2015, doi: 10.1242/dmm.019406.
- [275] K. Świtońska *et al.*, "Identification of Altered Developmental Pathways in Human Juvenile HD iPSC With 71Q and 109Q Using Transcriptome Profiling," (in eng), *Front Cell Neurosci*, vol. 12, p. 528, 2018, doi: 10.3389/fncel.2018.00528.
- [276] Y. Liu, F. Qiao, P. C. Leiferman, A. Ross, E. H. Schlenker, and H. Wang, "FOXOs modulate proteasome activity in human-induced pluripotent stem cells of Huntington's disease and their derived neural cells," (in eng), *Hum Mol Genet*, vol. 26, no. 22, pp. 4416-4428, 11 15 2017, doi: 10.1093/hmg/ddx327.
- [277] E. D. Nekrasov *et al.*, "Manifestation of Huntington's disease pathology in human induced pluripotent stem cell-derived neurons," (in eng), *Mol Neurodegener*, vol. 11, p. 27, Apr 14 2016, doi: 10.1186/s13024-016-0092-5.
- [278] A. Delli Carri *et al.*, "Developmentally coordinated extrinsic signals drive human pluripotent stem cell differentiation toward authentic DARPP-32+ medium-sized spiny neurons," (in eng), *Development*, vol. 140, no. 2, pp. 301-12, Jan 2013, doi: 10.1242/dev.084608.
- [279] S. Mu *et al.*, "Transplantation of induced pluripotent stem cells improves functional recovery in Huntington's disease rat model," (in eng), *PLoS One*, vol. 9, no. 7, p. e101185, 2014, doi: 10.1371/journal.pone.0101185.
- [280] A. Al-Gharaibeh *et al.*, "Induced Pluripotent Stem Cell-Derived Neural Stem Cell Transplantations Reduced Behavioral Deficits and Ameliorated Neuropathological Changes in YAC128 Mouse Model of Huntington's Disease," (in eng), *Front Neurosci*, vol. 11, p. 628, 2017, doi: 10.3389/fnins.2017.00628.

- [281] T. A. Juopperi *et al.*, "Astrocytes generated from patient induced pluripotent stem cells recapitulate features of Huntington's disease patient cells," (in eng), *Mol Brain*, vol. 5, p. 17, May 2012, doi: 10.1186/1756-6606-5-17.
- [282] N. Merienne *et al.*, "Cell-Type-Specific Gene Expression Profiling in Adult Mouse Brain Reveals Normal and Disease-State Signatures," (in eng), *Cell Rep*, vol. 26, no. 9, pp. 2477-2493.e9, 02 26 2019, doi: 10.1016/j.celrep.2019.02.003.
- [283] H. Phatnani and T. Maniatis, "Astrocytes in neurodegenerative disease," (in eng), *Cold Spring Harb Perspect Biol*, vol. 7, no. 6, Apr 15 2015, doi: 10.1101/cshperspect.a020628.
- [284] I. K. Cho, B. Yang, C. Forest, L. Qian, and A. W. S. Chan, "Amelioration of Huntington's disease phenotype in astrocytes derived from iPSC-derived neural progenitor cells of Huntington's disease monkeys," (in eng), *PLoS One*, vol. 14, no. 3, p. e0214156, 2019, doi: 10.1371/journal.pone.0214156.
- [285] V. J. Garcia *et al.*, "Huntington's Disease Patient-Derived Astrocytes Display Electrophysiological Impairments and Reduced Neuronal Support," (in eng), *Front Neurosci*, vol. 13, p. 669, 2019, doi: 10.3389/fnins.2019.00669.
- [286] J. F. Vasques, R. Mendez-Otero, and F. Gubert, "Modeling ALS using iPSCs: is it possible to reproduce the phenotypic variations observed in patients," (in eng), *Regen Med*, vol. 15, no. 7, pp. 1919-1933, 07 2020, doi: 10.2217/rme-2020-0067.
- [287] E. Kiskinis *et al.*, "Pathways disrupted in human ALS motor neurons identified through genetic correction of mutant SOD1," (in eng), *Cell Stem Cell*, vol. 14, no. 6, pp. 781-95, Jun 2014, doi: 10.1016/j.stem.2014.03.004.
- [288] H. Chen *et al.*, "Modeling ALS with iPSCs reveals that mutant SOD1 misregulates neurofilament balance in motor neurons," (in eng), *Cell Stem Cell*, vol. 14, no. 6, pp. 796-809, Jun 2014, doi: 10.1016/j.stem.2014.02.004.
- [289] J. H. Park, H. S. Park, S. Hong, and S. Kang, "Motor neurons derived from ALS-related mouse iPSCs recapitulate pathological features of ALS," (in eng), *Exp Mol Med*, vol. 48, no. 12, p. e276, 12 09 2016, doi: 10.1038/emm.2016.113.
- [290] B. J. Wainger *et al.*, "Intrinsic membrane hyperexcitability of amyotrophic lateral sclerosis patient-derived motor neurons," (in eng), *Cell Rep*, vol. 7, no. 1, pp. 1-11, Apr 2014, doi: 10.1016/j.celrep.2014.03.019.
- [291] M. Naujock *et al.*, "4-Aminopyridine Induced Activity Rescues Hypoexcitable Motor Neurons from Amyotrophic Lateral Sclerosis Patient-Derived Induced Pluripotent Stem Cells," (in eng), *Stem Cells*, vol. 34, no. 6, pp. 1563-75, 06 2016, doi: 10.1002/stem.2354.
- [292] L. Wang *et al.*, "CRISPR/Cas9-mediated targeted gene correction in amyotrophic lateral sclerosis patient iPSCs," (in eng), *Protein Cell*, vol. 8, no. 5, pp. 365-378, 05 2017, doi: 10.1007/s13238-017-0397-3.
- [293] C. J. Donnelly *et al.*, "RNA toxicity from the ALS/FTD C9ORF72 expansion is mitigated by antisense intervention," (in eng), *Neuron*, vol. 80, no. 2, pp. 415-28, Oct 2013, doi: 10.1016/j.neuron.2013.10.015.
- [294] D. Sareen *et al.*, "Targeting RNA foci in iPSC-derived motor neurons from ALS patients with a C9ORF72 repeat expansion," (in eng), *Sci Transl Med*, vol. 5, no. 208, p. 208ra149, Oct 2013, doi: 10.1126/scitranslmed.3007529.
- [295] R. Dafinca *et al.*, "C9orf72 Hexanucleotide Expansions Are Associated with Altered Endoplasmic Reticulum Calcium Homeostasis and Stress Granule Formation in Induced Pluripotent Stem Cell-Derived Neurons from Patients with Amyotrophic Lateral Sclerosis and Frontotemporal Dementia," (in eng), *Stem Cells*, vol. 34, no. 8, pp. 2063-78, 08 2016, doi: 10.1002/stem.2388.
- [296] B. T. Selvaraj *et al.*, "C9ORF72 repeat expansion causes vulnerability of motor neurons to Ca," (in eng), *Nat Commun*, vol. 9, no. 1, p. 347, 01 24 2018, doi: 10.1038/s41467-017-02729-0.

- [297] R. Lopez-Gonzalez *et al.*, "Poly(GR) in C9ORF72-Related ALS/FTD Compromises Mitochondrial Function and Increases Oxidative Stress and DNA Damage in iPSC-Derived Motor Neurons," (in eng), *Neuron*, vol. 92, no. 2, pp. 383-391, Oct 2016, doi: 10.1016/j.neuron.2016.09.015.
- [298] Y. Shi *et al.*, "Haploinsufficiency leads to neurodegeneration in C9ORF72 ALS/FTD human induced motor neurons," (in eng), *Nat Med*, vol. 24, no. 3, pp. 313-325, 03 2018, doi: 10.1038/nm.4490.
- [299] B. Bilican *et al.*, "Mutant induced pluripotent stem cell lines recapitulate aspects of TDP-43 proteinopathies and reveal cell-specific vulnerability," (in eng), *Proc Natl Acad Sci U S A*, vol. 109, no. 15, pp. 5803-8, Apr 2012, doi: 10.1073/pnas.1202922109.
- [300] X. Sun, J. Song, H. Huang, H. Chen, and K. Qian, "Modeling hallmark pathology using motor neurons derived from the family and sporadic amyotrophic lateral sclerosis patient-specific iPSCs," (in eng), *Stem Cell Res Ther*, vol. 9, no. 1, p. 315, 11 15 2018, doi: 10.1186/s13287-018-1048-1.
- [301] K. Fujimori *et al.*, "Modeling sporadic ALS in iPSC-derived motor neurons identifies a potential therapeutic agent," (in eng), *Nat Med*, vol. 24, no. 10, pp. 1579-1589, 10 2018, doi: 10.1038/s41591-018-0140-5.
- [302] N. Egawa *et al.*, "Drug screening for ALS using patient-specific induced pluripotent stem cells," (in eng), *Sci Transl Med*, vol. 4, no. 145, p. 145ra104, Aug 2012, doi: 10.1126/scitranslmed.3004052.
- [303] Y. Zhang *et al.*, "MRI signatures of brain macrostructural atrophy and microstructural degradation in frontotemporal lobar degeneration subtypes," (in eng), *J Alzheimers Dis*, vol. 33, no. 2, pp. 431-44, 2013, doi: 10.3233/JAD-2012-121156.
- [304] J. Lenzi *et al.*, "ALS mutant FUS proteins are recruited into stress granules in induced pluripotent stem cell-derived motoneurons," (in eng), *Dis Model Mech*, vol. 8, no. 7, pp. 755-66, Jul 01 2015, doi: 10.1242/dmm.020099.
- [305] H. Wang *et al.*, "Mutant FUS causes DNA ligation defects to inhibit oxidative damage repair in Amyotrophic Lateral Sclerosis," (in eng), *Nat Commun*, vol. 9, no. 1, p. 3683, 09 11 2018, doi: 10.1038/s41467-018-06111-6.
- [306] L. Marrone *et al.*, "FUS pathology in ALS is linked to alterations in multiple ALS-associated proteins and rescued by drugs stimulating autophagy," (in eng), *Acta Neuropathol*, vol. 138, no. 1, pp. 67-84, 07 2019, doi: 10.1007/s00401-019-01998-x.
- [307] R. De Santis *et al.*, "FUS Mutant Human Motoneurons Display Altered Transcriptome and microRNA Pathways with Implications for ALS Pathogenesis," (in eng), *Stem Cell Reports*, vol. 9, no. 5, pp. 1450-1462, 11 2017, doi: 10.1016/j.stemcr.2017.09.004.
- [308] J. Japtok *et al.*, "Stepwise acquirement of hallmark neuropathology in FUS-ALS iPSC models depends on mutation type and neuronal aging," (in eng), *Neurobiol Dis*, vol. 82, pp. 420-429, Oct 2015, doi: 10.1016/j.nbd.2015.07.017.
- [309] X. Liu *et al.*, "The fused in sarcoma protein forms cytoplasmic aggregates in motor neurons derived from integration-free induced pluripotent stem cells generated from a patient with familial amyotrophic lateral sclerosis carrying the FUS-P525L mutation," (in eng), *Neurogenetics*, vol. 16, no. 3, pp. 223-31, Jul 2015, doi: 10.1007/s10048-015-0448-y.
- [310] N. Ichiyanagi *et al.*, "Establishment of In Vitro FUS-Associated Familial Amyotrophic Lateral Sclerosis Model Using Human Induced Pluripotent Stem Cells," (in eng), *Stem Cell Reports*, vol. 6, no. 4, pp. 496-510, Apr 12 2016, doi: 10.1016/j.stemcr.2016.02.011.

- [311] S. Mitsuzawa *et al.*, "Reduced PHOX2B stability causes axonal growth impairment in motor neurons with TARDBP mutations," (in eng), *Stem Cell Reports*, vol. 16, no. 6, pp. 1527-1541, Jun 08 2021, doi: 10.1016/j.stemcr.2021.04.021.
- [312] T. Akiyama *et al.*, "Aberrant axon branching via Fos-B dysregulation in FUS-ALS motor neurons," (in eng), *EBioMedicine*, vol. 45, pp. 362-378, Jul 2019, doi: 10.1016/j.ebiom.2019.06.013.
- [313] A. Serio *et al.*, "Astrocyte pathology and the absence of non-cell autonomy in an induced pluripotent stem cell model of TDP-43 proteinopathy," (in eng), *Proc Natl Acad Sci U S A*, vol. 110, no. 12, pp. 4697-702, Mar 19 2013, doi: 10.1073/pnas.1300398110.
- [314] K. Qian *et al.*, "Sporadic ALS Astrocytes Induce Neuronal Degeneration In Vivo," (in eng), *Stem Cell Reports*, vol. 8, no. 4, pp. 843-855, 04 2017, doi: 10.1016/j.stemcr.2017.03.003.
- [315] C. E. Hall *et al.*, "Progressive Motor Neuron Pathology and the Role of Astrocytes in a Human Stem Cell Model of VCP-Related ALS," (in eng), *Cell Rep*, vol. 19, no. 9, pp. 1739-1749, 05 2017, doi: 10.1016/j.celrep.2017.05.024.
- [316] A. C. Lepore *et al.*, "Focal transplantation-based astrocyte replacement is neuroprotective in a model of motor neuron disease," (in eng), *Nat Neurosci*, vol. 11, no. 11, pp. 1294-301, Nov 2008, doi: 10.1038/nn.2210.
- [317] T. Kondo *et al.*, "Focal transplantation of human iPSC-derived glial-rich neural progenitors improves lifespan of ALS mice," (in eng), *Stem Cell Reports*, vol. 3, no. 2, pp. 242-9, Aug 12 2014, doi: 10.1016/j.stemcr.2014.05.017.
- [318] B. E. Clarke and R. Patani, "The microglial component of amyotrophic lateral sclerosis," (in eng), *Brain*, vol. 143, no. 12, pp. 3526-3539, 12 01 2020, doi: 10.1093/brain/awaa309.
- [319] W. Zheng, Q. Li, C. Zhao, Y. Da, H. L. Zhang, and Z. Chen, "Differentiation of Glial Cells From hiPSCs: Potential Applications in Neurological Diseases and Cell Replacement Therapy," (in eng), *Front Cell Neurosci*, vol. 12, p. 239, 2018, doi: 10.3389/fncel.2018.00239.
- [320] S. Agarwal, S. Saha, V. Balla, A. Pal, A. Barui, and S. Bodhak, "Current Developments in 3D Bioprinting for Tissue and Organ Regeneration—A Review," *Front. Mech. Eng.*, vol. 6:589171, 2020.
- [321] Q. Ramadan and M. Zourob, "3D Bioprinting at the Frontier of Regenerative Medicine, Pharmaceutical, and Food Industries," (in eng), *Front Med Technol*, vol. 2, p. 607648, 2020, doi: 10.3389/fmedt.2020.607648.
- [322] J. Groll *et al.*, "Biofabrication: reappraising the definition of an evolving field," (in eng), *Biofabrication*, vol. 8, no. 1, p. 013001, Jan 2016, doi: 10.1088/1758-5090/8/1/013001.
- [323] V. Mironov, N. Reis, and B. Derby, "Review: bioprinting: a beginning," (in eng), *Tissue Eng*, vol. 12, no. 4, pp. 631-4, Apr 2006, doi: 10.1089/ten.2006.12.631.
- [324] B. Guillotin *et al.*, "Laser assisted bioprinting of engineered tissue with high cell density and microscale organization," (in eng), *Biomaterials*, vol. 31, no. 28, pp. 7250-6, Oct 2010, doi: 10.1016/j.biomaterials.2010.05.055.
- [325] F. Guillemot, V. Mironov, and M. Nakamura, "Bioprinting is coming of age: Report from the International Conference on Bioprinting and Biofabrication in Bordeaux (3B'09)," (in eng), *Biofabrication*, vol. 2, no. 1, p. 010201, Mar 2010, doi: 10.1088/1758-5082/2/1/010201.
- [326] G. A., "Bioprinting: stato dell'arte ed applicazioni biomediche," Master thesis in Clinical Engineering, 2015.
- [327] R. J. Klebe, "Cytoscribing: a method for micropositioning cells and the construction of two- and three-dimensional synthetic tissues," (in eng), *Exp Cell Res*, vol. 179, no. 2, pp. 362-73, Dec 1988, doi: 10.1016/0014-4827(88)90275-3.

- [328] D. J. Odde and M. J. Renn, "Laser-guided direct writing for applications in biotechnology," (in eng), *Trends Biotechnol*, vol. 17, no. 10, pp. 385-9, Oct 1999, doi: 10.1016/s0167-7799(99)01355-4.
- [329] R. Landers, U. Hübner, R. Schmelzeisen, and R. Mülhaupt, "Rapid prototyping of scaffolds derived from thermoreversible hydrogels and tailored for applications in tissue engineering," (in eng), *Biomaterials*, vol. 23, no. 23, pp. 4437-47, Dec 2002, doi: 10.1016/s0142-9612(02)00139-4.
- [330] W. C. Wilson and T. Boland, "Cell and organ printing 1: protein and cell printers," (in eng), *Anat Rec A Discov Mol Cell Evol Biol*, vol. 272, no. 2, pp. 491-6, Jun 2003, doi: 10.1002/ar.a.10057.
- [331] P. Thayer, H. Martinez, and E. Gatenholm, "History and Trends of 3D Bioprinting," (in eng), *Methods Mol Biol*, vol. 2140, pp. 3-18, 2020, doi: 10.1007/978-1-0716-0520-2_1.
- [332] A. B. Dababneh and I. T. Ozbolat, "Bioprinting Technology: A Current State-of-the-Art Review," ed: J Manuf Sci Eng, 2014, p. 136.
- [333] X. Cui, D. Dean, Z. M. Ruggeri, and T. Boland, "Cell damage evaluation of thermal inkjet printed Chinese hamster ovary cells," (in eng), *Biotechnol Bioeng*, vol. 106, no. 6, pp. 963-9, Aug 15 2010, doi: 10.1002/bit.22762.
- [334] Z. Gu, J. Fu, H. Lin, and Y. He, "Development of 3D bioprinting: From printing methods to biomedical applications," (in eng), *Asian J Pharm Sci*, vol. 15, no. 5, pp. 529-557, Sep 2020, doi: 10.1016/j.ajps.2019.11.003.
- [335] C. Jamieson *et al.*, "A Review of Recent Advances in 3D Bioprinting With an Eye on Future Regenerative Therapies in Veterinary Medicine," (in eng), *Front Vet Sci*, vol. 7, p. 584193, 2020, doi: 10.3389/fvets.2020.584193.
- [336] A. N. Leberfinger *et al.*, "Bioprinting functional tissues," (in eng), *Acta Biomater*, vol. 95, pp. 32-49, 09 01 2019, doi: 10.1016/j.actbio.2019.01.009.
- [337] L. Elomaa, C. C. Pan, Y. Shanjani, A. Malkovskiy, J. V. Seppälä, and Y. Yang, "Three-dimensional fabrication of cell-laden biodegradable poly(ethylene glycol-," (in eng), *J Mater Chem B*, vol. 3, no. 42, pp. 8348-8358, Nov 14 2015, doi: 10.1039/c5tb01468a.
- [338] N. R. Schiele, D. T. Corr, Y. Huang, N. A. Raof, Y. Xie, and D. B. Chrisey, "Laser-based direct-write techniques for cell printing," (in eng), *Biofabrication*, vol. 2, no. 3, p. 032001, Sep 2010, doi: 10.1088/1758-5082/2/3/032001.
- [339] V. K. Lee and G. Dai, "Printing of Three-Dimensional Tissue Analogs for Regenerative Medicine," (in eng), *Ann Biomed Eng*, vol. 45, no. 1, pp. 115-131, 01 2017, doi: 10.1007/s10439-016-1613-7.
- [340] H. Gudapati, J. Yan, Y. Huang, and D. B. Chrisey, "Alginate gelation-induced cell death during laser-assisted cell printing," (in eng), *Biofabrication*, vol. 6, no. 3, p. 035022, Sep 2014, doi: 10.1088/1758-5082/6/3/035022.
- [341] Z. Wang, R. Abdulla, B. Parker, R. Samanipour, S. Ghosh, and K. Kim, "A simple and high-resolution stereolithography-based 3D bioprinting system using visible light crosslinkable bioinks," (in eng), *Biofabrication*, vol. 7, no. 4, p. 045009, Dec 22 2015, doi: 10.1088/1758-5090/7/4/045009.
- [342] R. Masaeli, K. Zandsalimi, and L. Tayebi, "Biomaterials Evaluation: Conceptual Refinements and Practical Reforms," (in eng), *Ther Innov Regul Sci*, vol. 53, no. 1, pp. 120-127, 01 2019, doi: 10.1177/2168479018774320.
- [343] M. Bordoni *et al.*, "Biomaterials in Neurodegenerative Disorders: A Promising Therapeutic Approach," (in eng), *Int J Mol Sci*, vol. 21, no. 9, May 2020, doi: 10.3390/ijms21093243.
- [344] D. F. Williams, "On the nature of biomaterials," (in eng), *Biomaterials*, vol. 30, no. 30, pp. 5897-909, Oct 2009, doi: 10.1016/j.biomaterials.2009.07.027.

- [345] V. Dos Santos, R. N. Brandalise, and M. Savaris, *Engineering of Biomaterials* (Topics in Mining, Metallurgy and Materials Engineering). Springer International Publishing, 2017, p. 94.
- [346] A. Bharadwaj, "An Overview on Biomaterials and Its Applications in Medical Science," 2021.
- [347] A. Ovsianikov, A. Khademhosseini, and V. Mironov, "The Synergy of Scaffold-Based and Scaffold-Free Tissue Engineering Strategies," (in eng), *Trends Biotechnol*, vol. 36, no. 4, pp. 348-357, 04 2018, doi: 10.1016/j.tibtech.2018.01.005.
- [348] K. R. Silva *et al.*, "Delivery of Human Adipose Stem Cells Spheroids into Lockyballs," (in eng), *PLoS One*, vol. 11, no. 11, p. e0166073, 2016, doi: 10.1371/journal.pone.0166073.
- [349] Z. Xie, M. Gao, A. O. Lobo, and T. J. Webster, "3D Bioprinting in Tissue Engineering for Medical Applications: The Classic and the Hybrid," (in eng), *Polymers (Basel)*, vol. 12, no. 8, Jul 31 2020, doi: 10.3390/polym12081717.
- [350] C. M. Smith *et al.*, "Three-dimensional bioassembly tool for generating viable tissue-engineered constructs," (in eng), *Tissue Eng*, vol. 10, no. 9-10, pp. 1566-76, 2004 Sep-Oct 2004, doi: 10.1089/ten.2004.10.1566.
- [351] N. C. Hunt and L. M. Grover, "Cell encapsulation using biopolymer gels for regenerative medicine," (in eng), *Biotechnol Lett*, vol. 32, no. 6, pp. 733-42, Jun 2010, doi: 10.1007/s10529-010-0221-0.
- [352] K. L. Spiller, S. A. Maher, and A. M. Lowman, "Hydrogels for the repair of articular cartilage defects," (in eng), *Tissue Eng Part B Rev*, vol. 17, no. 4, pp. 281-99, Aug 2011, doi: 10.1089/ten.TEB.2011.0077.
- [353] M. H. Cai *et al.*, "Design and Development of Hybrid Hydrogels for Biomedical Applications: Recent Trends in Anticancer Drug Delivery and Tissue Engineering," (in eng), *Front Bioeng Biotechnol*, vol. 9, p. 630943, 2021, doi: 10.3389/fbioe.2021.630943.
- [354] A. R. Murphy, A. Laslett, C. M. O'Brien, and N. R. Cameron, "Scaffolds for 3D in vitro culture of neural lineage cells," (in eng), *Acta Biomater*, vol. 54, pp. 1-20, 05 2017, doi: 10.1016/j.actbio.2017.02.046.
- [355] L. Rebers *et al.*, "Differentiation of physical and chemical cross-linking in gelatin methacryloyl hydrogels," (in eng), *Sci Rep*, vol. 11, no. 1, p. 3256, 02 05 2021, doi: 10.1038/s41598-021-82393-z.
- [356] A. B. Bello, D. Kim, H. Park, and S. H. Lee, "Engineering and Functionalization of Gelatin Biomaterials: From Cell Culture to Medical Applications," (in eng), *Tissue Eng Part B Rev*, vol. 26, no. 2, pp. 164-180, 04 2020, doi: 10.1089/ten.TEB.2019.0256.
- [357] K. Deshmukh , M. Ahamed , R. Deshmukh , S. Pasha , P. Bhagat , and K. Chidambaram "Biopolymer Composites With High Dielectric Performance: Interface Engineering," in *Biopolymer Composites in Electronics*: Elsevier, 2017, ch. 3, pp. 27-128.
- [358] H. Zhang, J. Cheng, and Q. Ao, "Preparation of Alginate-Based Biomaterials and Their Applications in Biomedicine," (in eng), *Mar Drugs*, vol. 19, no. 5, May 10 2021, doi: 10.3390/md19050264.
- [359] I. Lukin *et al.*, "Progress in Gelatin as Biomaterial for Tissue Engineering," (in eng), *Pharmaceutics*, vol. 14, no. 6, May 31 2022, doi: 10.3390/pharmaceutics14061177.
- [360] D. R. Sahoo and T. Biswal, "Alginate and its application to tissue engineering," *SN Appl. Sci.* , vol. 3, no. 30, 2021.
- [361] R. J. Hickey and A. E. Pelling, "Cellulose Biomaterials for Tissue Engineering," (in eng), *Front Bioeng Biotechnol*, vol. 7, p. 45, 2019, doi: 10.3389/fbioe.2019.00045.

- [362] S. M. F. Kabir, P. P. Sikdar, B. Haque, M. A. R. Bhuiyan, A. Ali, and M. N. Islam, "Cellulose-based hydrogel materials: chemistry, properties and their prospective applications," (in eng), *Prog Biomater*, vol. 7, no. 3, pp. 153-174, Sep 2018, doi: 10.1007/s40204-018-0095-0.
- [363] Z. Zhang, L. H. Klausen, M. Chen, and M. Dong, "Electroactive Scaffolds for Neurogenesis and Myogenesis: Graphene-Based Nanomaterials," (in eng), *Small*, vol. 14, no. 48, p. e1801983, 11 2018, doi: 10.1002/smll.201801983.
- [364] C. Xiang, Y. Zhang, W. Guo, and X. J. Liang, "Biomimetic carbon nanotubes for neurological disease therapeutics as inherent medication," (in eng), *Acta Pharm Sin B*, vol. 10, no. 2, pp. 239-248, Feb 2020, doi: 10.1016/j.apsb.2019.11.003.
- [365] N. Chen, L. Tian, L. He, and S. Ramakrishna, "Nanobiomaterials for neural regeneration," (in eng), *Neural Regen Res*, vol. 11, no. 9, pp. 1372-1374, Sep 2016, doi: 10.4103/1673-5374.191195.
- [366] V. Beachley and X. Wen, "Polymer nanofibrous structures: Fabrication, biofunctionalization, and cell interactions," (in eng), *Prog Polym Sci*, vol. 35, no. 7, pp. 868-892, Jul 01 2010, doi: 10.1016/j.progpolymsci.2010.03.003.
- [367] J. Cheng, Y. Jun, J. Qin, and S. H. Lee, "Electrospinning versus microfluidic spinning of functional fibers for biomedical applications," (in eng), *Biomaterials*, vol. 114, pp. 121-143, 01 2017, doi: 10.1016/j.biomaterials.2016.10.040.
- [368] G. Jin *et al.*, "Electrospun three-dimensional aligned nanofibrous scaffolds for tissue engineering," (in eng), *Mater Sci Eng C Mater Biol Appl*, vol. 92, pp. 995-1005, Nov 01 2018, doi: 10.1016/j.msec.2018.06.065.
- [369] S. Nemati, S. J. Kim, Y. M. Shin, and H. Shin, "Current progress in application of polymeric nanofibers to tissue engineering," (in eng), *Nano Converg*, vol. 6, no. 1, p. 36, Nov 08 2019, doi: 10.1186/s40580-019-0209-y.
- [370] D. Klemm *et al.*, "Nanocelluloses: a new family of nature-based materials," (in eng), *Angew Chem Int Ed Engl*, vol. 50, no. 24, pp. 5438-66, Jun 06 2011, doi: 10.1002/anie.201001273.
- [371] H. Du, W. Liu, M. Zhang, C. Si, X. Zhang, and B. Li, "Cellulose nanocrystals and cellulose nanofibrils based hydrogels for biomedical applications," (in eng), *Carbohydr Polym*, vol. 209, pp. 130-144, Apr 01 2019, doi: 10.1016/j.carbpol.2019.01.020.
- [372] V. Kumar, S. Naqvi, and P. Gopinath, "Applications of Nanofibers in Tissue," in *Micro and Nano Technologies, Applications of Nanomaterials.*, O. S. O. Sneha Mohan Bhagyaraj, Nandakumar Kalarikkal, Sabu Thomas Ed.: Woodhead Publishing, 2018, pp. 179-203.
- [373] D. Silva Adaya, L. Aguirre-Cruz, J. Guevara, and E. Ortiz-Islas, "Nanobiomaterials' applications in neurodegenerative diseases," (in eng), *J Biomater Appl*, vol. 31, no. 7, pp. 953-984, 02 2017, doi: 10.1177/0885328216659032.
- [374] M. Fathi-Achachelouei *et al.*, "Use of Nanoparticles in Tissue Engineering and Regenerative Medicine," (in eng), *Front Bioeng Biotechnol*, vol. 7, p. 113, 2019, doi: 10.3389/fbioe.2019.00113.
- [375] S. Lee *et al.*, "Self-Assembling Peptides and Their Application in the Treatment of Diseases," (in eng), *Int J Mol Sci*, vol. 20, no. 23, Nov 21 2019, doi: 10.3390/ijms20235850.
- [376] J. Chen and X. Zou, "Self-assemble peptide biomaterials and their biomedical applications," (in eng), *Bioact Mater*, vol. 4, pp. 120-131, Dec 2019, doi: 10.1016/j.bioactmat.2019.01.002.
- [377] D. R. Nisbet and R. J. Williams, "Self-assembled peptides: characterisation and in vivo response," (in eng), *Biointerphases*, vol. 7, no. 1-4, p. 2, Dec 2012, doi: 10.1007/s13758-011-0002-x.

- [378] F. L. Maclean, A. L. Rodriguez, C. L. Parish, R. J. Williams, and D. R. Nisbet, "Integrating Biomaterials and Stem Cells for Neural Regeneration," (in eng), *Stem Cells Dev*, vol. 25, no. 3, pp. 214-26, Feb 01 2016, doi: 10.1089/scd.2015.0314.
- [379] X. Zhao, "Design of self-assembling surfactant-like peptides and their applications," *Current Opinion in Colloid & Interface Science*, vol. 14, no. 5, pp. 340-348, 2009.
- [380] G. Pennarossa, S. Arcuri, T. De Iorio, F. Gandolfi, and T. A. L. Brevini, "Current Advances in 3D Tissue and Organ Reconstruction," (in eng), *Int J Mol Sci*, vol. 22, no. 2, Jan 15 2021, doi: 10.3390/ijms22020830.
- [381] N. Cubo, M. Garcia, J. F. Del Cañizo, D. Velasco, and J. L. Jorcano, "3D bioprinting of functional human skin: production and in vivo analysis," (in eng), *Biofabrication*, vol. 9, no. 1, p. 015006, 12 05 2016, doi: 10.1088/1758-5090/9/1/015006.
- [382] L. J. Pourchet *et al.*, "Human Skin 3D Bioprinting Using Scaffold-Free Approach," (in eng), *Adv Healthc Mater*, vol. 6, no. 4, Feb 2017, doi: 10.1002/adhm.201601101.
- [383] M. Varkey, D. O. Visscher, P. P. M. van Zuijlen, A. Atala, and J. J. Yoo, "Skin bioprinting: the future of burn wound reconstruction?," (in eng), *Burns Trauma*, vol. 7, p. 4, 2019, doi: 10.1186/s41038-019-0142-7.
- [384] C. S. Ong *et al.*, "Biomaterial-Free Three-Dimensional Bioprinting of Cardiac Tissue using Human Induced Pluripotent Stem Cell Derived Cardiomyocytes," (in eng), *Sci Rep*, vol. 7, no. 1, p. 4566, 07 04 2017, doi: 10.1038/s41598-017-05018-4.
- [385] K. Sung, N. R. Patel, N. Ashammakhi, and K. L. Nguyen, "3-Dimensional Bioprinting of Cardiovascular Tissues: Emerging Technology," (in eng), *JACC Basic Transl Sci*, vol. 6, no. 5, pp. 467-482, May 2021, doi: 10.1016/j.jacbts.2020.12.006.
- [386] Y. P. Singh, A. Bandyopadhyay, and B. B. Mandal, "3D Bioprinting Using Cross-Linker-Free Silk-Gelatin Bioink for Cartilage Tissue Engineering," (in eng), *ACS Appl Mater Interfaces*, vol. 11, no. 37, pp. 33684-33696, Sep 18 2019, doi: 10.1021/acsami.9b11644.
- [387] C. Antich *et al.*, "Bio-inspired hydrogel composed of hyaluronic acid and alginate as a potential bioink for 3D bioprinting of articular cartilage engineering constructs," (in eng), *Acta Biomater*, vol. 106, pp. 114-123, 04 01 2020, doi: 10.1016/j.actbio.2020.01.046.
- [388] J. C. Reichert, A. Heymer, A. Berner, J. Eulert, and U. Nöth, "Fabrication of polycaprolactone collagen hydrogel constructs seeded with mesenchymal stem cells for bone regeneration," (in eng), *Biomed Mater*, vol. 4, no. 6, p. 065001, Dec 2009, doi: 10.1088/1748-6041/4/6/065001.
- [389] T. Genova, I. Roato, M. Carossa, C. Motta, D. Cavagnetto, and F. Mussano, "Advances on Bone Substitutes through 3D Bioprinting," (in eng), *Int J Mol Sci*, vol. 21, no. 19, Sep 23 2020, doi: 10.3390/ijms21197012.
- [390] A. K. Amler *et al.*, "3D bioprinting of tissue-specific osteoblasts and endothelial cells to model the human jawbone," (in eng), *Sci Rep*, vol. 11, no. 1, p. 4876, 03 01 2021, doi: 10.1038/s41598-021-84483-4.
- [391] M. Rajput, P. Mondal, P. Yadav, and K. Chatterjee, "Light-based 3D bioprinting of bone tissue scaffolds with tunable mechanical properties and architecture from photocurable silk fibroin," (in eng), *Int J Biol Macromol*, vol. 202, pp. 644-656, Mar 31 2022, doi: 10.1016/j.ijbiomac.2022.01.081.
- [392] M. Cadena *et al.*, "3D Bioprinting of Neural Tissues," (in eng), *Adv Healthc Mater*, vol. 10, no. 15, p. e2001600, 08 2021, doi: 10.1002/adhm.202001600.

- [393] C. M. Owens, F. Marga, G. Forgacs, and C. M. Heesch, "Biofabrication and testing of a fully cellular nerve graft," (in eng), *Biofabrication*, vol. 5, no. 4, p. 045007, Dec 2013, doi: 10.1088/1758-5082/5/4/045007.
- [394] B. Lorber, W. K. Hsiao, I. M. Hutchings, and K. R. Martin, "Adult rat retinal ganglion cells and glia can be printed by piezoelectric inkjet printing," (in eng), *Biofabrication*, vol. 6, no. 1, p. 015001, Mar 2014, doi: 10.1088/1758-5082/6/1/015001.
- [395] Q. Gu *et al.*, "Functional 3D Neural Mini-Tissues from Printed Gel-Based Bioink and Human Neural Stem Cells," (in eng), *Adv Healthc Mater*, vol. 5, no. 12, pp. 1429-38, 06 2016, doi: 10.1002/adhm.201600095.
- [396] E. Abelseth, L. Abelseth, L. De la Vega, S. T. Beyer, S. J. Wadsworth, and S. M. Willerth, "3D Printing of Neural Tissues Derived from Human Induced Pluripotent Stem Cells Using a Fibrin-Based Bioink," (in eng), *ACS Biomater Sci Eng*, vol. 5, no. 1, pp. 234-243, Jan 14 2019, doi: 10.1021/acsbiomaterials.8b01235.
- [397] A. Altunbas, S. J. Lee, S. A. Rajasekaran, J. P. Schneider, and D. J. Pochan, "Encapsulation of curcumin in self-assembling peptide hydrogels as injectable drug delivery vehicles," (in eng), *Biomaterials*, vol. 32, no. 25, pp. 5906-14, Sep 2011, doi: 10.1016/j.biomaterials.2011.04.069.
- [398] A. Rajput, A. Bariya, A. Allam, S. Othman, and S. B. Butani, "In situ nanostructured hydrogel of resveratrol for brain targeting: in vitro-in vivo characterization," (in eng), *Drug Deliv Transl Res*, vol. 8, no. 5, pp. 1460-1470, 10 2018, doi: 10.1007/s13346-018-0540-6.
- [399] J. A. Loureiro, B. Gomes, G. Fricker, M. A. N. Coelho, S. Rocha, and M. C. Pereira, "Cellular uptake of PLGA nanoparticles targeted with anti-amyloid and anti-transferrin receptor antibodies for Alzheimer's disease treatment," (in eng), *Colloids Surf B Biointerfaces*, vol. 145, pp. 8-13, Sep 01 2016, doi: 10.1016/j.colsurfb.2016.04.041.
- [400] R. Barbara *et al.*, "Novel Curcumin loaded nanoparticles engineered for Blood-Brain Barrier crossing and able to disrupt Abeta aggregates," (in eng), *Int J Pharm*, vol. 526, no. 1-2, pp. 413-424, Jun 30 2017, doi: 10.1016/j.ijpharm.2017.05.015.
- [401] A. Smith, B. Giunta, P. C. Bickford, M. Fountain, J. Tan, and R. D. Shytle, "Nanolipidic particles improve the bioavailability and alpha-secretase inducing ability of epigallocatechin-3-gallate (EGCG) for the treatment of Alzheimer's disease," (in eng), *Int J Pharm*, vol. 389, no. 1-2, pp. 207-12, Apr 15 2010, doi: 10.1016/j.ijpharm.2010.01.012.
- [402] I. Carrera *et al.*, "A comparative evaluation of a novel vaccine in APP/PS1 mouse models of Alzheimer's disease," (in eng), *Biomed Res Int*, vol. 2015, p. 807146, 2015, doi: 10.1155/2015/807146.
- [403] Y. Yu, X. Jiang, S. Gong, L. Feng, Y. Zhong, and Z. Pang, "The proton permeability of self-assembled polymersomes and their neuroprotection by enhancing a neuroprotective peptide across the blood-brain barrier after modification with lactoferrin," (in eng), *Nanoscale*, vol. 6, no. 6, pp. 3250-8, Mar 21 2014, doi: 10.1039/c3nr05196j.
- [404] S. Al-Halifa, M. Babych, X. Zottig, D. Archambault, and S. Bourgault, "Amyloid self-assembling peptides: Potential applications in nanovaccine engineering and biosensing.," *Pept. Sci.*, no. 111 , e24095., 2019.
- [405] N. Mehrban *et al.*, "Functionalized α -Helical Peptide Hydrogels for Neural Tissue Engineering," (in eng), *ACS Biomater Sci Eng*, vol. 1, no. 6, pp. 431-439, Jun 08 2015, doi: 10.1021/acsbiomaterials.5b00051.
- [406] K. S. Hellmund and B. Koksich, "Self-Assembling Peptides as Extracellular Matrix Mimics to Influence Stem Cell's Fate," (in eng), *Front Chem*, vol. 7, p. 172, 2019, doi: 10.3389/fchem.2019.00172.

- [407] K. S. Senthilkumar, K. S. Saravanan, G. Chandra, K. M. Sindhu, A. Jayakrishnan, and K. P. Mohanakumar, "Unilateral implantation of dopamine-loaded biodegradable hydrogel in the striatum attenuates motor abnormalities in the 6-hydroxydopamine model of hemi-parkinsonism," (in eng), *Behav Brain Res*, vol. 184, no. 1, pp. 11-8, Nov 22 2007, doi: 10.1016/j.bbr.2007.06.025.
- [408] Y. Ren, X. Zhao, X. Liang, P. X. Ma, and B. Guo, "Injectable hydrogel based on quaternized chitosan, gelatin and dopamine as localized drug delivery system to treat Parkinson's disease," (in eng), *Int J Biol Macromol*, vol. 105, no. Pt 1, pp. 1079-1087, Dec 2017, doi: 10.1016/j.ijbiomac.2017.07.130.
- [409] T. Y. Wang, K. F. Bruggeman, J. A. Kauhausen, A. L. Rodriguez, D. R. Nisbet, and C. L. Parish, "Functionalized composite scaffolds improve the engraftment of transplanted dopaminergic progenitors in a mouse model of Parkinson's disease," (in eng), *Biomaterials*, vol. 74, pp. 89-98, Jan 2016, doi: 10.1016/j.biomaterials.2015.09.039.
- [410] B. Ucar and C. Humpel, "Therapeutic efficacy of glial cell-derived neurotrophic factor loaded collagen scaffolds in ex vivo organotypic brain slice Parkinson's disease models," (in eng), *Brain Res Bull*, vol. 149, pp. 86-95, 07 2019, doi: 10.1016/j.brainresbull.2019.04.012.
- [411] X. Yang, R. Zheng, Y. Cai, M. Liao, W. Yuan, and Z. Liu, "Controlled-release levodopa methyl ester/benserazide-loaded nanoparticles ameliorate levodopa-induced dyskinesia in rats," (in eng), *Int J Nanomedicine*, vol. 7, pp. 2077-86, 2012, doi: 10.2147/IJN.S30463.
- [412] S. Md *et al.*, "Bromocriptine loaded chitosan nanoparticles intended for direct nose to brain delivery: pharmacodynamic, pharmacokinetic and scintigraphy study in mice model," (in eng), *Eur J Pharm Sci*, vol. 48, no. 3, pp. 393-405, Feb 14 2013, doi: 10.1016/j.ejps.2012.12.007.
- [413] H. E. Gendelman *et al.*, "Nanoneuromedicines for degenerative, inflammatory, and infectious nervous system diseases," (in eng), *Nanomedicine*, vol. 11, no. 3, pp. 751-67, Apr 2015, doi: 10.1016/j.nano.2014.12.014.
- [414] S. Abdelrahman *et al.*, "A Parkinson's disease model composed of 3D bioprinted dopaminergic neurons within a biomimetic peptide scaffold," (in eng), *Biofabrication*, vol. 14, no. 4, 07 20 2022, doi: 10.1088/1758-5090/ac7eec.
- [415] V. M. Tatard *et al.*, "Pharmacologically active microcarriers: a tool for cell therapy," (in eng), *Biomaterials*, vol. 26, no. 17, pp. 3727-37, Jun 2005, doi: 10.1016/j.biomaterials.2004.09.042.
- [416] V. M. Tatard, P. Menei, J. P. Benoit, and C. N. Montero-Menei, "Combining polymeric devices and stem cells for the treatment of neurological disorders: a promising therapeutic approach," (in eng), *Curr Drug Targets*, vol. 6, no. 1, pp. 81-96, Feb 2005, doi: 10.2174/1389450053344885.
- [417] E. M. André, C. Passirani, B. Seijo, A. Sanchez, and C. N. Montero-Menei, "Nano and microcarriers to improve stem cell behaviour for neuroregenerative medicine strategies: Application to Huntington's disease," (in eng), *Biomaterials*, vol. 83, pp. 347-62, Mar 2016, doi: 10.1016/j.biomaterials.2015.12.008.
- [418] W. Cong, R. Bai, Y. F. Li, L. Wang, and C. Chen, "Selenium Nanoparticles as an Efficient Nanomedicine for the Therapy of Huntington's Disease," (in eng), *ACS Appl Mater Interfaces*, vol. 11, no. 38, pp. 34725-34735, Sep 25 2019, doi: 10.1021/acsami.9b12319.
- [419] M. M. Adil *et al.*, "hPSC-Derived Striatal Cells Generated Using a Scalable 3D Hydrogel Promote Recovery in a Huntington Disease Mouse Model," (in eng), *Stem Cell Reports*, vol. 10, no. 5, pp. 1481-1491, 05 08 2018, doi: 10.1016/j.stemcr.2018.03.007.

- [420] T. Osaki, S. G. M. Uzel, and R. D. Kamm, "Microphysiological 3D model of amyotrophic lateral sclerosis (ALS) from human iPS-derived muscle cells and optogenetic motor neurons," (in eng), *Sci Adv*, vol. 4, no. 10, p. eaat5847, 10 2018, doi: 10.1126/sciadv.aat5847.
- [421] I. Malysz-Cymborska *et al.*, "MRI-guided intrathecal transplantation of hydrogel-embedded glial progenitors in large animals," (in eng), *Sci Rep*, vol. 8, no. 1, p. 16490, 11 07 2018, doi: 10.1038/s41598-018-34723-x.
- [422] S. Vieira *et al.*, "Methacrylated gellan gum and hyaluronic acid hydrogel blends for image-guided neurointerventions," (in eng), *J Mater Chem B*, vol. 8, no. 27, pp. 5928-5937, 07 15 2020, doi: 10.1039/d0tb00877j.
- [423] X. Xu *et al.*, "A perspective on therapies for amyotrophic lateral sclerosis: can disease progression be curbed?," (in eng), *Transl Neurodegener*, vol. 10, no. 1, p. 29, 08 10 2021, doi: 10.1186/s40035-021-00250-5.
- [424] S. Naz *et al.*, "Cerium oxide nanoparticles: a 'radical' approach to neurodegenerative disease treatment," (in eng), *Nanomedicine (Lond)*, vol. 12, no. 5, pp. 545-553, Mar 2017, doi: 10.2217/nmm-2016-0399.
- [425] X. Niu, J. Chen, and J. Gao, "Nanocarriers as a powerful vehicle to overcome blood-brain barrier in treating neurodegenerative diseases: Focus on recent advances," (in eng), *Asian J Pharm Sci*, vol. 14, no. 5, pp. 480-496, Sep 2019, doi: 10.1016/j.ajps.2018.09.005.
- [426] B. Nabi, S. Rehman, M. Fazil, S. Khan, S. Baboota, and J. Ali, "Riluzole-loaded nanoparticles to alleviate the symptoms of neurological disorders by attenuating oxidative stress," (in eng), *Drug Dev Ind Pharm*, vol. 46, no. 3, pp. 471-483, Mar 2020, doi: 10.1080/03639045.2020.1730396.
- [427] J. A. Davies, "Organoids and mini-organs: Introduction, history, and potential," in *Organoids and Mini-Organs*, J. A. Davies and M. L. Lawrence Eds., no. 2-23): Academic Press, 2018, ch. 1.
- [428] W. R. Duryee and J. K. Doherty, "Nuclear and cytoplasmic organoids in the living cell," (in eng), *Ann N Y Acad Sci*, vol. 58, no. 7, pp. 1210-31, Nov 17 1954, doi: 10.1111/j.1749-6632.1954.tb45904.x.
- [429] D. S. Heller, C. P. Frydman, R. E. Gordon, J. Jagirdar, and I. S. Schwartz, "An unusual organoid tumor. Alveolar soft part sarcoma or paraganglioma?," (in eng), *Cancer*, vol. 67, no. 7, pp. 1894-9, Apr 01 1991, doi: 10.1002/1097-0142(19910401)67:7<1894::aid-cnrc2820670713>3.0.co;2-w.
- [430] D. Chen *et al.*, "Organoid Cultures Derived From Patients With Papillary Thyroid Cancer," (in eng), *J Clin Endocrinol Metab*, vol. 106, no. 5, pp. 1410-1426, 04 23 2021, doi: 10.1210/clinem/dgab020.
- [431] C. Corrà, L. Novellademunt, and V. S. W. Li, "A brief history of organoids," (in eng), *Am J Physiol Cell Physiol*, vol. 319, no. 1, pp. C151-C165, 07 01 2020, doi: 10.1152/ajpcell.00120.2020.
- [432] M. A. Lancaster and J. A. Knoblich, "Organogenesis in a dish: modeling development and disease using organoid technologies," (in eng), *Science*, vol. 345, no. 6194, p. 1247125, Jul 18 2014, doi: 10.1126/science.1247125.
- [433] M. Huch and B. K. Koo, "Modeling mouse and human development using organoid cultures," (in eng), *Development*, vol. 142, no. 18, pp. 3113-25, Sep 15 2015, doi: 10.1242/dev.118570.
- [434] N. D. Amin and S. P. Paşca, "Building Models of Brain Disorders with Three-Dimensional Organoids," (in eng), *Neuron*, vol. 100, no. 2, pp. 389-405, 10 24 2018, doi: 10.1016/j.neuron.2018.10.007.
- [435] H. V. Wilson, "Development of sponges from dissociated tissue cells.," *Bull. US Bureau Fisheries* pp. 1-30, 1910.

- [436] A. Moscona and H. Moscona, "The dissociation and aggregation of cells from organ rudiments of the early chick embryo," (in eng), *J Anat*, vol. 86, no. 3, pp. 287-301, Jul 1952.
- [437] A. Moscona, "Cell suspensions from organ rudiments of chick embryos," *Exp Cell Res.*, vol. 3, pp. 535-539, 1952.
- [438] A. Moscona, "The development in vitro of chimeric aggregated of dissociated embryonic chick and mouse cells" (in eng), *Proc Natl Acad Sci U S A*, vol. 43, no. 1, pp. 184-94, Jan 15 1957, doi: 10.1073/pnas.43.1.184.
- [439] R. Auerbach and C. Grobstein, "Inductive interaction of embryonic tissues after dissociation and reaggregation," (in eng), *Exp Cell Res*, vol. 15, no. 2, pp. 384-97, Oct 1958, doi: 10.1016/0014-4827(58)90039-9.
- [440] M. Unbekandt and J. A. Davies, "Dissociation of embryonic kidneys followed by reaggregation allows the formation of renal tissues," (in eng), *Kidney Int*, vol. 77, no. 5, pp. 407-16, Mar 2010, doi: 10.1038/ki.2009.482.
- [441] M. S. Steinberg, "Reconstruction of tissues by dissociated cells. Some morphogenetic tissue movements and the sorting out of embryonic cells may have a common explanation," (in eng), *Science*, vol. 141, no. 3579, pp. 401-8, Aug 02 1963, doi: 10.1126/science.141.3579.401.
- [442] D. Duguay, R. A. Foty, and M. S. Steinberg, "Cadherin-mediated cell adhesion and tissue segregation: qualitative and quantitative determinants," (in eng), *Dev Biol*, vol. 253, no. 2, pp. 309-23, Jan 15 2003, doi: 10.1016/s0012-1606(02)00016-7.
- [443] J. A. Davies and E. Cachat, "Synthetic biology meets tissue engineering," (in eng), *Biochem Soc Trans*, vol. 44, no. 3, pp. 696-701, 06 15 2016, doi: 10.1042/BST20150289.
- [444] M. S. Noël-Hudson *et al.*, "Human epidermis reconstructed on synthetic membrane: influence of experimental conditions on terminal differentiation," (in eng), *In Vitro Cell Dev Biol Anim*, vol. 31, no. 7, pp. 508-15, 1995 Jul-Aug 1995, doi: 10.1007/BF02634028.
- [445] Z. Lodin, V. Fleischmannová, B. Hájková, J. Faltin, and J. Hartman, "Reaggregation of human, chick, and human embryonic brain cells. Factors influencing the formation of a histiotypic unit," (in eng), *Z Mikrosk Anat Forsch*, vol. 95, no. 5, pp. 701-20, 1981.
- [446] M. McCarthy, L. Resnick, F. Taub, R. V. Stewart, and R. D. Dix, "Infection of human neural cell aggregate cultures with a clinical isolate of cytomegalovirus," (in eng), *J Neuropathol Exp Neurol*, vol. 50, no. 4, pp. 441-50, Jul 1991, doi: 10.1097/00005072-199107000-00005.
- [447] A. Barnea and J. Roberts, "An improved method for dissociation and aggregate culture of human fetal brain cells in serum-free medium," (in eng), *Brain Res Brain Res Protoc*, vol. 4, no. 2, pp. 156-64, Jul 1999, doi: 10.1016/s1385-299x(99)00015-x.
- [448] E. Y. Choi *et al.*, "Thymocytes positively select thymocytes in human system," (in eng), *Hum Immunol*, vol. 54, no. 1, pp. 15-20, Apr 15 1997, doi: 10.1016/s0198-8859(97)00012-8.
- [449] T. Ishikawa *et al.*, "Characterization of in vitro gutlike organ formed from mouse embryonic stem cells," (in eng), *Am J Physiol Cell Physiol*, vol. 286, no. 6, pp. C1344-52, Jun 2004, doi: 10.1152/ajpcell.00392.2003.
- [450] X. M. Guo *et al.*, "Creation of engineered cardiac tissue in vitro from mouse embryonic stem cells," (in eng), *Circulation*, vol. 113, no. 18, pp. 2229-37, May 09 2006, doi: 10.1161/CIRCULATIONAHA.105.583039.
- [451] H. Mizumoto, K. Aoki, K. Nakazawa, H. Ijima, K. Funatsu, and T. Kajiwara, "Hepatic differentiation of embryonic stem cells in HF/organoid culture," (in eng),

- Transplant Proc*, vol. 40, no. 2, pp. 611-3, Mar 2008, doi: 10.1016/j.transproceed.2008.01.023.
- [452] T. Sato *et al.*, "Single Lgr5 stem cells build crypt-villus structures in vitro without a mesenchymal niche," (in eng), *Nature*, vol. 459, no. 7244, pp. 262-5, May 14 2009, doi: 10.1038/nature07935.
- [453] M. Eiraku *et al.*, "Self-organized formation of polarized cortical tissues from ESCs and its active manipulation by extrinsic signals," (in eng), *Cell Stem Cell*, vol. 3, no. 5, pp. 519-32, Nov 06 2008, doi: 10.1016/j.stem.2008.09.002.
- [454] I. Tortorella, C. Argentati, C. Emiliani, S. Martino, and F. Morena, "The role of physical cues in the development of stem cell-derived organoids," (in eng), *Eur Biophys J*, vol. 51, no. 2, pp. 105-117, Mar 2022, doi: 10.1007/s00249-021-01551-3.
- [455] A. A. Kurmann *et al.*, "Regeneration of Thyroid Function by Transplantation of Differentiated Pluripotent Stem Cells," (in eng), *Cell Stem Cell*, vol. 17, no. 5, pp. 527-42, Nov 05 2015, doi: 10.1016/j.stem.2015.09.004.
- [456] M. J. Workman *et al.*, "Engineered human pluripotent-stem-cell-derived intestinal tissues with a functional enteric nervous system," (in eng), *Nat Med*, vol. 23, no. 1, pp. 49-59, 01 2017, doi: 10.1038/nm.4233.
- [457] M. Hohwieler *et al.*, "Human pluripotent stem cell-derived acinar/ductal organoids generate human pancreas upon orthotopic transplantation and allow disease modelling," (in eng), *Gut*, vol. 66, no. 3, pp. 473-486, 03 2017, doi: 10.1136/gutjnl-2016-312423.
- [458] J. G. Camp *et al.*, "Multilineage communication regulates human liver bud development from pluripotency," (in eng), *Nature*, vol. 546, no. 7659, pp. 533-538, 06 22 2017, doi: 10.1038/nature22796.
- [459] V. Velasco, S. A. Shariati, and R. Esfandyarpour, "Microtechnology-based methods for organoid models," (in eng), *Microsyst Nanoeng*, vol. 6, p. 76, 2020, doi: 10.1038/s41378-020-00185-3.
- [460] E. Garreta *et al.*, "Fine tuning the extracellular environment accelerates the derivation of kidney organoids from human pluripotent stem cells," (in eng), *Nat Mater*, vol. 18, no. 4, pp. 397-405, 04 2019, doi: 10.1038/s41563-019-0287-6.
- [461] J. C. Valdoz *et al.*, "The ECM: To Scaffold, or Not to Scaffold, That Is the Question," (in eng), *Int J Mol Sci*, vol. 22, no. 23, Nov 24 2021, doi: 10.3390/ijms222312690.
- [462] M. Cavo, M. Caria, I. Pulsoni, F. Beltrame, M. Fato, and S. Scaglione, "A new cell-laden 3D Alginate-Matrigel hydrogel resembles human breast cancer cell malignant morphology, spread and invasion capability observed "in vivo"." *Sci Rep*, vol. 8, p. 5333, 2018.
- [463] T. K. Mercer and S. V. Murphy, "Hydrogels for 3D Bioprinting Applications," in *Essentials of 3D Biofabrication and Translation*, A. Atala and J. J. Yoo Eds.: Academic Press, 2015, ch. 14, pp. 249-270.
- [464] E. A. Aisenbrey and W. L. Murphy, "Synthetic alternatives to Matrigel," (in eng), *Nat Rev Mater*, vol. 5, no. 7, pp. 539-551, Jul 2020, doi: 10.1038/s41578-020-0199-8.
- [465] S. Kim *et al.*, "Tissue extracellular matrix hydrogels as alternatives to Matrigel for culturing gastrointestinal organoids," (in eng), *Nat Commun*, vol. 13, no. 1, p. 1692, 03 30 2022, doi: 10.1038/s41467-022-29279-4.
- [466] I. Burova, I. Wall, and R. J. Shipley, "Mathematical and computational models for bone tissue engineering in bioreactor systems," (in eng), *J Tissue Eng*, vol. 10, p. 2041731419827922, 2019 Jan-Dec 2019, doi: 10.1177/2041731419827922.

- [467] T. Nakano *et al.*, "Self-formation of optic cups and storable stratified neural retina from human ESCs," (in eng), *Cell Stem Cell*, vol. 10, no. 6, pp. 771-785, Jun 14 2012, doi: 10.1016/j.stem.2012.05.009.
- [468] X. Qian, F. Jacob, M. M. Song, H. N. Nguyen, H. Song, and G. L. Ming, "Generation of human brain region-specific organoids using a miniaturized spinning bioreactor," (in eng), *Nat Protoc*, vol. 13, no. 3, pp. 565-580, 03 2018, doi: 10.1038/nprot.2017.152.
- [469] M. Stephenson and W. Grayson, "Recent advances in bioreactors for cell-based therapies," (in eng), *F1000Res*, vol. 7, 2018, doi: 10.12688/f1000research.12533.1.
- [470] M. Z. Ismadi *et al.*, "Flow characterization of a spinner flask for induced pluripotent stem cell culture application," (in eng), *PLoS One*, vol. 9, no. 10, p. e106493, 2014, doi: 10.1371/journal.pone.0106493.
- [471] R. Jeske *et al.*, "Agitation in a Microcarrier-based Spinner Flask Bioreactor Modulates Homeostasis of Human Mesenchymal Stem Cells," (in eng), *Biochem Eng J*, vol. 168, Apr 2021, doi: 10.1016/j.bej.2021.107947.
- [472] M. A. Phelan, P. I. Lelkes, and A. Swaroop, "Mini and customized low-cost bioreactors for optimized high-throughput generation of tissue organoids," (in eng), *Stem Cell Investig*, vol. 5, p. 33, 2018, doi: 10.21037/sci.2018.09.06.
- [473] K. G. Choi, B. C. Wu, A. H. Lee, B. Baquir, and R. E. W. Hancock, "Utilizing Organoid and Air-Liquid Interface Models as a Screening Method in the Development of New Host Defense Peptides," (in eng), *Front Cell Infect Microbiol*, vol. 10, p. 228, 2020, doi: 10.3389/fcimb.2020.00228.
- [474] J. T. Neal *et al.*, "Organoid Modeling of the Tumor Immune Microenvironment," (in eng), *Cell*, vol. 175, no. 7, pp. 1972-1988.e16, 12 13 2018, doi: 10.1016/j.cell.2018.11.021.
- [475] L. K. Esser *et al.*, "Cultivation of Clear Cell Renal Cell Carcinoma Patient-Derived Organoids in an Air-Liquid Interface System as a Tool for Studying Individualized Therapy," (in eng), *Front Oncol*, vol. 10, p. 1775, 2020, doi: 10.3389/fonc.2020.01775.
- [476] H. Tseng, A. C. Daquinag, G. R. Souza, and M. G. Kolonin, "Three-Dimensional Magnetic Levitation Culture System Simulating White Adipose Tissue," (in eng), *Methods Mol Biol*, vol. 1773, pp. 147-154, 2018, doi: 10.1007/978-1-4939-7799-4_12.
- [477] J. N. Ferreira *et al.*, "A magnetic three-dimensional levitated primary cell culture system for the development of secretory salivary gland-like organoids," (in eng), *J Tissue Eng Regen Med*, vol. 13, no. 3, pp. 495-508, 03 2019, doi: 10.1002/term.2809.
- [478] X. Qian, H. Song, and G. L. Ming, "Brain organoids: advances, applications and challenges," (in eng), *Development*, vol. 146, no. 8, pp. 1660-1674, 04 16 2019, doi: 10.1242/dev.166074.
- [479] N. Sachs *et al.*, "Long-term expanding human airway organoids for disease modeling," (in eng), *EMBO J*, vol. 38, no. 4, pp. 1525-1536, 02 15 2019, doi: 10.15252/embj.2018100300.
- [480] J. Kim, B. K. Koo, and J. A. Knoblich, "Human organoids: model systems for human biology and medicine," (in eng), *Nat Rev Mol Cell Biol*, vol. 21, no. 10, pp. 571-584, 10 2020, doi: 10.1038/s41580-020-0259-3.
- [481] M. A. Lancaster and M. Huch, "Disease modelling in human organoids," (in eng), *Dis Model Mech*, vol. 12, no. 7, pp. 1-12, 07 29 2019, doi: 10.1242/dmm.039347.
- [482] J. L. Fowler, L. T. Ang, and K. M. Loh, "A critical look: Challenges in differentiating human pluripotent stem cells into desired cell types and organoids," (in eng), *Wiley Interdiscip Rev Dev Biol*, vol. 9, no. 3, p. e368, 05 2020, doi: 10.1002/wdev.368.

- [483] G. A. Figtree, K. J. Bubb, O. Tang, E. Kizana, and C. Gentile, "Vascularized Cardiac Spheroids as Novel 3D in vitro Models to Study Cardiac Fibrosis," (in eng), *Cells Tissues Organs*, vol. 204, no. 3-4, pp. 191-198, 2017, doi: 10.1159/000477436.
- [484] C. R. Archer, R. Sargeant, J. Basak, J. Pilling, J. R. Barnes, and A. Pointon, "Characterization and Validation of a Human 3D Cardiac Microtissue for the Assessment of Changes in Cardiac Pathology," (in eng), *Sci Rep*, vol. 8, no. 1, p. 10160, 07 05 2018, doi: 10.1038/s41598-018-28393-y.
- [485] L. Polonchuk *et al.*, "Cardiac spheroids as promising in vitro models to study the human heart microenvironment," (in eng), *Sci Rep*, vol. 7, no. 1, p. 7005, 08 01 2017, doi: 10.1038/s41598-017-06385-8.
- [486] H. K. Voges, R. J. Mills, D. A. Elliott, R. G. Parton, E. R. Porrello, and J. E. Hudson, "Development of a human cardiac organoid injury model reveals innate regenerative potential," (in eng), *Development*, vol. 144, no. 6, pp. 1118-1127, 03 15 2017, doi: 10.1242/dev.143966.
- [487] R. K. Iyer, L. L. Chiu, and M. Radisic, "Microfabricated poly(ethylene glycol) templates enable rapid screening of triculture conditions for cardiac tissue engineering," (in eng), *J Biomed Mater Res A*, vol. 89, no. 3, pp. 616-31, Jun 2009, doi: 10.1002/jbm.a.32014.
- [488] M. Devarasetty *et al.*, "Optical Tracking and Digital Quantification of Beating Behavior in Bioengineered Human Cardiac Organoids," (in eng), *Biosensors (Basel)*, vol. 7, no. 3, Jun 23 2017, doi: 10.3390/bios7030024.
- [489] T. Takebe *et al.*, "Vascularized and functional human liver from an iPSC-derived organ bud transplant," (in eng), *Nature*, vol. 499, no. 7459, pp. 481-4, Jul 25 2013, doi: 10.1038/nature12271.
- [490] F. Wu *et al.*, "Generation of hepatobiliary organoids from human induced pluripotent stem cells," (in eng), *J Hepatol*, vol. 70, no. 6, pp. 1145-1158, 06 2019, doi: 10.1016/j.jhep.2018.12.028.
- [491] S. P. Harrison, S. F. Baumgarten, R. Verma, O. Lunov, A. Dejneka, and G. J. Sullivan, "Liver Organoids: Recent Developments, Limitations and Potential," (in eng), *Front Med (Lausanne)*, vol. 8, p. 574047, 2021, doi: 10.3389/fmed.2021.574047.
- [492] S. D. Forsythe *et al.*, "Environmental Toxin Screening Using Human-Derived 3D Bioengineered Liver and Cardiac Organoids," (in eng), *Front Public Health*, vol. 6, p. 103, 2018, doi: 10.3389/fpubh.2018.00103.
- [493] M. A. Lancaster *et al.*, "Cerebral organoids model human brain development and microcephaly," (in eng), *Nature*, vol. 501, no. 7467, pp. 373-9, Sep 19 2013, doi: 10.1038/nature12517.
- [494] G. Nzou *et al.*, "Human Cortex Spheroid with a Functional Blood Brain Barrier for High-Throughput Neurotoxicity Screening and Disease Modeling," (in eng), *Sci Rep*, vol. 8, no. 1, p. 7413, 05 09 2018, doi: 10.1038/s41598-018-25603-5.
- [495] C. E. Barkauskas, M. I. Chung, B. Fioret, X. Gao, H. Katsura, and B. L. Hogan, "Lung organoids: current uses and future promise," (in eng), *Development*, vol. 144, no. 6, pp. 986-997, 03 15 2017, doi: 10.1242/dev.140103.
- [496] T. S. Leach, A. Dominijanni, S. V. Murphy, and A. Atala, "Tissue organoid models and applications," in *Principles of Tissue Engineering*, R. Lanza, R. Langer, J. P. Vacanti, and A. Atala Eds., Fifth ed.: Academic Press, 2020, ch. 83, pp. 1537-1549.
- [497] J. R. Rock *et al.*, "Basal cells as stem cells of the mouse trachea and human airway epithelium," (in eng), *Proc Natl Acad Sci U S A*, vol. 106, no. 31, pp. 12771-5, Aug 04 2009, doi: 10.1073/pnas.0906850106.

- [498] A. Skardal *et al.*, "Multi-tissue interactions in an integrated three-tissue organ-on-a-chip platform," (in eng), *Sci Rep*, vol. 7, no. 1, p. 8837, 08 18 2017, doi: 10.1038/s41598-017-08879-x.
- [499] Y. W. Chen *et al.*, "A three-dimensional model of human lung development and disease from pluripotent stem cells," (in eng), *Nat Cell Biol*, vol. 19, no. 5, pp. 542-549, May 2017, doi: 10.1038/ncb3510.
- [500] S. Ishikawa, K. Ishimori, and S. Ito, "A 3D epithelial-mesenchymal co-culture model of human bronchial tissue recapitulates multiple features of airway tissue remodeling by TGF- β 1 treatment," (in eng), *Respir Res*, vol. 18, no. 1, p. 195, 11 22 2017, doi: 10.1186/s12931-017-0680-0.
- [501] A. J. Miller *et al.*, "Generation of lung organoids from human pluripotent stem cells in vitro," (in eng), *Nat Protoc*, vol. 14, no. 2, pp. 518-540, 02 2019, doi: 10.1038/s41596-018-0104-8.
- [502] J. Kong *et al.*, "Lung organoids, useful tools for investigating epithelial repair after lung injury," (in eng), *Stem Cell Res Ther*, vol. 12, no. 1, p. 95, 01 30 2021, doi: 10.1186/s13287-021-02172-5.
- [503] T. Sato *et al.*, "Paneth cells constitute the niche for Lgr5 stem cells in intestinal crypts," (in eng), *Nature*, vol. 469, no. 7330, pp. 415-8, Jan 20 2011, doi: 10.1038/nature09637.
- [504] T. Zietek, E. Rath, D. Haller, and H. Daniel, "Intestinal organoids for assessing nutrient transport, sensing and incretin secretion," (in eng), *Sci Rep*, vol. 5, p. 16831, Nov 19 2015, doi: 10.1038/srep16831.
- [505] M. Kasendra *et al.*, "Development of a primary human Small Intestine-on-a-Chip using biopsy-derived organoids," (in eng), *Sci Rep*, vol. 8, no. 1, p. 2871, 02 13 2018, doi: 10.1038/s41598-018-21201-7.
- [506] G. Altay *et al.*, "Self-organized intestinal epithelial monolayers in crypt and villus-like domains show effective barrier function," (in eng), *Sci Rep*, vol. 9, no. 1, p. 10140, 07 12 2019, doi: 10.1038/s41598-019-46497-x.
- [507] D. P. Gómez and F. Boudreau, "Organoids and Their Use in Modeling Gut Epithelial Cell Lineage Differentiation and Barrier Properties During Intestinal Diseases," (in eng), *Front Cell Dev Biol*, vol. 9, p. 732137, 2021, doi: 10.3389/fcell.2021.732137.
- [508] R. Nishinakamura, "Human kidney organoids: progress and remaining challenges," (in eng), *Nat Rev Nephrol*, vol. 15, no. 10, pp. 613-624, 10 2019, doi: 10.1038/s41581-019-0176-x.
- [509] B. S. Freedman, "Physiology assays in human kidney organoids," (in eng), *Am J Physiol Renal Physiol*, vol. 322, no. 6, pp. F625-F638, 06 01 2022, doi: 10.1152/ajprenal.00400.2021.
- [510] L. Alzamil, K. Nikolakopoulou, and M. Y. Turco, "Organoid systems to study the human female reproductive tract and pregnancy," (in eng), *Cell Death Differ*, vol. 28, no. 1, pp. 35-51, 01 2021, doi: 10.1038/s41418-020-0565-5.
- [511] V. D. Venkata *et al.*, "Development and characterization of human fetal female reproductive tract organoids to understand Müllerian duct anomalies," (in eng), *Proc Natl Acad Sci U S A*, vol. 119, no. 30, p. e2118054119, 07 26 2022, doi: 10.1073/pnas.2118054119.
- [512] C. M. Fligor *et al.*, "Three-Dimensional Retinal Organoids Facilitate the Investigation of Retinal Ganglion Cell Development, Organization and Neurite Outgrowth from Human Pluripotent Stem Cells," (in eng), *Sci Rep*, vol. 8, no. 1, p. 14520, 09 28 2018, doi: 10.1038/s41598-018-32871-8.
- [513] J. van der Vaart *et al.*, "Adult mouse and human organoids derived from thyroid follicular cells and modeling of Graves' hyperthyroidism," (in eng), *Proc Natl Acad Sci U S A*, vol. 118, no. 51, 12 21 2021, doi: 10.1073/pnas.2117017118.

- [514] R. A. Wimmer *et al.*, "Human blood vessel organoids as a model of diabetic vasculopathy," (in eng), *Nature*, vol. 565, no. 7740, pp. 505-510, 01 2019, doi: 10.1038/s41586-018-0858-8.
- [515] T. Takebe *et al.*, "Vascularized and Complex Organ Buds from Diverse Tissues via Mesenchymal Cell-Driven Condensation," (in eng), *Cell Stem Cell*, vol. 16, no. 5, pp. 556-65, May 07 2015, doi: 10.1016/j.stem.2015.03.004.
- [516] X. Zhao *et al.*, "Review on the Vascularization of Organoids and Organoids-on-a-," (in eng), *Front Bioeng Biotechnol*, vol. 9, p. 637048, 2021, doi: 10.3389/fbioe.2021.637048.
- [517] F. Duzagac, G. Saorin, L. Memeo, V. Canzonieri, and F. Rizzolio, "Microfluidic Organoids-on-a-Chip: Quantum Leap in Cancer Research," (in eng), *Cancers (Basel)*, vol. 13, no. 4, Feb 10 2021, doi: 10.3390/cancers13040737.
- [518] E. Lee, H. G. Song, and C. S. Chen, "Biomimetic on-a-chip platforms for studying cancer metastasis," (in eng), *Curr Opin Chem Eng*, vol. 11, pp. 20-27, Feb 2016, doi: 10.1016/j.coche.2015.12.001.
- [519] X. Liu *et al.*, "Tumor-on-a-chip: from bioinspired design to biomedical application," (in eng), *Microsyst Nanoeng*, vol. 7, p. 50, 2021, doi: 10.1038/s41378-021-00277-8.
- [520] G. Imparato, F. Urciuolo, and P. A. Netti, "Organ on Chip Technology to Model Cancer Growth and Metastasis," (in eng), *Bioengineering (Basel)*, vol. 9, no. 1, Jan 11 2022, doi: 10.3390/bioengineering9010028.
- [521] I. Maschmeyer *et al.*, "A four-organ-chip for interconnected long-term co-culture of human intestine, liver, skin and kidney equivalents," (in eng), *Lab Chip*, vol. 15, no. 12, pp. 2688-99, Jun 21 2015, doi: 10.1039/c5lc00392j.
- [522] K. H. Benam *et al.*, "Small airway-on-a-chip enables analysis of human lung inflammation and drug responses in vitro," (in eng), *Nat Methods*, vol. 13, no. 2, pp. 151-7, Feb 2016, doi: 10.1038/nmeth.3697.
- [523] S. Wray, "Modelling neurodegenerative disease using brain organoids," (in eng), *Semin Cell Dev Biol*, vol. 111, pp. 60-66, 03 2021, doi: 10.1016/j.semcdb.2020.05.012.
- [524] S. Moore *et al.*, "APP metabolism regulates tau proteostasis in human cerebral cortex neurons," (in eng), *Cell Rep*, vol. 11, no. 5, pp. 689-96, May 05 2015, doi: 10.1016/j.celrep.2015.03.068.
- [525] C. Arber *et al.*, "Familial Alzheimer's disease patient-derived neurons reveal distinct mutation-specific effects on amyloid beta," (in eng), *Mol Psychiatry*, vol. 25, no. 11, pp. 2919-2931, 11 2020, doi: 10.1038/s41380-019-0410-8.
- [526] S. H. Choi *et al.*, "A three-dimensional human neural cell culture model of Alzheimer's disease," (in eng), *Nature*, vol. 515, no. 7526, pp. 274-8, Nov 13 2014, doi: 10.1038/nature13800.
- [527] W. K. Raja *et al.*, "Self-Organizing 3D Human Neural Tissue Derived from Induced Pluripotent Stem Cells Recapitulate Alzheimer's Disease Phenotypes," (in eng), *PLoS One*, vol. 11, no. 9, p. e0161969, 2016, doi: 10.1371/journal.pone.0161969.
- [528] C. Gonzalez, E. Armijo, J. Bravo-Alegria, A. Becerra-Calixto, C. E. Mays, and C. Soto, "Modeling amyloid beta and tau pathology in human cerebral organoids," (in eng), *Mol Psychiatry*, vol. 23, no. 12, pp. 2363-2374, 12 2018, doi: 10.1038/s41380-018-0229-8.
- [529] M. A. Hernández-Sapiéns, E. E. Reza-Zaldívar, R. R. Cevallos, A. L. Márquez-Aguirre, K. Gazarian, and A. A. Canales-Aguirre, "A Three-Dimensional Alzheimer's Disease Cell Culture Model Using iPSC-Derived Neurons Carrying A246E Mutation in PSEN1," (in eng), *Front Cell Neurosci*, vol. 14, p. 151, 2020, doi: 10.3389/fncel.2020.00151.

- [530] J. Jo *et al.*, "Midbrain-like Organoids from Human Pluripotent Stem Cells Contain Functional Dopaminergic and Neuromelanin-Producing Neurons," (in eng), *Cell Stem Cell*, vol. 19, no. 2, pp. 248-257, 08 04 2016, doi: 10.1016/j.stem.2016.07.005.
- [531] L. M. Smits *et al.*, "Modeling Parkinson's disease in midbrain-like organoids," (in eng), *NPJ Parkinsons Dis*, vol. 5, p. 5, 2019, doi: 10.1038/s41531-019-0078-4.
- [532] J. Jarazo *et al.*, "Parkinson's Disease Phenotypes in Patient Neuronal Cultures and Brain Organoids Improved by 2-Hydroxypropyl- β -Cyclodextrin Treatment," (in eng), *Mov Disord*, vol. 37, no. 1, pp. 80-94, 01 2022, doi: 10.1002/mds.28810.
- [533] S. W. Kim *et al.*, "Neural stem cells derived from human midbrain organoids as a stable source for treating Parkinson's disease: Midbrain organoid-NSCs (Og-NSC) as a stable source for PD treatment," (in eng), *Prog Neurobiol*, vol. 204, p. 102086, 09 2021, doi: 10.1016/j.pneurobio.2021.102086.
- [534] P. Conforti *et al.*, "Faulty neuronal determination and cell polarization are reverted by modulating HD early phenotypes," (in eng), *Proc Natl Acad Sci U S A*, vol. 115, no. 4, pp. E762-E771, 01 23 2018, doi: 10.1073/pnas.1715865115.
- [535] J. Zhang *et al.*, "Expanded huntingtin CAG repeats disrupt the balance between neural progenitor expansion and differentiation in human cerebral organoids," 2020.
- [536] J. J. Metzger *et al.*, "Deep-learning analysis of micropattern-based organoids enables high-throughput drug screening of Huntington's disease models," (in eng), *Cell Rep Methods*, vol. 2, no. 9, p. 100297, Sep 19 2022, doi: 10.1016/j.crmeth.2022.100297.
- [537] C. Liu *et al.*, "Mitochondrial HSF1 triggers mitochondrial dysfunction and neurodegeneration in Huntington's disease," (in eng), *EMBO Mol Med*, vol. 14, no. 7, p. e15851, 07 07 2022, doi: 10.15252/emmm.202215851.
- [538] C. Cepeda, N. Wu, V. M. André, D. M. Cummings, and M. S. Levine, "The corticostriatal pathway in Huntington's disease," (in eng), *Prog Neurobiol*, vol. 81, no. 5-6, pp. 253-71, Apr 2007, doi: 10.1016/j.pneurobio.2006.11.001.
- [539] R. Monk and B. Connor, "Cell Reprogramming to Model Huntington's Disease: A Comprehensive Review," (in eng), *Cells*, vol. 10, no. 7, 06 22 2021, doi: 10.3390/cells10071565.
- [540] A. Virlogeux *et al.*, "Reconstituting Corticostriatal Network on-a-Chip Reveals the Contribution of the Presynaptic Compartment to Huntington's Disease," (in eng), *Cell Rep*, vol. 22, no. 1, pp. 110-122, 01 02 2018, doi: 10.1016/j.celrep.2017.12.013.
- [541] J. M. Faustino Martins *et al.*, "Self-Organizing 3D Human Trunk Neuromuscular Organoids," (in eng), *Cell Stem Cell*, vol. 26, no. 2, pp. 172-186.e6, 02 06 2020, doi: 10.1016/j.stem.2019.12.007.
- [542] J. D. Pereira *et al.*, "Human sensorimotor organoids derived from healthy and amyotrophic lateral sclerosis stem cells form neuromuscular junctions," (in eng), *Nat Commun*, vol. 12, no. 1, p. 4744, 08 06 2021, doi: 10.1038/s41467-021-24776-4.
- [543] K. Szebényi *et al.*, "Human ALS/FTD brain organoid slice cultures display distinct early astrocyte and targetable neuronal pathology," (in eng), *Nat Neurosci*, vol. 24, no. 11, pp. 1542-1554, 11 2021, doi: 10.1038/s41593-021-00923-4.
- [544] Y. Tamaki *et al.*, "Spinal cord extracts of amyotrophic lateral sclerosis spread TDP-43 pathology in cerebral organoids," 2021.
- [545] M. Filosto *et al.*, "A Novel Mutation in the Stalk Domain of," (in eng), *J Clin Med*, vol. 8, no. 1, Dec 22 2018, doi: 10.3390/jcm8010017.
- [546] V. Fantini *et al.*, "Bioink Composition and Printing Parameters for 3D Modeling Neural Tissue," (in eng), *Cells*, vol. 8, no. 8, 08 2019, doi: 10.3390/cells8080830.

- [547] E. Scarian *et al.*, "Patients' Stem Cells Differentiation in a 3D Environment as a Promising Experimental Tool for the Study of Amyotrophic Lateral Sclerosis," (in eng), *Int J Mol Sci*, vol. 23, no. 10, May 11 2022, doi: 10.3390/ijms23105344.
- [548] H. Yi *et al.*, "Derivation and Identification of Motor Neurons from Human Urine-Derived Induced Pluripotent Stem Cells," (in eng), *Stem Cells Int*, vol. 2018, p. 3628578, 2018, doi: 10.1155/2018/3628578.
- [549] A. Bernal and L. Arranz, "Nestin-expressing progenitor cells: function, identity and therapeutic implications," (in eng), *Cell Mol Life Sci*, vol. 75, no. 12, pp. 2177-2195, 06 2018, doi: 10.1007/s00018-018-2794-z.
- [550] L. Xie, X. Zeng, J. Hu, and Q. Chen, "Characterization of Nestin, a Selective Marker for Bone Marrow Derived Mesenchymal Stem Cells," (in eng), *Stem Cells Int*, vol. 2015, p. 762098, 2015, doi: 10.1155/2015/762098.
- [551] H. Fong, K. A. Hohenstein, and P. J. Donovan, "Regulation of self-renewal and pluripotency by Sox2 in human embryonic stem cells," (in eng), *Stem Cells*, vol. 26, no. 8, pp. 1931-8, Aug 2008, doi: 10.1634/stemcells.2007-1002.
- [552] M. Pagin *et al.*, "Sox2 controls neural stem cell self-renewal through a Fos-centered gene regulatory network," (in eng), *Stem Cells*, vol. 39, no. 8, pp. 1107-1119, Aug 2021, doi: 10.1002/stem.3373.
- [553] T. C. Archer, J. Jin, and E. S. Casey, "Interaction of Sox1, Sox2, Sox3 and Oct4 during primary neurogenesis," (in eng), *Dev Biol*, vol. 350, no. 2, pp. 429-40, Feb 15 2011, doi: 10.1016/j.ydbio.2010.12.013.
- [554] M. Elkouris *et al.*, "Sox1 maintains the undifferentiated state of cortical neural progenitor cells via the suppression of Prox1-mediated cell cycle exit and neurogenesis," (in eng), *Stem Cells*, vol. 29, no. 1, pp. 89-98, Jan 2011, doi: 10.1002/stem.554.
- [555] X. Zhang *et al.*, "Pax6 is a human neuroectoderm cell fate determinant," (in eng), *Cell Stem Cell*, vol. 7, no. 1, pp. 90-100, Jul 02 2010, doi: 10.1016/j.stem.2010.04.017.
- [556] S. Shin, H. Xue, M. P. Mattson, and M. S. Rao, "Stage-dependent Olig2 expression in motor neurons and oligodendrocytes differentiated from embryonic stem cells," (in eng), *Stem Cells Dev*, vol. 16, no. 1, pp. 131-41, Feb 2007, doi: 10.1089/scd.2006.0023.
- [557] M. A. Tischfield *et al.*, "Human TUBB3 mutations perturb microtubule dynamics, kinesin interactions, and axon guidance," (in eng), *Cell*, vol. 140, no. 1, pp. 74-87, Jan 08 2010, doi: 10.1016/j.cell.2009.12.011.
- [558] G. Morello and S. Cavallaro, "Transcriptional analysis reveals distinct subtypes in amyotrophic lateral sclerosis: implications for personalized therapy," (in eng), *Future Med Chem*, vol. 7, no. 10, pp. 1335-59, 2015, doi: 10.4155/fmc.15.60.
- [559] W. Veit, D. B. B. S.J. Enna, Ed. *Choline Acetyltransferase* (xPharm: The Comprehensive Pharmacology Reference). Elsevier, , 2007.
- [560] M. C. Chiang, C. J. B. Nicol, C. H. Lin, S. J. Chen, C. Yen, and R. N. Huang, "Nanogold induces anti-inflammation against oxidative stress induced in human neural stem cells exposed to amyloid-beta peptide," (in eng), *Neurochem Int*, vol. 145, p. 104992, 05 2021, doi: 10.1016/j.neuint.2021.104992.
- [561] L. Chung, "A Brief Introduction to the Transduction of Neural Activity into Fos Signal," (in eng), *Dev Reprod*, vol. 19, no. 2, pp. 61-7, Jun 2015, doi: 10.12717/DR.2015.19.2.061.
- [562] M. M. A. K. Shawan *et al.*, "Fabrication of Xanthan gum: Gelatin (Xnt:Gel) Hybrid Composite Hydrogels for Evaluating Skin Wound Healing Efficacy," *Modern Applied Science*, vol. 13, No. 3, pp. 101-111, 2019, doi: 10.5539/mas.v13n3p101.

- [563] B. Piola, M. Sabbatini, S. Gino, M. Invernizzi, and F. Renò, "3D Bioprinting of Gelatin-Xanthan Gum Composite Hydrogels for Growth of Human Skin Cells," (in eng), *Int J Mol Sci*, vol. 23, no. 1, Jan 04 2022, doi: 10.3390/ijms23010539.
- [564] A. W. Asohan, R. Hashim, K. M. K. Ishak, Z. A. A. Hamid, N. Jasme, and Y. Bustami, "Preparation and Characterisation of Cellulose Nanocrystal/Alginate/Polyethylene Glycol Diacrylate (CNC/Alg/PEGDA) Hydrogel Using Double Network Crosslinking Technique for Bioprinting Application " *Applied Sciences*, vol. 12, no. 2, p. 771, 2022, doi: 10.3390/app12020771
- [565] F. M., "Measuring cell fluorescence using ImageJ.."
- [566] Y. Xu, P. Li, M. Wang, J. Zhang, and W. Wang, "Imaging the brain in 3D using a combination of CUBIC and immunofluorescence staining," (in eng), *Biomed Opt Express*, vol. 10, no. 4, pp. 2141-2149, Apr 01 2019, doi: 10.1364/BOE.10.002141.
- [567] S. Zucca *et al.*, "RNA-Seq profiling in peripheral blood mononuclear cells of amyotrophic lateral sclerosis patients and controls," (in eng), *Sci Data*, vol. 6, p. 190006, 02 05 2019, doi: 10.1038/sdata.2019.6.
- [568] W. Walter, F. Sánchez-Cabo, and M. Ricote, "GOplot: an R package for visually combining expression data with functional analysis," (in eng), *Bioinformatics*, vol. 31, no. 17, pp. 2912-4, Sep 01 2015, doi: 10.1093/bioinformatics/btv300.
- [569] M. V. Kuleshov *et al.*, "Enrichr: a comprehensive gene set enrichment analysis web server 2016 update," (in eng), *Nucleic Acids Res*, vol. 44, no. W1, pp. W90-7, 07 08 2016, doi: 10.1093/nar/gkw377.
- [570] G. Cidonio, M. Cooke, M. Glinka, J. I. Dawson, L. Grover, and R. O. C. Oreffo, "Printing bone in a gel: using nanocomposite bioink to print functionalised bone scaffolds," (in eng), *Mater Today Bio*, vol. 4, p. 100028, Sep 2019, doi: 10.1016/j.mtbio.2019.100028.
- [571] C. A. Dyer *et al.*, "GFAP-positive and myelin marker-positive glia in normal and pathologic environments," (in eng), *J Neurosci Res*, vol. 60, no. 3, pp. 412-26, May 01 2000, doi: 10.1002/(SICI)1097-4547(20000501)60:3<412::AID-JNR16>3.0.CO;2-E.
- [572] Z. Yang and K. K. Wang, "Glial fibrillary acidic protein: from intermediate filament assembly and gliosis to neurobiomarker," (in eng), *Trends Neurosci*, vol. 38, no. 6, pp. 364-74, Jun 2015, doi: 10.1016/j.tins.2015.04.003.
- [573] X. Liang *et al.*, "Isl1 is required for multiple aspects of motor neuron development," (in eng), *Mol Cell Neurosci*, vol. 47, no. 3, pp. 215-22, Jul 2011, doi: 10.1016/j.mcn.2011.04.007.
- [574] M. Erb, B. Lee, S. Yeon Seo, J. W. Lee, S. Lee, and S. K. Lee, "The Isl1-Lhx3 Complex Promotes Motor Neuron Specification by Activating Transcriptional Pathways that Enhance Its Own Expression and Formation," (in eng), *eNeuro*, vol. 4, no. 2, 2017 Mar-Apr 2017, doi: 10.1523/ENEURO.0349-16.2017.
- [575] S. Arber, B. Han, M. Mendelsohn, M. Smith, T. M. Jessell, and S. Sockanathan, "Requirement for the homeobox gene Hb9 in the consolidation of motor neuron identity," (in eng), *Neuron*, vol. 23, no. 4, pp. 659-74, Aug 1999, doi: 10.1016/s0896-6273(01)80026-x.
- [576] C. J. Alves *et al.*, "Gene expression profiling for human iPS-derived motor neurons from sporadic ALS patients reveals a strong association between mitochondrial functions and neurodegeneration," (in eng), *Front Cell Neurosci*, vol. 9, p. 289, 2015, doi: 10.3389/fncel.2015.00289.
- [577] V. M. Gun'ko, I. N. Savina, and S. V. Mikhalovsky, "Properties of Water Bound in Hydrogels," (in eng), *Gels*, vol. 3, no. 4, Oct 19 2017, doi: 10.3390/gels3040037.

- [578] M. Jonoobi, J. Harun, A. P. Mathew, M. Z. B. Hussein, and K. Oksman, "Preparation of cellulose nanofibers with hydrophobic surface characteristics," *Cellulose*, vol. 17, pp. 299-307, 2010, doi: 10.1007/s10570-009-9387-9.
- [579] S. Maiti and L. Kumari, "Smart Nanopolysaccharides for the Delivery of Bioactives," in *Nanoarchitectonics for Smart Delivery and Drug Targeting*, A. M. G. Alina Maria Holban Ed.: William Andrew Publishing, 2016, ch. 3, pp. 67-94.
- [580] N. Antill-O'Brien, J. Bourke, and C. D. O'Connell, "Layer-By-Layer: The Case for 3D Bioprinting Neurons to Create Patient-Specific Epilepsy Models," (in eng), *Materials (Basel)*, vol. 12, no. 19, Oct 01 2019, doi: 10.3390/ma12193218.
- [581] L. Wang and J. P. Stegemann, "Extraction of high quality RNA from polysaccharide matrices using cetyltrimethylammonium bromide," (in eng), *Biomaterials*, vol. 31, no. 7, pp. 1612-8, Mar 2010, doi: 10.1016/j.biomaterials.2009.11.024.
- [582] K. A. Burgess, V. L. Workman, M. A. Elsayy, A. F. Miller, D. Oceandy, and A. Saiani, "RNA extraction from self-assembling peptide hydrogels to allow qPCR analysis of encapsulated cells," (in eng), *PLoS One*, vol. 13, no. 6, p. e0197517, 2018, doi: 10.1371/journal.pone.0197517.
- [583] H. Jeon *et al.*, "Generation of Multilayered 3D Structures of HepG2 Cells Using a Bio-printing Technique," (in eng), *Gut Liver*, vol. 11, no. 1, pp. 121-128, Jan 15 2017, doi: 10.5009/gnl16010.
- [584] M. Venere, Y. G. Han, R. Bell, J. S. Song, A. Alvarez-Buylla, and R. Blelloch, "Sox1 marks an activated neural stem/progenitor cell in the hippocampus," (in eng), *Development*, vol. 139, no. 21, pp. 3938-49, Nov 2012, doi: 10.1242/dev.081133.
- [585] D. M. Suter, D. Tirefort, S. Julien, and K. H. Krause, "A Sox1 to Pax6 switch drives neuroectoderm to radial glia progression during differentiation of mouse embryonic stem cells," (in eng), *Stem Cells*, vol. 27, no. 1, pp. 49-58, Jan 2009, doi: 10.1634/stemcells.2008-0319.
- [586] J. Gao, J. Wang, Y. Wang, W. Dai, and L. Lu, "Regulation of Pax6 by CTCF during induction of mouse ES cell differentiation," (in eng), *PLoS One*, vol. 6, no. 6, p. e20954, 2011, doi: 10.1371/journal.pone.0020954.
- [587] O. von Bohlen Und Halbach, "Immunohistological markers for staging neurogenesis in adult hippocampus," (in eng), *Cell Tissue Res*, vol. 329, no. 3, pp. 409-20, Sep 2007, doi: 10.1007/s00441-007-0432-4.
- [588] H. E. S. Marei *et al.*, "Cholinergic and dopaminergic neuronal differentiation of human adipose tissue derived mesenchymal stem cells," (in eng), *J Cell Physiol*, vol. 233, no. 2, pp. 936-945, Feb 2018, doi: 10.1002/jcp.25937.
- [589] S. Halpain and L. Dehmelt, "The MAP1 family of microtubule-associated proteins," (in eng), *Genome Biol*, vol. 7, no. 6, p. 224, 2006, doi: 10.1186/gb-2006-7-6-224.
- [590] N. R. Cashman *et al.*, "Neuroblastoma x spinal cord (NSC) hybrid cell lines resemble developing motor neurons," (in eng), *Dev Dyn*, vol. 194, no. 3, pp. 209-21, Jul 1992, doi: 10.1002/aja.1001940306.
- [591] M. H. Qiu, M. C. Chen, Z. L. Huang, and J. Lu, "Neuronal activity (c-Fos) delineating interactions of the cerebral cortex and basal ganglia," (in eng), *Front Neuroanat*, vol. 8, p. 13, 2014, doi: 10.3389/fnana.2014.00013.
- [592] A. S. Perrin-Terrin *et al.*, "The c-FOS Protein Immunohistological Detection: A Useful Tool As a Marker of Central Pathways Involved in Specific Physiological Responses In Vivo and Ex Vivo," (in eng), *J Vis Exp*, no. 110, 04 25 2016, doi: 10.3791/53613.

- [593] A. E. Hudson, "Genetic Reporters of Neuronal Activity: c-Fos and G-CaMP6," (in eng), *Methods Enzymol*, vol. 603, pp. 197-220, 2018, doi: 10.1016/bs.mie.2018.01.023.
- [594] Y. C. Chiu, E. M. Brey, and V. H. Pérez-Luna, "A study of the intrinsic autofluorescence of poly (ethylene glycol)-co-(L-lactic acid) diacrylate," (in eng), *J Fluoresc*, vol. 22, no. 3, pp. 907-13, May 2012, doi: 10.1007/s10895-011-1029-6.
- [595] A. Birger, M. Ottolenghi, L. Perez, B. Reubinoff, and O. Behar, "ALS-related human cortical and motor neurons survival is differentially affected by Sema3A," (in eng), *Cell Death Dis*, vol. 9, no. 3, p. 256, 02 15 2018, doi: 10.1038/s41419-018-0294-6.
- [596] J. H. Hor *et al.*, "ALS motor neurons exhibit hallmark metabolic defects that are rescued by SIRT3 activation," (in eng), *Cell Death Differ*, vol. 28, no. 4, pp. 1379-1397, 04 2021, doi: 10.1038/s41418-020-00664-0.
- [597] O. S. Agboola, X. Hu, Z. Shan, Y. Wu, and L. Lei, "Brain organoid: a 3D technology for investigating cellular composition and interactions in human neurological development and disease models in vitro," (in eng), *Stem Cell Res Ther*, vol. 12, no. 1, p. 430, 07 31 2021, doi: 10.1186/s13287-021-02369-8.
- [598] C. A. Thomas *et al.*, "Modeling of TREG1-Dependent Autoimmune Disease using Human Stem Cells Highlights L1 Accumulation as a Source of Neuroinflammation," (in eng), *Cell Stem Cell*, vol. 21, no. 3, pp. 319-331.e8, Sep 07 2017, doi: 10.1016/j.stem.2017.07.009.
- [599] L. Chi *et al.*, "Motor neuron degeneration promotes neural progenitor cell proliferation, migration, and neurogenesis in the spinal cords of amyotrophic lateral sclerosis mice," (in eng), *Stem Cells*, vol. 24, no. 1, pp. 34-43, Jan 2006, doi: 10.1634/stemcells.2005-0076.
- [600] Y. J. Guan *et al.*, "Increased stem cell proliferation in the spinal cord of adult amyotrophic lateral sclerosis transgenic mice," (in eng), *J Neurochem*, vol. 102, no. 4, pp. 1125-38, Aug 2007, doi: 10.1111/j.1471-4159.2007.04610.x.
- [601] F. Zhou *et al.*, "Screening the expression characteristics of several miRNAs in G93A-SOD1 transgenic mouse: altered expression of miRNA-124 is associated with astrocyte differentiation by targeting Sox2 and Sox9," (in eng), *J Neurochem*, vol. 145, no. 1, pp. 51-67, 04 2018, doi: 10.1111/jnc.14229.
- [602] M. J. Castellanos-Montiel, M. Chaineau, and T. M. Durcan, "The Neglected Genes of ALS: Cytoskeletal Dynamics Impact Synaptic Degeneration in ALS," (in eng), *Front Cell Neurosci*, vol. 14, p. 594975, 2020, doi: 10.3389/fncel.2020.594975.
- [603] A. R. Mehta *et al.*, "Mitochondrial bioenergetic deficits in C9orf72 amyotrophic lateral sclerosis motor neurons cause dysfunctional axonal homeostasis," (in eng), *Acta Neuropathol*, vol. 141, no. 2, pp. 257-279, Feb 2021, doi: 10.1007/s00401-020-02252-5.
- [604] F. Benninger, M. J. Glat, D. Offen, and I. Steiner, "Glial fibrillary acidic protein as a marker of astrocytic activation in the cerebrospinal fluid of patients with amyotrophic lateral sclerosis," (in eng), *J Clin Neurosci*, vol. 26, pp. 75-8, Apr 2016, doi: 10.1016/j.jocn.2015.10.008.
- [605] L. Martínez-Palma, E. Miquel, V. Lagos-Rodríguez, L. Barbeito, A. Cassina, and P. Cassina, "Mitochondrial Modulation by Dichloroacetate Reduces Toxicity of Aberrant Glial Cells and Gliosis in the SOD1G93A Rat Model of Amyotrophic Lateral Sclerosis," (in eng), *Neurotherapeutics*, vol. 16, no. 1, pp. 203-215, 01 2019, doi: 10.1007/s13311-018-0659-7.
- [606] O. H. Tam *et al.*, "Postmortem Cortex Samples Identify Distinct Molecular Subtypes of ALS: Retrotransposon Activation, Oxidative Stress, and Activated Glia," (in eng), *Cell Rep*, vol. 29, no. 5, pp. 1164-1177.e5, 10 29 2019, doi: 10.1016/j.celrep.2019.09.066.

- [607] J. L. Mougeot, Z. Li, A. E. Price, F. A. Wright, and B. R. Brooks, "Microarray analysis of peripheral blood lymphocytes from ALS patients and the SAFE detection of the KEGG ALS pathway," (in eng), *BMC Med Genomics*, vol. 4, p. 74, Oct 25 2011, doi: 10.1186/1755-8794-4-74.
- [608] M. Garofalo *et al.*, "Alzheimer's, Parkinson's Disease and Amyotrophic Lateral Sclerosis Gene Expression Patterns Divergence Reveals Different Grade of RNA Metabolism Involvement," (in eng), *Int J Mol Sci*, vol. 21, no. 24, Dec 14 2020, doi: 10.3390/ijms21249500.
- [609] D. Sproviero *et al.*, "Extracellular Vesicles Derived From Plasma of Patients With Neurodegenerative Disease Have Common Transcriptomic Profiling," (in eng), *Front Aging Neurosci*, vol. 14, p. 785741, 2022, doi: 10.3389/fnagi.2022.785741.
- [610] R. M. Marton *et al.*, "Differentiation and maturation of oligodendrocytes in human three-dimensional neural cultures," (in eng), *Nat Neurosci*, vol. 22, no. 3, pp. 484-491, 03 2019, doi: 10.1038/s41593-018-0316-9.
- [611] S. N. Lanjewar and S. A. Sloan, "Growing Glia: Cultivating Human Stem Cell Models of Gliogenesis in Health and Disease," (in eng), *Front Cell Dev Biol*, vol. 9, p. 649538, 2021, doi: 10.3389/fcell.2021.649538.
- [612] S. J. Rabin *et al.*, "Sporadic ALS has compartment-specific aberrant exon splicing and altered cell-matrix adhesion biology," (in eng), *Hum Mol Genet*, vol. 19, no. 2, pp. 313-28, Jan 15 2010, doi: 10.1093/hmg/ddp498.
- [613] S. Lorenzl, "Stem cells and the modeling of the extracellular matrix--the library of cells needs suitable bookshelves," (in eng), *J Mol Med (Berl)*, vol. 88, no. 6, pp. 531-3, Jun 2010, doi: 10.1007/s00109-010-0612-7.
- [614] G. Maguire, "Amyotrophic lateral sclerosis as a protein level, non-genomic disease: Therapy with S2RM exosome released molecules," (in eng), *World J Stem Cells*, vol. 9, no. 11, pp. 187-202, Nov 26 2017, doi: 10.4252/wjsc.v9.i11.187.
- [615] M. Singh, C. R. Foster, S. Dalal, and K. Singh, "Osteopontin: role in extracellular matrix deposition and myocardial remodeling post-MI," (in eng), *J Mol Cell Cardiol*, vol. 48, no. 3, pp. 538-43, Mar 2010, doi: 10.1016/j.yjmcc.2009.06.015.
- [616] U. Talts, U. Kuhn, G. Roos, and U. Rauch, "Modulation of extracellular matrix adhesiveness by neurocan and identification of its molecular basis," (in eng), *Exp Cell Res*, vol. 259, no. 2, pp. 378-88, Sep 15 2000, doi: 10.1006/excr.2000.4987.
- [617] U. Rauch, K. Feng, and X. H. Zhou, "Neurocan: a brain chondroitin sulfate proteoglycan," (in eng), *Cell Mol Life Sci*, vol. 58, no. 12-13, pp. 1842-56, Nov 2001, doi: 10.1007/PL00000822.
- [618] Z. Su *et al.*, "Neurocan, an extracellular chondroitin sulfate proteoglycan, stimulates neuroblastoma cells to promote malignant phenotypes," (in eng), *Oncotarget*, vol. 8, no. 63, pp. 106296-106310, Dec 05 2017, doi: 10.18632/oncotarget.22435.
- [619] V. Arpino, M. Brock, and S. E. Gill, "The role of TIMPs in regulation of extracellular matrix proteolysis," (in eng), *Matrix Biol*, vol. 44-46, pp. 247-54, 2015 May-Jul 2015, doi: 10.1016/j.matbio.2015.03.005.
- [620] S. Cornfine *et al.*, "The kinesin KIF9 and reggie/flotillin proteins regulate matrix degradation by macrophage podosomes," (in eng), *Mol Biol Cell*, vol. 22, no. 2, pp. 202-15, Jan 15 2011, doi: 10.1091/mbc.E10-05-0394.
- [621] C. Gauthier-Rouvière, S. Bodin, F. Comunale, and D. Planchon, "Flotillin membrane domains in cancer," (in eng), *Cancer Metastasis Rev*, vol. 39, no. 2, pp. 361-374, 06 2020, doi: 10.1007/s10555-020-09873-y.
- [622] C. Tohda and M. Tohda, "Extracellular cathepsin L stimulates axonal growth in neurons," (in eng), *BMC Res Notes*, vol. 10, no. 1, p. 613, Nov 23 2017, doi: 10.1186/s13104-017-2940-y.

- [623] G. Lombardi *et al.*, "Cathepsin-L influences the expression of extracellular matrix in lymphoid organs and plays a role in the regulation of thymic output and of peripheral T cell number," (in eng), *J Immunol*, vol. 174, no. 11, pp. 7022-32, Jun 01 2005, doi: 10.4049/jimmunol.174.11.7022.
- [624] C. P. Gomes *et al.*, "Cathepsin L in COVID-19: From Pharmacological Evidences to Genetics," (in eng), *Front Cell Infect Microbiol*, vol. 10, p. 589505, 2020, doi: 10.3389/fcimb.2020.589505.
- [625] J. Behmoaras, S. Slove, S. Seve, R. Vranckx, P. Sommer, and M. P. Jacob, "Differential expression of lysyl oxidases LOXL1 and LOX during growth and aging suggests specific roles in elastin and collagen fiber remodeling in rat aorta," (in eng), *Rejuvenation Res*, vol. 11, no. 5, pp. 883-9, Oct 2008, doi: 10.1089/rej.2008.0760.
- [626] A. G. Greene, S. B. Eivers, E. W. J. Dervan, C. J. O'Brien, and D. M. Wallace, "Lysyl Oxidase Like 1: Biological roles and regulation," (in eng), *Exp Eye Res*, vol. 193, p. 107975, 04 2020, doi: 10.1016/j.exer.2020.107975.
- [627] N. Yang, D. F. Cao, X. X. Yin, H. H. Zhou, and X. Y. Mao, "Lysyl oxidases: Emerging biomarkers and therapeutic targets for various diseases," (in eng), *Biomed Pharmacother*, vol. 131, p. 110791, Nov 2020, doi: 10.1016/j.biopha.2020.110791.
- [628] L. J. Sosa, A. Cáceres, S. Dupraz, M. Oksdath, S. Quiroga, and A. Lorenzo, "The physiological role of the amyloid precursor protein as an adhesion molecule in the developing nervous system," (in eng), *J Neurochem*, vol. 143, no. 1, pp. 11-29, 10 2017, doi: 10.1111/jnc.14122.
- [629] K. T. Nguyen Ba-Charvet, Y. von Boxberg, S. Guazzi, E. Boncinelli, and P. Godement, "A potential role for the OTX2 homeoprotein in creating early 'highways' for axon extension in the rostral brain," (in eng), *Development*, vol. 125, no. 21, pp. 4273-82, Nov 1998, doi: 10.1242/dev.125.21.4273.
- [630] A. Planques, V. Oliveira Moreira, C. Dubreuil, A. Prochiantz, and A. A. Di Nardo, "OTX2 Signals from the Choroid Plexus to Regulate Adult Neurogenesis," (in eng), *eNeuro*, vol. 6, no. 2, 2019 Mar/Apr 2019, doi: 10.1523/ENEURO.0262-18.2019.
- [631] H. Xu *et al.*, "Col9a2 gene deletion accelerates the degeneration of intervertebral discs," (in eng), *Exp Ther Med*, vol. 23, no. 3, p. 207, Mar 2022, doi: 10.3892/etm.2022.11130.
- [632] B. Goyer, M. Thériault, S. P. Gendron, I. Brunette, P. J. Rochette, and S. Proulx, "Extracellular Matrix and Integrin Expression Profiles in Fuchs Endothelial Corneal Dystrophy Cells and Tissue Model," (in eng), *Tissue Eng Part A*, vol. 24, no. 7-8, pp. 607-615, 04 2018, doi: 10.1089/ten.TEA.2017.0128.
- [633] S. Spada, A. Tocci, F. Di Modugno, and P. Nisticò, "Fibronectin as a multiregulatory molecule crucial in tumor matrisome: from structural and functional features to clinical practice in oncology," (in eng), *J Exp Clin Cancer Res*, vol. 40, no. 1, p. 102, Mar 17 2021, doi: 10.1186/s13046-021-01908-8.
- [634] R. P. Toth and J. D. Atkin, "Dysfunction of Optineurin in Amyotrophic Lateral Sclerosis and Glaucoma," (in eng), *Front Immunol*, vol. 9, p. 1017, 2018, doi: 10.3389/fimmu.2018.01017.
- [635] S. V. Mousavi, E. Agah, and A. Tafakhori, "The Role of Osteopontin in Amyotrophic Lateral Sclerosis: A Systematic Review," *Arch Neurosci.*, vol. 7(3):e94205, 2020.
- [636] K. L. Moya and R. T. Ibad, "OTX2 signaling in retinal dysfunction, degeneration and regeneration," (in eng), *Neural Regen Res*, vol. 16, no. 10, pp. 2002-2003, Oct 2021, doi: 10.4103/1673-5374.308094.

- [637] H. Mizuno, H. Warita, M. Aoki, and Y. Itoyama, "Accumulation of chondroitin sulfate proteoglycans in the microenvironment of spinal motor neurons in amyotrophic lateral sclerosis transgenic rats," (in eng), *J Neurosci Res*, vol. 86, no. 11, pp. 2512-23, Aug 15 2008, doi: 10.1002/jnr.21702.
- [638] A. Oohira, F. Matsui, Y. Tokita, S. Yamauchi, and S. Aono, "Molecular interactions of neural chondroitin sulfate proteoglycans in the brain development," (in eng), *Arch Biochem Biophys*, vol. 374, no. 1, pp. 24-34, Feb 01 2000, doi: 10.1006/abbi.1999.1598.
- [639] S. Lorenzl *et al.*, "Tissue inhibitors of matrix metalloproteinases are elevated in cerebrospinal fluid of neurodegenerative diseases," (in eng), *J Neurol Sci*, vol. 207, no. 1-2, pp. 71-6, Mar 15 2003, doi: 10.1016/s0022-510x(02)00398-2.
- [640] I. Niebroj-Dobosz, P. Janik, B. Sokołowska, and H. Kwiecinski, "Matrix metalloproteinases and their tissue inhibitors in serum and cerebrospinal fluid of patients with amyotrophic lateral sclerosis," (in eng), *Eur J Neurol*, vol. 17, no. 2, pp. 226-31, Feb 2010, doi: 10.1111/j.1468-1331.2009.02775.x.
- [641] J. Zhai *et al.*, "Proteomic characterization of lipid raft proteins in amyotrophic lateral sclerosis mouse spinal cord," (in eng), *FEBS J*, vol. 276, no. 12, pp. 3308-23, Jun 2009, doi: 10.1111/j.1742-4658.2009.07057.x.
- [642] T. Pushkarsky *et al.*, "Abundance of Nef and p-Tau217 in Brains of Individuals Diagnosed with HIV-Associated Neurocognitive Disorders Correlate with Disease Severance," (in eng), *Mol Neurobiol*, vol. 59, no. 2, pp. 1088-1097, Feb 2022, doi: 10.1007/s12035-021-02608-2.
- [643] P. A. Li *et al.*, "Up-regulation and altered distribution of lysyl oxidase in the central nervous system of mutant SOD1 transgenic mouse model of amyotrophic lateral sclerosis," (in eng), *Brain Res Mol Brain Res*, vol. 120, no. 2, pp. 115-22, Jan 05 2004, doi: 10.1016/j.molbrainres.2003.10.013.
- [644] J. L. Gonzalez de Aguilar *et al.*, "Gene profiling of skeletal muscle in an amyotrophic lateral sclerosis mouse model," (in eng), *Physiol Genomics*, vol. 32, no. 2, pp. 207-18, Jan 17 2008, doi: 10.1152/physiolgenomics.00017.2007.
- [645] J. B. Bryson *et al.*, "Amyloid precursor protein (APP) contributes to pathology in the SOD1(G93A) mouse model of amyotrophic lateral sclerosis," (in eng), *Hum Mol Genet*, vol. 21, no. 17, pp. 3871-82, Sep 01 2012, doi: 10.1093/hmg/dds215.
- [646] S. Stanga *et al.*, "A Role for GDNF and Soluble APP as Biomarkers of Amyotrophic Lateral Sclerosis Pathophysiology," (in eng), *Front Neurol*, vol. 9, p. 384, 2018, doi: 10.3389/fneur.2018.00384.
- [647] S. Apolloni and N. D'Ambrosi, "Fibrosis as a common trait in amyotrophic lateral sclerosis tissues," (in eng), *Neural Regen Res*, vol. 17, no. 1, pp. 97-98, Jan 2022, doi: 10.4103/1673-5374.314302.
- [648] J. Ma *et al.*, "Extracellular Matrix Proteins Involved in Alzheimer's Disease," (in eng), *Chemistry*, vol. 26, no. 53, pp. 12101-12110, Sep 21 2020, doi: 10.1002/chem.202000782.
- [649] F. Dangond *et al.*, "Molecular signature of late-stage human ALS revealed by expression profiling of postmortem spinal cord gray matter," (in eng), *Physiol Genomics*, vol. 16, no. 2, pp. 229-39, Jan 15 2004, doi: 10.1152/physiolgenomics.00087.2001.
- [650] S. Ono *et al.*, "Decreased type IV collagen of skin and serum in patients with amyotrophic lateral sclerosis," (in eng), *Neurology*, vol. 51, no. 1, pp. 114-20, Jul 1998, doi: 10.1212/wnl.51.1.114.
- [651] H. G. Yi, H. Kim, J. Kwon, Y. J. Choi, J. Jang, and D. W. Cho, "Application of 3D bioprinting in the prevention and the therapy for human diseases," (in eng), *Signal Transduct Target Ther*, vol. 6, no. 1, p. 177, 05 14 2021, doi: 10.1038/s41392-021-00566-8.

- [652] A. G. Turhan *et al.*, "iPSC-Derived Organoids as Therapeutic Models in Regenerative Medicine and Oncology," (in eng), *Front Med (Lausanne)*, vol. 8, p. 728543, 2021, doi: 10.3389/fmed.2021.728543.
- [653] S. Fernandes, C. Vyas, P. Lim, R. F. Pereira, A. Virós, and P. Bártolo, "3D Bioprinting: An Enabling Technology to Understand Melanoma," (in eng), *Cancers (Basel)*, vol. 14, no. 14, Jul 20 2022, doi: 10.3390/cancers14143535.